IMPACT OF DAMPER FAILURE ON VEHICLE HANDLING DURING CRITICAL DRIVING SITUATIONS

A THESIS SUBMITTED TO
THE GRADUATE SCHOOL OF NATURAL AND APPLIED SCIENCES
OF
MIDDLE EAST TECHNICAL UNIVERSITY

BY

MUSTAFA DURUKAN BEDÜK

IN PARTIAL FULLFILLMENT OF THE REQUIREMENTS
FOR
THE DEGREE OF MASTER OF SCIENCE
IN
MECHANICAL ENGINEERING

NOVEMBER 2009

Approval of the thesis:

IMPACT OF DAMPER FAILURE ON VEHICLE HANDLING DURING CRITICAL DRIVING SITUATIONS

submitted by **MUSTAFA DURUKAN BEDÜK** in partial fulfillment of the requirements for the degree of **Master of Science in Mechanical Engineering Department, Middle East Technical University** by,

Prof. Dr. Canan Özgen _____
Dean, Graduate School of **Natural and Applied Sciences**

Prof. Dr. Suha Oral _____
Head of Department, **Mechanical Engineering**

Prof. Dr. Y. Samim Ünlüsoy _____
Supervisor, **Mechanical Engineering Dept., METU**

Examining Committee Members:

Prof. Dr. Metin Akkök _____
Mechanical Engineering Dept., METU

Prof. Dr. Y. Samim Ünlüsoy _____
Mechanical Engineering Dept., METU

Assist. Prof. Dr. Yiğit Yazıcıoğlu _____
Mechanical Engineering Dept., METU

Assist. Prof. Dr. Gökhan O. Özgen _____
Mechanical Engineering Dept., METU

Assist. Prof. Dr. Kutluk Bilge Arıkan _____
Mechatronics Engineering Dept., Atılım University

Date:

I hereby declare that all information in this document has been obtained and presented in accordance with academic rules and ethical conduct. I also declare that, as required by these rules and conduct, I have fully cited and referenced all material and results that are not original to this work.

Name, Last name : **Mustafa Durukan Bedük**

Signature :

ABSTRACT

IMPACT OF DAMPER FAILURE ON VEHICLE HANDLING DURING CRITICAL DRIVING SITUATIONS

Bedük, Mustafa Durukan

M.S., Department of Mechanical Engineering

Supervisor: Prof. Dr. Y. Samim Ünlüsoy

November 2009, 179 pages

Capturing what is going on and what may happen related to vehicle handling behaviour in cases of desired or non-desired actions and interventions has a crucial importance. Strategies implemented to improve vehicle stability or algorithms and control modules designed to compensate the non-desired effects on handling behavior may appear to be inadequate as the vehicle goes through uncountable experiences. The importance of understanding and introducing the possible sources of undesired effects which may be encountered throughout driving action cannot be underemphasized.

One of the possibilities that may lead the driver face with unexpected results concerning vehicle's handling is suspension damper failure, which has not yet been dealt with adequately in the literature. The fast developing technology and consequently the expanding utilization of chassis electronics and electronic vehicle components make the investigation of damper failure phenomenon essential since reliability decreases by the continuously increasing introduction of electronic means. In this study, possible failure types of dampers including electrical failure are taken into account, their effects on vehicle stability under critical driving conditions are examined. Shortcomings and comments are made on criticality of failed damper and its failure point. This work as a result, constitutes a particular contribution to the literature in that it brings up a concrete knowledge to the stated research area.

Keywords: Suspension damper, damper failure, chassis component malfunction, vehicle stability, vehicle handling,

ÖZ

KRİTİK SEYİR DURUMLARINDA AMÖRTİSÖR ARIZALARININ YOL TUTUŞ DAVRANIŞI ÜZERİNDEKİ ETKİLERİ

Bedük, Mustafa Durukan
Yüksek Lisans, Makina Mühendisliği Bölümü
Tez Yöneticisi: Prof. Dr. Y. Samim Ünlüsoy

Kasım 2009, 179 sayfa

Hareket halindeki araçlara istenen ve istenmeyen etkileşim ve müdahale durumunda, aracın yol tutuş davranışında neler olabileceğini algılayabilmek a önemlidir. Araç kararlılığını arttırmak için kullanılan stratejiler veya araç yol tutuşu üzerindeki istenmeyen etkileri karşılayabilmek için tasarlanan algoritma ve denetim modülleri, araç beklenmedik bir arızaya maruz kaldığında yetersiz kalabilir. Bu nedenlerle, sürüş esnasında karşılaşılabilecek ve istenmeyen bir davranış yaratabilecek tüm durumları anlayabilmek ve kestirebilmenin önemi vurgulanmalıdır.

Sürücüyü istenmeyen bir yol tutuş durumuyla karşı karşıya bırakabilecek, ilgili literatürün bugüne kadar çok üzerinde durmadığı olasılıklardan biri de amortisör arızalarıdır. Şasi elektronik sistemleri ve araç elektronik komponentlerinin artan teknolojisi ve uygulamaları, elektronik komponentlerin güvenilirliğinin de daha az olmasından dolayı amortisör arızası durumunun incelenmesini gerekli kılmıştır. Bu çalışmada, mümkün görülen tüm amortisör arıza tipleri, amortisörlerdeki elektronik bozulmaları da kapsayacak şekilde hesaba katılmıştır. Kritik seyir durumlarında bunların yol tutuş ve araç kararlılığı üzerindeki etkileri ve bu etkilerin ne şekilde ortaya çıktığı incelenmiş ve sürüş ve bozulma tipine göre kritik amortisör ve kritik bozulma zamanları belirlenmiştir.

Sonuç olarak bu çalışma, literatüre ilgili alanda bir kaynak olması açısından önemli bir katkı sağlamaktadır.

Anahtar kelimeler: Amortisör bozulması, Şasi komponent işlev bozuklukları, araç kararlılığı, araç yol tutuşu,

Dedicated to my family, who always supported me throughout my life…

ACKNOWLEDGEMENTS

Firstly, I would like to express my special appreciations to Prof. Dr. Y. Samim Ünlüsoy who supervised and guided me with his useful and sophisticated insights throughout this thesis.

Also I would like to put my special thankfulness to Prof. Dr.-Ing. Ferit Küçükay into words, who has provided me the opportunity to make use of the technical literature supplied by Institute für Fahrzeugtechnik, TU Braunschweig.

I would like to state my special thanks to Dr. Kemal Çalışkan, who has patiently guided me with his technical contribution and practical advises throughout my study. Additionally, I am also grateful for the beneficial recommendations of Dr.-Ing. Roman Henze who provided useful technical support during the thesis.

My special thankfulness also goes to Andaç Töre Şamiloğlu, Emir Kutluay, Görkem Oktay, Taner Yılmaz and Torben Pawellek who have patiently stimulated me with their enjoyable and kind attitude during my career in automotive engineering.

My last, but not the least thanks go to my valuable family; the most precious people in my life, who unconditionally supported me throughout my life with their love and understanding and in all kinds of manner.

TABLE OF CONTENTS

LIST OF TABLES

LIST OF FIGURES

LIST OF SYMBOLS

a0..a7,b0..b8,c0..c10	Pacejka coefficients which include the influence of wheel load, slip angle, slip ratio and camber
a_y	Lateral acceleration
$a_{y\max}$	Time point indicating maximum lateral acceleration
cw1, cw2 and *cw3*	Air resistance coefficients
cst_h	Torsional stiffness value of the rear anti-roll bar
cst_v	Torsional stiffness value of the front anti-roll bar
fr	Rolling resistance coefficient
g	Gravitational acceleration
h	Pitch centre height
h_a	Body (sprung) mass centre height
h_h	Rear axle unsprung mass centre of gravity height
h_v	Front axle unsprung mass centre of gravity height
h'	Moment arm for the roll moment
i_{Li}	Steering gear ratio
l	Wheelbase
l_h	Centre of mass distance from the rear axle
l_v	Centre of mass distance from the front axle
l_{ha}	Distance between the body centre of gravity and rear axle
l_{hn}	Distance of the pitch centre from the rear axle
l_{va}	Distance between the body centre of gravity and front axle
l_{vn}	Distance between the pitch centre and front axle

m	Total mass of the vehicle
m_a	Body (sprung) mass of the vehicle
m_f	Total unsprung mass
m_h	Rear axle unsprung mass
m_v	Front axle unsprung mass
$n_0(\delta_{Vi})$	Castor offset with wheel steer angle dependence
p_h	Roll centre height for rear suspension
p_v	Roll centre height for front suspension
r_{dyn}	Dynamical rotating tire radius
r_p	Radius of the planet gear of differential
r_s	Radius of the sun gear of differential
r_{st1}	Outer radius of the differential cage
r_{st2}	Inner radius of the differential cage
r_h	Radius of the ring gear of differential
r_{GA}	Final drive ratio
r_L	Offset due to steering axis inclination with kingpin offset dependence
$r_\sigma(\delta_{Vi})$	Offset due to steering axis inclination with wheel steer angle dependence
s_h	Rear track width
s_v	Front track width
v_0	Initial longitudinal speed of the vehicle (input to the system)
$v_{lat,i}$	Linear velocity component of tire parallel to the lateral axis of the body
$v_{long,i}$	Linear velocity component of tire parallel to the longitudinal axis of the body

ω_i	Angular speed of the wheel
$\dot{\omega}_1$	Angular acceleration of the front left wheel
$\dot{\omega}_2$	Angular acceleration of the front right wheel
$\dot{x}$	Longitudinal velocity of the vehicle
$\ddot{x}$	Longitudinal acceleration of the vehicle
z	Vertical displacement of the body
z_{0i}	Individual static deflection of the suspensions
z_i	Individual suspension deflections
$\dot{z}$	Vertical velocity of the body
$\dot{z}_i$	Individual suspension relative velocity
$\ddot{z}$	Body vertical acceleration
F_{Di}	Damper force
F_{Fi}	Spring force
F_{GA}	Driving force entering the differential input
F_L	Air resistance
F_P	Total net drive force entering the differential
F_{Ri}	Rolling resistance of the individual wheel
F_{Xi}	Longitudinal tire force
F_{Yi}	Lateral tire force
F_{Zi}	Vertical tire force
F_{Z0_i}	Individual static loads on the tires
J_{st}	Rotational inertia for the differential cage
J_p	Rotational inertia for the planet gear
J_R	Rotational inertia of the wheel
J_X	Roll moment of inertia around the centre of gravity
J_Y	Pitch moment of inertia around the pitch centre

J_Z	Yaw moment of inertia of the vehicle
M_1	Net moment on the front left wheel
M_2	Net moment on the front right wheel
M_{B1}	Braking moment on the front left wheel
M_{B2}	Braking moment on the front right wheel
M_{GA}	Torque entering the differential input
M_{Zi}	Self aligning torque
Sp	Slip percentage
S_{Xi}	Longitudinal slip values of the individual tires
V_{Xi}	Individual longitudinal linear wheel velocities parallel to wheel rolling plane
α_i	Tire slip angle
β	Side slip angle
$\beta_{\max}$	Time point indicating maximum side slip angle
$\dot{\beta}$	Side slip angular velocity
δ_{SCi}	Deviation due to aligning steer-torques
δ_{SW}	Steering wheel angle
δ_{V0}	Static toe angle given to the wheels
δ_{Vi}	The overall wheel steer angle
$\delta_{Vi}(F_{Xi})$	Angular elastic deformation due to longitudinal tire forces
$\delta_{Vi}(F_{Yi})$	Angular elastic deformation due to lateral tire forces
$\delta_{Vi}(\kappa)$	Angular elastic deformation due to roll angle κ
ε	Support angle between the suspension arms and the vertical axis
γ_i	Dynamic camber
κ	Roll angle

$\kappa_{\max}$	Time point indicating maximum roll angle
$\dot{\kappa}_{\max}$	Time point indicating maximum roll velocity
$\ddot{\kappa}$	Roll acceleration
$\tau(\delta_{V_i})$	Dynamical castor angle with wheel steer angle dependence
$\varphi_{\max}$	Time point indicating maximum pitch angle
$\dot{\varphi}$	Pitch velocity
$\dot{\varphi}_{\max}$	Time point indicating maximum pitch velocity
$\ddot{\varphi}$	Pitch acceleration
$\dot{\psi}$	Yaw velocity of the vehicle
$\dot{\psi}_{\max}$	Time point indicating maximum yaw velocity
$\ddot{\psi}$	Yaw acceleration

CHAPTER 1

INTRODUCTION

Vehicle dynamics and stability control task has always had a profound importance in automotive engineering. The factors influencing vehicle handling and stability are worth to be examined since they may have a great impact on vehicle handling in that the vehicle stability and safety may be affected in a hazardous manner. These impacts may be sourcing from outer factors (road disturbances due to travelling, driver effects etc.) and inner factors (effects due to vehicle components).

Inner factors also include the chassis component failures which may constitute a deep impact on vehicle stability. Chassis component parametrization (parameter selection) has a significant value in defining vehicle handling characteristics, thus a failure occurring in one of them may alter the vehicle handling behaviour changing the parameters of that particular component.

Only a few researches, studies, and publications can be found in the literature, which focus on effects of vehicle component parametrization on handling behaviour and failure mechanics of some vehicle components. Recently, vehicle components have started to exhibit a tendency in increasing use of electrical power instead of mechanical means. As a result, the failure risk of components increases with decreasing reliability.

One of the most common usages of electrical power is in the suspension components, especially in active suspensions. Electrically driven dampers are typical examples. The literature up to now has covered the effects of parameter variation of dampers on vehicle handling i.e. the damper wear and the control strategies applied in switchable dampers, in only a few publications. However, even those studies do not go beyond gathering some results concerning changes occurring in vehicle handling behaviour with parameter alteration; they do not

examine the critical driving situations in which the deepest impact may occur on vehicle stability and handling in case of a parameter change as a result of failure.

The goal of this study is to examine the impact of damper failure on vehicle handling during critical driving conditions with all possible means of damper failure. By such means the study carried out will contribute to the related work on the subject. In the study, a detailed vehicle model is developed, a large number of simulation case studies concerning the damper failure are carried out, the results are interpreted, and some general shortcomings are uncovered.

Modern dampers can be split into several classes in terms of working principles. Traditionally, dampers used in automobile suspensions are of hydraulic type. During the operation of hydraulic dampers, the piston moves through the fluid in its bore and the valves restrict the fluid flow through the piston which creates the damping force. Normally, a damper consists of leak restriction, port restriction, and spring controlled blow-off valves. Adjustment of these valves provides the damping coefficient of the hydraulic damper [1]. There are 2 main structural configurations of hydraulic dampers:

1.1 TWIN -TUBE DAMPERS

These dampers consist of one operating (pressure) tube and one reverse (balancing) tube, Figure 1.1. When the wheels are subjected to bump, piston moves down and oil flows out of the lower working chamber through the valve into the upper chamber. The oil goes into the equalization chamber through the base valve. This produces the main forces necessary for the compression damping and only if this does not suffice, the valve on the piston can become effective.

When the axle rebounds, there is overpressure between the piston and the piston rod guide. As this happens, the main oil volume is pushed to the adjustable valve, which causes the jounce damping. The minor fluid is squeezed through the gap between the guide and the piston rod. If the rod extends, this leads to a lack of

oil in the working chamber. The missing liquid is sucked from the equalization chamber and flows through the return valve [2].

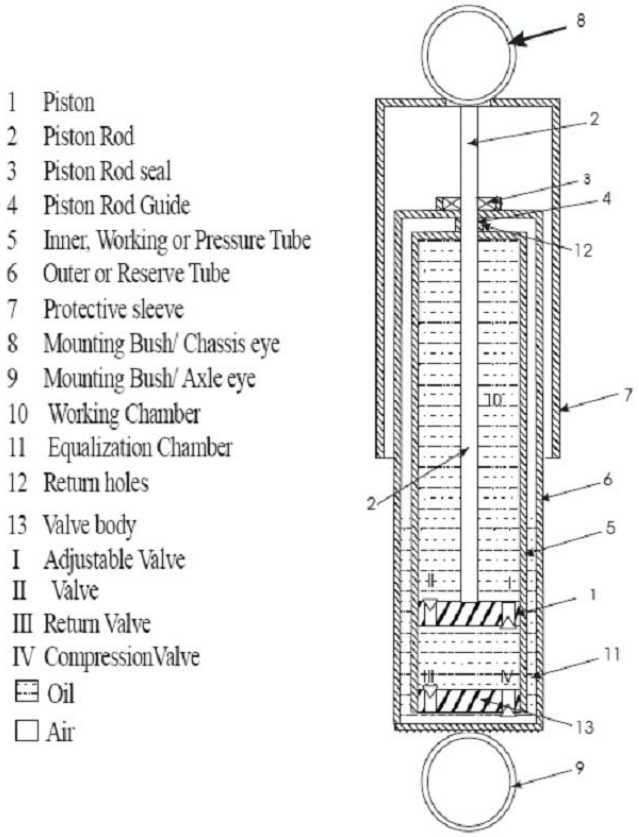

Figure 1.1 Structure of the Twin Tube Damper [2]

1.2 SINGLE -TUBE DAMPERS

These dampers consist of a single operating (pressure) tube with a floating piston separating oil and gas chambers as illustrated in Figure 1.2 [2]. When the wheel jounces, the oil flows through the jounce state valve from the bottom to the top part of the working chamber. The gas pressures in the equalization chamber forces the dividing piston to follow. If the wheel goes into the travel bump, the compression valve is charged, and the dividing piston moves upwards through the

oncoming rod volume. The entire piston surface is available for bump damping. Because tube is longer, it is difficult to apply this design to passenger cars.

However, it is an original equipment of many imported and domestic passenger cars such as SUV and light truck applications. The difference in actual application is that in a single-tube design, the dividing piston makes it possible to install the damper in any position; it can be mounted upside down or right side up and will work either way.

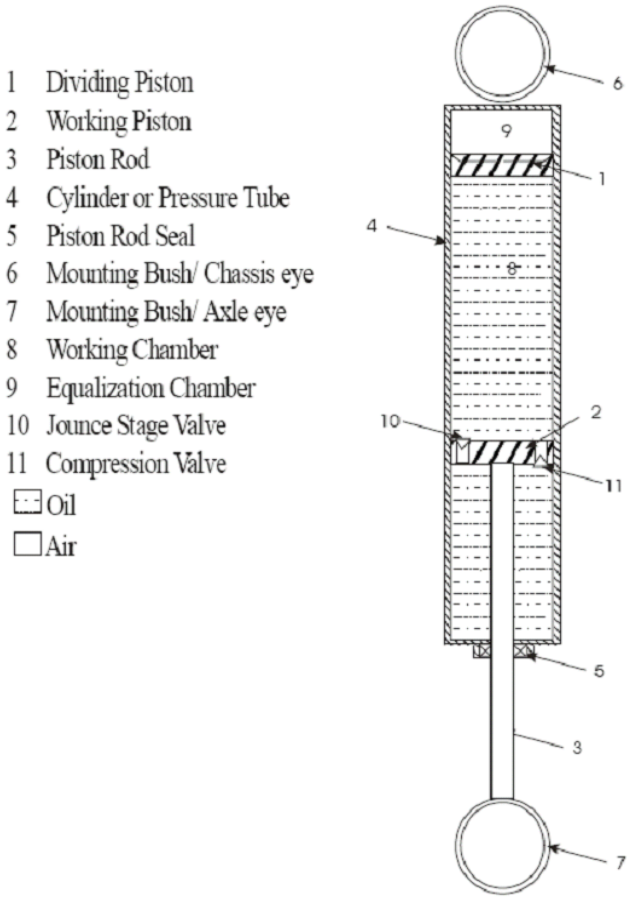

Figure 1.2 Structure of the Single Tube Damper [2]

In modern systems, there exist also the electrical, magnetorheological (MR), and electrorheological (ER) type dampers [2].

1.3 ELECTRIC DAMPER

An electric damper converts the kinetic energy into electric energy. This energy can be used to charge a battery and to improve drive efficiency. It consists of a permanent magnet linear synchronous generator, a spring, and an electric energy accumulator. The linear generator consists of two parts:

- Primary part with three-phase winding placed in the slots of primary core, and
- Secondary part with permanent magnets attached to the iron core.

The electric energy accumulator consists of a controlled rectifier and a battery connected to it, as illustrated in Figure 1.3.

During the oscillation of the vehicle, the secondary part is moving with respect to the primary part. Due to the relative linear motion of primary winding and secondary permanent magnets, an AC voltage is induced in the coils. This voltage is then rectified by the 3-phase controlled converter and supplies a battery. Since the magnetic field produced by the permanent magnets alternates with respect to the primary part, the core of this part must be laminated to decrease the eddy current losses and hysteresis losses. The secondary core can be made of solid iron since the magnetic flux is steady in it. The damping force is actually the resisting magnetic force created by means of the motion of the windings inside that magnetic flux.

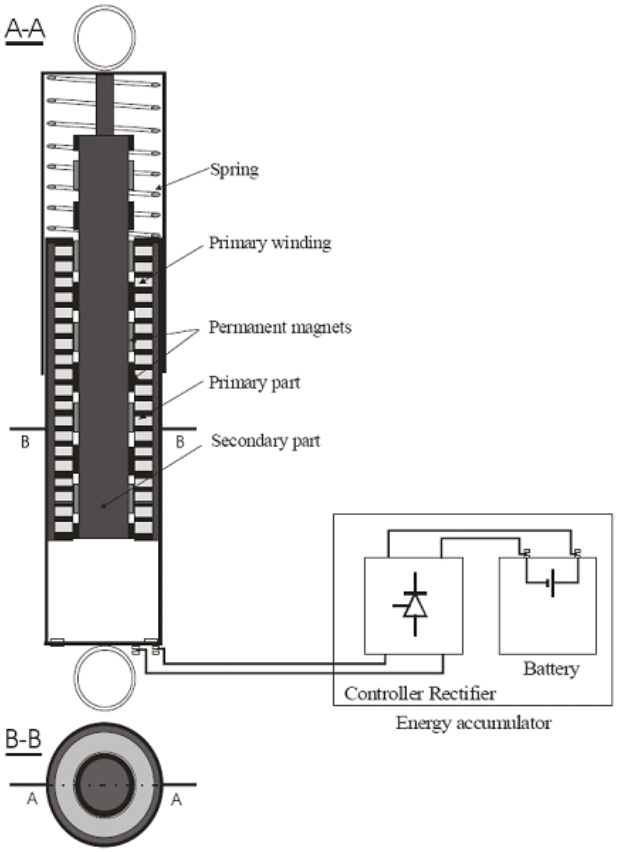

Figure 1.3 Structure of the Electric Damper [2]

The modern versions of electric (electromagnetic) dampers are commonly used for the sake of semi-active automobile suspensions where the usage of semi-active suspensions is preferable to full active suspensions due to lower costs. As a less expensive alternative to active suspensions, semi-active dissipative suspensions were proposed in which an active force generator is replaced by a damper that can vary its characteristic with sufficient speed. *Such a damper can adjust the coefficient of damping by varying the cross sectional area of the oil flow in the dampers.* In principle, the damping force generated by such a damper can track the force that would be obtained by an active device as long as it is dissipative, i.e. does not require supply of energy [3].

In some applications of electric dampers thermal energy generated by the compressed oil is converted into mechanical energy by a wheel-like turbine and then it is converted to electrical energy by a small generator. This energy can be used for charging purposes of heavy vehicle batteries or for assistance purposes of hybrid vehicle powertrains [4].

1.4 MAGNETORHEOLOGICAL DAMPERS

Recently, magnetorheological (MR) dampers have received increasing attention in vehicle active suspension designs due to their mechanical simplicity, wide operation bandwidth, and high reliability. Although the MR dampers are superior to traditional variable solenoid dampers, they are much more difficult to model and control because of their inherent hysteresis and other nonlinear dynamics [5].

Today, magnetorheological dampers have also attracted interest in using controllable actuators for their quick response and low energy consumption. The load-levelling suspension system (with MR dampers) has a unique advantage over the traditional suspension system because its damping can be changed by controlling the MR damper in the system. This property can potentially be used to solve the conflict of suspension system ride comfort and handling property.

The control methods implemented with MR dampers are the skyhook control, LQG control, and sliding mode control. These methods depend on varying the system's damping ratio without changing the system stiffness [6].

1.5 MATHEMATICAL MODELLING

The modern damper modelling for simulations can be separated into 3 types. The first one is the analytical modelling which consists of calculation of the damper forces dependent on displacement, velocity, or acceleration based on the

geometrical and physical parameters of the damper. This modelling is complex, therefore not preferable for computer simulations.

The second modelling type is the experimental modelling in which the damper characteristics will rely purely on experimental data. Models which describe input and output relationships are developed through these measurements.

The other methods for damper modelling are the restoring-force mapping method which is based on tests carried out at a fixed frequency with various amplitudes, the artificial neural network, and empirical dynamics methods which use testing to obtain the damper characteristics. These models have also the ability to predict the damper characteristics beyond the testing conditions [1].

CHAPTER 2

LITERATURE SURVEY

In modern systems, damper characteristics are usually captured via high speed data acquisition which gives the force-displacement and force-velocity relation of the damper. However, in vehicle simulation studies a linear or a non-linear damper model in terms of velocity-force dependence is frequently used. In the bilinear model there exist actually two linear regions (one for extensive and one for compressive sections) which correspond to high velocity ranges. Inside the boundaries of low velocity range the damping curve is non-linear [7]. During the simulation workout, this type of a damper characteristic curve is employed. In Figures 2.1 and 2.2, experimentally obtained damper characteristics for different mileage levels (53k and 103k) are shown.

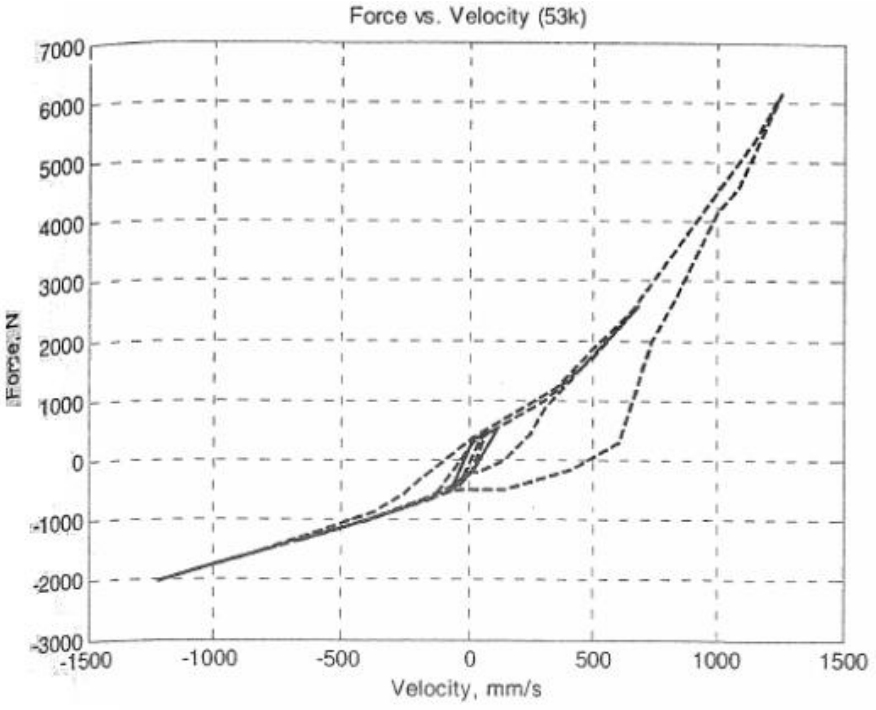

Figure 2.1 Experimental Damper Characteristics for a Damper with 53k [7]

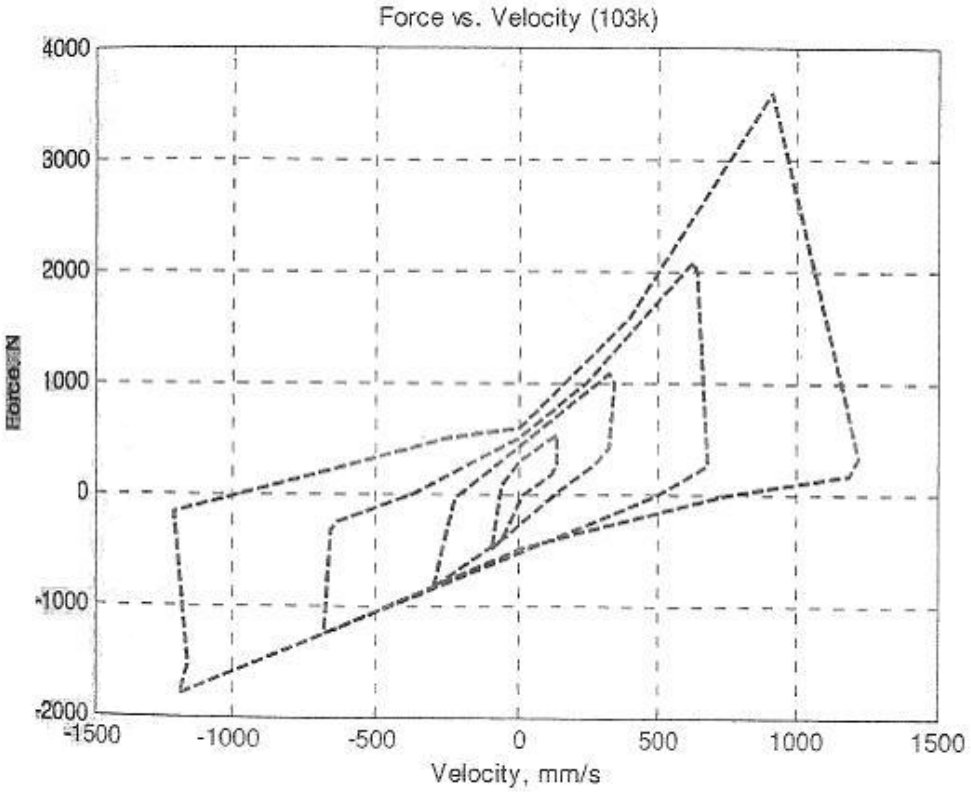

Figure 2.2 Experimental Damper Characteristics for a Damper with 103k [7]

The asymmetric damping characteristics of the modern dampers are examined in [8] in which a broad frequency range excitation testing with alternative excitation amplitudes is carried out. The test results indicate that the compression and rebound peak velocities are different then each other. This means that the damper characteristics are asymmetric in compression and tension. The effects of temperature and frictional forces in gas dampers, which play an important role in terms of the overall ride height and mass jerking response indirectly, are also referred to in that publication. In Figure 2.3, velocity and displacement dependent damper characteristics obtained through frequency range excitation testing are shown.

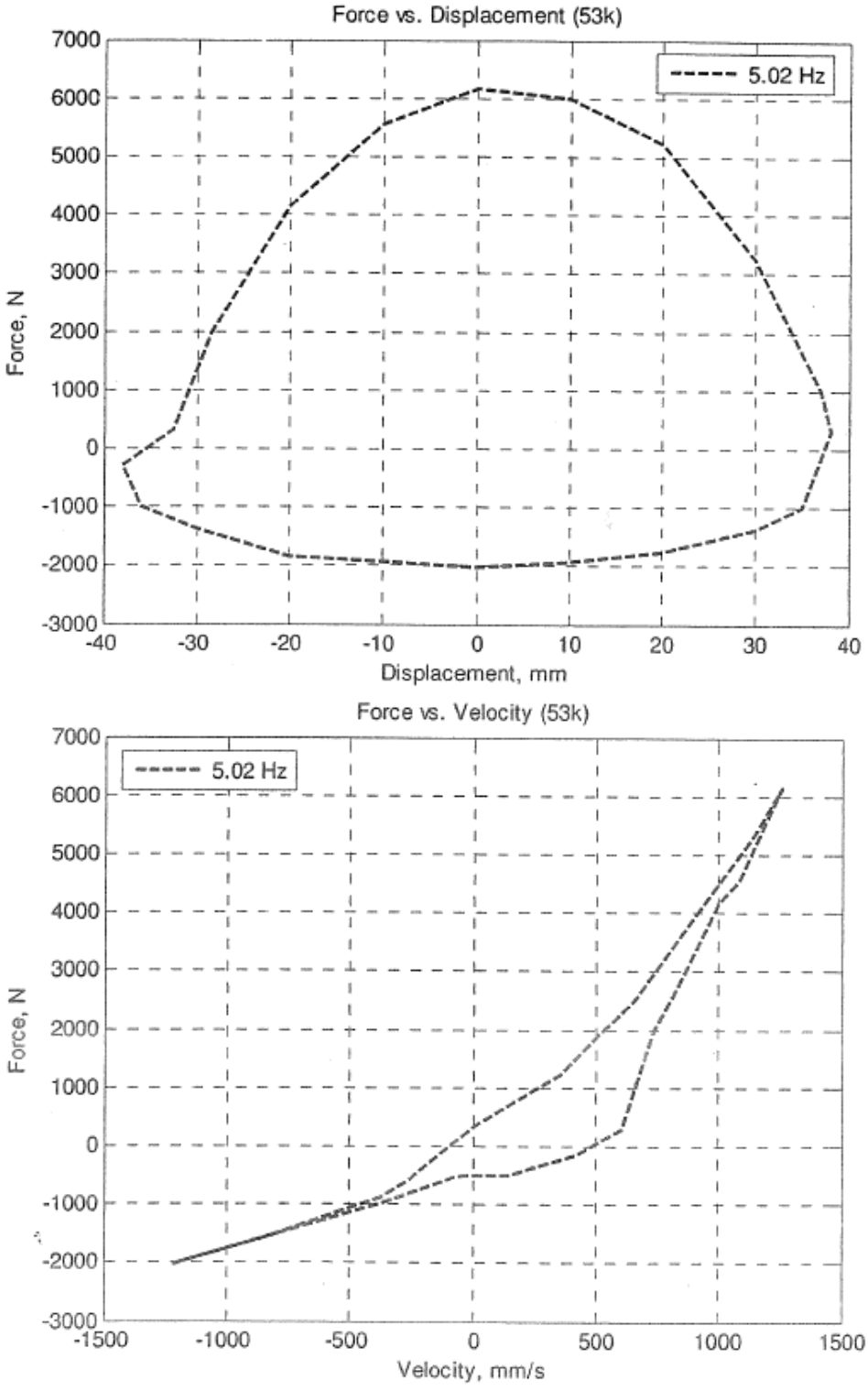

Figure 2.3 Representative Force vs. Displacement (above) and Force vs. Velocity [7]

There are also a number of publications in the literature which examine the adaptive control strategies for a switchable damper. One of these publications [9] investigates the impact of two main control strategies based on optimization via minimization of wheel acceleration and suspension deflection. The test simulations performed with a quarter car model, Figure 2.4, having parameters: body mass of 250 kg, wheel mass of 50 kg, tire stiffness of 120000 N/m, and switchable damper stiffnesses of 650, 1500 and 2900 Ns/m. As a result of that study, control strategy based on minimization of suspension travel gave an improvement in body acceleration and dynamic tire load up to 15 %, whereas the other control strategy based on minimization of wheel acceleration had an improvement up to 22 % in comparison with the passive damper vehicle.

Switchable damper modelling is studied in [10], in which the conclusions from the software analysis indicate significant improvements of 13 % and 17 % in body acceleration, and 7 % and 8 % in dynamic tire load relative to a passive system for two-state and three-state switchable dampers respectively. The during-switch characteristics from hard to soft and soft to hard are measured in terms of dead time duration. The dead time occurs to be 30 ms to attain 63 % harder or softer characteristics than original for the damper used in measurements. It took more than 50 ms to attain to complete hard to complete soft or vice versa. During the damper force change throughout these considerably short switch times due to variable orifice change, a first order polynomial approach is applied. As a result, it could be obviously considered that the switch times for switchable type dampers are substantially short to count for a significant effect on vehicle handling.

The use of magnetorheological dampers has attracted attention in some publications. For example, in [6] it is shown that the low frequency rolling in curves and low frequency pitching during braking are possible to control by use of magnetorheological dampers, but also the load-levelling is possible by such means.

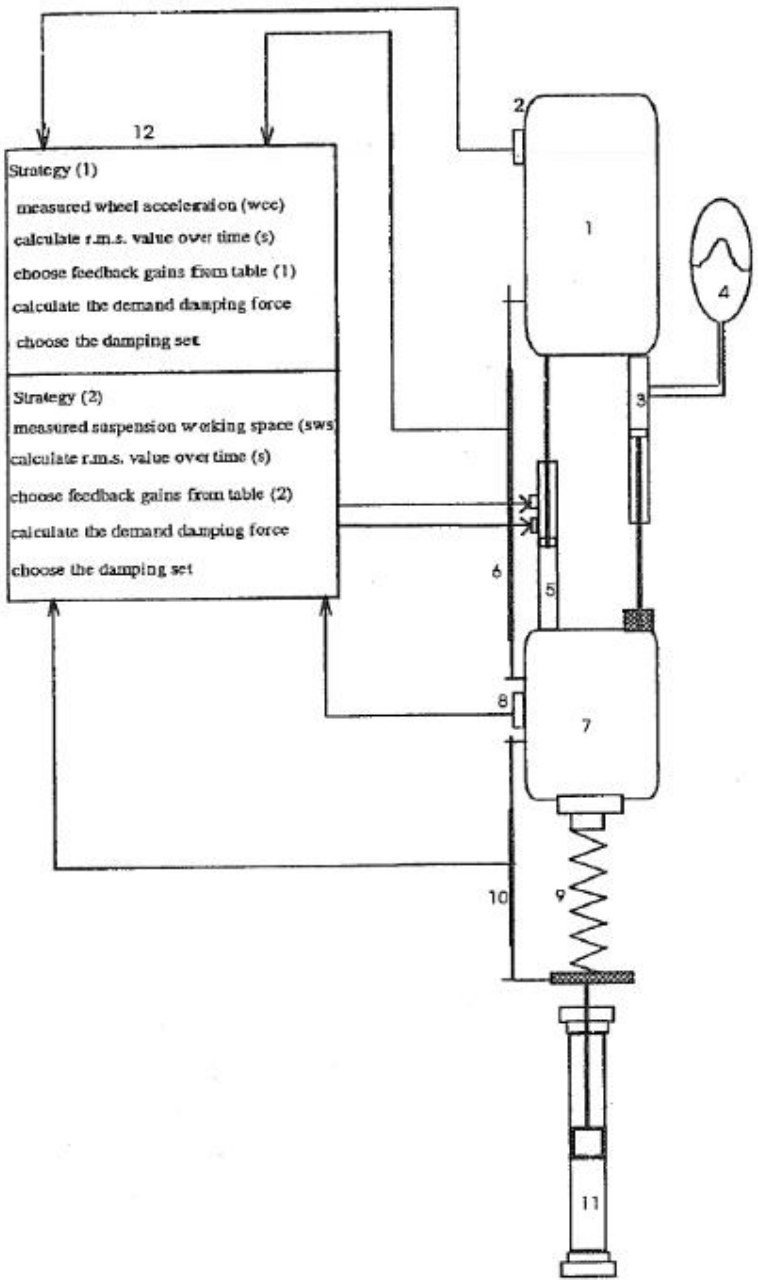

Figure 2.4 Structure of the Three State Switchable Damper used in [9]

It is also commented in that reference [11] that the stability of the vehicle can be changed drastically due to small variations on tire force characteristics,

especially during cornering maneuvers performed close to the limit of adhesion. The gravity of those boundary maneuvers in terms of vehicle handling characteristics lies behind the fact that the tire forces, at boundaries, are limited by the surface coefficient of adhesion. Thus the longitudinal tire force, which is primarily a function of tire longitudinal slip, and tire lateral force, which exhibits very similar characteristic to tire slip angle as a function of it are both saturated through limits of adhesion, in other terms the tire normal force due to friction circle. Because of these tire properties, vehicle response to driver inputs can change rather dramatically when the limit of adhesion is reached. From those findings the significance of factors that may affect the tire normal forces throughout critical driving maneuvers could obviously be realised, so that due to those influences the stability characteristics may also be changed.

Control strategies adjusting the damper stiffness for the sake of introduction of new chassis control systems have also attracted some attention in some publications. In [1], which focuses on the fundamental research for development of adaptive damper modelling, the necessity of damper stiffness adjustment during cornering is also highlighted as a vital future work, which would be implemented together with the ESP for the sake of vehicle trajectory improvement. *That information also obviously clarifies the requirement of understanding the effects of alternating damper characteristics on vehicle handling in an extensive scale*.

The evaluation of some damper models for vehicle simulation and their conformability is handled in [7] in which the modelling of worn dampers for computer simulation are practiced by basing on a switching between Force-Displacement and Force-Velocity characteristics depending upon the driving situation. For the purpose of vehicle handling investigation J-Turn and Fishhook

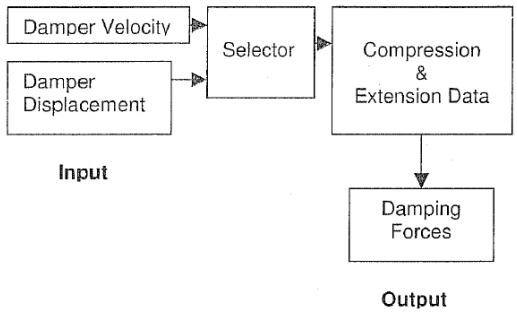

Figure 2.5 Basic Concept of the Damper Model used for Worn Damper Modelling [7]

maneuvers basing upon The National Highway Traffic Safety Administration (NHTSA) rollover investigation maneuvers are performed which are claimed to be *good maneuvers to use for rollover research*. Bound to its observations, that study concludes that with the damper model for worn damper representation, the peak roll rate has increased to an extent of 2.0 deg/s on a J-Turn maneuver at 30 mph.

Another publication, which constitutes as a further work for the above mentioned study, has an intention to investigate the impact of worn dampers on vehicle handling and stability via dynamic model simulation [12]. As simulation maneuvers, Slowly Increasing Steer (SIS), J-Turn, Fishhook and Straight-line Braking on a Smooth Surface dynamic simulations with some certain author defined velocity, steering wheel angle and rotation rate, lateral acceleration and braking deceleration and braking ratio parameters are used. Damper characteristics are obtained by means of a damper data acquisition from individual dampers of a Grand Cherokee via dynamometer testing whose data is afterwards interpolated to build the damper characteristic splines.

According to the results from [12] with increasing mileage roll velocity amplitudes increase albeit slightly. For the sake of an illustration, it is observed in that analysis that there is a 10 % increase in the peak roll rate for the J-Turn maneuver at 40 mph. It is also mentioned in that study, that the maximum amount of roll rates that occur during the simulations are around 25 deg/s which relate to

250 mm/s translational damper velocities. To demonstrate deeper impact of worn dampers, harsher maneuvers are to be carried out.

In addition to those, artificially worn dampers through removal of some amount of working fluid from the damper are tested on dynamometer to obtain damper characteristics of worn dampers. As a result of a more detailed analysis, it is concluded that the largest roll rate response is obtained with a model with worn front outside damper. The general conclusion resulting from the overall analysis remarks that:

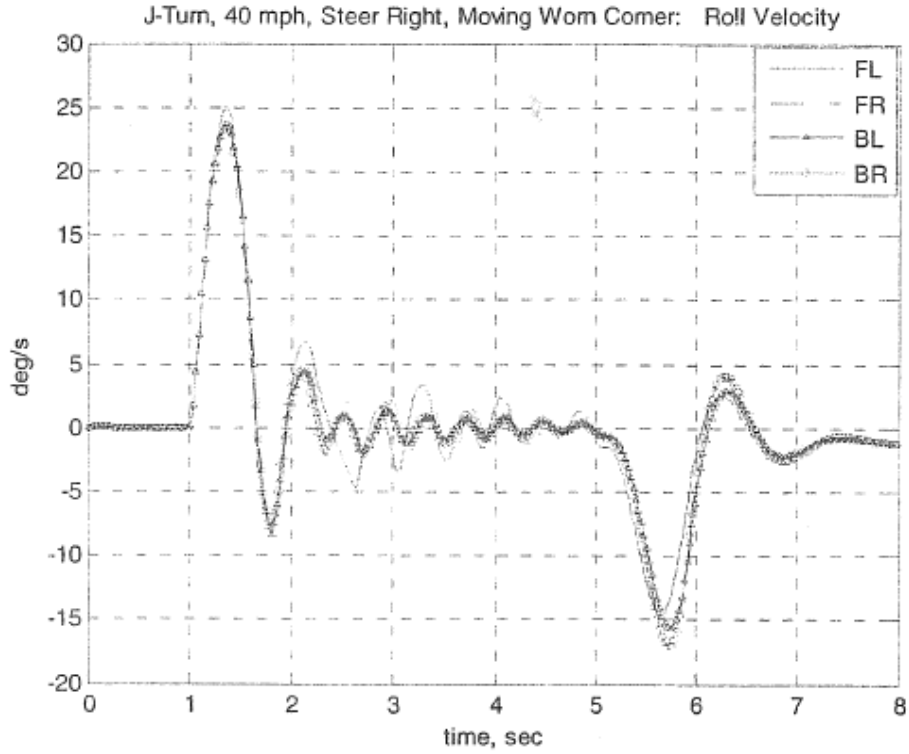

Figure 2.6 Roll Rates Depending on the Worn Damper Location (Right J-Turn 40 mph) [12]

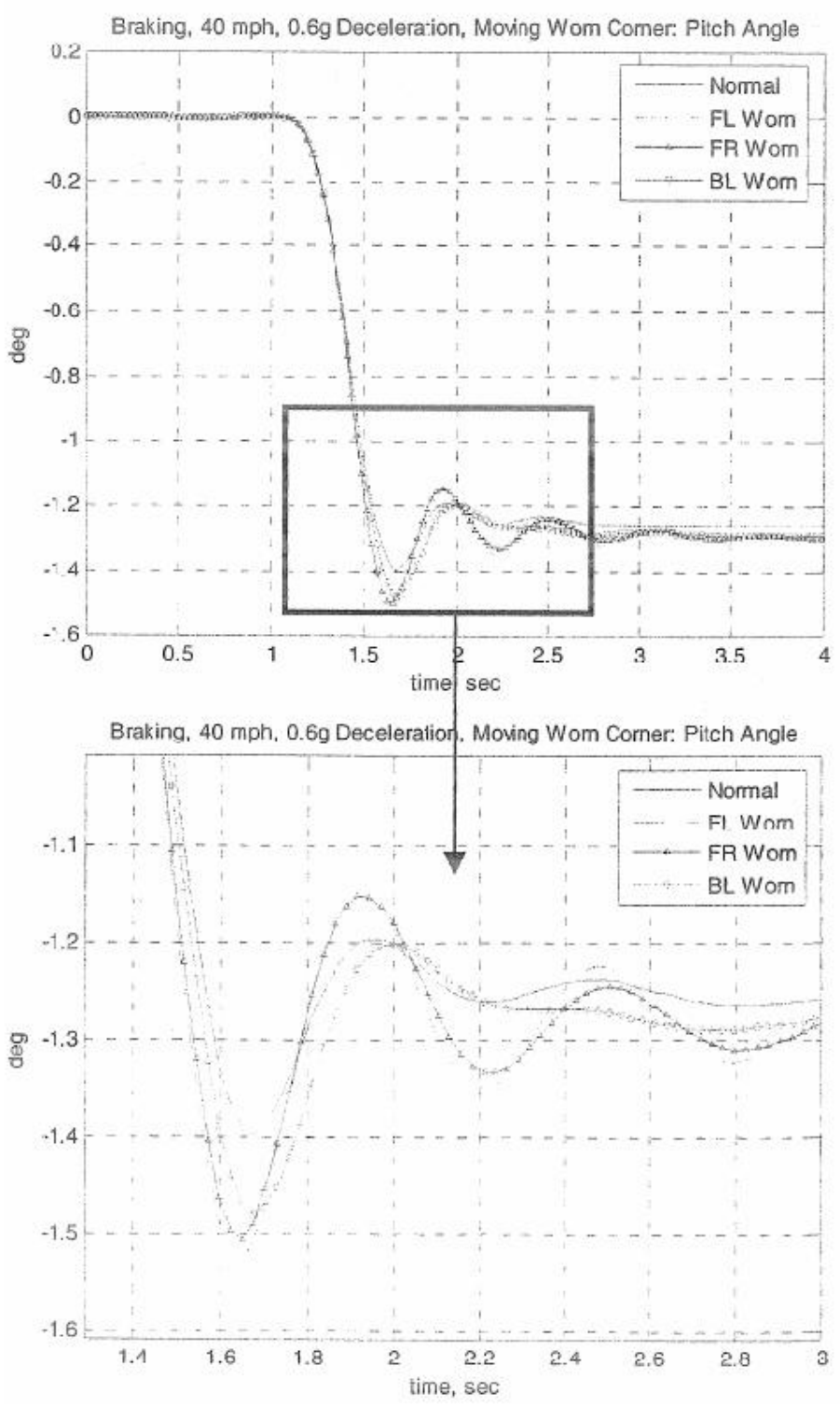

Figure 2.7 Pitch Angles Depending on the Worn Damper Location (Braking 40 mph) [12]

- the loss of damping reduces the ability to dissipate kinetic energy,
- during flat road steering and braking type maneuvers higher mileage results with higher levels of roll and pitch responses,
- the front outside location (damper) is the most critical one for steering and either front one is the most critical for braking maneuvers on flat road in terms of worn damper location. The Figures 2.6 and 2.7 above show the roll and pitch rates changing with the worn damper location.

In another publication examining the effects of aging process of dampers on vehicle handling and ride characteristics [13], it is observed that during an emergency brake test (including braking and lane change on an irregular surface) used dampers (matches with 60000-80000 km usage), modelled with 50 % of a damping coefficient corresponding to a new damper, results in 37.8 m brake distance whereas the new ones end up with 33.9 m, which makes a significant difference. In the second test, (performed with a double lane change maneuver carried out on an irregular surface) the driver could maneuver at a speed of only 52 km/h with old dampers, whereas the maneuverable top speed with new dampers was 59 km/h, which again indicates a high difference.

In another test with straight ahead braking, carried out with 80 km/h speed and 25 % aging, the braking difference came out to be just 0.2 m. However, for a drive on a curve test with a pothole on the road and with the same steering input, it is observed that the model with old dampers spins more than the model with new dampers do after the pothole due to loss of tire grip. This proves that, the aging process of dampers is critical on irregular surfaces. According to that paper, the main consequences of the damper aging process are:

- aquaplaning danger at lower speeds
- irregular tires wear
- loss of grip on curves
- dazzle due to light beam oscillations

- increase of the braking distance even with ABS system
- loss of comfort and motion sickness danger in passengers

The impact of a structural factor on vehicle handling and stability is studied in [14], examining the effects of lift kits and oversize tires by means of handling tests including straight line braking, trapezoidal steering, braking in a turn, steady state turning, and sinusoidal steering. To obtain a proper measure of vehicle handling characteristics; vehicle speed, steering wheel angle, brake pedal force, longitudinal and lateral accelerations, yaw rate, roll, pitch and side slip angles and front/rear brake line pressure are observed by means of sensors. According to the outcomes of this publication, owing to larger rolling diameters and increased ride-height, vehicles equipped with life kits and oversize tires are subjected to decreased braking efficiency, increased rollover risk, increased understeer tendency and decreased steering sensitivity, and an increased tendency towards chassis component failures. Also the crash risk is specified to be increased depending upon Collision Severity and Collusion Frequency Terms accepted by The Virginia Crash Investigation Team (1991), [15] especially because of rolling radius values higher than an acceptable limit of 34 inches.

In a reference that intends to investigate the failure and stress analysis of the longitudinal stringer of an automobile chassis, it is mentioned that the most common vehicle component failure type is that of engine with 41 % and the chassis component failures constitute 7 % [16]. However it is also stated that the chassis failures may be catastrophic with serious consequences through heavy costs and bad publicity. There are also a number of publications examining the fatigue failures and durability tests, but only a few aiming to study the impact of those failures on vehicle handling and stability.

In [17], it is mentioned that there exists a non-negligible contribution of vehicular factors on traffic accidents. However, the statistical data from some particular official records relating traffic accidents only due to wheel failure or

misuse are taken, considering wheel failures as the main source of chassis failures leading to traffic accidents.

In a study based on vehicle stability control, estimation of side slip angle is accounted and on which vehicle handling with the help of side slip angle observation is the aim of interest, the characteristic maneuvers like lane change, slalom, steady-state turn, and J-Turn are performed [18]. Since it builds up a close example due to its similarity to this study, [18] is used as a representative in terms of vehicle handling maneuver selection.

The literature survey has indicated that there is a gap related to studies of the effect of chassis component failures on vehicle handling and stability. In this thesis, an attempt is made to reveal the effects of the damper failure on vehicle handling and stability together with further physical explanations of the phenomena to contribute to the literature.

CHAPTER 3

VEHICLE MODEL

In order to observe the outcomes of damper failure process, a mathematical vehicle model at a certain level of accuracy and real-life compatibility is needed. In modern applications a compromise between model complexity and simulation speed must be achieved. An adequate model complexity ensures that the outcomes of the simulations are well-matched to real life and thus helps to avoid possible deviations from the exact results. On the other hand, with simpler models it is possible to obtain faster results and make easier modifications on the model when needed. Therefore, the trouble-shooting capability is increased with simpler simulation models to a great extent.

Concerning the aim of this study and the goals to be achieved, model complexity is to be emphasized. It is observed in some of the publications in the literature survey that in some cases modified damper characteristics may lead to so sensitive results that the differences between the original responses and the ones with damper failure may not be distinguishable. Considering the fact that the results may come out to be close to the ones without damper failure, it is decided to use a detailed model at the expense of long simulations. Thus, it is hoped to eliminate the possibility of incorrect results.

3.1 MATHEMATICAL MODEL OF THE VEHICLE

In order to represent the vehicle in a detailed manner, a 10 degree of freedom model is constructed using the software MATLAB/Simulink. The degrees of freedom provided are

- 4 rotational motions of the wheels

- vehicle translational, lateral, and yaw motions
- body vertical, roll, and pitch motions

As seen the model complexity reveals itself firstly in terms of the number of degrees of freedom. In the literature investigating vehicle dynamics studies, most detailed mathematical vehicle simulation models usually consist of those 10 degrees of freedom. The main goal of this study is to examine vehicle handling and stability characteristics as a consequence of damper failure, body related degrees of freedom of the vehicle model may not be considered essential and may be neglected for the sake of simplicity. However, as it will be clarified in the next chapters, suspension related degrees of freedom (i.e. vertical dynamics of the vehicle) play the most significant role on damper failure dynamics. Therefore, it is essential that a detailed suspension representation be included in the simulation model.

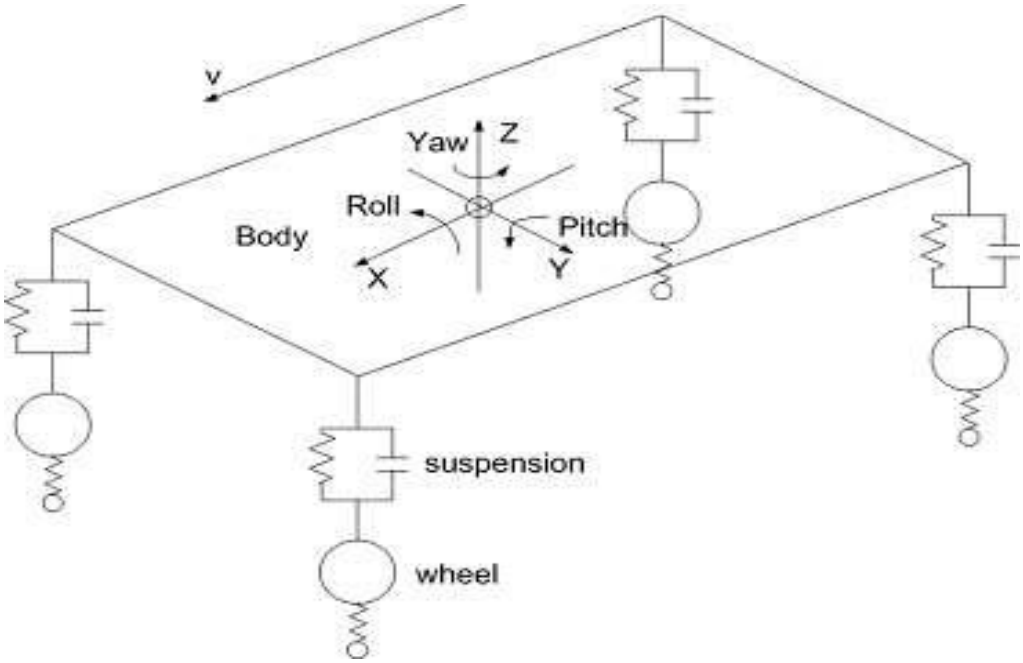

Figure 3.1 Degrees of Freedom included in the model

3.2 SIMULINK MODEL AND MATHEMATICAL REPRESENTATION

The vehicle model is constructed using Matlab/Simulink. The details of the model are given in the following sections.

3.2.1 STEERING SYSTEM

The relation between the steering wheel angle (which is a system input) and front wheel steer angles are constructed such that the change of steer angle due to steering system elasto-kinematics and aligning steer-torque are also taken into account. In general, the mathematical vehicle models involve a rational relation between the steering wheel angle and wheel steer angles. So the formulae for wheel steer angle estimation are as follows:

$$\delta_{Vi} = \delta_{Li} + \delta_{V0} + \delta_{Vi}(\kappa) + \delta_{Vi}(F_{Xi}) + \delta_{Vi}(F_{Yi}) \tag{3.1}$$

where δ_{Vi} is the overall wheel steer angle,

δ_{V0} is static toe angle given to the wheels,

$\delta_{Vi}(\kappa)$ is the angular elastic deformation due to roll angle κ

$\delta_{Vi}(F_{Xi})$ and $\delta_{Vi}(F_{Yi})$ are the angular elastic deformation due to longitudinal and lateral tire forces respectively.

The elasto-kinematics behaviour of the tires (i.e. the wheel steer angle deviations due to roll angle, longitudinal and lateral tire forces) are obtained through kinematical suspension test processes held on the *VW Golf V GTI* vehicle which is the base vehicle for which the data set is referenced, Appendix A.

δ_{Li} denotes for the pure steer angle occurring on the wheels without any elasto-kinematical effects. It is calculated through:

$$\delta_{Li} = \delta_{SW} * i_{Li} + \delta_{SCi} \tag{3.2}$$

where δ_{SW} is the steering wheel angle,

i_{Li} is the steering gear ratios corresponding to left and right wheels (it is the geometrical parameter connected with the steering linkage geometry which relates the amount of steering wheel to the amount of wheel rotation),

δ_{SCi} is the deviation due to aligning steer-torques. It should be noted that this term only exists for the front wheels since the vehicle model is constructed as a front wheel steer car.

The steering gear ratios are obtained through the data set of the *VW Golf V GTI* vehicle, Appendix A.

δ_{SCi} is calculated concerning the geometrical construction of the steering and suspension systems through the following formula:

$$\delta_{SCi} = \frac{M_{Zi} + F_{Yi} * (r_{dyn} * \sin(\tau(\delta_{Vi})) - n_0(\delta_{Vi})) + F_{Xi} * (r_\sigma(\delta_{Vi})\{r_L\})}{Cl} * \frac{1}{Tl \cdot s + 1} \tag{3.3}$$

The numerator in the first term stands for the total aligning steer-torque, whereas the denominator (*Cl*) is the steering stiffness; and the second term is the transfer function representing the time delay with a time constant *Tl*. It indicates that the aligning torque has a lag when it triggers the deviation in the wheel steer angles.

The aligning steer-torque (the term in the denominator) is calculated in accordance with the steering and suspension system construction and compliance parameters.

M_{Zi} is the self aligning torque from the tires,

r_{dyn} is the dynamical rotating tire radius,

$\tau(\delta_{Vi})$ is the dynamical castor angle with wheel steer angle dependence,

$n_0(\delta_{Vi})$ is the castor offset with wheel steer angle dependence,

$r_\sigma(\delta_{Vi})$ and r_L are the offset due to steering axis inclination with wheel steer angle dependence and the kingpin offsets respectively. It should be noted that the moment arms $r_\sigma(\delta_{Vi})$ and r_L switch to each other depending on whether the longitudinal force is a traction force or a braking force. Regarding the fact that the tractive reaction force is created on the wheel centre (and similarly for braking on it is created on the contact patch), $r_\sigma(\delta_{Vi})$ and r_L are considered as the moment arms in case of traction and braking respectively.

Subscript *i* stands for the wheel index throughout the formulations. The wheel steer angle dependences for the dynamical parameters, the steering stiffness and the delay function for the aligning steer torque are obtained from the data set of the *VW Golf V GTI* vehicle, Appendix A.

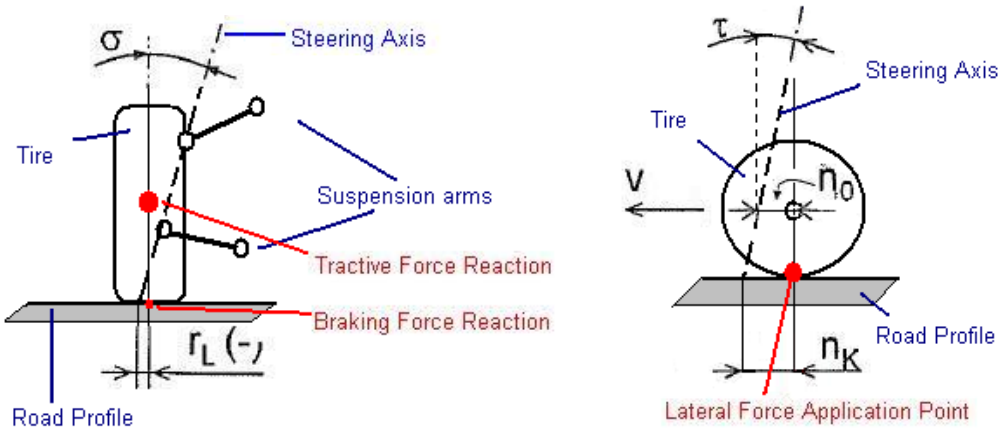

Figures 3.2 and 3.3 Steering axis and suspension constructions taken into account in the formulations

3.2.2 TIRE MODEL

Tire models in vehicle simulation are always important, since tires constitute the only contact between the vehicle and the road. The dynamic forces that influence and identify the overall driving behaviour of the vehicle are created through this contact. Therefore, it is always required to build or use a proper type of tire model in vehicle computer simulations.

Tire models are basically (in simulation work) mathematical algorithms which output mainly the longitudinal and lateral forces, together with the self aligning torque as a function of inputs (tire normal loads, longitudinal slips, tire slip angles and coefficient of adhesion between the tires and the road surface) and some model-dependent parameters.

In this study, Pacejka Magic Formula tire force estimation algorithm is used for tire model. Magic Formula algorithm is commonly used for its precision, sufficient detail and in cases where a particular level of accuracy in the results is needed. Despite its content of a high level of non-linearity, it is preferred in most of the software simulation work due to its good real-life competence and reliability. According to Magic Formula, tire forces (longitudinal and lateral) and the self

aligning torque formulas are deviced using the general formula and with some corresponding modifications on the constants:

$$y = D_i * \sin[C_i * \arctan(B_i - E_i * [B_i * x_i - \arctan(B_i * x_i)])] \quad (3.4)$$

That general formula is deviced by Pacejka [19] in order to fit the resulting tire outputs to a particular curve, as illustrated in Figure 3.4. In general B is known as the *stiffness factor* whereas C and D are known as the *peak value* and the *shape factor,* respectively. In addition to the parameters introduced in the above formula, there are two other parameters *Sv* and *Sh shown* in the figure, which are added to the algorithm in order to create some offsets from the origin. These intend to take the effects of ply steer (which appear because of the direction and method with which the plies are manufactured into the tire) and conicity forces (which appear because the tire may look a bit like a cone) into account respectively.

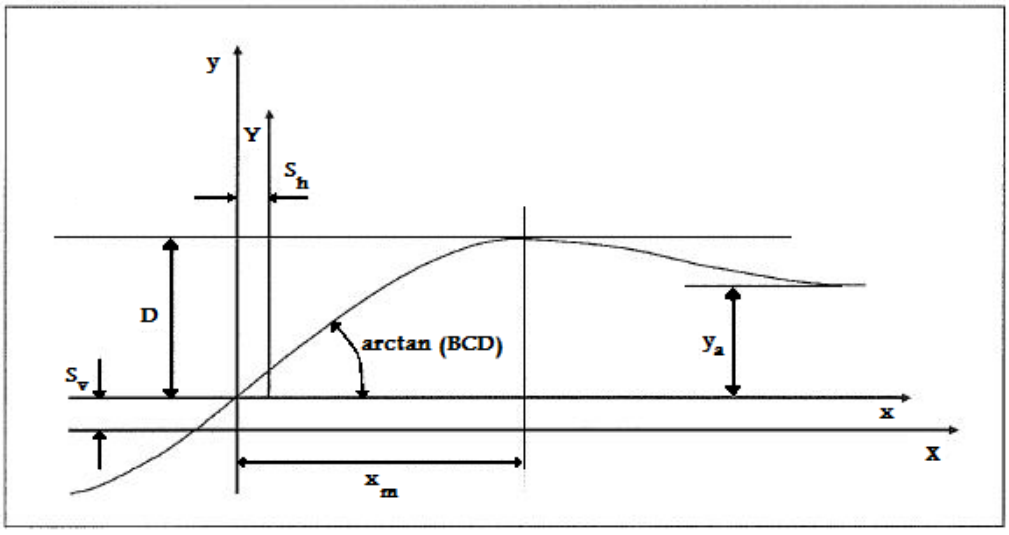

Figure 3.4 Demonstration of tire algorithm outputs and the coefficients of Pacejka Magic Formula [20]

So according to that general formula **tire longitudinal force** calculation is given as follows [21]:

$$F_{X\,i} = D_i * \sin(C_i * \arctan(B_i * (1 - E_i) * Sp + E_i * \arctan(B_i * Sp))) \quad (3.5)$$

where

$$C_i = b0 \quad (3.6)$$

$$D_i = (b1 * F_{Z\,i} + b2) * F_{Z\,i} \quad (3.7)$$

$$B_i = ((b3 * F_{Z\,i}{}^2 + b4 * F_{Z\,i}) * \exp(-b5 * F_{Z\,i})) / (C_i * D_i) \quad (3.8)$$

$$E_i = b6 * F_{Z\,i}{}^2 + b7 * F_{Z\,i} + b8 \quad (3.9)$$

$F_{X\,i}$ is the longitudinal tire force,

$F_{Z\,i}$ is the vertical tire force,

Sp is the slip percentage calculated by (longitudinal slip ratio)*100,

b0, b1, b2, b3, b4, b5, b6, b7 and *b8* are the coefficients which include the influence of wheel load, slip angle, slip ratio and camber.

The lateral force formula is given by [21]:

$$F_{Y\,i} = D_i * \sin(C_i * \arctan(B_i * (1 - E_i) * \alpha_i + E_i * \arctan(B_i * \alpha_i))) \quad (3.10)$$

where

$$C_i = a0 \quad (3.11)$$

$$D_i = (a1 * F_{Zi} + a2) * F_{Zi} \tag{3.12}$$

$$B_i = lateral\ stiffness / (C_i * D_i) \tag{3.13}$$

$$lateral\ stiffness = a3 * \sin(2 * \arctan(F_{Zi} / a4)) * (1 - a5 * abs(\gamma_i)) \tag{3.14}$$

$$E_i = a6 * F_{Zi} + a7 \tag{3.15}$$

F_{Yi} is the lateral tire force,

α_i is the tire slip angle,

γ_i is the dynamic camber,

a0, a1, a2, a3, a4, a5, a6 and *a7* are the coefficients which include the influence of wheel load, slip angle, slip ratio and camber.

Lateral stiffness used in the formula is also known as the *cornering stiffness* of the tire. In case of small tire slip angles, the lateral force can be also linearly computed by multiplying the cornering stiffness and tire slip angle. The multiplication of *B, C* and *D* parameters in the Pacejka Algorithm gives the so called lateral stiffness of the tire. Generally spoken, in case of linear simulations, that product is simply given to the model as a single value instead of that complex algorithm.

The self aligning torque expression is given as follows [22]:

$$M_{Zi} = D_i * \sin(C_i * \arctan(B_i * (1 - E_i) * \alpha_i + E_i * \arctan(B_i * \alpha_i))) \tag{3.16}$$

where

$$C_i = c0 \tag{3.17}$$

$$D_i = c1 * F_{Zi}{}^2 + c2 * F_{Zi} \tag{3.18}$$

$$E_i = (c7 * F_{Zi}{}^2 + c8 * F_{Zi} + c9) * (1 - c10 * abs(\gamma_i)) \tag{3.19}$$

$$B_i = ((c3 * F_{Zi}{}^2 + c4 * F_{Zi}) * (1 - c6 * abs(\gamma_i)) * \exp(-c5 * F_{Zi})) / (C_i * D_i) \tag{3.20}$$

M_{Zi} is the self aligning torque,

α_i is the tire slip angle,

γ_i is the dynamic camber,

c0, c1, c2, c3, c4, c5, c6, c7, c8, c9 and *c10* are the coefficients which include the influence of wheel load, slip angle, slip ratio and camber.

Additionally, the formulation of combined slip condition, on which the simultaneous longitudinal and lateral motion is taken into account, are given as follows. So, the combined longitudinal forces are [21]:

$$F_{Xi} = F_X 0_i * Gx\alpha_i \tag{3.21}$$

$$Gx\alpha_i = \frac{\cos[Cx\alpha_i * \arctan\{Bx\alpha_i * (\alpha^*{}_i + SHx\alpha_i)\}]}{\cos[Cx\alpha_i * \arctan(Bx\alpha_i * SHx\alpha_i)]} \tag{3.22}$$

$$Bx\alpha_i = Bxy * \cos[\arctan(B2xy * k_i)] * \lambda xy \tag{3.23}$$

$$Cx\alpha_i = Cxy \tag{3.24}$$

where $Gx\alpha_i$ is the weighting factor,

Bxy and $B2xy$ are the stiffness factors,

Cxy is the shape factor,

$SHx\alpha_i$ is the horizontal shift fort he curve fitting,

k_i and α^*_i are the longitudinal and lateral slip ratios respectively,

λxy is the influence factor for tire slip angles for the combined slip formula.

The combined lateral forces have the similar formulation and constants with combined longitudinal forces.

The constant series (parameters) *a, b* and *c* are taken as a data set from the testing results of tire *Bridgestone Potenza 245/40 R18* [23]. The verified tire model constants according to combined slip Pacejka Magic Formula are given in Appendix A.

3.2.3 POWERTRAIN AND DIFFERENTIAL

In order to model the longitudinal dynamics of the vehicle effectively, an appropriate and sufficient drivetrain (powertrain and differential) representation is to be ensured. That should include the wheel rotational equations and consequently the longitudinal slip creation formulae and which should mainly take the wheel linear speeds, engine torque, and brake torques as inputs.

In this study, the modelling of a detailed engine is omitted since the lateral dynamics inspection is the focus of intent. However, for the sake of real-life compatibility, a differential model is already included. So the differential (that also takes the effects of inertial resistances and viscous frictions due to different rotational speeds of the front right and left tires) distributes the forces to the driven (front) wheels according to the following formula:

$$F_{GA} = M_{GA} / r_{GA} \tag{3.25}$$

$$F_P = \frac{F_{GA} * r_{st1} - \frac{\dot{\omega}_1 + \dot{\omega}_2}{2} * J_{st}}{2 * r_{st2}} \tag{3.26}$$

$$M_1 = \left[\frac{(\dot{\omega}_2 - \dot{\omega}_1) * r_h}{2 * r_p} * \frac{J_p}{r_p} + F_P \right] * 0.5 * 2 * r_s + M_{B1} \tag{3.27}$$

$$M_2 = \left(F_P - \left[\frac{(\dot{\omega}_2 - \dot{\omega}_1) * r_h}{2 * r_p} * \frac{J_p}{r_p} + F_P \right] * 0.5 \right) * 2 * r_h + M_{B2} \tag{3.28}$$

where M_{GA} is the torque value entering the differential input,

F_{GA} and r_{GA} are the driving force entering the differential input and the final drive ratio respectively,

F_P is the total net drive force entering the differential (the inertial resistance for the differential is subtracted),

$\dot{\omega}_1$ and $\dot{\omega}_2$ are the angular accelerations for the front left and front right wheels, respectively,

J_{st} and J_p are the rotational inertias for the differential cage and the planet gear, respectively,

M_1 and M_2 are the net moments on the front left and front right wheels, respectively,

M_{B1} and M_{B2} are the braking moments on the front left and front right wheels, respectively,

r_{st1} and r_{st2} are the outer and inner radii of the differential cage, respectively,

r_s, r_p and r_h are the radii of the sun, planet and ring gear, respectively.

The wheel angular speeds and accelerations are calculated according to the rotational equations of motion for the wheels and can be expressed by:

$$\dot{\omega}_i = \frac{M_i - (F_{Xi} + F_{Ri}) * r_{dyn}}{J_R} \tag{3.29}$$

$$\omega_i = \int \dot{\omega}_i + \frac{v_0}{r_{dyn}} \tag{3.30}$$

where

$$F_{R_i} = F_{Zi} * fr \tag{3.31}$$

ω_i is the angular speed of the individual wheel,

v_0 is the initial longitudinal speed of the vehicle (input to the system),

J_R is the rotational inertia of the individual wheel,

fr is the rolling resistance coefficient,

F_{Ri} is the rolling resistance of the individual wheel.

It should be noted that the *Mi'*s for the driven wheels would also involve the tractive torque whereas for the rear axle the input torque would only include the brake torque as the input. *v0* is the initial velocity of the vehicle, which would also indicate that the calculation the angular speeds of the wheels constitute the initial step of the iterations held by the software. Then, the longitudinal slips, which the tire model takes as an input, are calculated in that manner:

$$S_{X\,i} = \frac{\omega_i * r_{dyn} - V_{X\,i}}{\omega_i * r_{dyn}} \qquad \text{if} \quad \omega_i * r_{dyn} > V_{X\,i} \quad \text{(tractive slip)} \qquad (3.32)$$

$$S_{X\,i} = (-1) * \frac{V_{X\,i} - \omega_i * r_{dyn}}{V_{X\,i}} \qquad \text{if} \quad \omega_i * r_{dyn} < V_{X\,i} \quad \text{(brake slip)} \qquad (3.33)$$

where r_{dyn} is the dynamic rolling radius of the tires,

$S_{X\,i}$ is the longitudinal slip values of the individual tires,

$V_{X\,i}$ is the individual longitudinal linear wheel velocities parallel to wheel rolling plane.

3.2.3.1 DRIVER ASSISTANCE SYSTEMS REPRESENTATIONS

In order to represent the vehicle more realistically, some driver assistance functions are also integrated to the vehicle model which a modern vehicle basically tends to have. By such means, the study would be more meaningful and attract more attention due to its up-to-date property.

The first driver assistance system representation embedded to the model is the **ABS** System. Anti-lock Brake System (ABS) is an electronic control program in the modern automobiles, that prevents the tire lock (which may be pretty dangerous on harsh braking cases) by inputting the tires a continuous high frequency step input when the tires tend to lock-up. This feature is represented with a slip limitation to the value of *0.3*, which is a commonly used value for slip saturation in computer simulations that ensures the function of ABS, albeit very roughly.

The second system that is considered as a driver assistance requirement to the system is the **Cruise Control** function. Besides being a necessary tool to model the modern vehicle accessories, it is furthermore needed not to lose the lateral dynamics characteristics during the simulation, since beginning from a particular

initial speed the vehicle slows down through the existence of air resistance, inertial resistance and the rolling resistance. Since the speed is required to be kept constant in order not to alter the lateral characteristics of the vehicle, a very simple and basic cruise control function is also embedded to the model. The control strategy applied in Cruise Control model is explained in the Appendix B.

3.2.4 LONGITUDINAL EQUATION OF MOTION

Vehicle longitudinal characteristics are determined with the Newton's 2nd Law of Motion which will give the acceleration of the vehicle and then consequently the velocity by integration. Longitudinal equations of motion block is so constructed that no assumptions (and linearizations) in terms of side slip angle is made. That is because of the fact that the vehicle velocity vector and the vehicle body longitudinal axis would constitute a relative high angle (namely the side slip angle), due to harsh maneuvers throughout the study, whose effect can not be neglected. It should be noted that, the longitudinal velocity vector, generally spoken, is at a right angle to the lateral acceleration vector, but not parallel to vehicle longitudinal axis. The formulation is as follows:

$$\ddot{x} = \frac{\sum F_{X_i} * \cos(\pm\delta_{V_i} - \beta) - \sum F_{Y_i} * \sin(\pm\delta_{V_i} - \beta) + m_a * h' * \ddot{\kappa} * \sin(\beta) - F_L}{m} \tag{3.34}$$

$$F_L = cw1 * \dot{x} + cw2 * \dot{x}^2 + cw3 * \dot{x}^3 \tag{3.35}$$

where $\dot{x}$ and $\ddot{x}$ are the longitudinal velocity and accelerations of the vehicle, respectively,

m and m_a are the total mass and body (sprung) masses of the vehicle, respectively,

$\ddot{\kappa}$ and h' are the roll acceleration and the moment arm for the roll moment (distance between the roll axis and the centre of gravity), respectively,

β is the side slip angle,

F_L is the air resistance,

cw1, *cw2* and *cw3* are the air resistance coefficients.

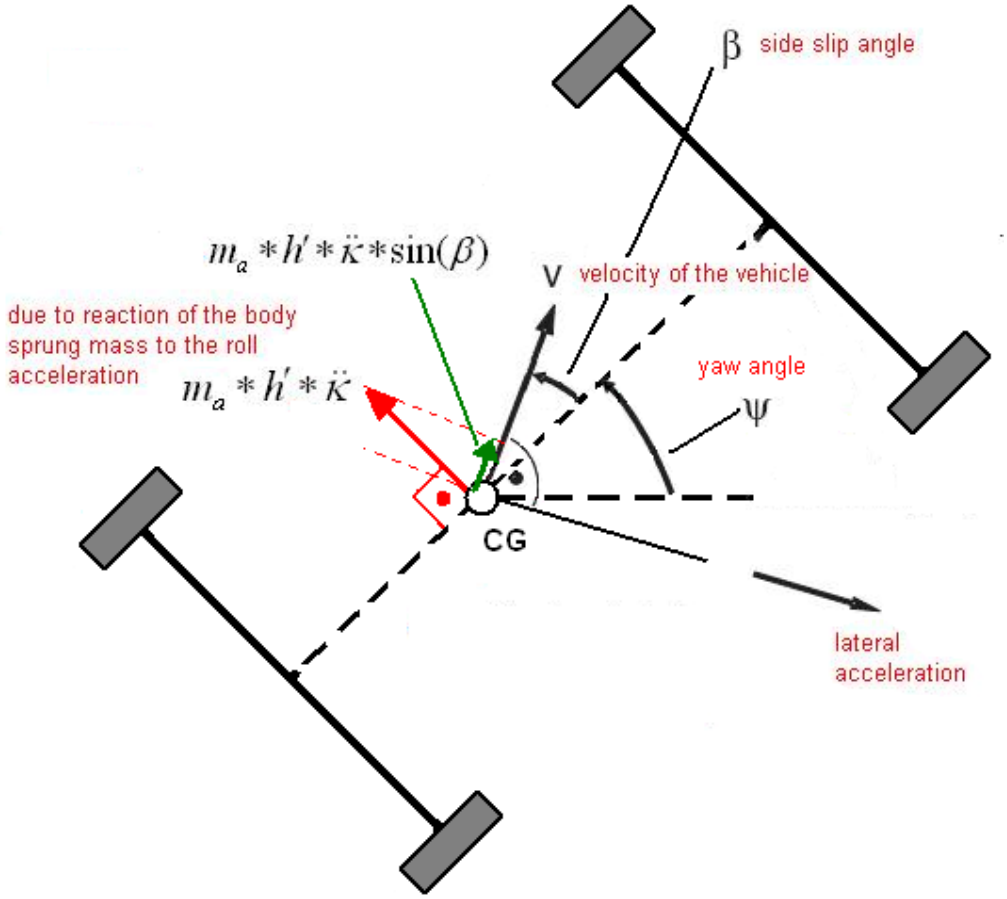

Figure 3.5 Effect of roll motion on the longitudinal dynamics

3.2.5 BODY (SPRUNG MASS) DYNAMICS

Concerning the roll, pitch, and vertical ride degrees of freedom of the vehicle body, a body dynamics block involving the equations of motion in terms of

these DOF s is constructed. This ensures a sufficient modelling and representation of the suspension and the influence of the rolling, pitching and riding on the lateral dynamics as well. **The vertical body acceleration** (and consequently velocity and displacement by integration) is calculated as follows:

$$\ddot{z} = \frac{\sum F_{F\,i} + \sum F_{D\,i} - m_a * g + m_a * \ddot{\kappa} * h' * \sin(\kappa) \pm \sum F_{X\,i} * \tan(\varepsilon)}{m_a} \tag{3.36}$$

where $\ddot{z}$ is the body vertical acceleration,

$F_{F\,i}$ and $F_{D\,i}$ are the spring and damper forces, respectively,

m_a and g are the body (sprung mass) mass and gravitational acceleration, respectively,

κ is the roll angle

ε is the support angle between the suspension arms and the vertical axis. Here, the influence of longitudinal forces in vertical forces due to suspension construction is also taken into account.

The roll acceleration (and consequently velocity and displacement by integration) is calculated by taking the moments of components about roll axis as follows:

$$\ddot{\kappa} = \frac{\pm \sum F_{F\,i} * \frac{s_{v,h}}{2} \pm \sum F_{D\,i} * \frac{s_{v,h}}{2} - cst_{v,h} * \kappa + \sum M_{ma}}{J_X + m_a * h'^2} \tag{3.37}$$

$$\sum M_{ma} = m_a * a_y * h' * \cos(\kappa) + m_a * g * h' * \sin(\kappa) \tag{3.38}$$

where s_v and s_h are the track widths at the front or rear axle depending upon the situation respectively,

cst_v and cst_h are the torsional stiffness values of the front or rear anti-roll bars depending upon the situation respectively,

J_X is the roll moment of inertia around the centre of gravity,

a_y is the lateral acceleration.

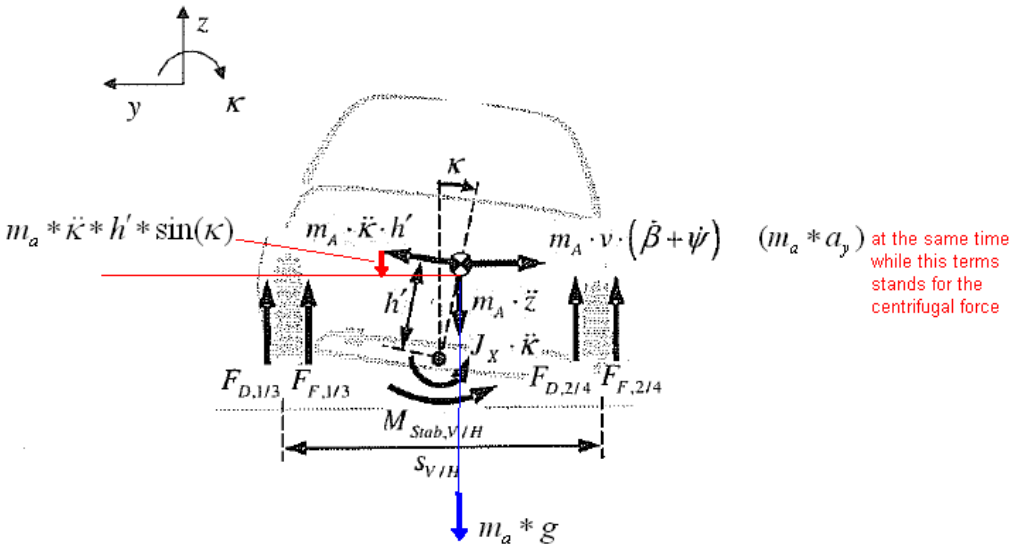

Figure 3.6 Schematic for equations of motion for roll and vertical motions [24]

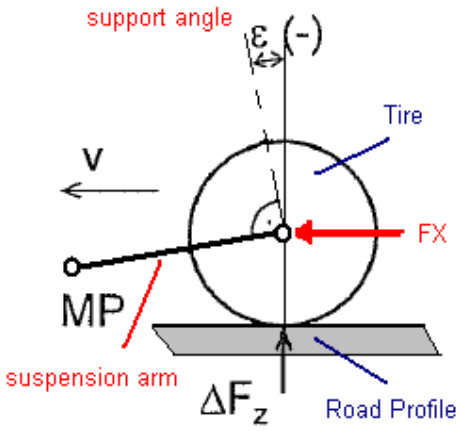

Figure 3.7 Effect of suspension support angle on vehicle vertical dynamics

The pitch acceleration (and consequently velocity and displacement by integration) is calculated by taking the moments of components about pitch centre as follows:

$$\ddot{\varphi} = \frac{\pm \sum F_{Fi} * l_{v,hn} \pm \sum F_{Di} * l_{v,hn} + m_a * g * (l_{vn} - l_{va}) - m_a * \ddot{x} * (h_a - h)}{J_Y} \tag{3.39}$$

where $\ddot{\varphi}$ is the pitch acceleration,

l_{vn} and l_{hn} are the distances of the pitch centre from the front or rear axle depending upon the situation, respectively,

l_{vn} and l_{va} are the distances between the pitch centre and front axle and between the body (sprung) mass centre of gravity and front axle, respectively,

h_a and h are the body (sprung) mass centre and pitch centre heights, respectively,

J_Y is the pitch moment of inertia around the pitch centre,

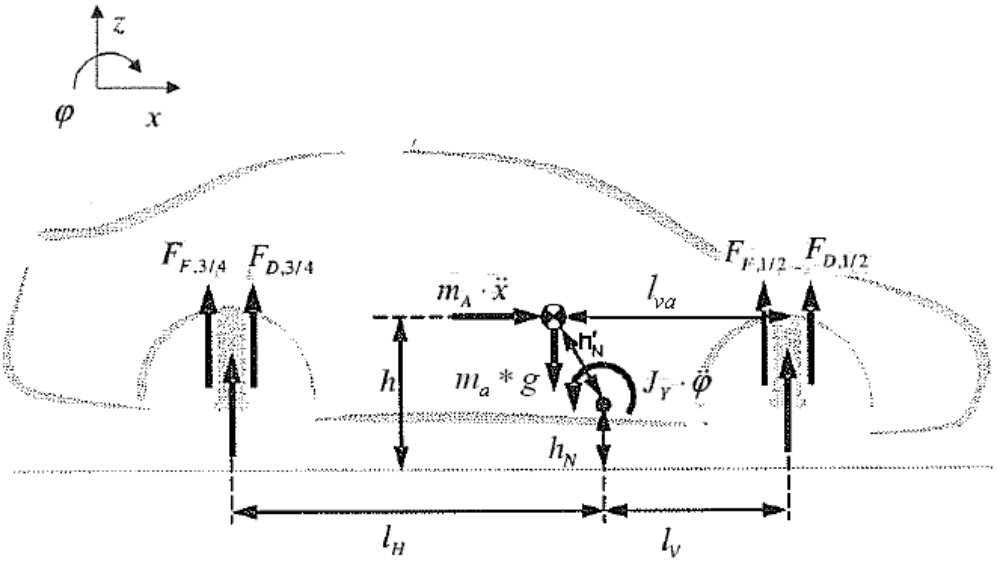

Figure 3.8 Schematic for equation of motion for pitch motion [24]

Under real conditions, the pitch centre is variant with alternating longitudinal forces. However, the specified effect is too complicated to model in simulation software and has no wide effect on the results. Therefore, the pitch centre could be assumed to be steady during the analysis.

The spring and damper forces are calculated with the help of spring and damper characteristic curves read from the vehicle data, which relate the suspension deflection to spring force and suspension relative velocity to damper force, Appendix A. The individual tire suspension travel and velocities are calculated as follows:

$$z_i = z_{0i} - z \pm \kappa * \frac{s_{v,h}}{2} \pm \varphi * l_{v,hn} \quad \text{where } z_{0i} \text{ is a function of } FZ0i \text{ and} \tag{3.40}$$

$$F_{Z0_i} = m_a * g * \frac{l_{h,va}}{l} * \frac{\frac{s_{v,h}}{2} \pm \kappa * h'}{s_{v,h}} \tag{3.41}$$

$$\dot{z}_i = -\dot{z} \pm \dot{\kappa} * \frac{s_{v,h}}{2} \pm \dot{\varphi} * l_{v,hn} \tag{3.42}$$

where z_{0_i} is the individual static deflection of the suspensions,

F_{Z0_i} is the individual static loads on the tires,

z_i and z are the individual suspension deflections and the vertical displacement of the body respectively,

$\dot{z}_i$ and $\dot{z}$ are the individual suspension relative velocities and the vertical velocity of the body respectively,

φ and $\dot{\varphi}$ are the pitch angle and velocities of the body respectively,

l_{ha} and l_{va} are the distances between the body centre of gravity and rear axle and front axle depending upon the situation respectively,

l is the wheelbase.

The static loads (*FZ0i*) on the wheels are calculated by distributing the body (sprung) mass weight around the individual wheels. However, among the same axle the individual tire static load are distributed to the wheels in a way that the effect of roll angle is also taken into account (the moment arm on the tilted side decreases due to κ), since it shifts the weight towards the tilted side albeit slightly. The relation between the static deflection (*z0i*) and static load (*FZ0i*) is taken from the spring characteristics of the vehicle data.

3.2.5.1 DYNAMIC TIRE LOADS

Estimation of tire loads is especially important through the modelling, since the study has a major focus on the tire load deviations. It is the key aspect in that study to evaluate the tire normal load variations in an approximate manner in case of a damper failure, since the overall results arise from the deviation of vertical tire forces, which further influences the tire forces calculated via the tire model. Therefore, the dynamic tire load approach is used in calculation of vertical forces to involve the effects of dynamic motions of the body sprung mass on the normal tire loads. By such means, the further analysis may be more reliable. **The dynamic tire loads** are calculated using the following formulation:

$$F_{Z\,i} = \pm F_{X\,i} * \tan(\varepsilon) + F_{F\,i} + F_{D\,i} + \frac{m_{v,h}}{2} \pm \frac{cst_{v,h} * \kappa}{s_{v,h}} \pm \sum F_{dyn} \tag{3.43}$$

$$\sum F_{dyn} = \left[(m_a * p_{v,h} + m_f * h_{v,h}) * (\ddot{x} * \sin(\beta) + a_y) - m_a * p_{v,h} * h' * \ddot{\kappa} \right] * \frac{l_{v,h}}{l * s_{v,h}} \tag{3.44}$$

where m_v and m_h are the unsprung masses (suspension mass) for the front and rear axles depending upon the situation respectively,

l_v and l_h are the centre of mass distances from the front axle and rear axle depending upon the situation respectively,

p_v and p_h are the heights roll centres for front and rear tracks depending upon the situation respectively,

h_v and h_h are the unsprung mass centre of gravity heights for the front and rear axles depending upon the situation respectively,

m_f is the total unsprung mass.

It could be noted that the formulation is based upon the distribution of the roll (tilting) moments together with the spring and damper forces. The dynamic force term (*Fdyn)* bases on the calculation of individual moments due to lateral forces on the unsprung masses sourcing from combined lateral acceleration $(\ddot{x} * \sin(\beta) + a_y)$ at the front and rear axles about their own centre of gravity heights together with the distributions of the moment due to body lateral force sourcing from combined lateral acceleration $(\ddot{x} * \sin(\beta) + a_y)$ and the distribution of body inertia moment due to body roll acceleration to the individual axles. I should be also noted that, roll moment component due to anti-roll bars is involved in the former equation.

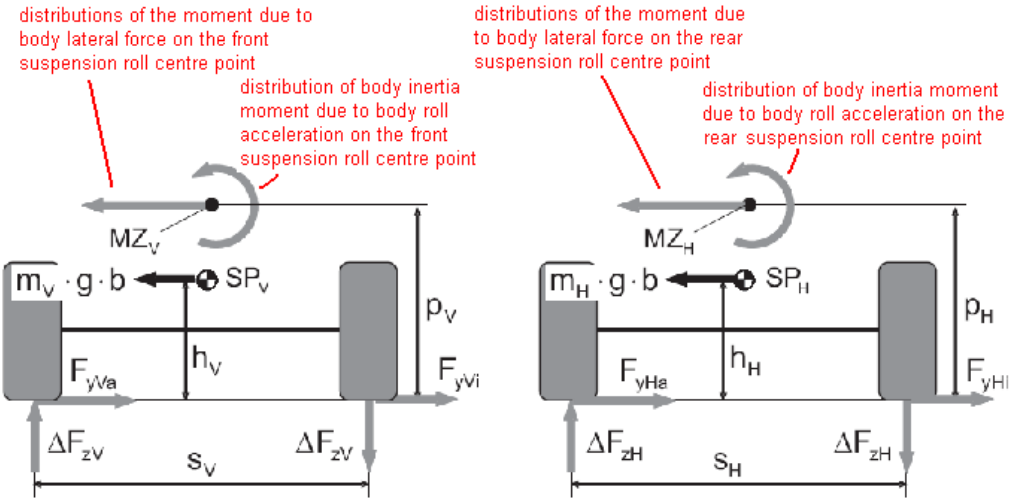

Figure 3.9 Schematic of calculation of dynamic tire loads for front(right) and rear axles [25]

3.2.6 LATERAL DYNAMICS

Vehicle yaw velocity, side slip angle and lateral acceleration (in general the lateral dynamics parameters) together with the tire slip angles and linear velocities are calculated via a lateral dynamics block including the lateral equations of motion. The main focus of intent of this study is the inspection of vehicle handling behaviour, so a detailed model involving all effects on the lateral dynamics equations is constructed. **The yaw velocity** of the vehicle (by calculating the yaw moment and determining yaw acceleration and then integrating) is calculated through the following equation:

$$\ddot{\psi} = \frac{\sum M_{FY} + \sum M_{FX} - \sum M_{Z_i}}{J_Z} \tag{3.45}$$

$$\sum M_{FY} = \pm \sum F_{Y_i} * \left(\cos(\delta_{V_i}) * l_{v,h} \pm \sin(\delta_{V_i}) * (\frac{s_{v,h}}{2} \pm h' * \sin(\kappa)) \right) \tag{3.46}$$

$$\sum M_{FX} = \pm \sum F_{X\,i} * \left(\sin(\delta_{V\,i}) * l_{v,h} \pm \cos(\delta_{V\,i}) * (\frac{s_{v,h}}{2} \pm h' * \sin(\kappa)) \right) \quad (3.47)$$

where $\ddot{\psi}$ is the yaw acceleration,

J_Z is the yaw moment of inertia of the vehicle. It should be noted that, the shifting of centre of gravity due to roll motion is also taken into account here.

The side slip angular velocity (consequently the side slip angle by integration) is obtained through dynamic force equilibrium in the direction of lateral acceleration vector as follows:

$$\dot{\beta} = \frac{\sum F_{Y\,i} * \cos(\pm\delta_{V\,i} - \beta) + \sum F_{X\,i} * \sin(\pm\delta_{V\,i} - \beta) + m_a * \ddot{\kappa} * h' * \cos(\beta)}{m * \dot{x}} - \dot{\psi}$$

(3.48)

where $\dot{\beta}$ is the side slip angular velocity. It should be noted that $m \cdot \dot{x} \cdot (\dot{\beta} + \dot{\psi})$ the centrifugal acceleration to which the total vehicle lateral force (dynamic force sum in the direction of lateral acceleration) must be equal.

Another block for the calculation of the lateral acceleration and the tire slip angles (together with the wheel linear velocities which are accounted in the slip calculations of the wheels) is constructed. The equations are:

$$a_y = \dot{x} * (\dot{\beta} + \dot{\psi}) \quad (3.49)$$

$$\alpha_i = \delta_{V\,i} - \arctan\left(\frac{v_{lat,i}}{v_{long,i}} \right) \quad (3.50)$$

$$v_{long,i} = \dot{x} * \cos(\beta) \pm \frac{s_{v,h}}{2} * \dot{\psi} \quad (3.51)$$

$$v_{lat,i} = \dot{x} * \sin(\beta) \pm l_{v,h} * \dot{\psi} \tag{3.52}$$

then , the longitudinal wheel linear velocities parallel to wheel plane are:

$$V_{X\,i} = \left(\sqrt{v_{long,i}{}^2 + v_{lat,i}{}^2} \right) * \cos(\alpha_i) \tag{3.53}$$

where a_y is the lateral acceleration,

α_i is the individual tire slip angle,

$\dot{\psi}$ is the yaw velocity of the vehicle.

$v_{long,i}$ and $v_{lat,i}$ are the linear velocity components of the individual tires parallel to the longitudinal axis and lateral axis of the body respectively.

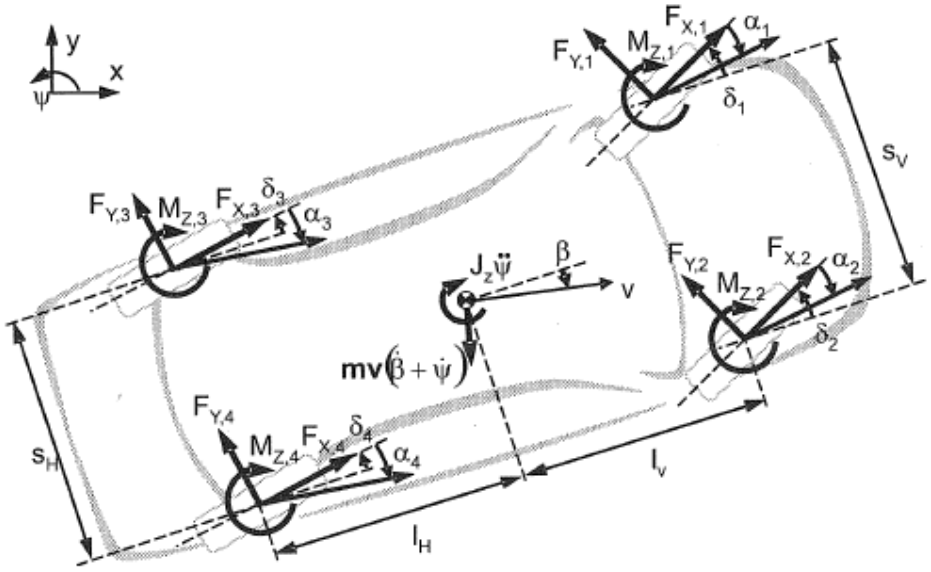

Figure 3.10 Schematic of lateral dynamics equations of motion [24]

3.3 SIMULATION INTERFACE:GUI

In order to interact with the vehicle model so that the required manipulations are input to the model such that the damper failure indication is also ensured, a graphical user interface (GUI) is prepared. The purposes of building up a GUI are:

- to ensure the convenience in setting the input parameters to the simulation model,
- to ensure the easiness in performing consequent simulations without too much effort,
- to visualise the responses more comfortably and
- to express and demonstrate the differences among the simulation cases more clearly.

The GUI mainly offers the user a simulation maneuver selection possibility with corresponding input parameters and the means to convey user selected (edited) damper failure time point and the failed damper selection (i.e. front left, rear right etc.). The control script is so written that the damper failure simulation takes place after an original maneuver (without damper failure) is already simulated, which gives the user the possibility to understand the behaviour of the maneuver completely and clearly select the desired time point for damper failure accordingly. In case of a further analysis, a second box for damper failure process is built (which would take place at a later time point than the first damper failure).

Figure 3.11 A general view of the graphical user interface

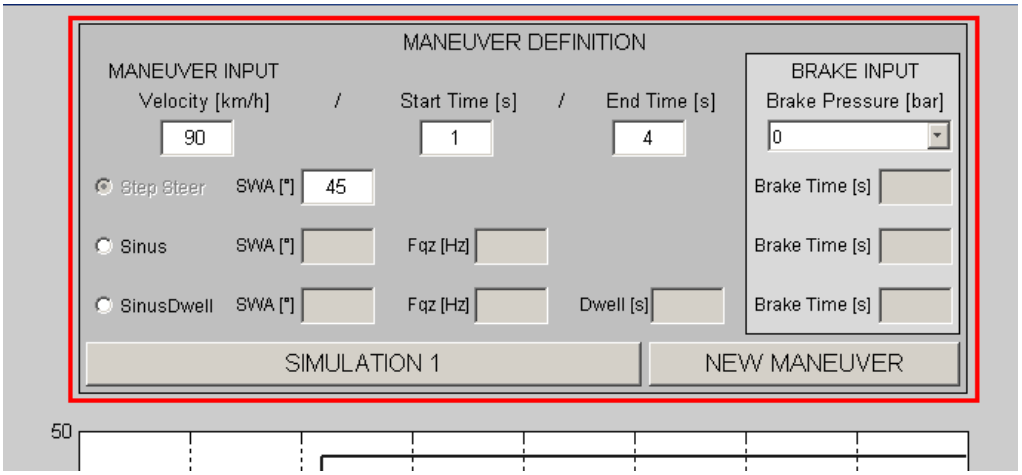

Figure 3.12 A section from the maneuver input of the GUI

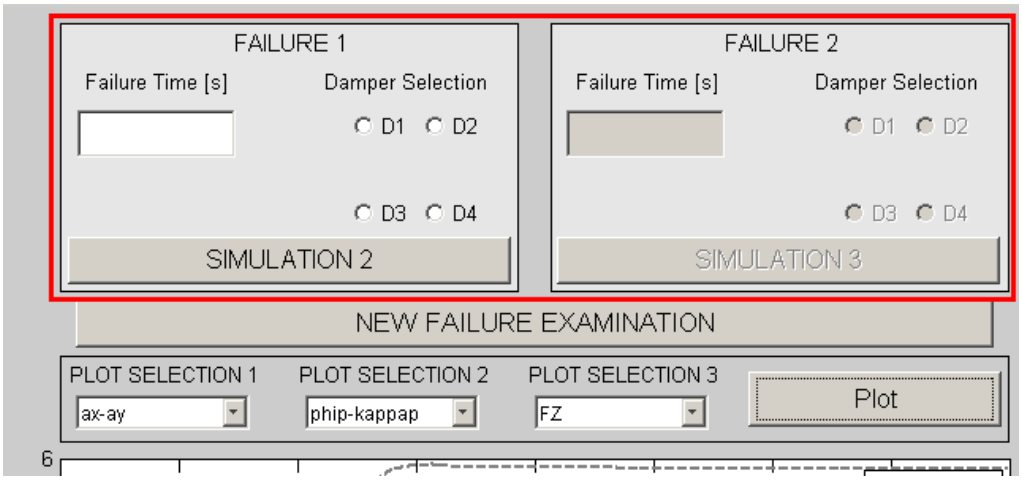

Figure 3.13 A section from the failure input of the GUI

The outputs (vehicle dynamics responses that are to be examined as a result of the maneuvers) are taken from the MATLAB/Simulink Software and revealed in the plots section of the GUI. The main parameters (that are superimposed onto each other in case of damper break out maneuvers) are always held on the GUI and they are the steering wheel angle and the major vehicle dynamics parameters yaw velocity ($\dot{\psi}$) and side slip angle (β). The other parameters, that are required to be inspected to capture the mechanism of damper failure process, are revealed optionally in case the user intends to inspect them. They are namely:

- vertical, lateral and longitudinal forces on the tires as well as the spring and damper forces on the suspensions,
- damper velocities,
- roll and pitch velocities and angular displacements,
- longitudinal and lateral accelerations,
- tire slip angles and
- velocity of the vehicle.

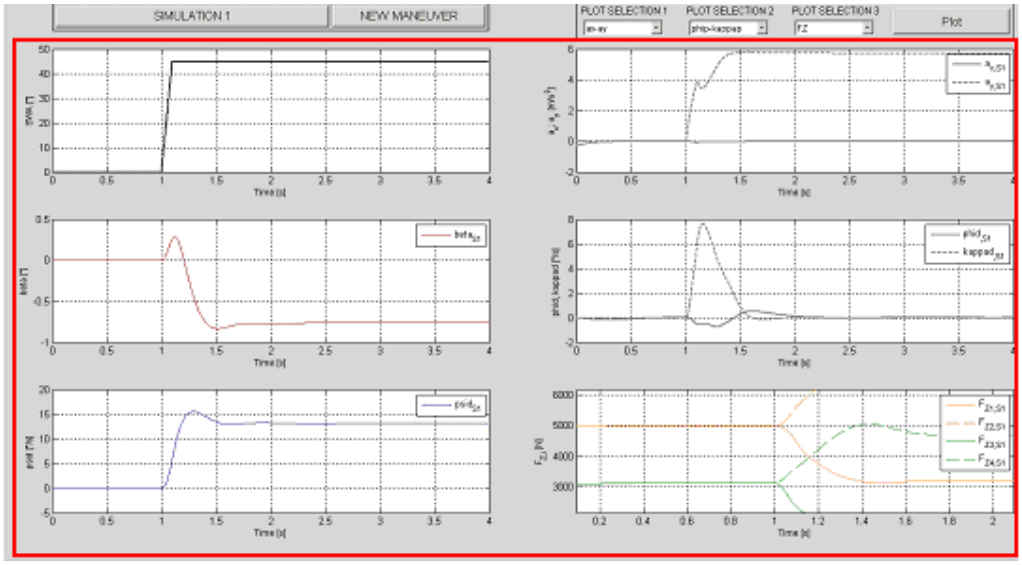

Figure 3.14 A section from the result output of the GUI

Also when needed, some small subscripts are written which controls the GUI so that the inputs are automatically given and the model is run especially when consecutive simulations are to be carried out in case studies.

CHAPTER 4

SIMULATIONS

The effects of damper failure on handling behaviour during critical driving situations are examined in this chapter by means of some representative dynamic driving maneuvers. The results coming out from the mechanical or software type of failure for electrical dampers together with the electrical failure effects are analysed, interpreted in a detailed way, which would give the user a broad idea about what would happen if a damper fails at a *characteristic* time point. For that purpose, the explanations or definitions for a characteristic time point are also made. MATLAB/Simulink vehicle model is used for simulations and the GUI is made use of for inputting and running the simulations. First, the critical driving maneuver is simulated, consequently the characteristic time points are identified and then all four dampers (at each corner of the vehicle) are intentionally made to fail at those characteristic time points. The maneuvers are held on normal environmental conditions, i.e. the vehicle is driven on dry asphalt surface. To satisfy this, the adhesion coefficient between the tires and the road surface is taken as **1**.

4.1 MANEUVERS

As discussed and decided as a result of the literature survey study, three main maneuvers, which are consistent with standard handling maneuvers in the literature, are selected to represent the critical driving situations. These are namely:

- Step Steer Input
- Continuous Sine Steer Input
- Sine-Dwell Steer Input

4.1.1 STEP STEER INPUT

Keeping the velocity constant during the simulation, a step input of desired angle is given to the steering wheel. There is a slight deviation from the step function due to a little time delay between the time points corresponding to step begin and step end. The time dependence of the step representing the time delay is given in Appendix B. The purpose for such an approach is to model the real case more approximately. This maneuver is also known as the J-Turn Maneuver in the literature. The GUI inputs representing the Step Steer Response simulation are:

- Maneuver start (starting point of steering wheel input) and end times,
- Initial velocity of the vehicle that should be kept constant,
- Step value of the steering wheel angle,
- Brake time (if any braking is included)

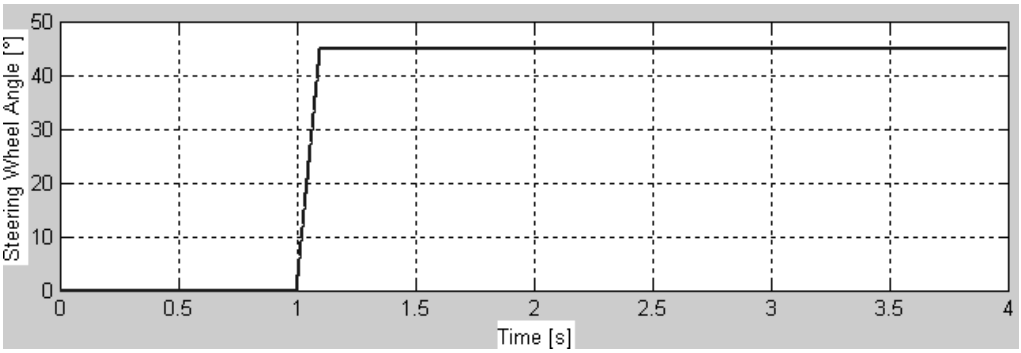

Figure 4.1 Step steer input used in the simulations

4.1.2 CONTINUOUS SINE STEER INPUT

Keeping the vehicle velocity constant, a sinusoidal input with a specified frequency is given as a steering wheel angle input which continues until the

maneuver end time. The GUI inputs representing the Continuous Sine Steer Response simulation are:

- Maneuver start (starting point of steering wheel input) and end times,
- Initial velocity of the vehicle that should be kept constant,
- Amplitude and frequency of sine steering wheel angle function,
- Brake time (if any braking is included)

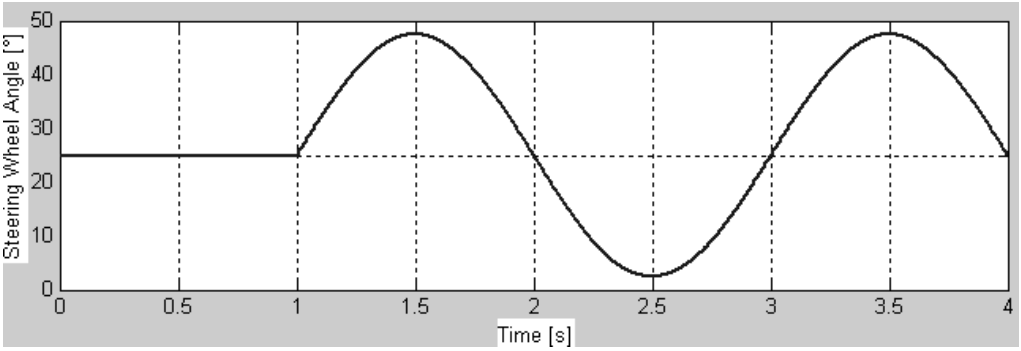

Figure 4.2 Continuous sine steer input used in the simulations

4.1.3 SINE-DWELL STEER INPUT

Keeping the vehicle velocity constant, a sine-dwell input with defined amplitude, frequency, and a dwell period is given as a steering wheel angle input. The whole function includes one period including the sine and dwell periods as used also in the standard driving maneuvers in the literature. The GUI inputs representing the Sine-Dwell Steer Response simulation are:

- Maneuver start (starting point of steering wheel input) and end times,
- Initial velocity of the vehicle that should be kept constant,

- Amplitude, frequency and dwell time of sine-dwell steering wheel angle function,
- Brake time (if any braking is included)

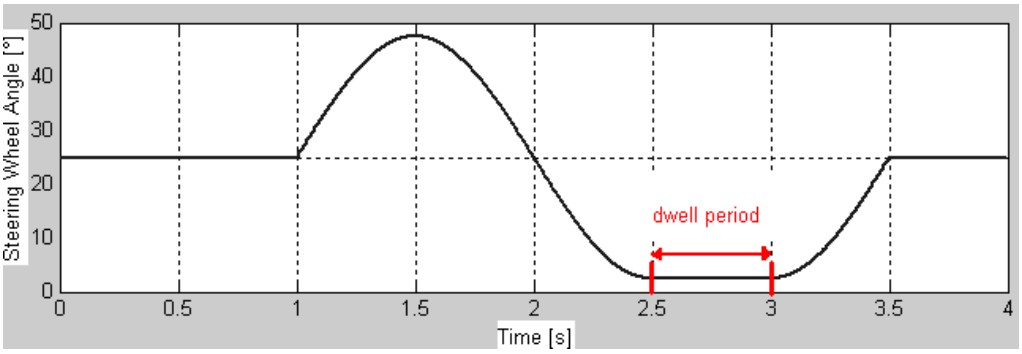

Figure 4.3 Sine-Dwell steer input used in the simulations

4.2 DAMPER FAILURE SIMULATIONS

The maneuvers used in the damper failure simulations are shown in Table 4.1. As shown in the maneuver definitions, a time interval of 1 second at the beginning is used before the steering input starts in each maneuver in order to be sure that the simulation errors (due to iterations in Simulink) have already vanished. It should be noted that for each type of failure phenomena those six representative maneuvers are used. The numbers in red indicate the case number used in the simulations.

The failure process is to take place at the critical time points which indicate some energy present in the system in terms of vehicle dynamics and stability (i.e. point on which lateral acceleration , yaw velocity, side slip angle are maximum. On the other hand, it is also obvious that, in order to face with some significant effect as a result of damper failure process, there ought to be some potential (damper force, i.e. damper relative velocity) to influence the system (vehicle handling) when

switched. Therefore, it could be foreseen that the combination of dynamics and the potential on the damper failure point decide the criticality of the damper failure. Characteristic candidate points for damper failure are listed in Table 4.2.

Table 4.1 Maneuvers used in the Simulations

ManeuverInfo		V[km/h]	Steering Wheel Angle [°]	Frequency [Hz]	Dwell [s]	Brake Time [s]
Without Braking	Step Steer [1]	100	90			
	Cont. Sine [2]	100	90	0.5		
	Sine-Dwell [3]	100	90	0.5	0.5	
With Braking	Step Steer [4]	80	10			1
	Cont. Sine [5]	105	5	1		0.88
	Sine-Dwell [6]	95	5	0.5	0.5	2.36

Table 4.2 Characteristic Candidate Points for Damper Failure

POINT	Explanations about the Characteristics of the Point
Start	Considering the entire dynamics of whole maneuver
$\dot{\kappa}_{max}$	Maximum damper velocity (damper force)
$\dot{\varphi}_{max}$	Maximum damper velocity (damper force) [for braking maneuvers]
φ_{max}	Maximum suspension travel (spring force) [for braking maneuvers]
$a_{y\,max}$	Maximum lateral acceleration (lateral force sum)
$\dot{\psi}_{max}$	Maximum yaw dynamics (yaw moment = 0)
κ_{max}	Maximum suspension travel (spring force)
β_{max}	Side slip angular velocity is 0 (instantaneous balance)

The most critical scene in each damper selection (among the characteristic damper failure points) is identified and the phenomenon is explained physically for that most critical case in each damper selection. This procedure is performed for four times (for each damper of the vehicle) concerning the Step Steer Responses and once (worst case among the four most critical cases for each damper) concerning the Sine and Sine-Dwell Responses.

Lateral dynamics characteristics of the vehicle are expressed by means of s signals produced in the Simulink Model (Lateral Dynamics Block) which demonstrates the lateral behaviour of the vehicle. The signals are derived from the formula (3.44) as follows:

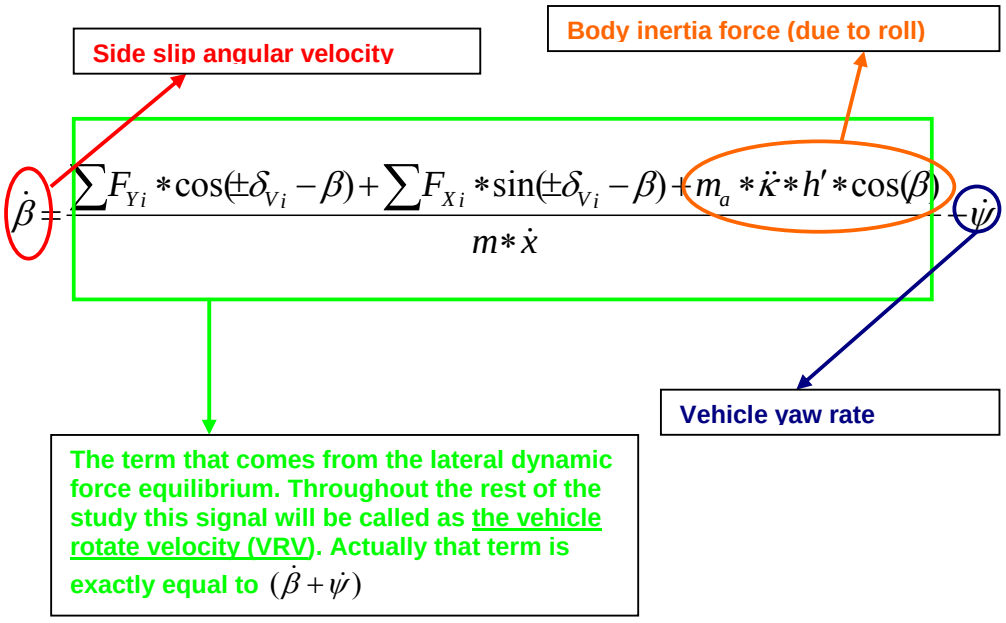

For the sake of consistence, the positive steering wheel angle is taken as a left hand steer during the simulations, meaning that the maneuvers always start with a left hand turn. In sinusoidal maneuvers the second half cycle corresponds as a

matter of course to the right hand turn. The wheel indices which are randomly matched are also given in Figure 4.4.

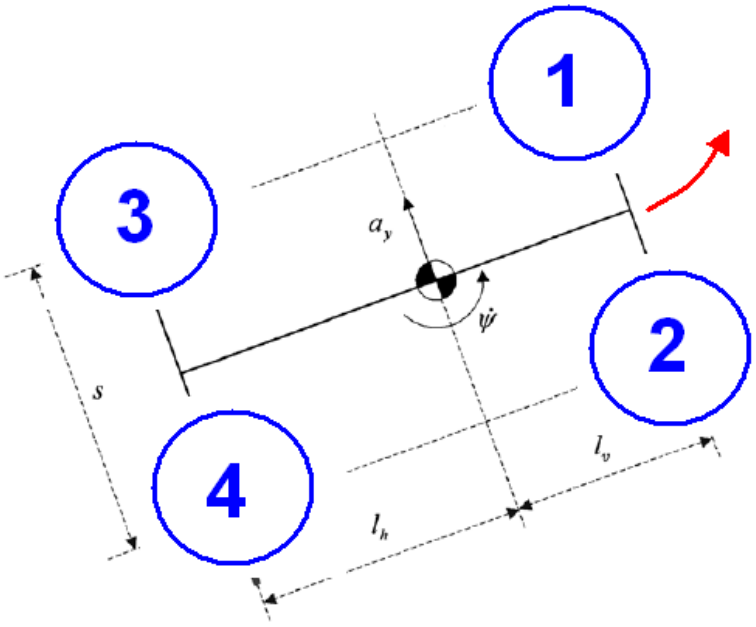

Figure 4.4 Tire Numbering for the simulations

4.2.1 MECHANICAL OR SOFTWARE FAILURE ANALYSIS

Mechanical or software type of failures in dampers result in disappearance of the damper forces created by the dampers. As discussed in the literature survey, the sources are mechanical (crush down of the damper case or piston structure, etc…) and software type (in which case the electrically controlled damper characteristic is *accidentally* switched to 0, such that the damper orifices are accidentally fully open). These two cases are rather theoretical cases which may contribute to the subject in a more obvious manner.

4.2.1.1 CASE 1: STEP STEER RESPONSE

Carrying out the simulation for the original maneuver, (without damper failure), the following responses and the characteristic failure points are obtained:

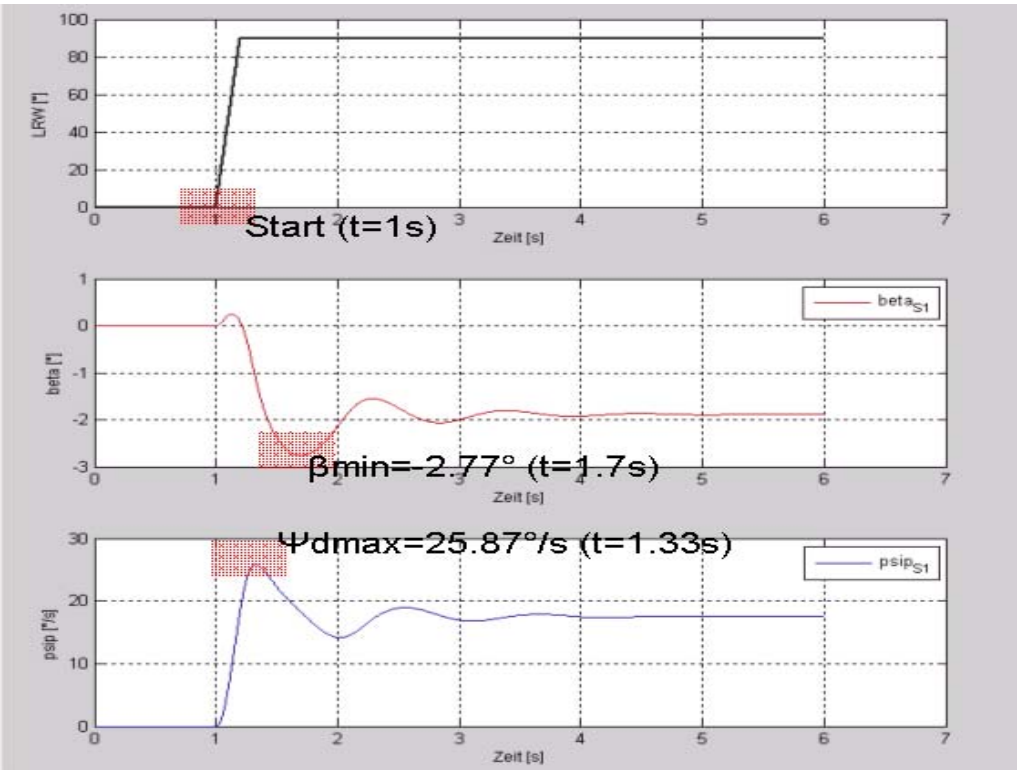

Figure 4.5 Characteristic Failure Points for Case1(a)

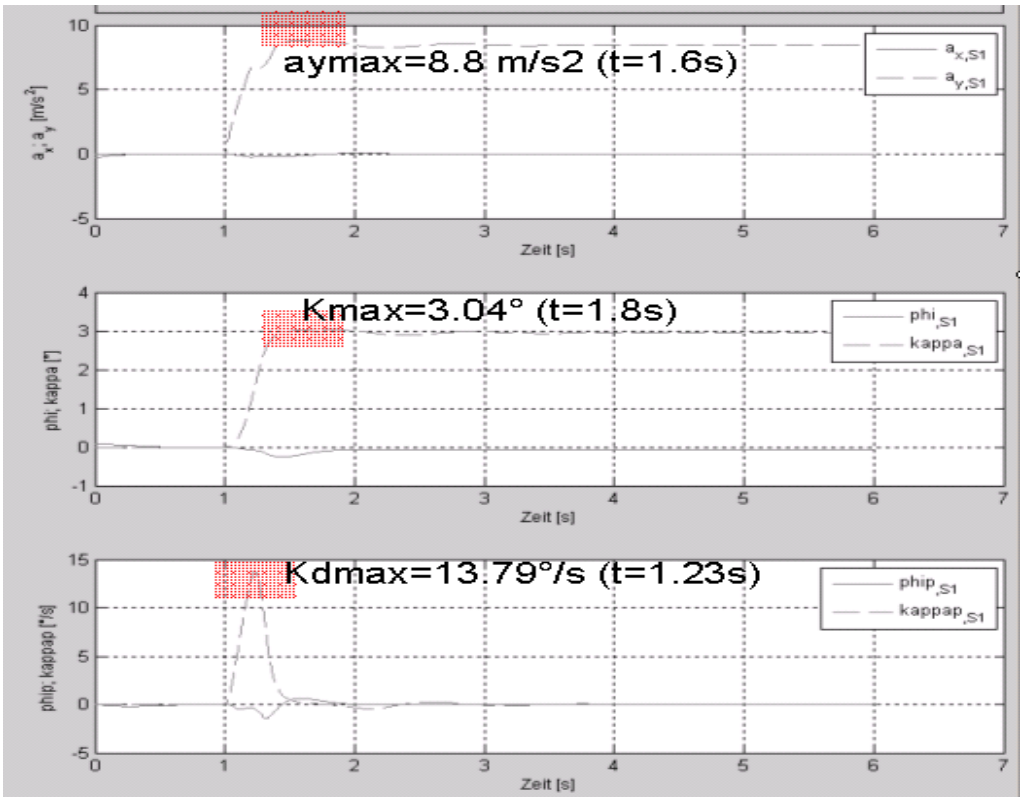

Figure 4.6 Characteristic Failure Points for Case1(b)

As can be seen in the Figures 4.5 and 4.6 that maneuver is a dynamic step steer response maneuver with a maximum yaw rate of 25.87 °/s and lateral acceleration of 8.8 m/s^2. The roll angle reaches above 3°.

4.2.1.1.1 Failure of Damper 3 (worst case)

With a failure of the damper 3 at the starting point of steering input, the body roll and pitch motions are faster and give sharper responses. The vehicle body leans more towards the tire 2. The pitching motion (in that case there is only a small amount due to reaction to rolling and re-settling) is overall greater towards the front in the absence of resisting dampers force from the tire 3.

The decisive factor in that case is the decrease in the yaw moment of the tire 4 due to less pitching and consequently reduced vertical force. It should be noted that the moment arm of the tire 4 is the longest and the lateral force from the tire 4 is relatively high which makes the yaw moment 4 the greatest, Figure 4.11. Therefore, the total yaw moment rises and the side slip angle consequently increases. The starting point of the maneuver is the most critical characteristic point for the failure of the damper 3 since the entire maneuver is influenced in such case. Figures 4.7-4.12 demonstrate the influence of the failure explained above.

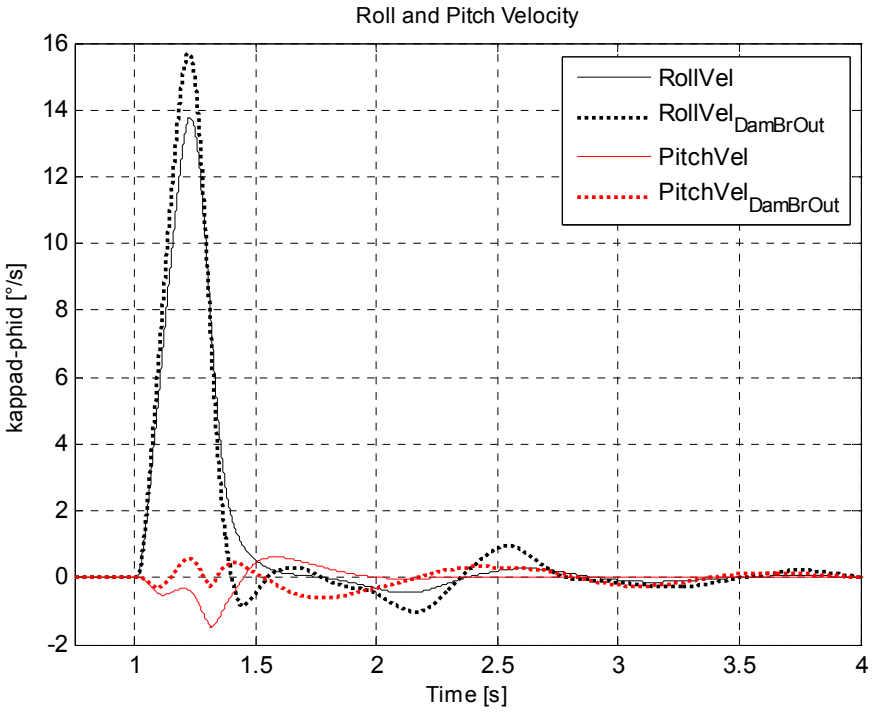

Figure 4.7 Roll and Pitch Velocities for Case 1-Damper3 Failure

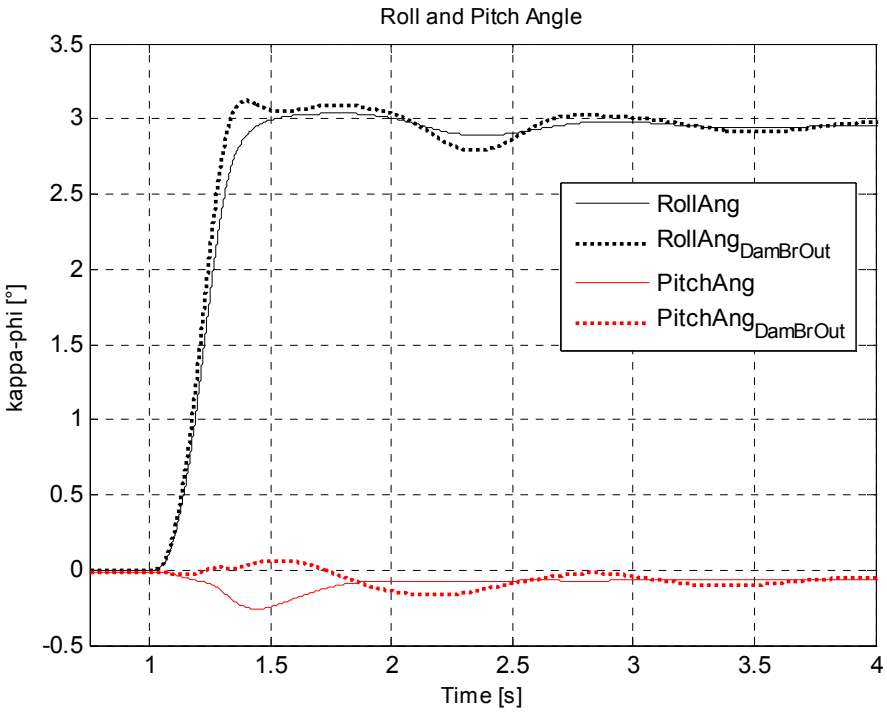

Figure 4.8 Roll and Pitch Angles for Case 1-Damper3 Failure

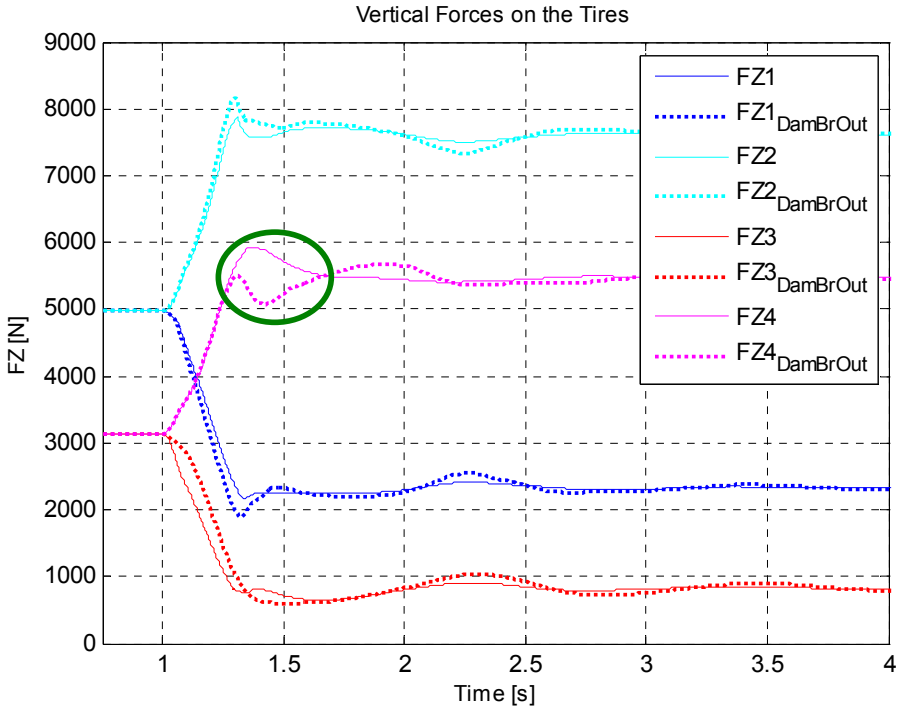

Figure 4.9 Vertical Tire Loads for Case 1-Damper3 Failure

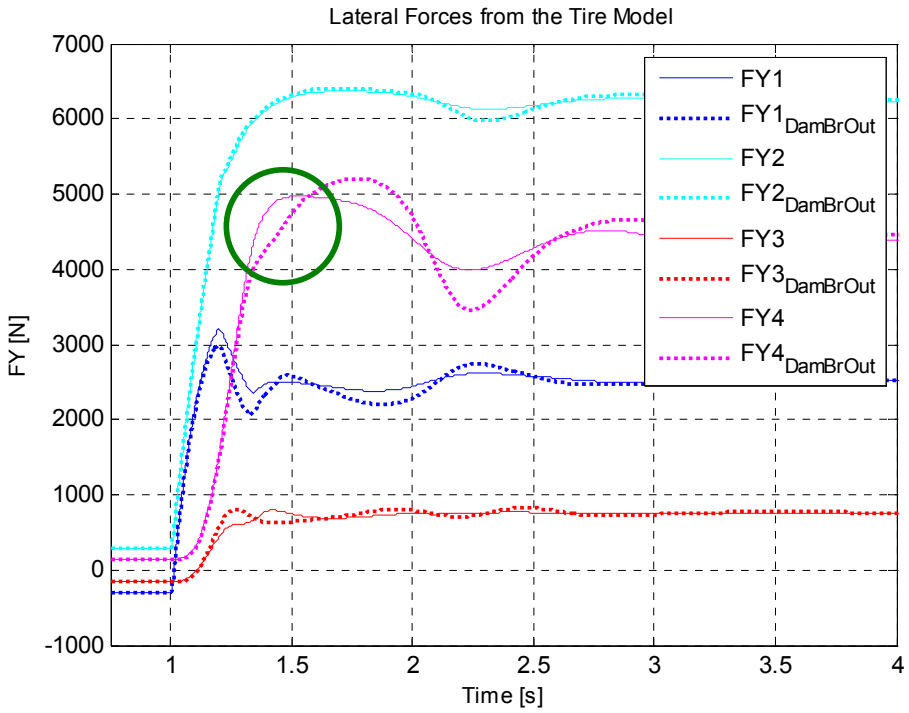

Figure 4.10 Lateral Tire Forces for Case 1-Damper3 Failure

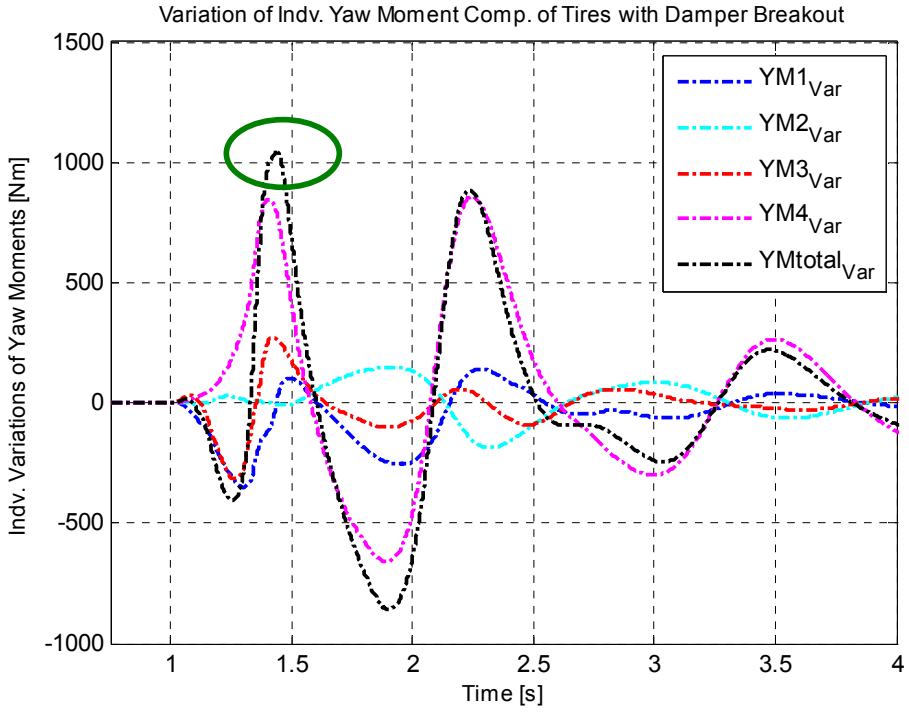

Figure 4.11 Variation of Yaw Moments for Case 1-Damper3 Failure

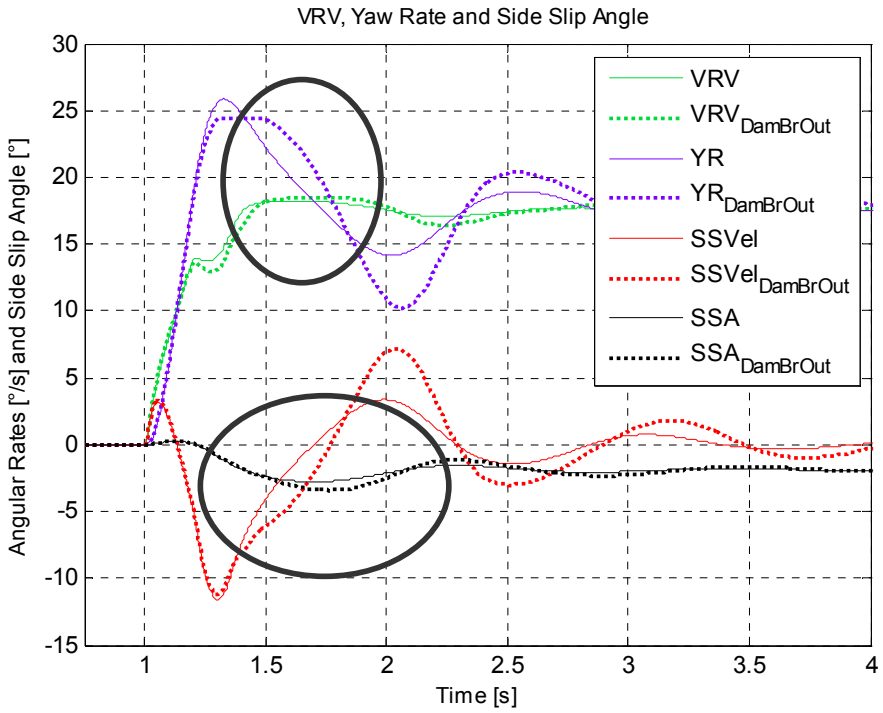

Figure 4.12 Calculation of Side Slip Angle for Case 1-Damper3 Failure

4.2.1.2 CASE 2: CONTINUOUS SINE RESPONSE

In that sinusoidal maneuver, there is the possibility of influencing the vehicle towards instability in both turning directions (leftwards and rightwards). This is obviously because of the two directional steering inputs to the system, steering towards left during a half sine cycle and rightwards during the other one. Therefore, the maxima and the minima corresponding to the characteristic damper failure points are to be taken into account, every half period taken as a single maneuver.

Carrying out the simulation for the original maneuver the following characteristic failure points are obtained:

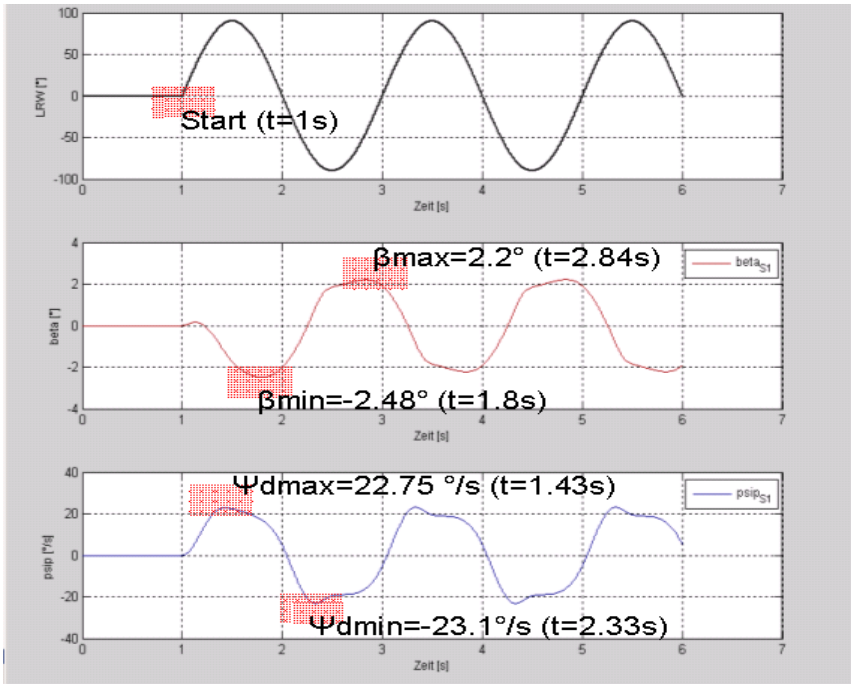

Figure 4.13 Characteristic Failure Points for Case2(a)

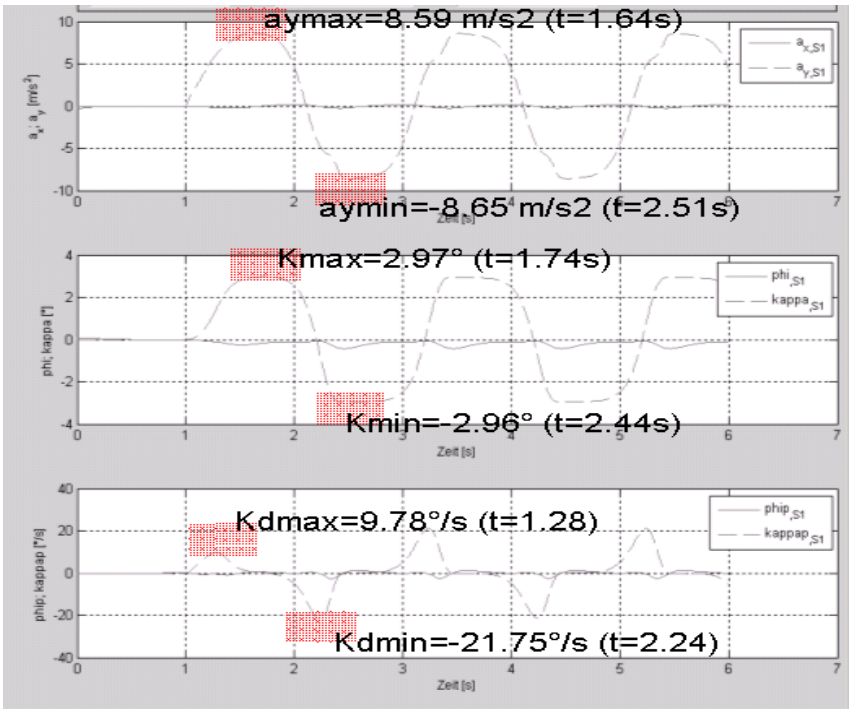

Figure 4.14 Characteristic Failure Points for Case2(b)

4.2.1.2.1 Failure of Damper 3 (worst case)

In this maneuver the maximum yaw velocity attains a value of 22.75 °/s whereas the maximum values of lateral acceleration and roll angle are 8.59 m/s^2 and 2.97° respectively, Figure 4.13 and 4.14. This is also quite a dynamic maneuver, which is obtained by implementing an additional reasonable frequency input to the previous step steer function.

The most critical damper failure scene (worst case) is obtained with damper 3 failure at the characteristic point $\dot{\psi}_{max}$. This is the point at which the yaw rate starts to decrease (and increase in the other direction due to the rightwards steer half cycle). In the region where one complete sine cycle is attained, the body normally makes a settling roll and pitch. Due to absence of resisting damper 3 force these motions are faster and greater in magnitude, roll angle is smaller, Figure 4.15. Therefore, that region affects the vertical loads of the tires 3 and 4 (which are decisive in this case) so that they decrease to produce less amount of lateral force to create greater amount of total yaw moment and side slip angle.

On the point leads $\dot{\psi}_{max}$ a damper failure of tire 3 also creates a vertical force bounce which, due to resulting lateral force, creates a negative yaw moment. Since this adds up with the effect explained above when the vehicle turns to right due to second half sine, it is an additional factor which makes the point $\dot{\psi}_{max}$ the most critical. It should also be noted that, that maneuver gives the same damper selection as the most critical one due to similar clarifications with the step steer response, but which changed the most critical characteristic failure point in this case is the additional affect on $\dot{\psi}_{max}$, as already explained. Figures 4.15-4.20 demonstrate the influence of the failure explained above.

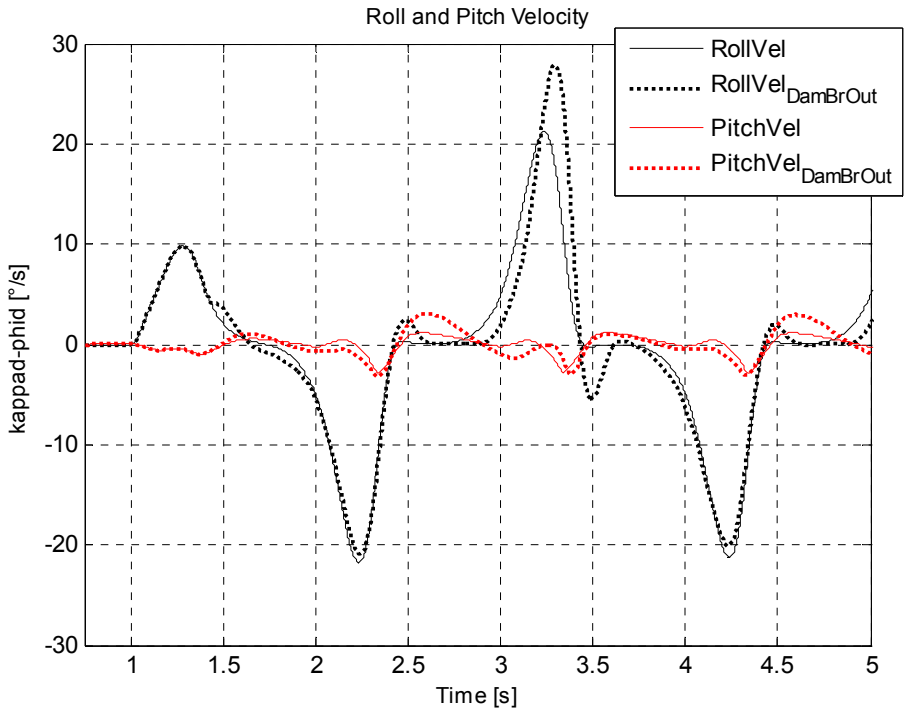

Figure 4.15 Roll and Pitch Velocities for Case 2-Damper 3 Failure

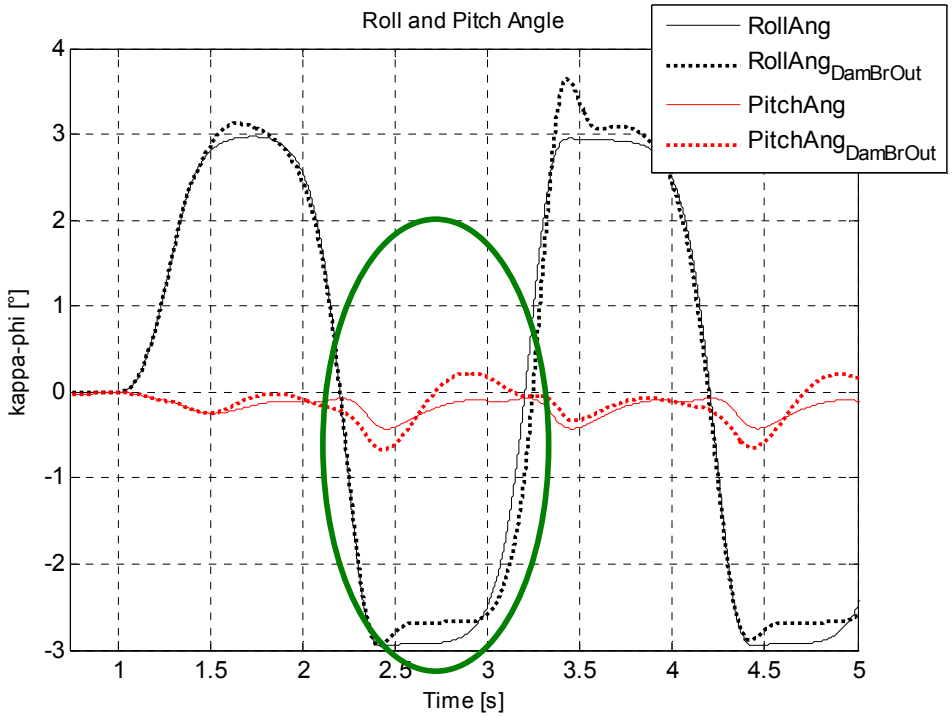

Figure 4.16 Roll and Pitch Angles for Case 2-Damper 3 Failure

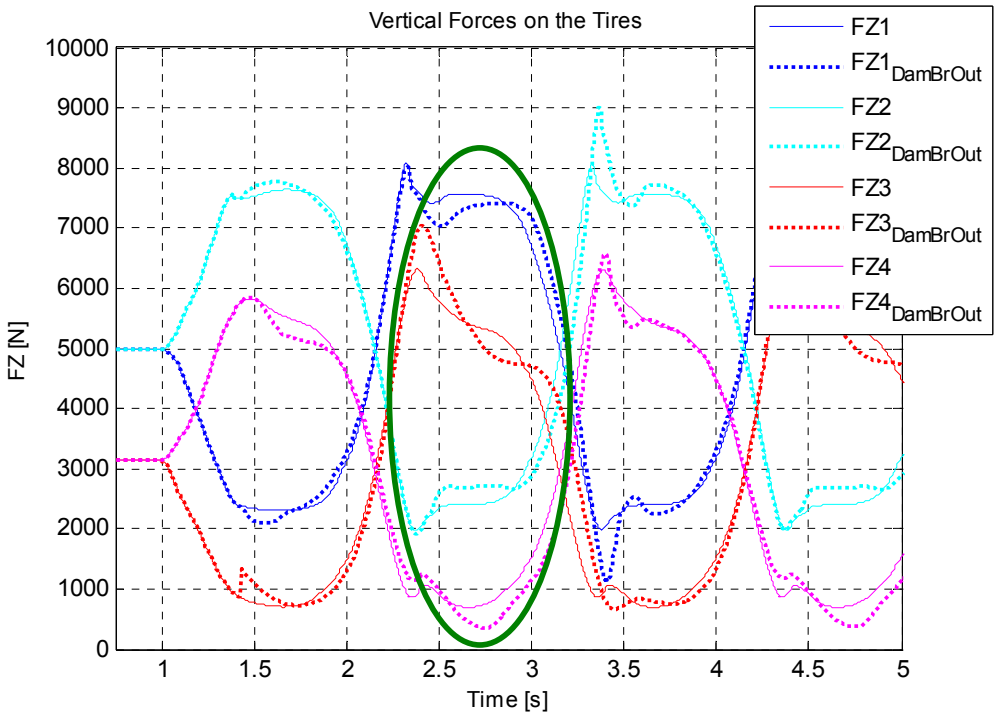

Figure 4.17 Vertical Tire Loads for Case 2-Damper 3Failure

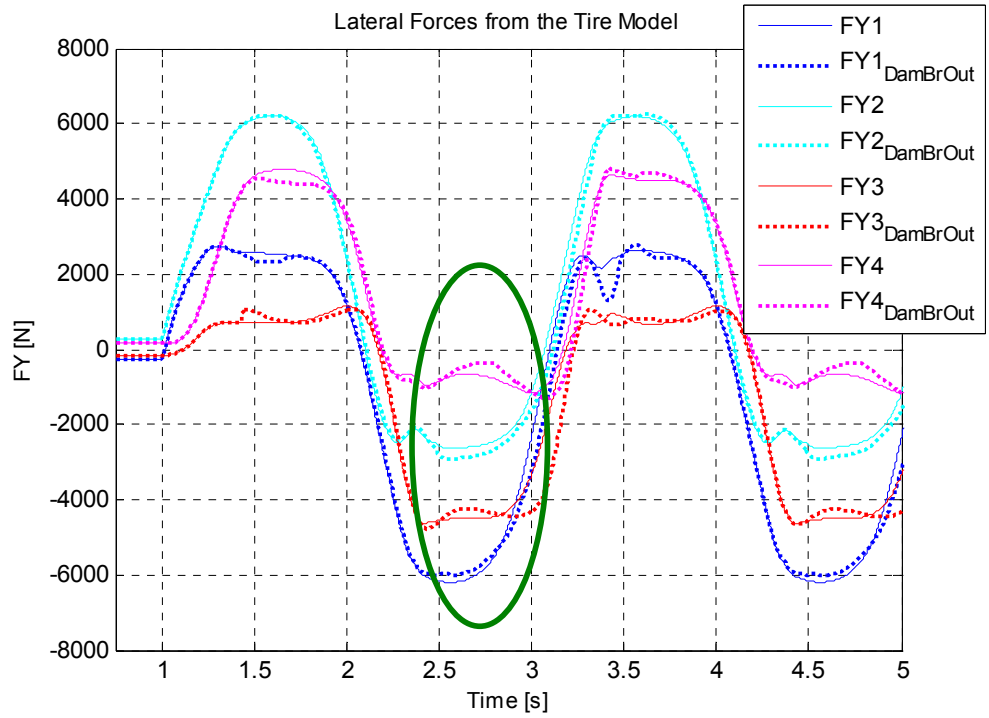

Figure 4.18 Lateral Tire Forces for Case 2-Damper 3Failure

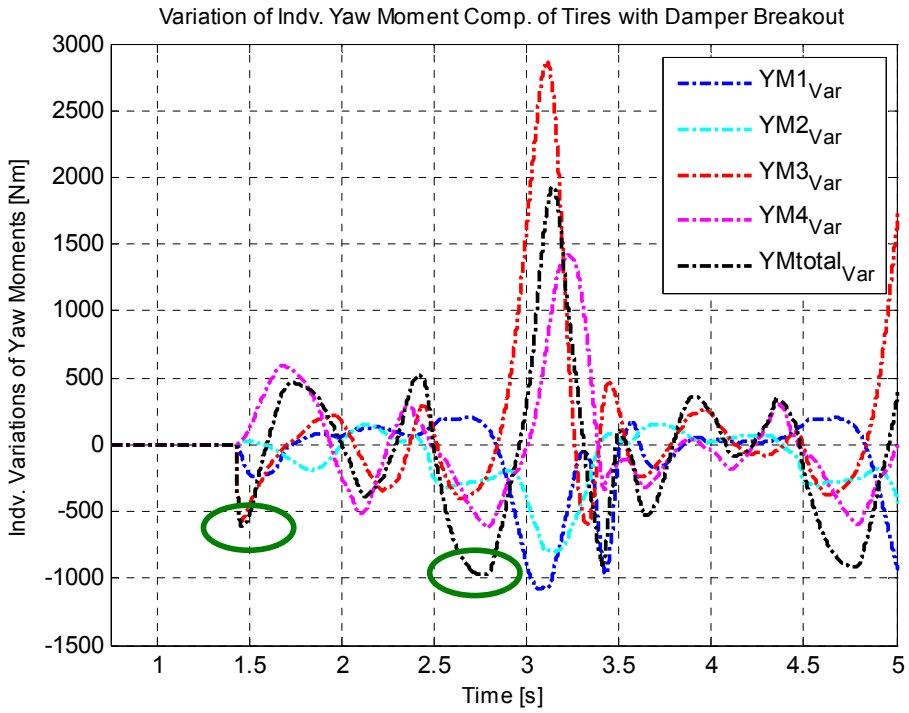

Figure 4.19 Variation of Yaw Moments for Case 2-Damper 3Failure

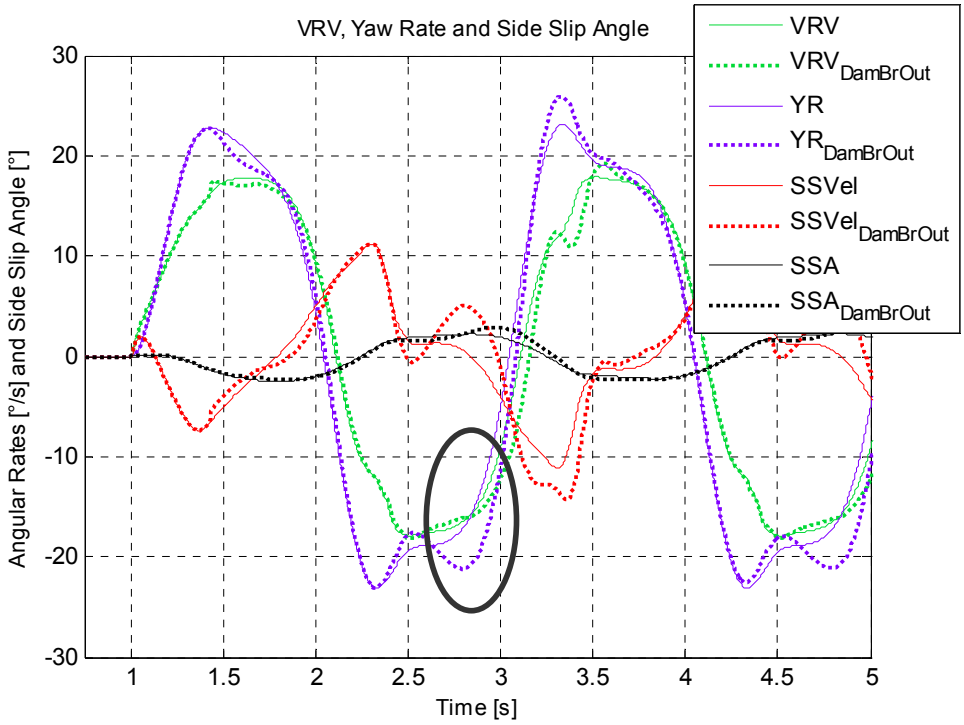

Figure 4.20 Calculation of Side Slip Angle for Case 2-Damper 3Failure

4.2.1.3 CASE 3: SINE-DWELL RESPONSE

Contrary to continuous sine response, sine–dwell consists of single period. Still the maxima and the minima corresponding to the characteristic damper failure points are to be taken into account (treating every half period as a single maneuver). The maneuver is obtained by implementing an additional dwell time to the previous sine function. Simulating the original maneuver, the following characteristic points are obtained:

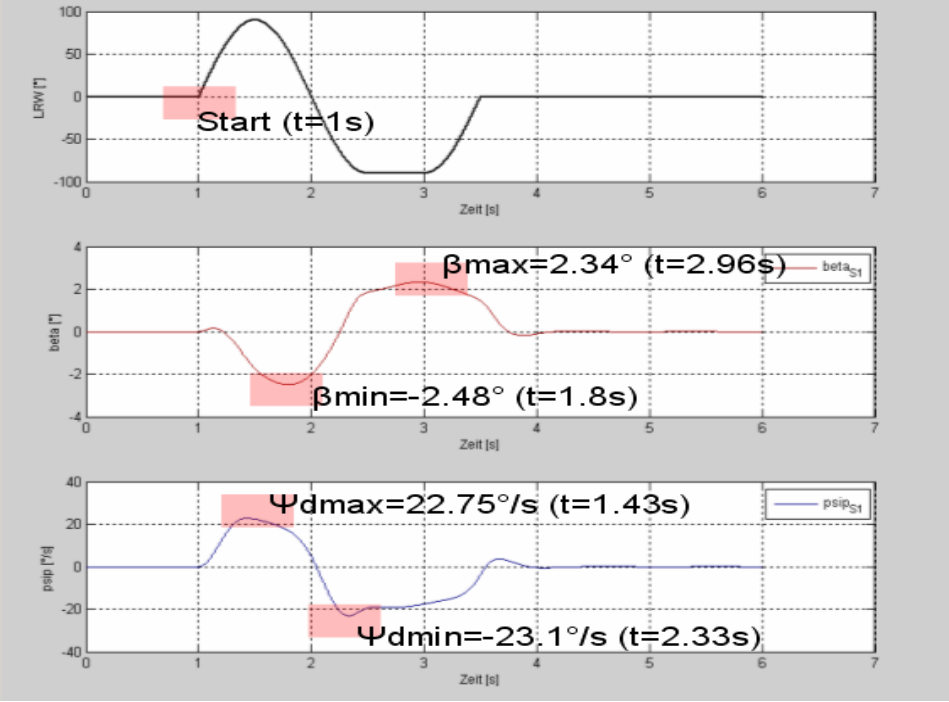

Figure 4.21 Characteristic Failure Points for Case3(a)

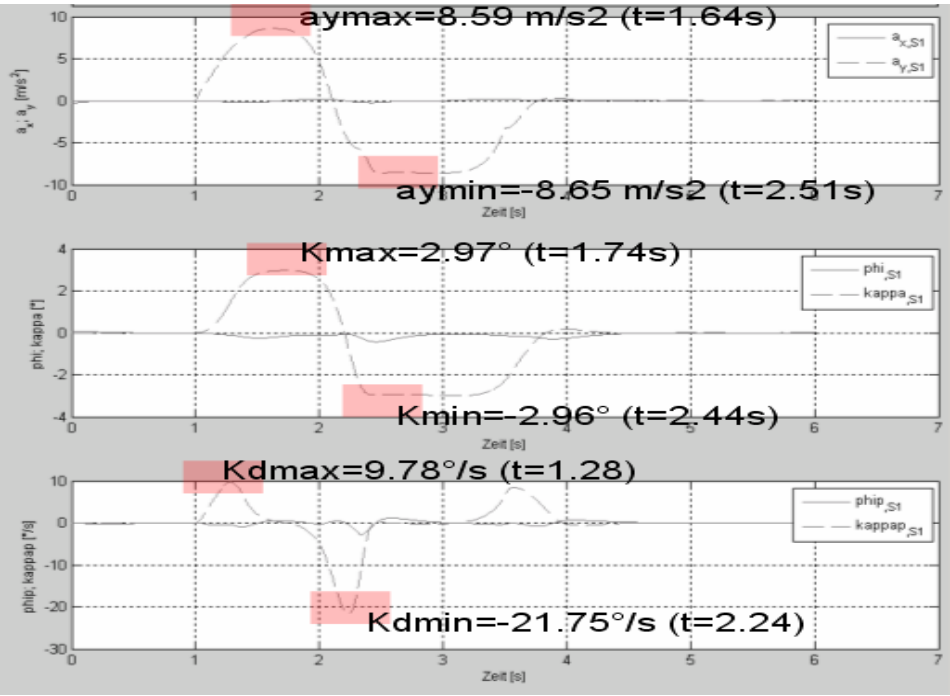

Figure 4.22 Characteristic Failure Points for Case3(b)

4.2.1.3.1 Failure of Damper 3 (worst case)

It is observed that the maneuver is similar to the previous one, since a common parametrization is used. The maximum yaw velocity attains a value of 22.75 °/s whereas the maximum values of lateral acceleration and roll angle are 8.59 m/s2 and 2.97° respectively, Figure 4.21 and 4.22.

Since the structures of the maneuvers are similar (this maneuver is no more than one period of the sine maneuver with dwell) the physical clarification of the damper failure phenomena is the same here. Thus the most critical damper failure point is $\dot{\psi}_{\max}$ due to same reasons. This can be observed from the plots and the similar tendencies marked on the graphs. Figures 4.23-4.28 demonstrate the influence of the failure explained above.

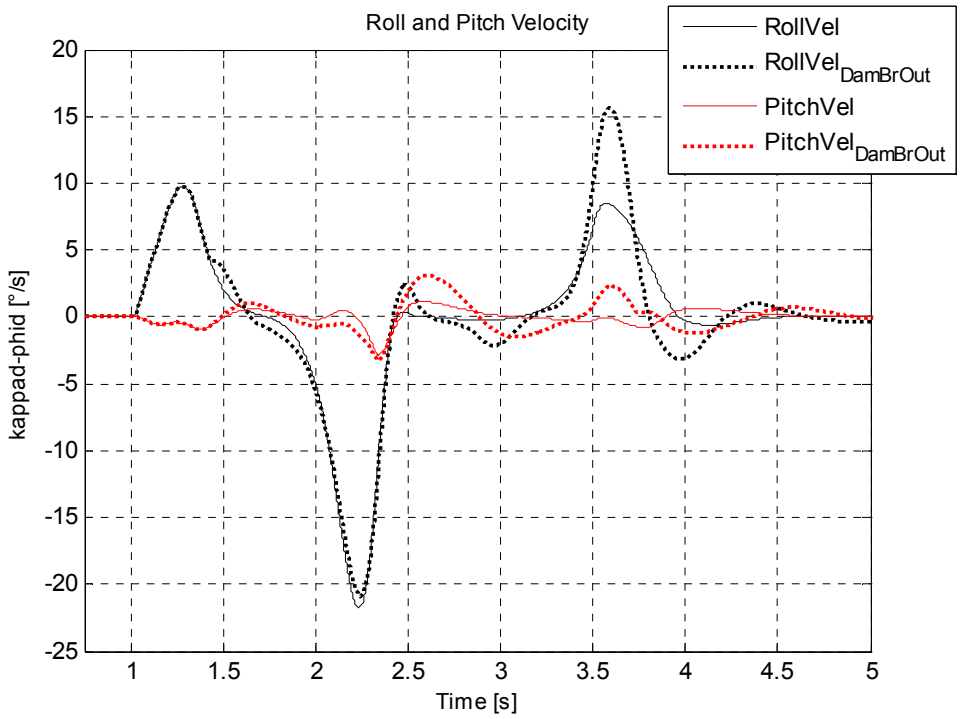

Figure 4.23 Roll and Pitch Velocities for Case 3-Damper 3Failure

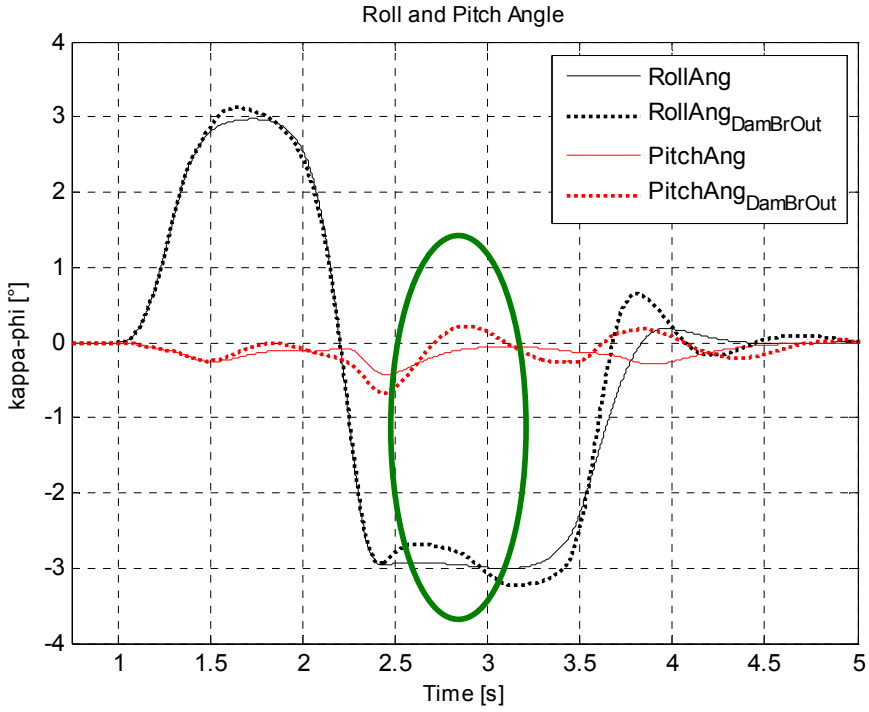

Figure 4.24 Roll and Pitch Angles for Case 3-Damper 3Failure

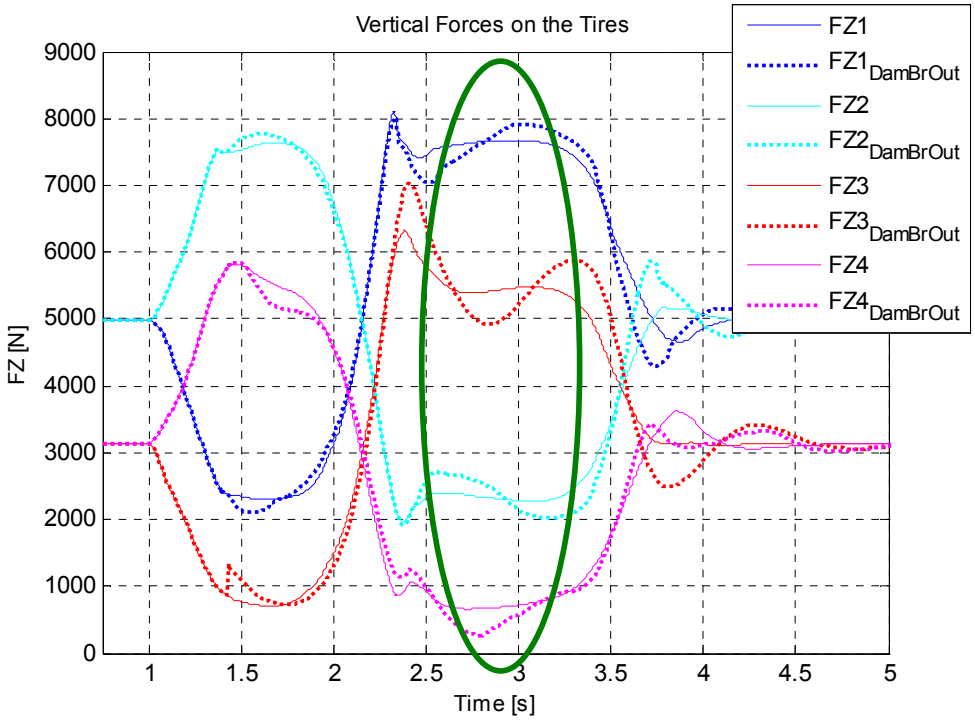

Figure 4.25 Vertical Tire Loads for Case 3-Damper 3Failure

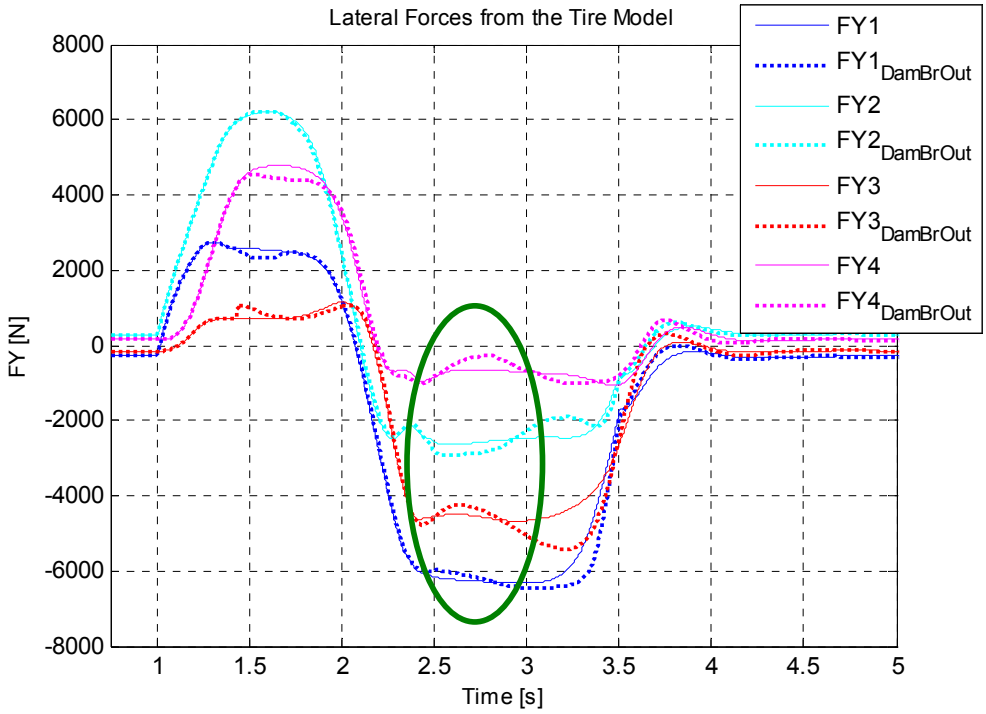

Figure 4.26 Lateral Tire Forces for Case 3-Damper 3 Failure

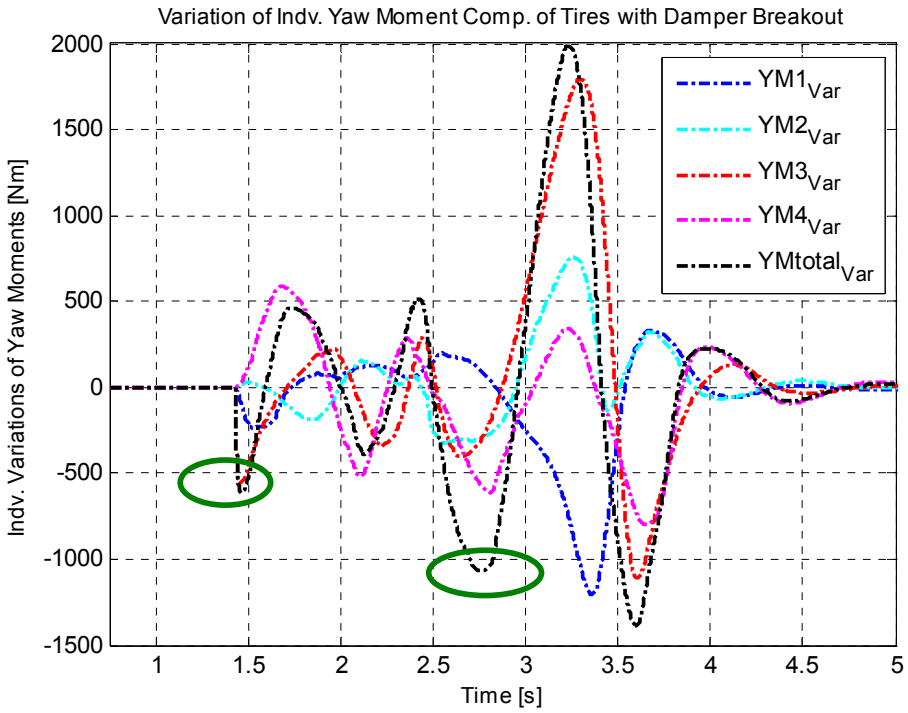

Figure 4.27 Variation of Yaw Moments for Case 3-Damper 3 Failure

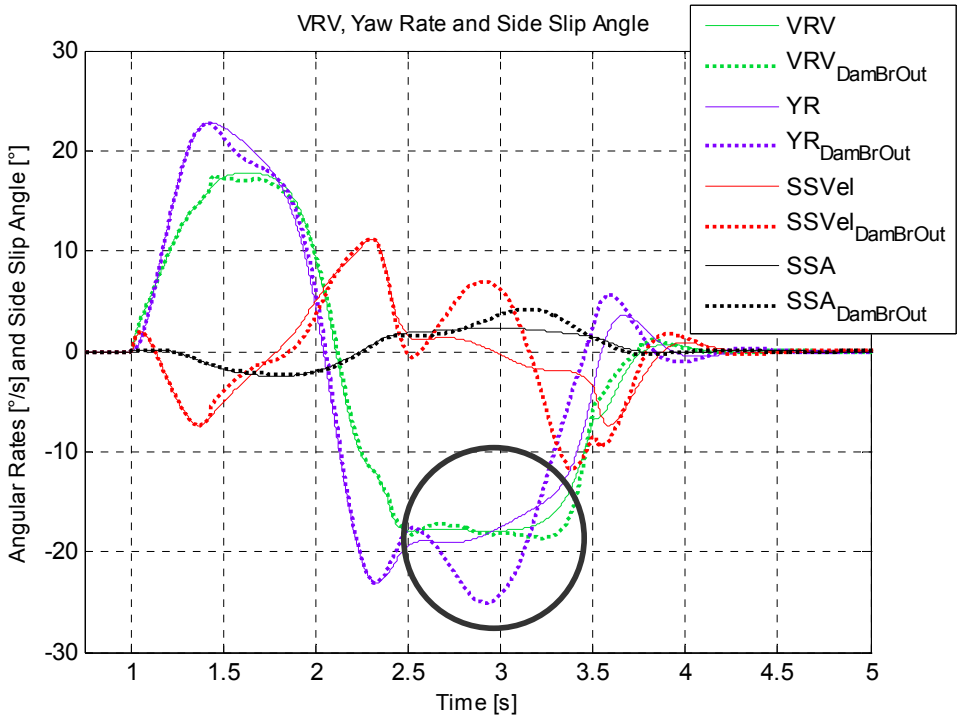

Figure 4.28 Calculation of Side Slip Angle for Case 3-Damper 3Failure

4.2.1.4 CASE 4: STEP STEER RESPONSE WITH BRAKING

In this maneuver an additional braking is implemented, which starts at the beginning of the steering input. With that sort of braking, the most critical driving situation is obtained. The maneuver is constructed by selection of velocity and step steer input value parameters and then simulating together with the braking. The velocity and steering step value are so selected that at the end the whole maneuver ends up with a critical and dynamic one. The maximum yaw velocity rises up to 15.09°/s, the lateral acceleration attains a maximum of 2.63 m/s^2 and the maximum pitch angle is around 1.89°, Figure 4.29 and 4.30. The following characteristic damper failure points are obtained as a result of this maneuver:

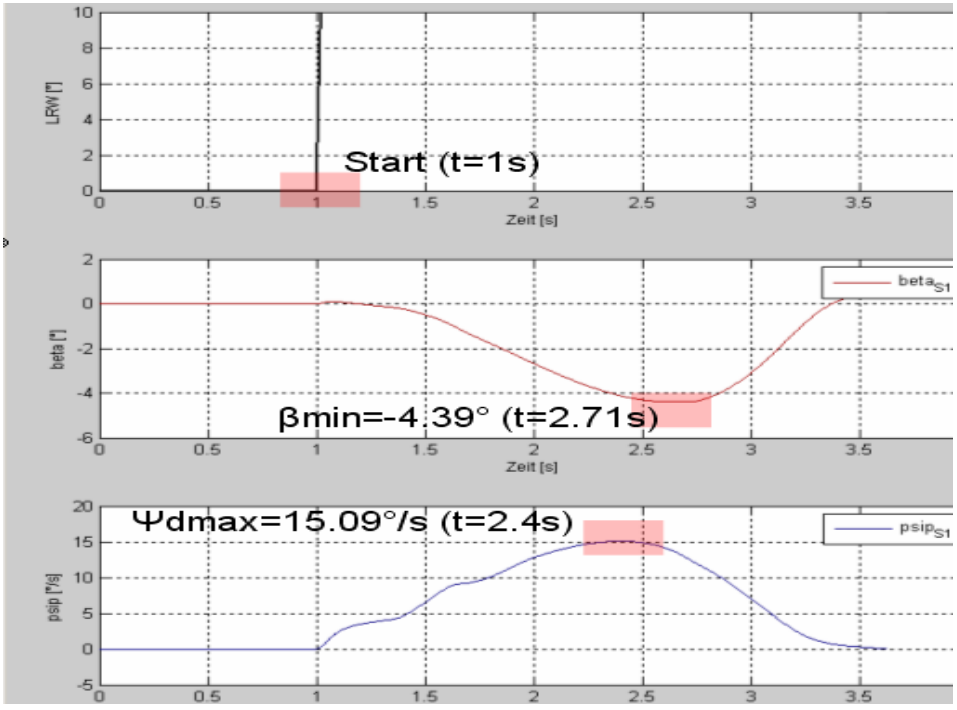

Figure 4.29 Characteristic Failure Points for Case4(a)

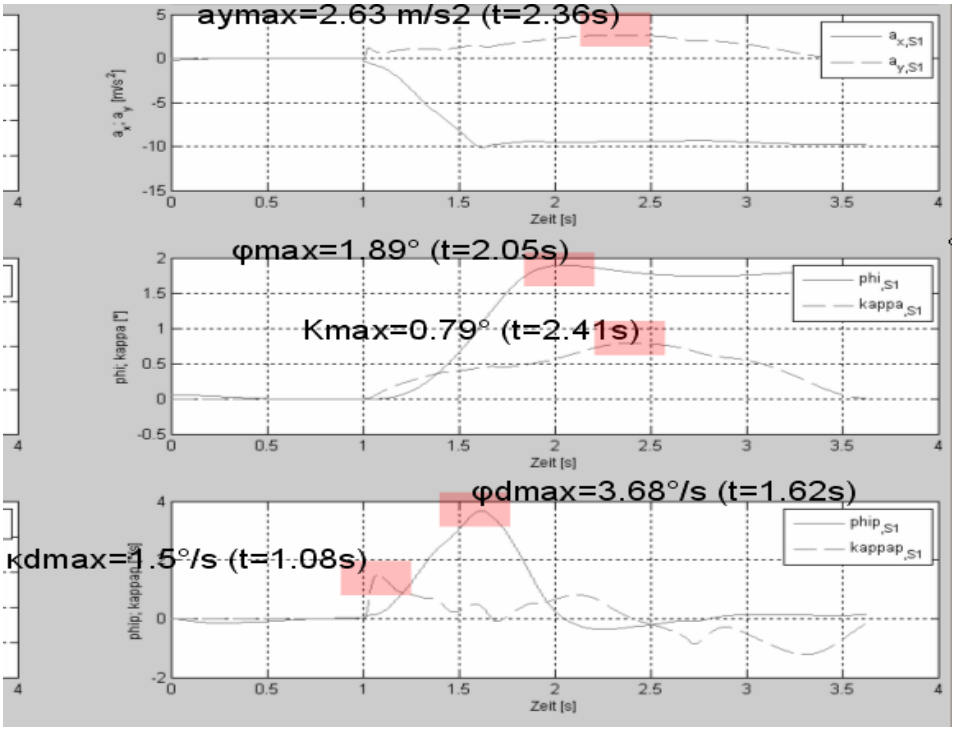

Figure 4.30 Characteristic Failure Points for Case4(b)

4.2.1.4.1 Failure of Damper 3 (worst case)

$\dot{\kappa}_{max}$ is the most critical point for damper3 failure since it accelerates the body pitch and roll motions to the greatest extent. It should be noted that $\dot{\kappa}_{max}$ point is the last dynamic point before the fore motion occurs due to braking. With a damper failure on this point the pitching during the fore motion and the roll motion become greater, Figure 4.31. It can be also imagined that within the absence of resisting damper force on tire 3, as a result of harsh braking the body leans on the tire 2 more. Therefore, the vertical forces on tires change (i.e. FX3 greater, FX4 greater and FY2 greater) so that the longitudinal and lateral tire forces at the end create a total yaw moment which rises up. It should be here noted that all of the increase in vertical tire load on tire 2 is distributed to lateral tire force FY2 through the friction circle since FX2 has reached to its mechanical maximum. Figures 4.31-4.37 demonstrate the influence of the failure explained above.

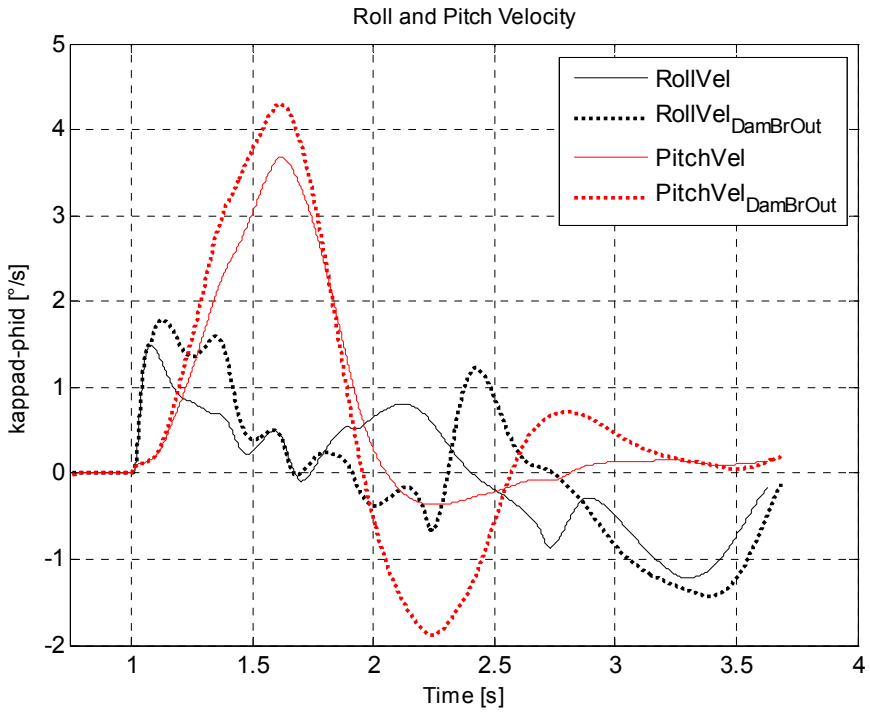

Figure 4.31 Roll and Pitch Velocities for Case 4-Damper 3 Failure

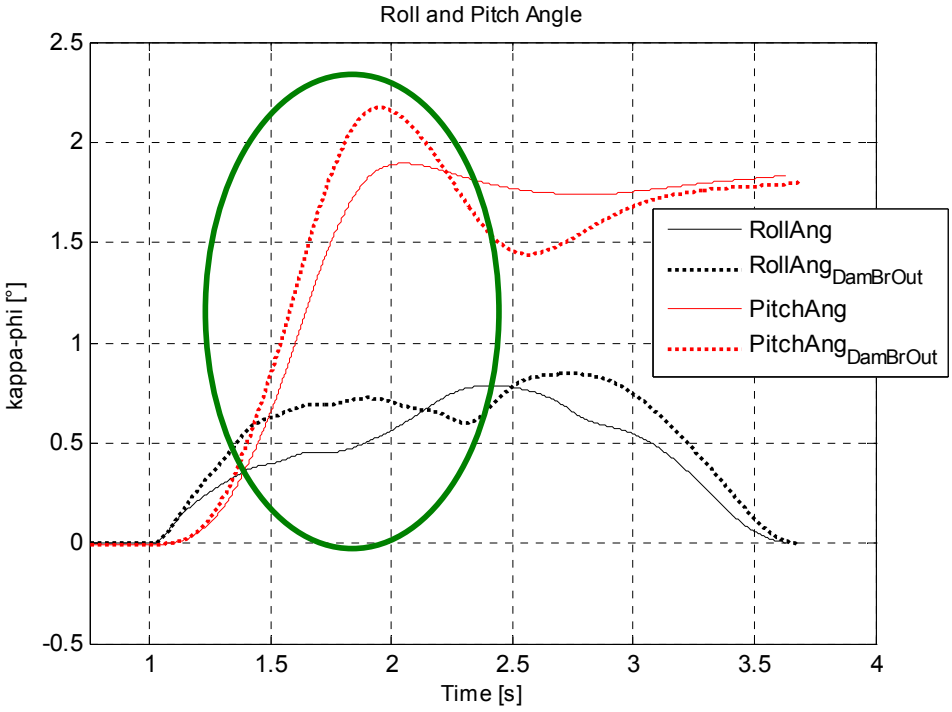

Figure 4.32 Roll and Pitch Angles for Case 4-Damper 3 Failure

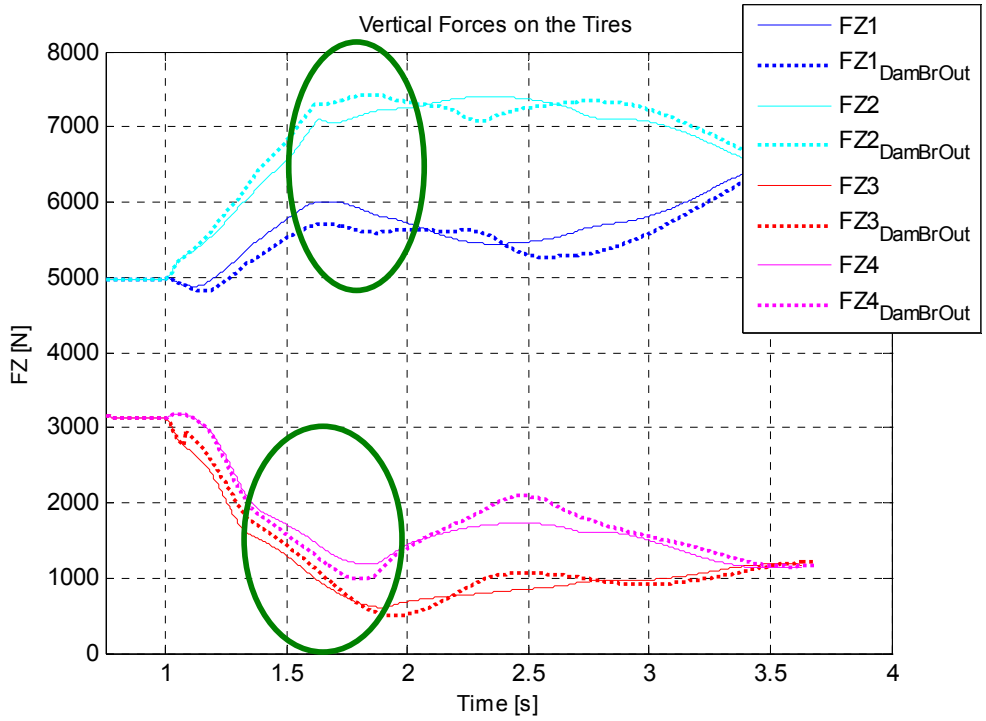

Figure 4.33 Vertical Tire Loads for Case 4-Damper 3 Failure

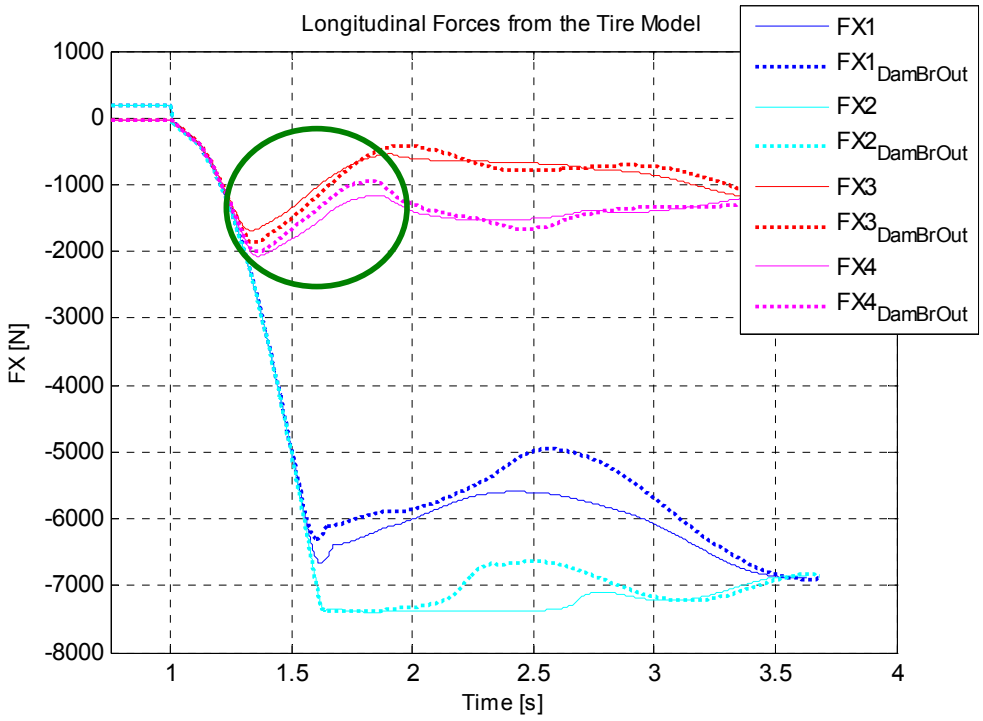

Figure 4.34 Longitudinal Tire Forces for Case 4-Damper 3 Failure

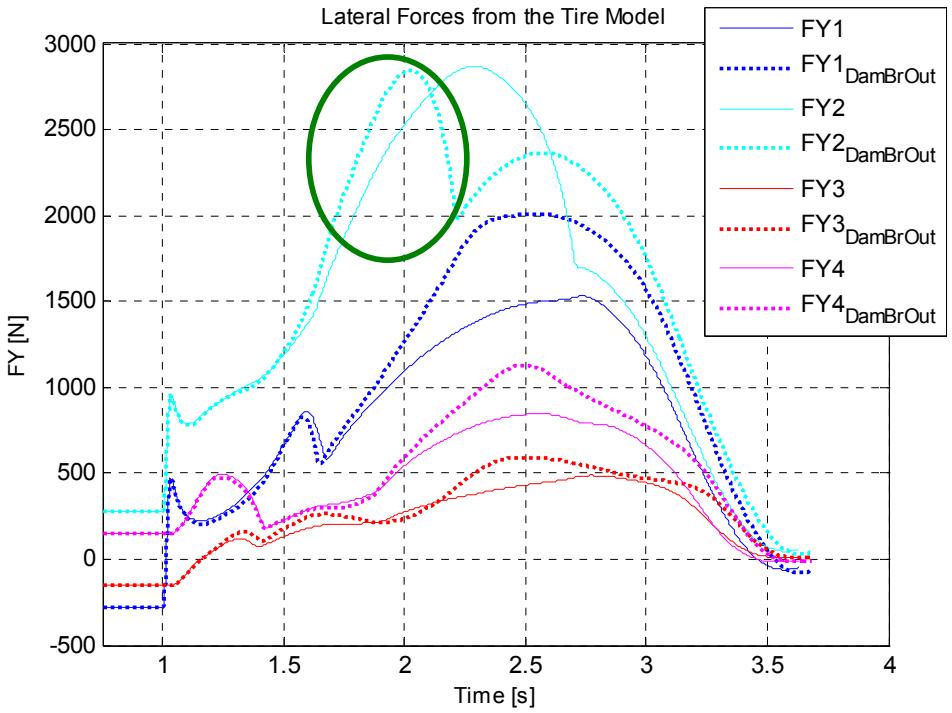

Figure 4.35 Lateral Tire Forces for Case 4-Damper 3 Failure

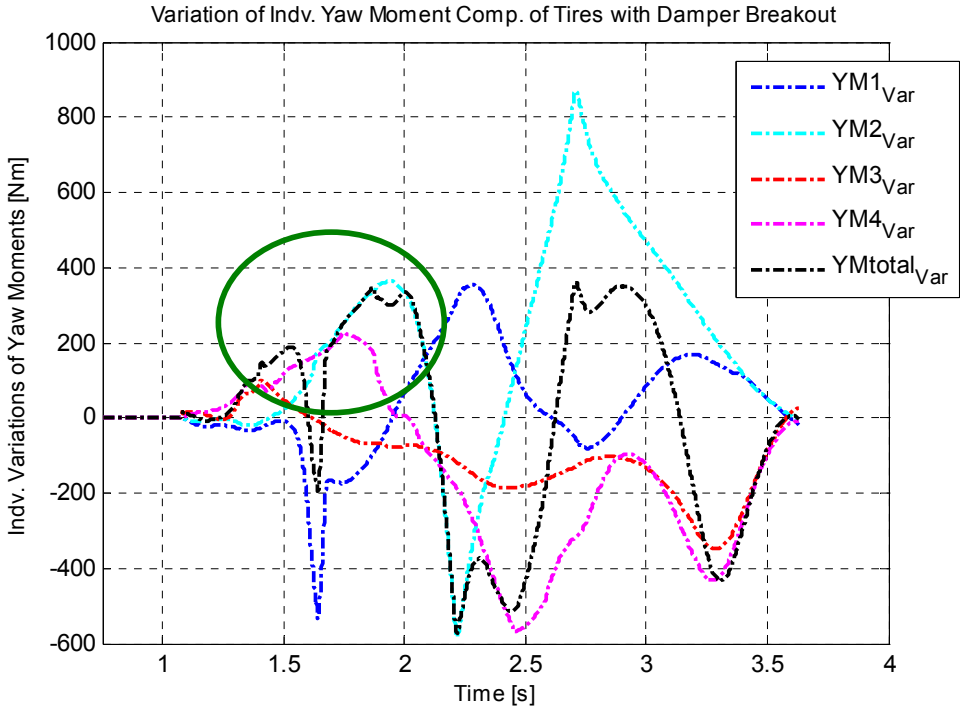

Figure 4.36Variation of Yaw moments for Case 4-Damper 3 Failure

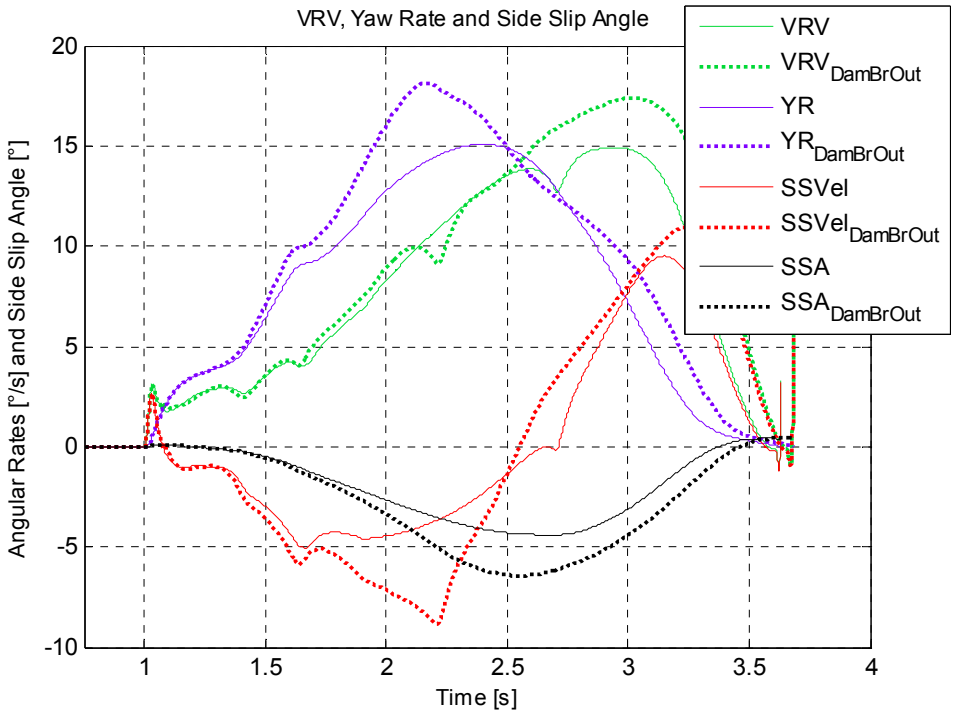

Figure 4.37 Calculation of Side Slip Angle for Case 4-Damper 3 Failure

4.2.1.5 CASE 5: CONTINUOUS SINE RESPONSE WITH BRAKING

An additional braking is implemented together with sine wave input parameters to build up a critical driving condition. In addition to steering wheel peak value, the frequency of sine input and the vehicle velocity, the braking time is also added to the input parameters. Braking time is so selected that at the end a critical and dynamic situation is obtained. The time point on which the maximum braking pressure is attained must coincide with the region where the maximum-minimum roll angle or lateral acceleration is obtained without braking, Appendix B. The maximum yaw rate is about 10.85°/s, the lateral acceleration is 2.14 m/s^2 and the maximum pitch angle is about 2°, Figure 4.38 and 4.39. The characteristic damper failure points are obtained as follows. Note that the starting point of braking is also taken as a characteristic point for damper failure.

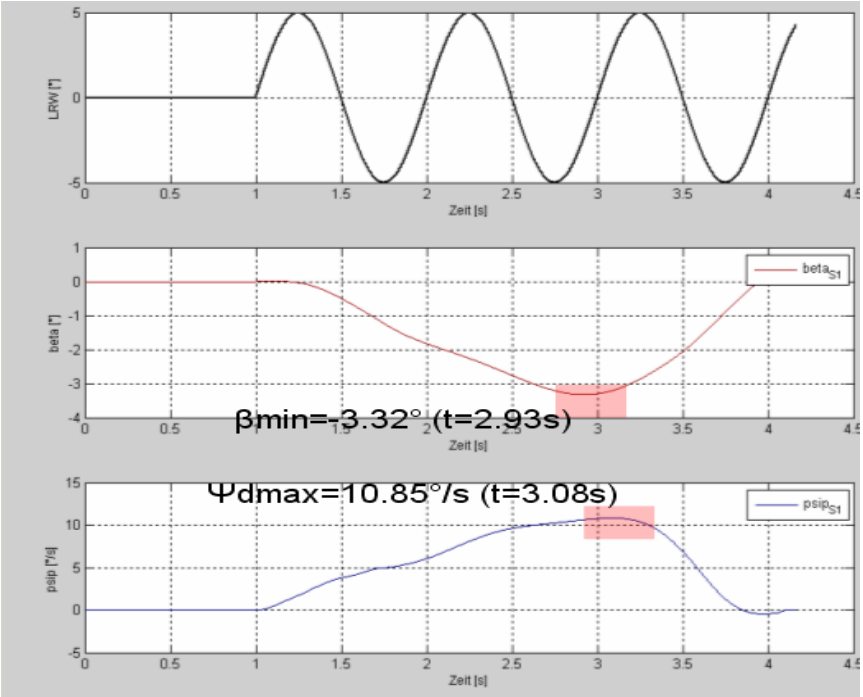

Figure 4.38 Characteristic Failure Points for Case5(a)

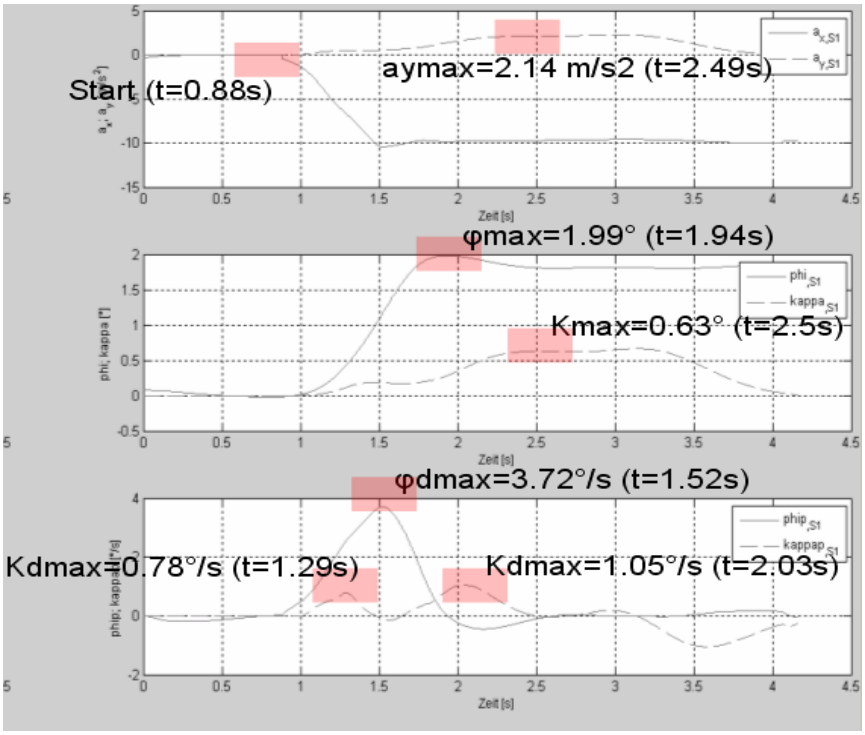

Figure 4.39 Characteristic Failure Points for Case5(b)

4.2.1.5.1 Failure of Damper 1 (worst case)

In that scenario the effect of braking force on the roll angle change with damper failure is decisive. The braking starts before the steering sine is given, therefore at the first step the body appears to lean towards tire1 more within the absence of resisting damper force, roll is smaller and pitch is greater. However, spring compression on tire 1 is not enough to exceed the vertical force without damper failure due to absence of high damper force. What makes the vertical load on tire 1 here is the tire slip angle increase due to altered dynamics. Consequently, FY1 and the total yaw moment are greater at the first step, Figure 4.44 and 4.45.

Secondly during braking and in the second region where roll angle is greater than the one without damper failure FY2 has and increase due to greater roll and consequently greater vertical load on tire 2, FX2 is at its mechanical limit. That increases the yaw moment in the second region. Figures 4.40-4.46 demonstrate the influence of the failure explained above.

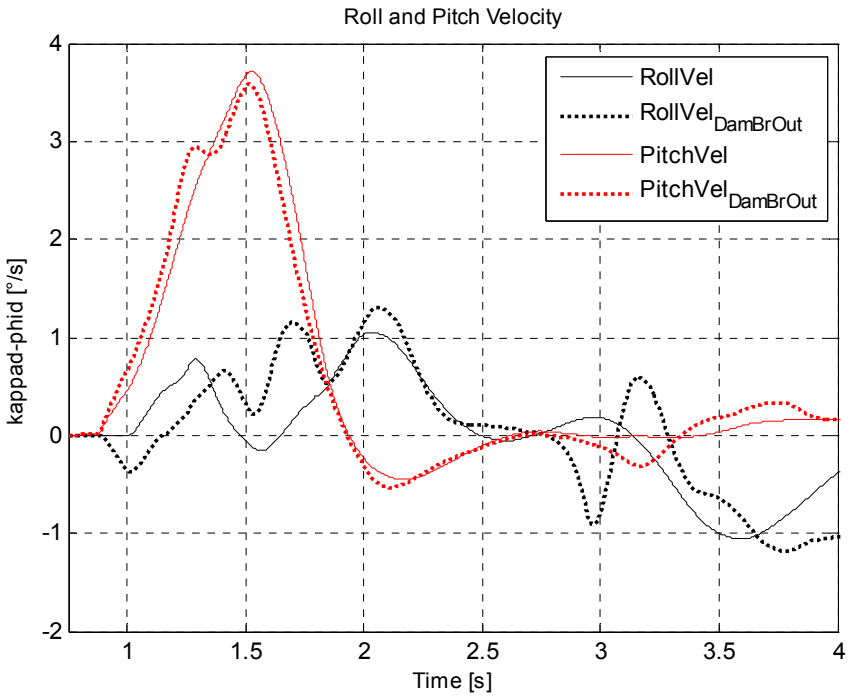

Figure 4.40 Roll and Pitch Velocities for Case 5-Damper 1 Failure

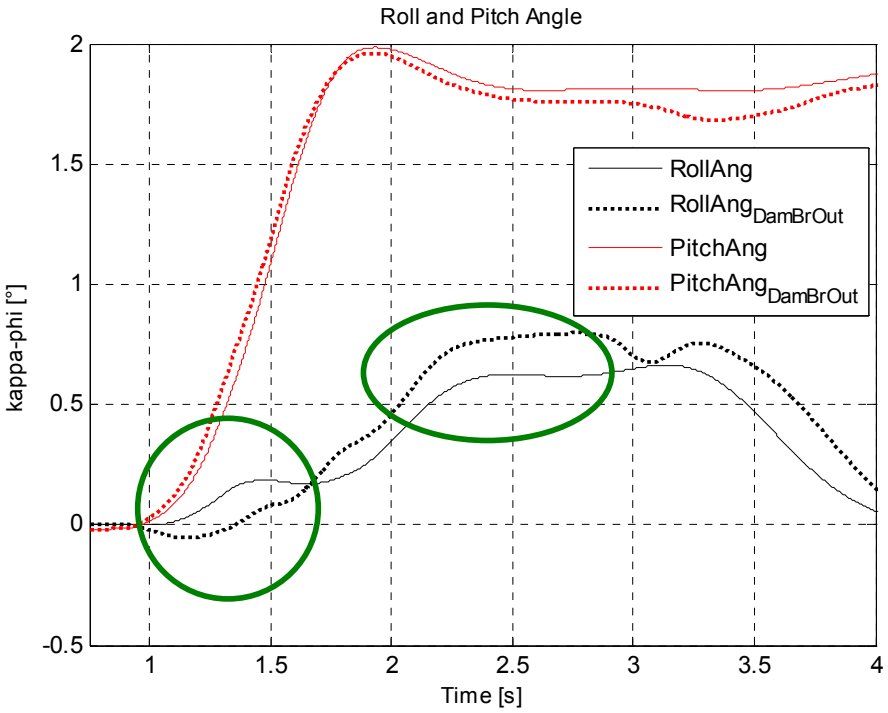

Figure 4.41 Roll and Pitch Angles for Case 5-Damper 1 Failure

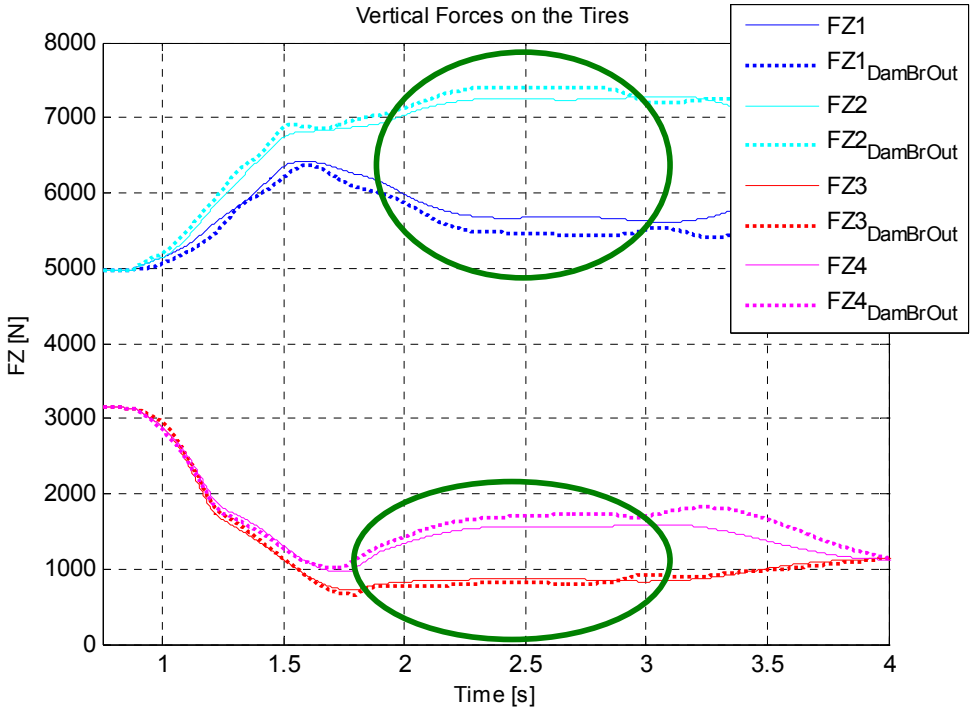

Figure 4.42 Vertical Tire Loads for Case 5-Damper 1 Failure

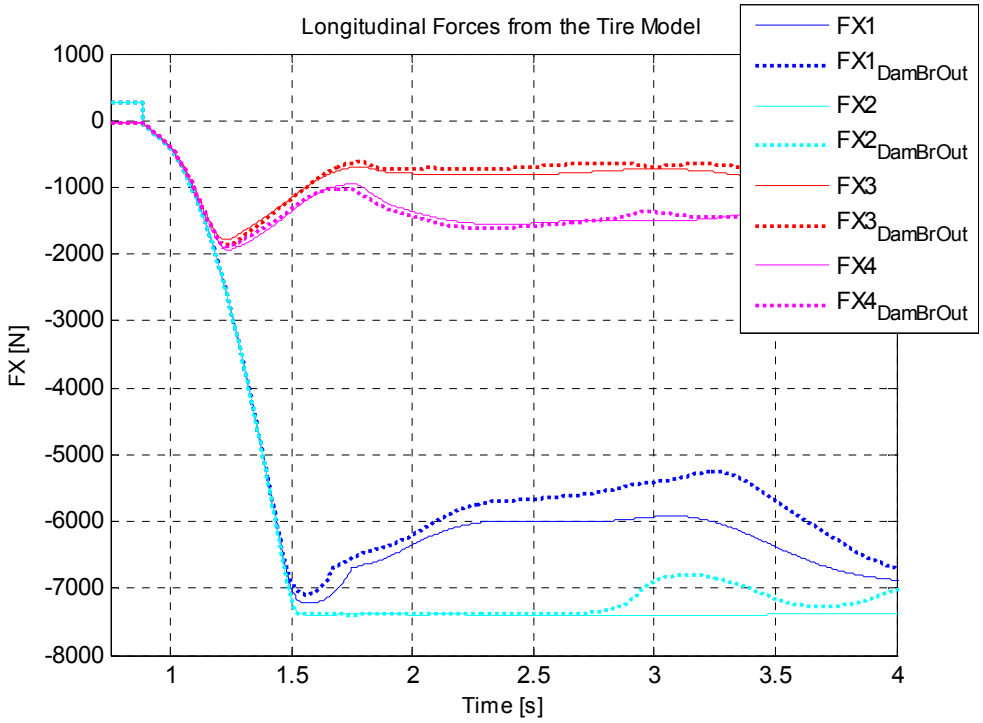

Figure 4.43 Longitudinal Tire Forces for Case 5-Damper 1 Failure

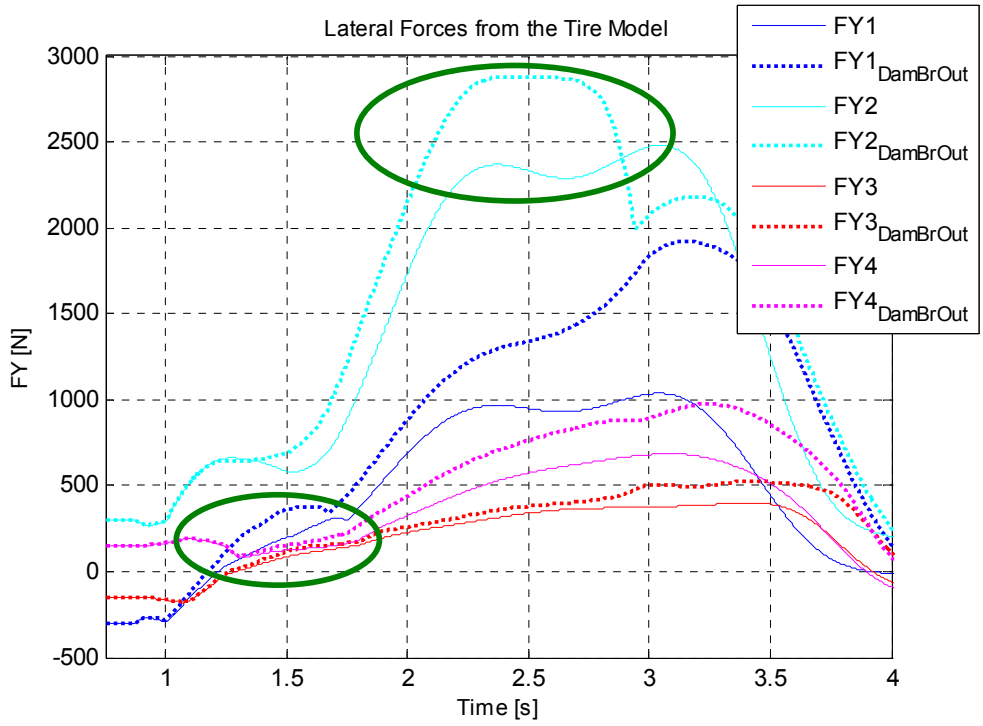

Figure 4.44 Lateral Tire Forces for Case 5-Damper 1Failure

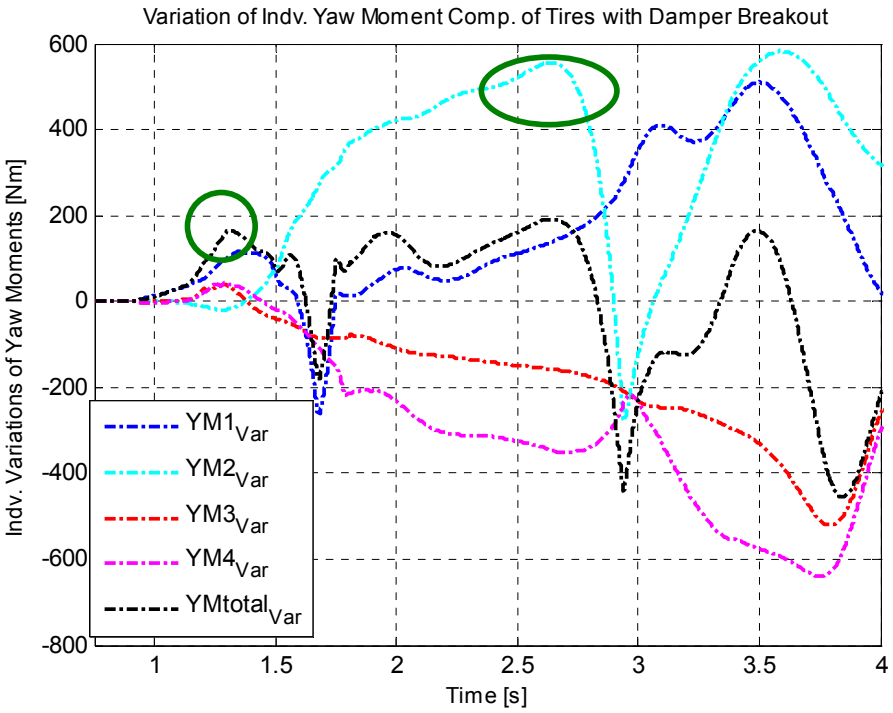

Figure 4.45 Variation of Yaw Moments for Case 5-Damper 1 Failure

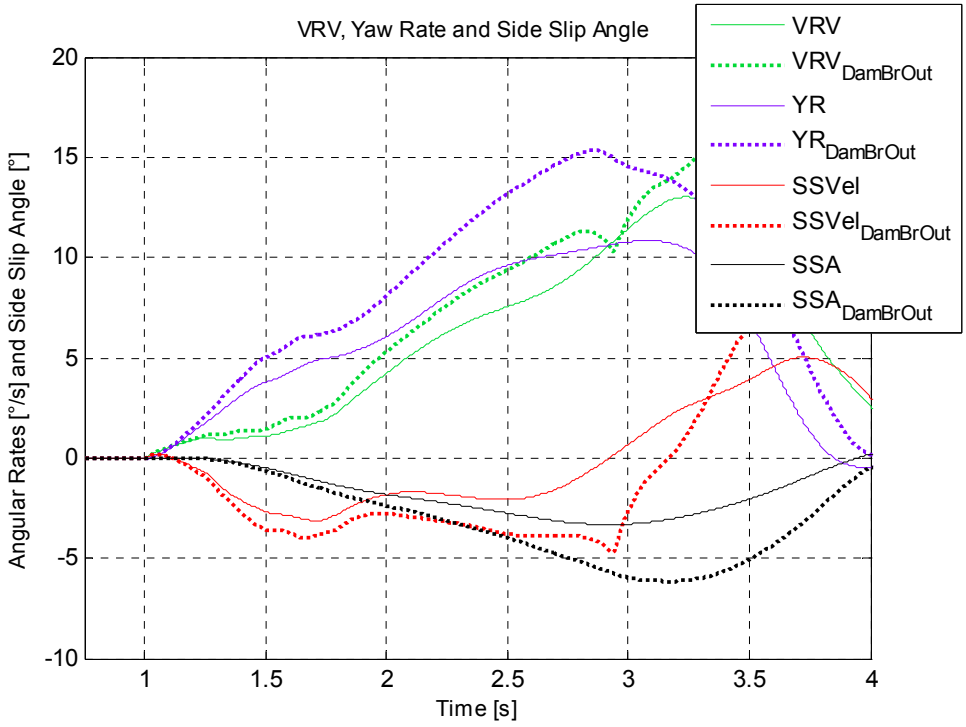

Figure 4.46 Calculation of Side Slip Angle for Case 5-Damper 1 Failure

4.2.1.6 CASE 6: SINE-DWELL RESPONSE WITH BRAKING

An additional braking is implemented together with sine-dwell input parameters to build up a critical driving condition. In addition to steering wheel peak value, the frequency, the dwell time and the vehicle velocity, the braking time are also added to the input parameters. Similar to sine wave input, the time point on which the maximum braking pressure is attained must coincide with the region where the maximum-minimum roll angle or lateral acceleration is obtained without braking, Appendix B. In this case, the maximum braking force is to be attained in the dwell region where the *minimum* lateral acceleration and the roll angle are obtained. The minimum yaw rate is about -14.8°/s, the lateral acceleration is -2.66 m/s^2 and the maximum pitch angle is about 2°, Figure 4.47 and 4.48. The characteristic damper failure points are obtained as follows:

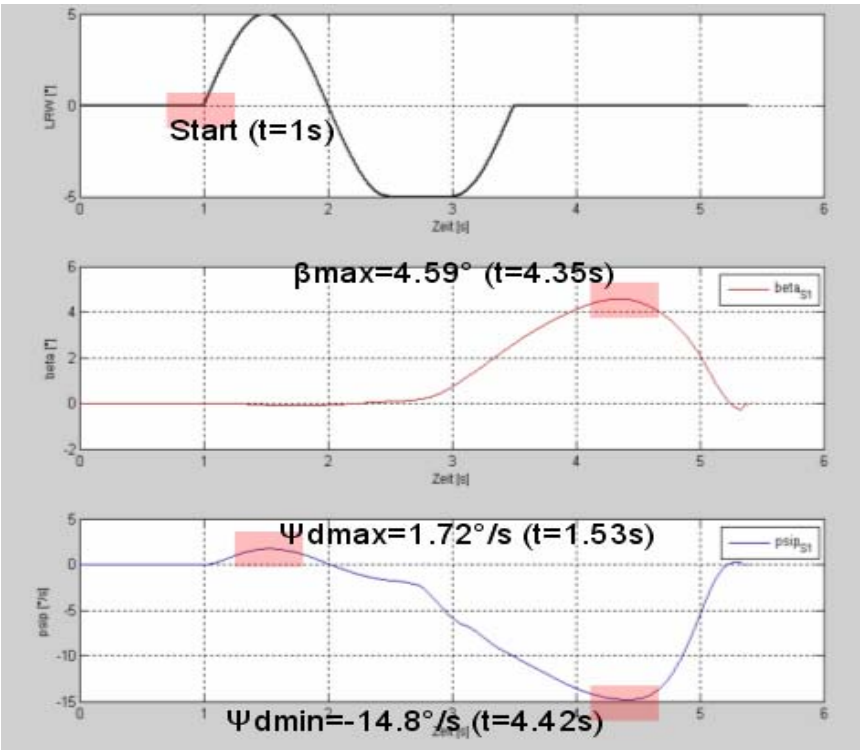

Figure 4.47 Characteristic Failure Points for Case6(a)

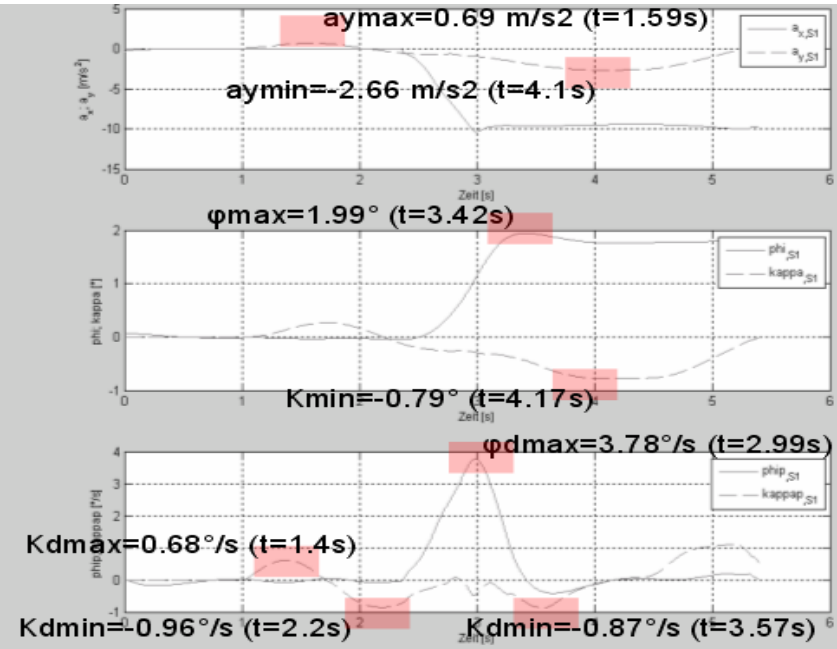

Figure 4.48 Characteristic Failure Points for Case6(b)

4.2.1.6.1 Failure of Damper 4 (worst case)

$\dot{\kappa}_{\min}$ is the most critical point for damper 4 failure . With a damper failure on tire 4, the body motions are increased in the most rapid manner. This case is completely similar to the case of damper failure 3 in step steer response with braking, with a difference that the inner tire on the rear axle is in this case 3 instead of 4, considering that the vehicle yaw rotation is in the other way in this case. So with the damper failure at that point, the last characteristic point before brake pitch starts, the body makes a smaller roll and greater pitch through braking due to absence of damper force on tire 4, which varies the vertical loads on 1, 2 and 4 so that the tire forces on these tires ensure a greater yaw moment, Figure 4.51 and 4.54. Here the decisive variation is on FY1 due to increasing FZ1 since FX1 is already reached to its mechanical limit. Note that in this case the outer tire on front axle is rather 1 but not 2, which was the decisive for some previous cases. Figures 4.49-4.55 demonstrate the influence of the failure explained above.

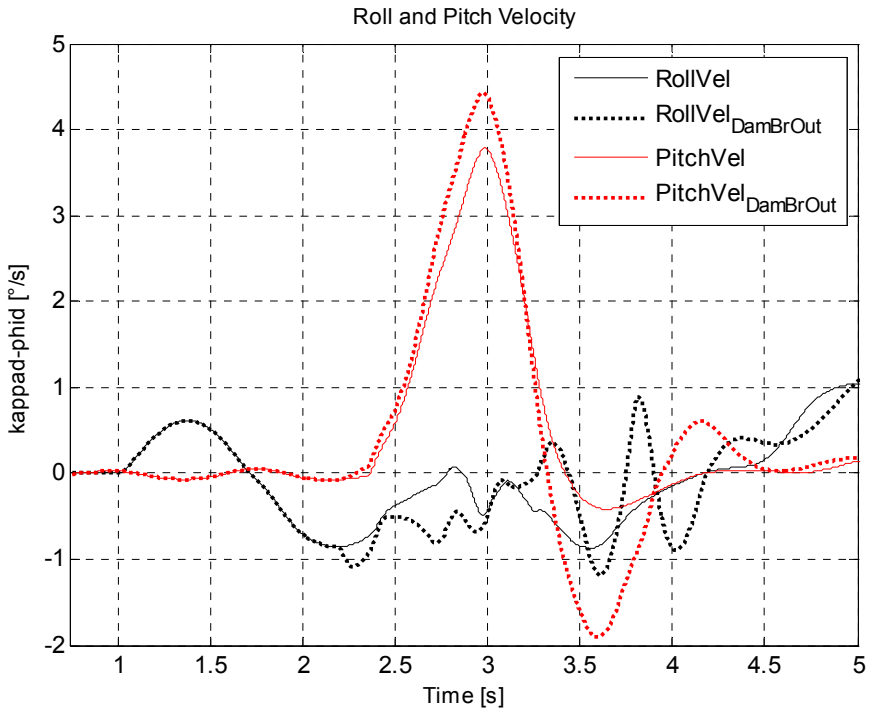

Figure 4.49 Roll and Pitch Velocities for Case 6-Damper 4 Failure

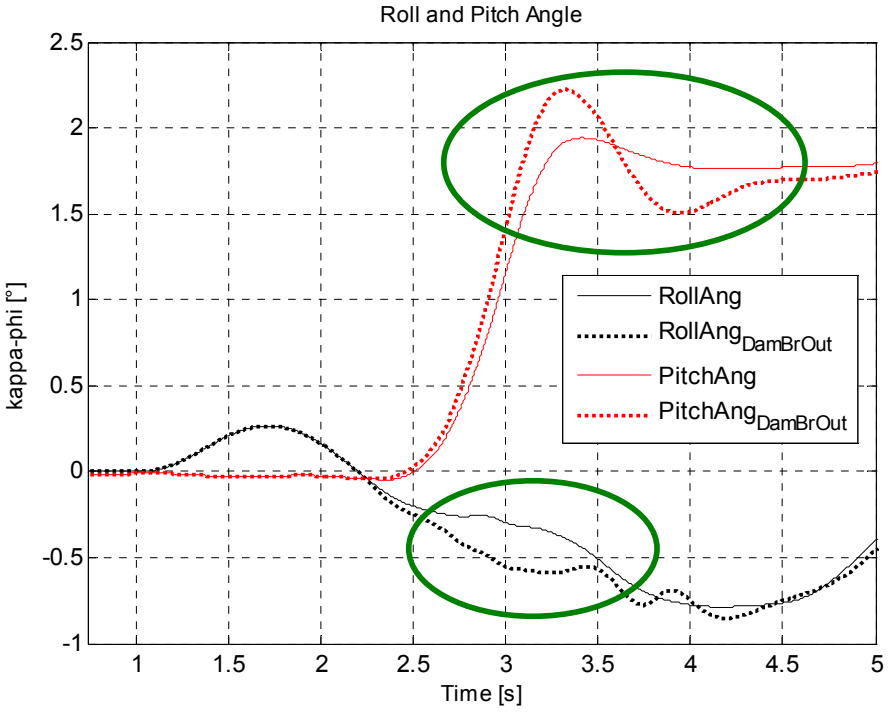

Figure 4.50 Roll and Pitch Angles for Case 6-Damper 4 Failure

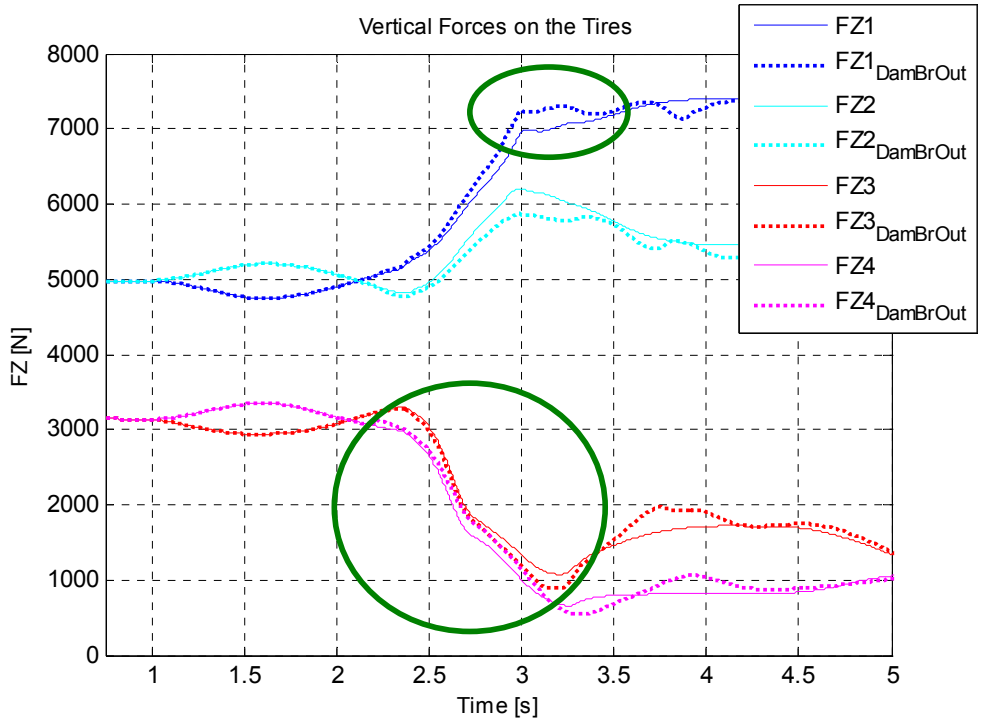

Figure 4.51 Vertical Tire Loads for Case 6-Damper 4 Failure

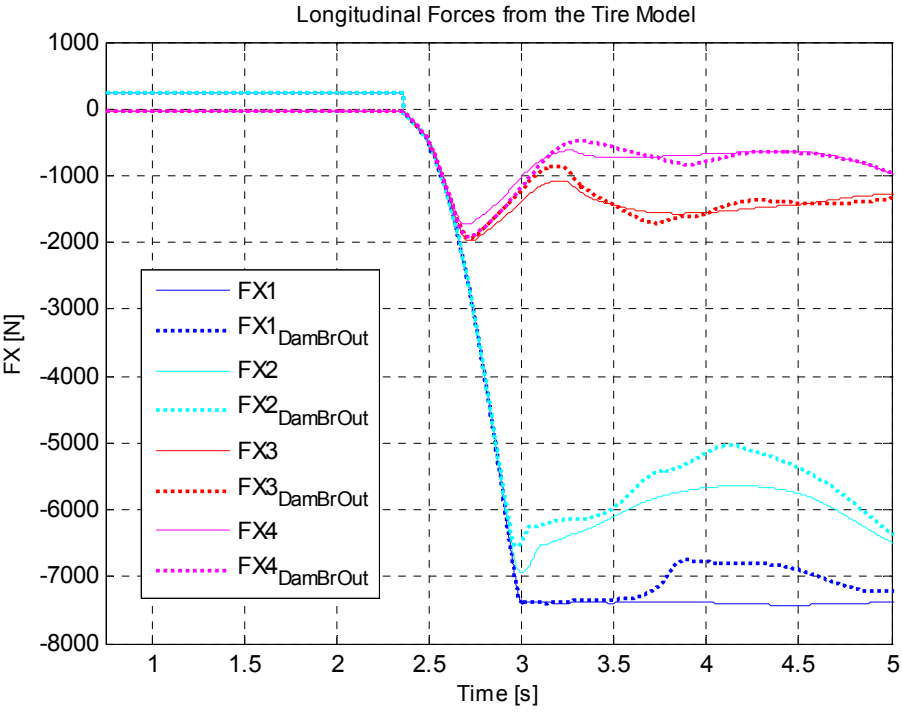

Figure 4.52 Longitudinal Tire Forces for Case 6-Damper 4 Failure

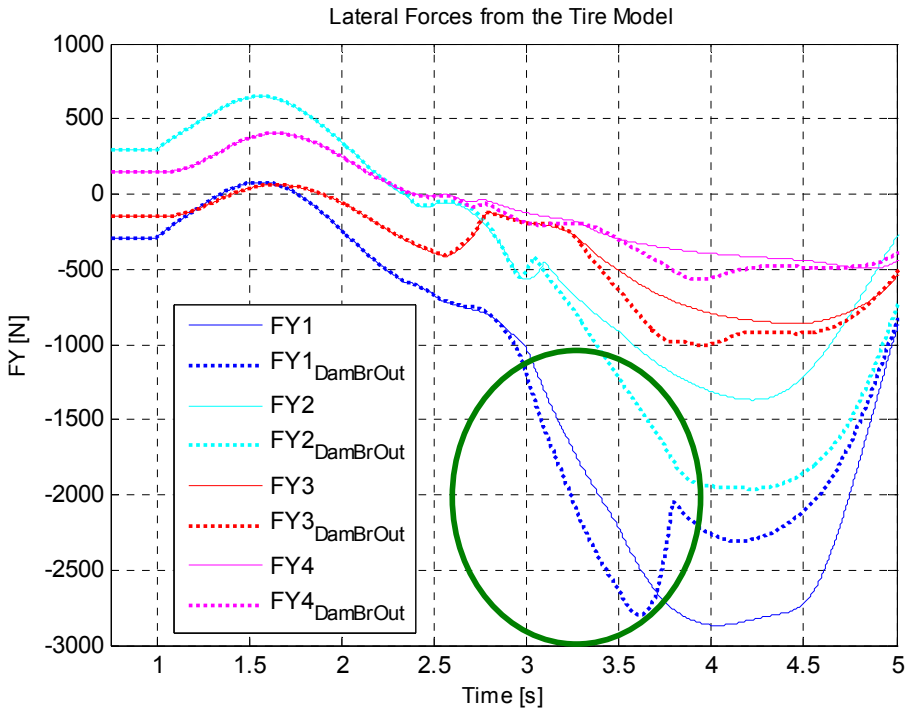

Figure 4.53 Lateral Tire Forces for Case 6-Damper 4 Failure

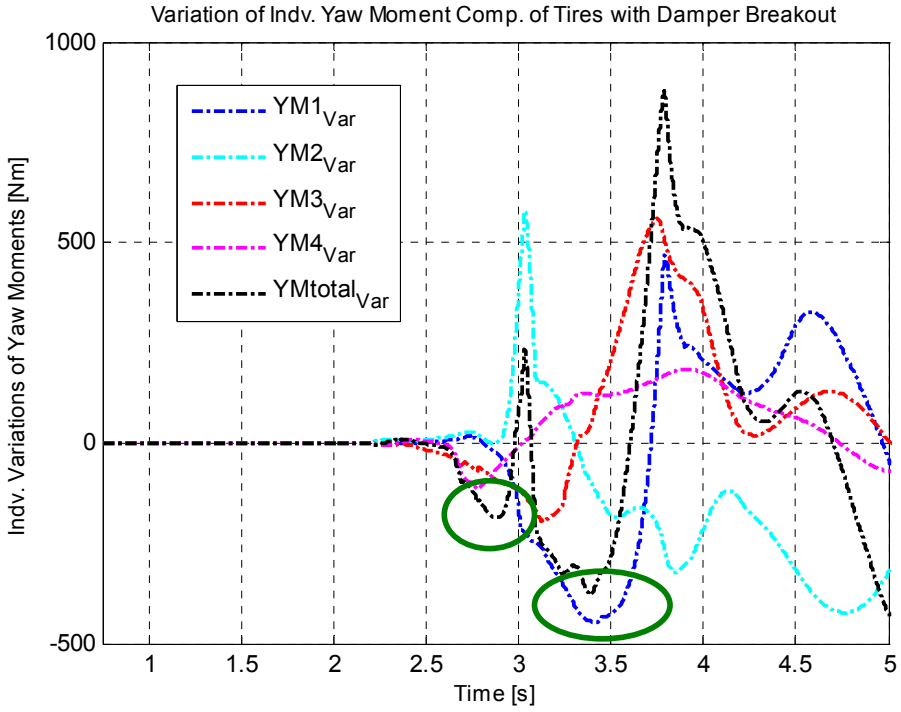

Figure 4.54 Variation of Yaw Moments for Case 6-Damper 4 Failure

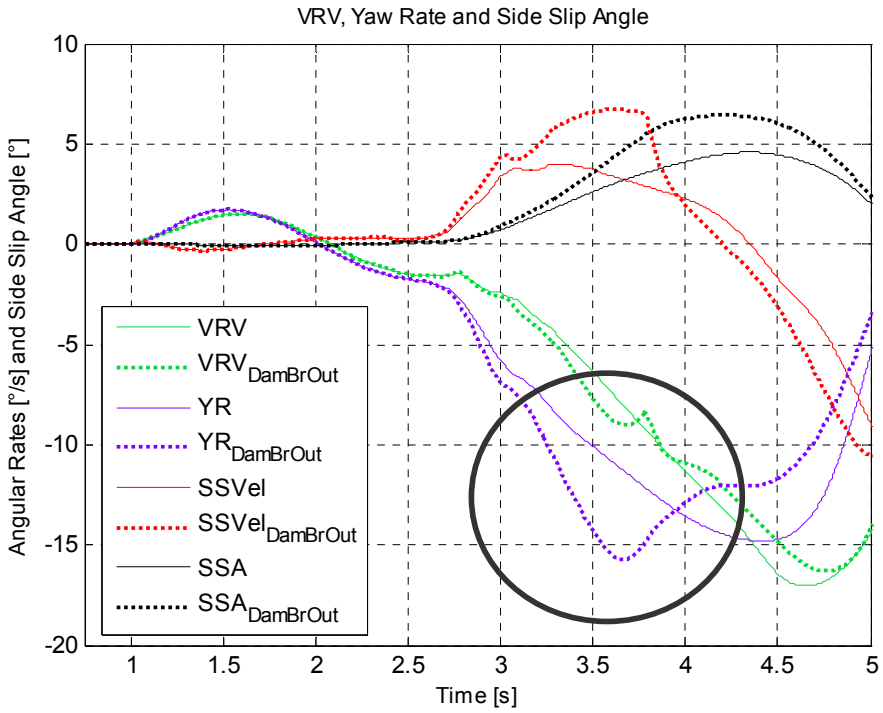

Figure 4.55 Calculation of Side Slip Angle for Case 6-Damper 4 Failure

4.2.2 ELECTRICAL FAILURE ANALYSIS

Electrical damper failure is the type which may be experienced on an electrically driven damper. Orifice width is adjusted with the help of electrical power in these types of dampers. When the electrical machinery fails, the orifice gap switches to a nearly closed state, which as a results leads to higher damping coefficient. Higher damper forces produced, consequently lead to harder damping. In this part the effects of electrical damper failure is examined with the help of the Simulink model, on which the damper characteristics are switched to a harder set on the damper failure points. In order to examine the results obviously, in those simulations damper characteristic curve is switched from the half of the damping curve of the original vehicle data to a harder one with factor 1.5 of this damping curve at the failure point.

The maneuvers used in the electrical failure analysis are the same as introduced in Table 4.1, but it should be noted that the case numbers are different since the scenarios are completely of different type. In these analyses the cases are defined such that case numbers are obtained adding 6 to the ones belonging to the previous analyses, i.e. Case **7** belongs to Step Steer Response without braking since 7-6=1.

The original responses (responses without damper failure) obtained in these analyses are also similar to the ones for the previous analyses since the maneuvers are the same. However, the values like yaw velocity maximum, side slip angle maximum etc., may slightly differ due to a slight difference of parametrization in original maneuvers. It should be reminded that the original maneuvers in these analyses have the damper characteristics half of the ones in the previous analyses. Nevertheless, the original responses in this case give approximate tendencies and the same order of the characteristic points during the maneuver. Therefore, the characteristic failure points on the original maneuver responses are not repeated in this part.

4.2.2.1 CASE 7: STEP STEER RESPONSE

4.2.2.1.1 Failure of Damper 4 (worst case)

The most critical situation in damper4 failure is obtained when the damper fails at the starting point of steering input. This is the most critical point since the entire maneuver is influenced by the failed damper. The body roll and pitch motions reveals a more damped tendency in that the body makes a higher fore motion and slower roll, the tensile force on tire 4 is greater in the region of settling pitch. This results in the variations of vertical loads of tires 1, 3 and 4, but in this case the decisive ones are the reductions of vertical loads on the rear axle (tire 3 and 4) and consequently the lateral tire forces, Figure 4.58 and 4.59. As a result, the total yaw moment is higher also the resulting side slip angle. Figures 4.56-4.61 demonstrate the influence of the failure explained above.

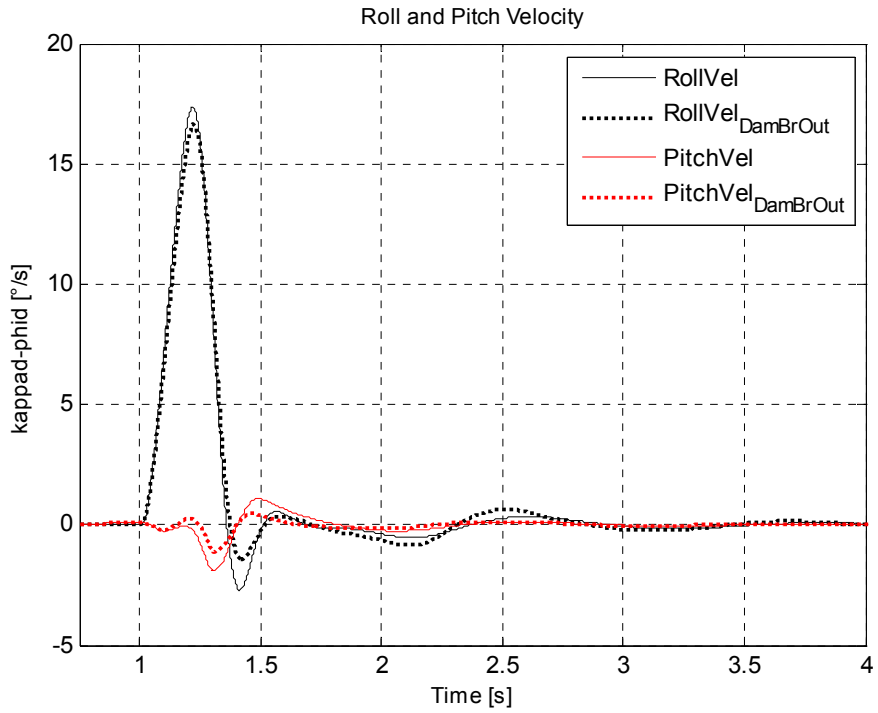

Figure 4.56 Roll and Pitch Velocities for Case 7-Damper 4 Failure

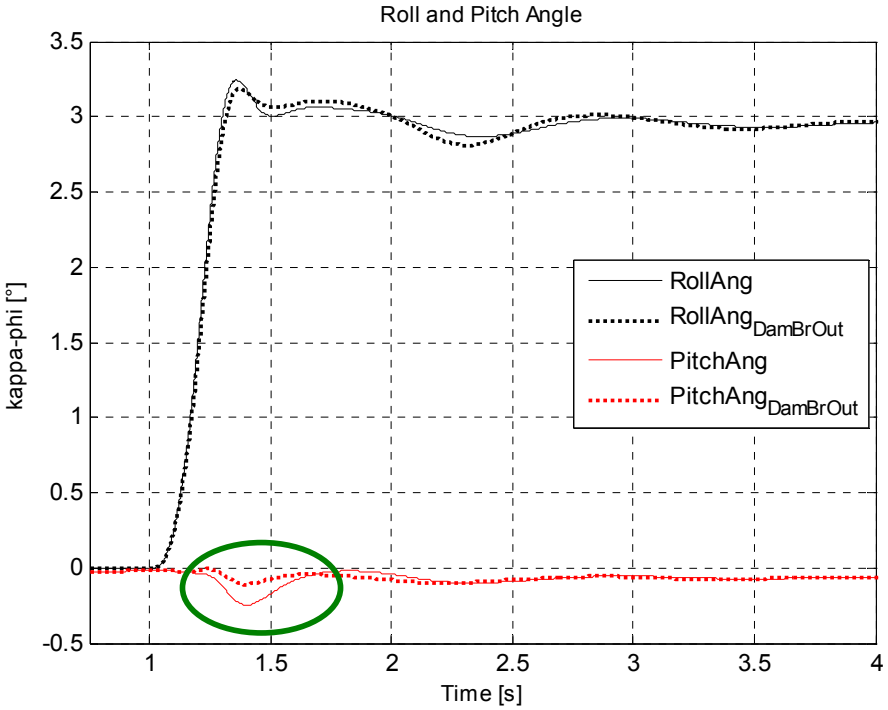

Figure 4.57 Roll and Pitch Angles for Case 7- Damper 4 Failure

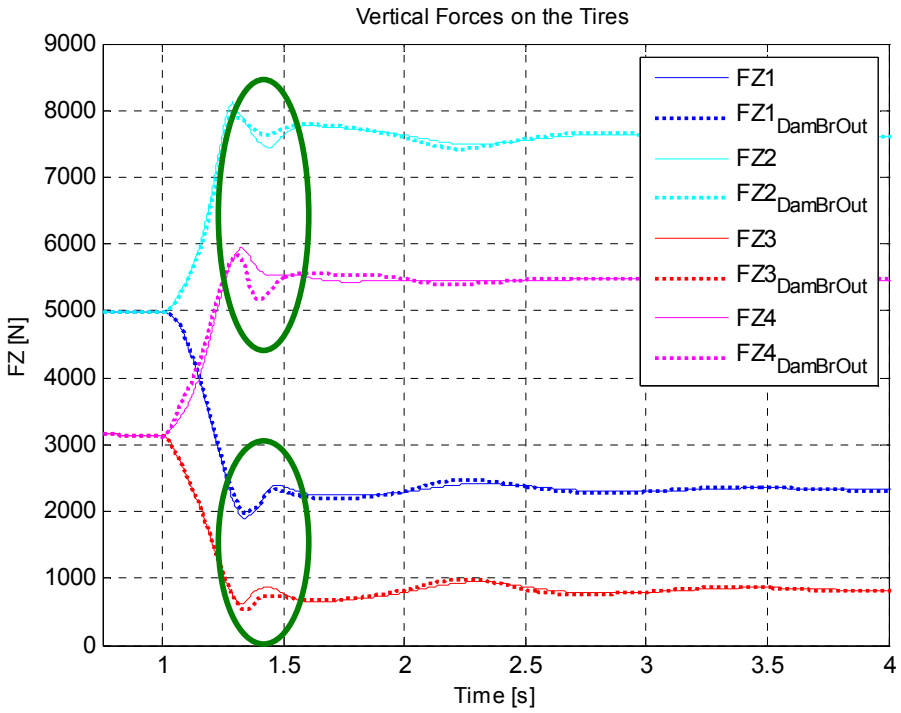

Figure 4.58 Vertical Tire Loads for Case 7- Damper 4 Failure

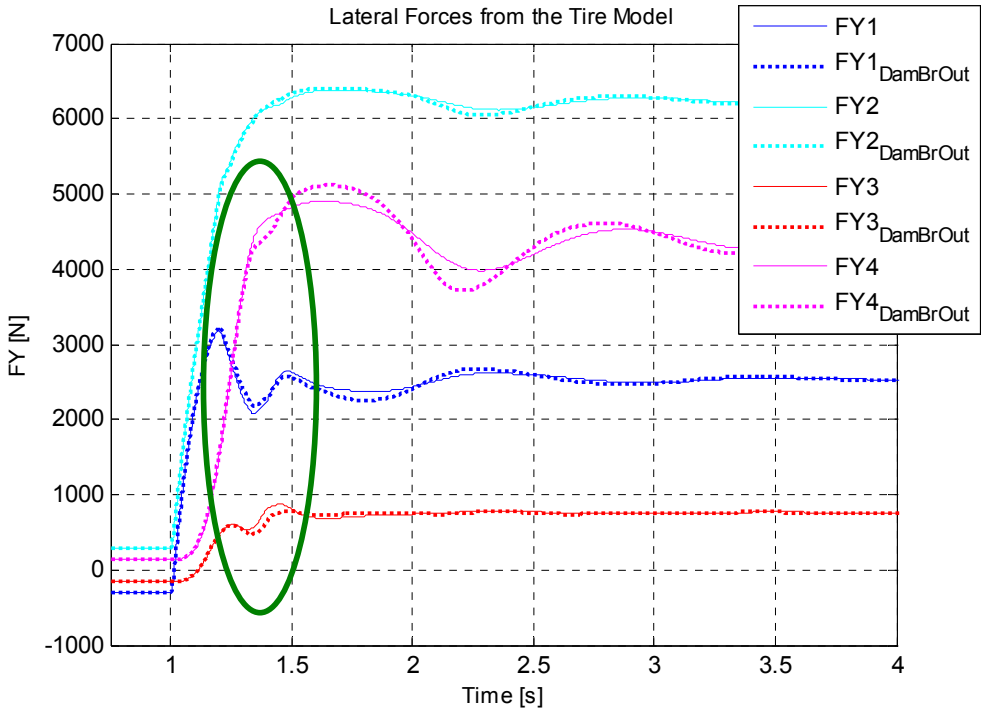

Figure 4.59 Lateral Tire Forces for Case 7- Damper 4 Failure

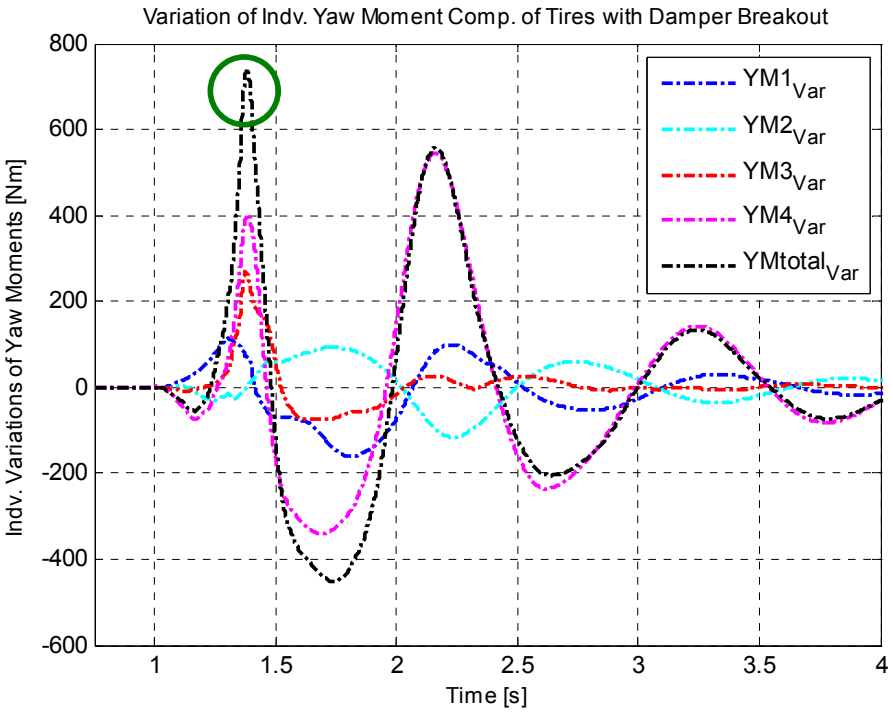

Figure 4.60 Variation of yaw Moments for Case 7- Damper 4 Failure

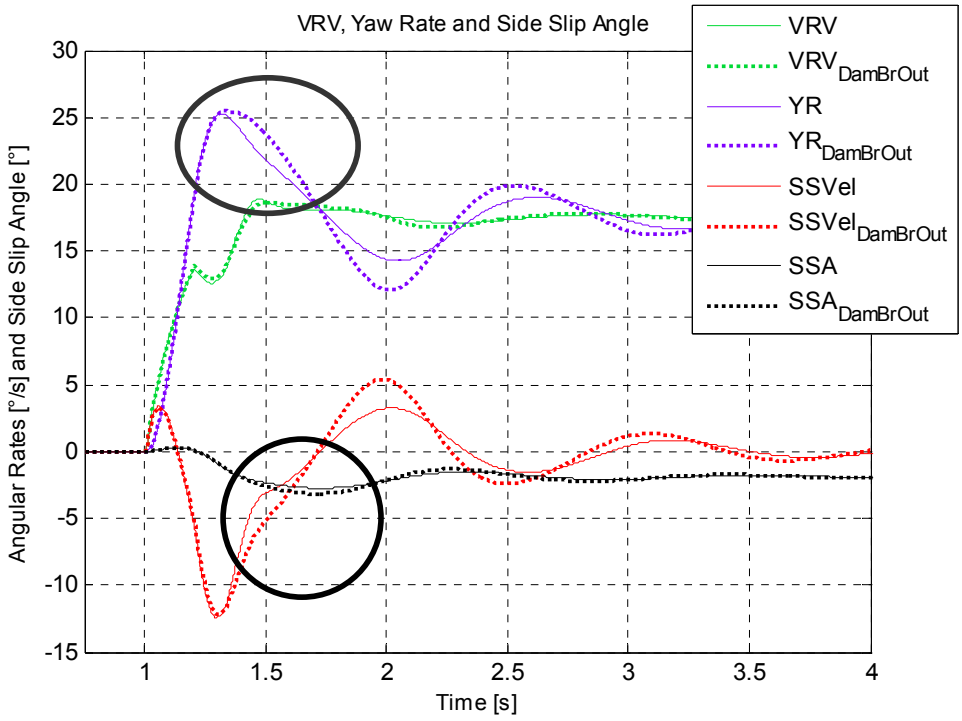

Figure 4.61 Calculation of Side Slip Angle for Case 7- Damper 4 Failure

4.2.2.2 CASE 8: CONTINUOUS SINE RESPONSE

4.2.2.2.1 Failure of Damper 4 (worst case)

In this maneuver, the settling pitch region is affected from a damper failure on the side of tire 4 at the starting point. This is the most critical characteristic point since the entire dynamics of the maneuver is influenced. With the damper failure, higher damper force on tire 4 pulls the body towards itself in the settling region, the region where the second half sine cycle is already finished and the body makes a settling pitching towards the front axle. It results in smaller roll and pitching, Figure 4.63. Vertical loads are consequently so oriented that at the end total yaw moment rises up. It should be noted that, here the decrease in the vertical load of tire 4 has the greatest influence on dynamics. The reason behind that unexpected rise despite the lean towards tire 4 is the relatively high damper force which exerts an extensional force on the tire and decreases the vertical load. Figures 4.62-4.67 demonstrate the influence of the failure explained above.

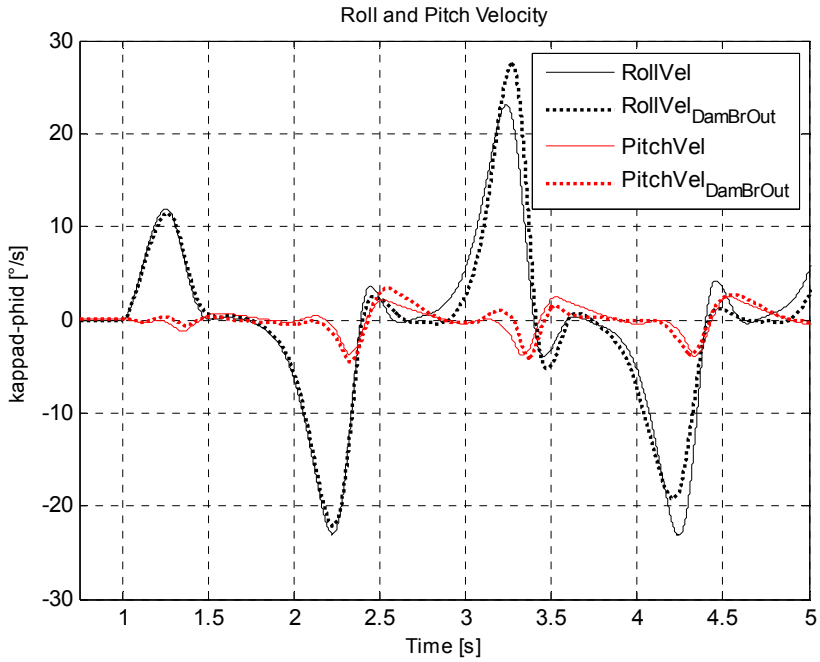

Figure 4.62 Roll and Pitch Velocities for Case 8- Damper 4 Failure

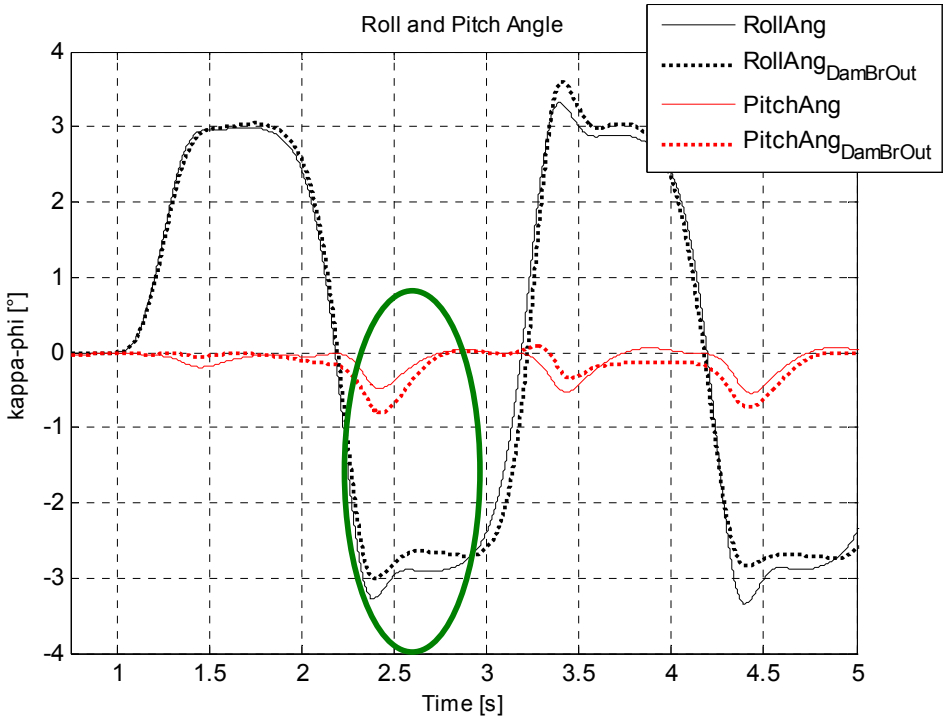

Figure 4.63 Roll and Pitch Angles for Case 8- Damper 4 Failure

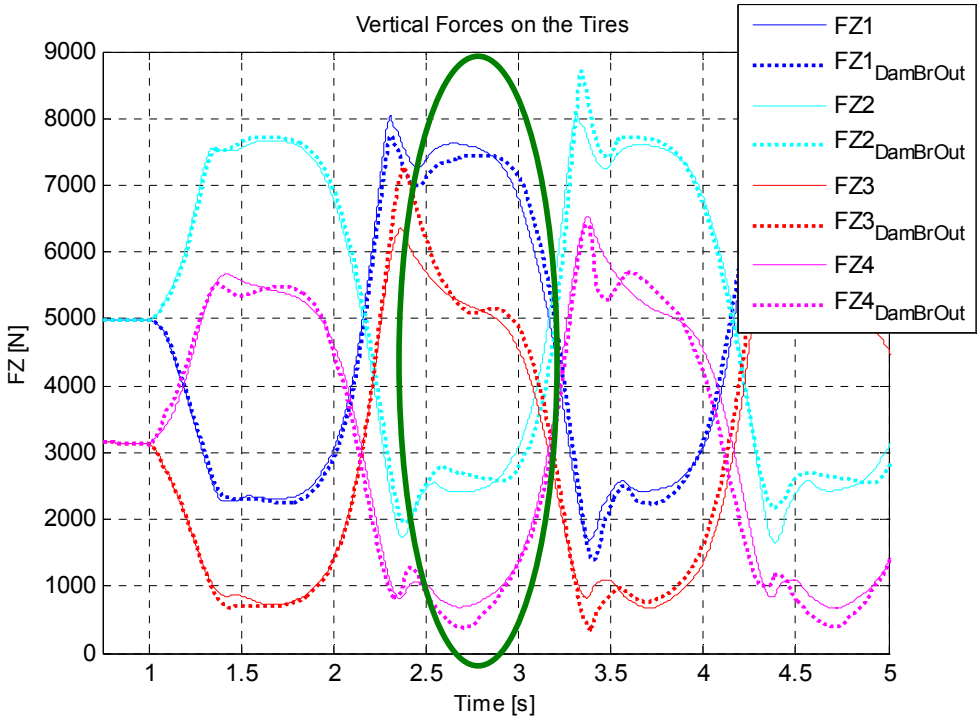

Figure 4.64 Vertical Tire Loads for Case 8- Damper 4 Failure

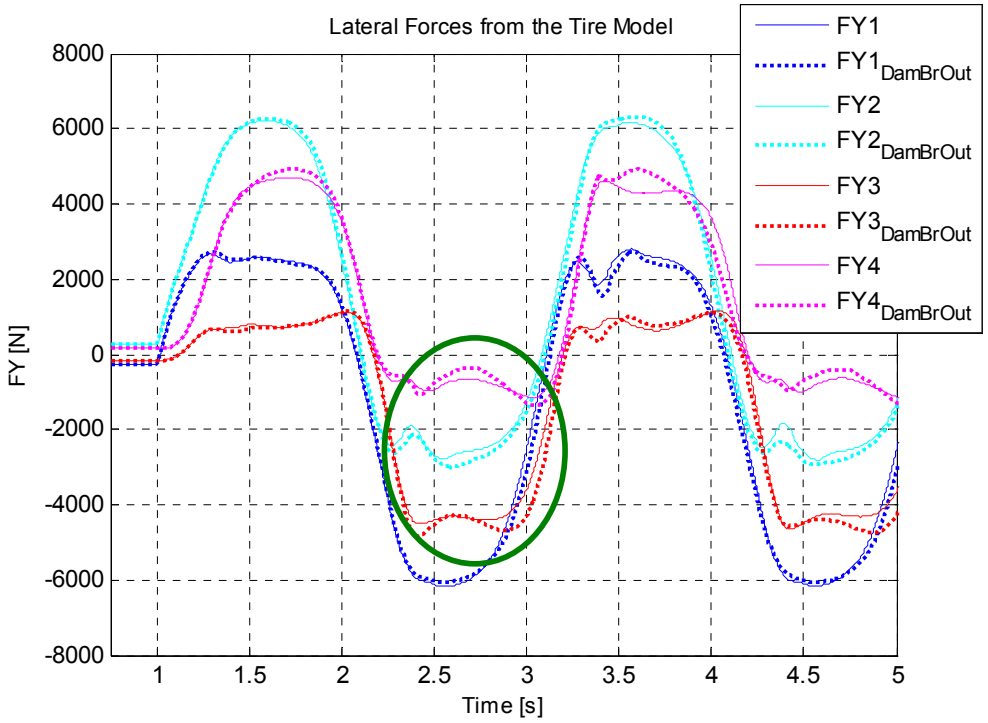

Figure 4.65 Lateral Tire Forces for Case 8- Damper 4 Failure

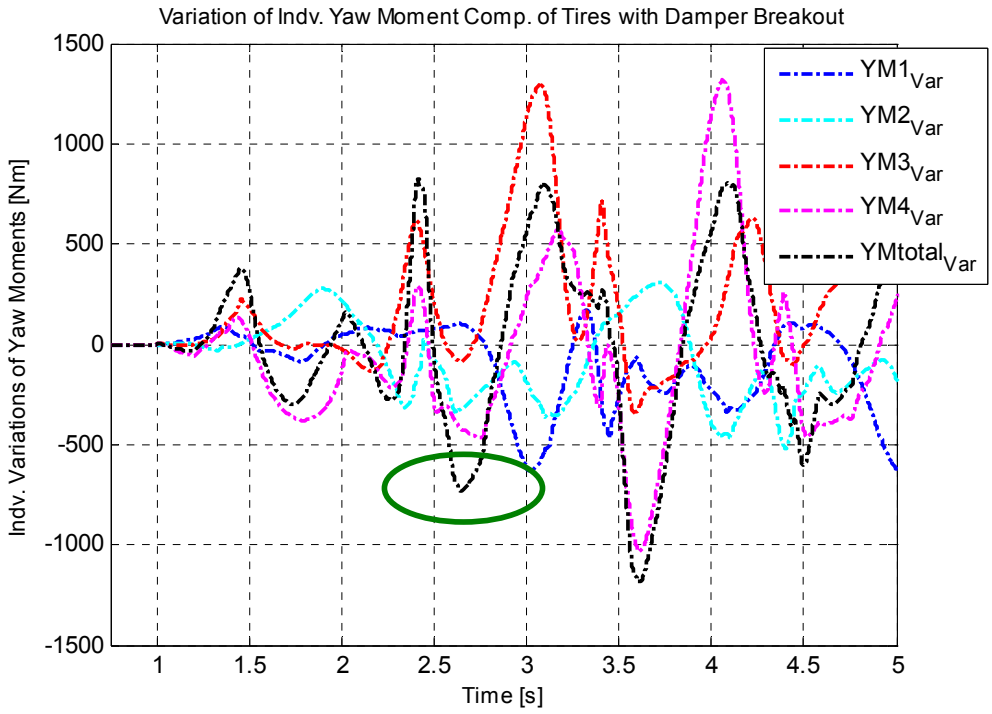

Figure 4.66 Variation of Yaw Moments for Case 8- Damper 4 Failure

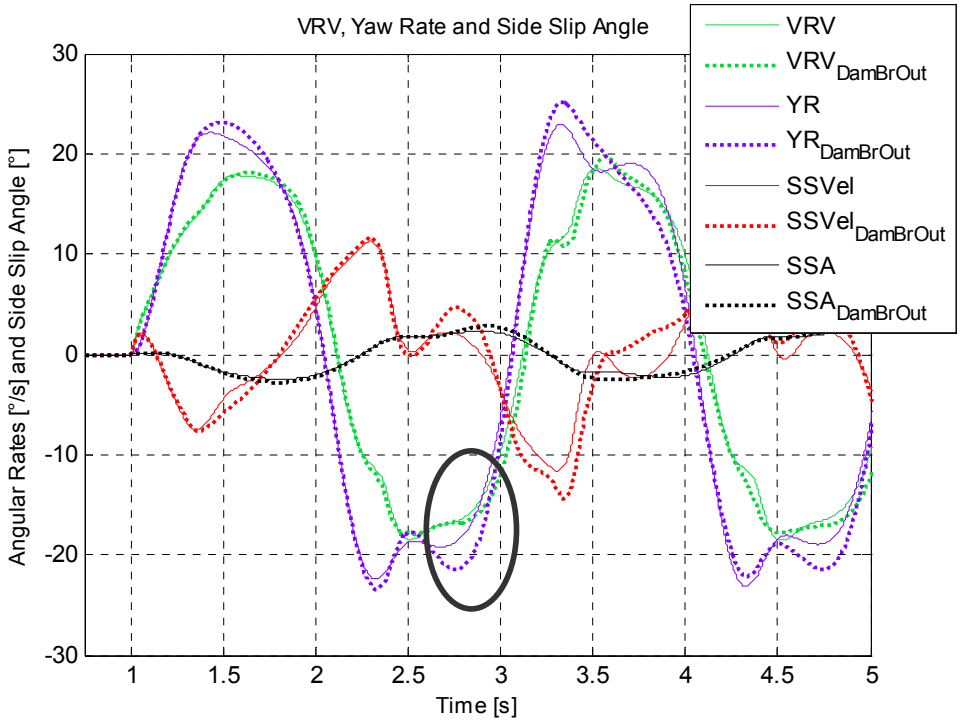

Figure 4.67 Calculation of Side Slip Angle for Case 8- Damper 4 Failure

4.2.2.3 CASE 9: SINE-DWELL RESPONSE

4.2.2.3.1 Failure of Damper 4 (worst case)

The most critical damper failure scenario for this maneuver comes out to be the damper failure of tire 4 at characteristic failure point starting time of steering input. The explanation and the physical interpretation is the same with Case 8, since both maneuvers are similar to each other concerning the first 2 half cycles. The plots demonstrating the failure scenario are given in Figures 4.68-4.73.

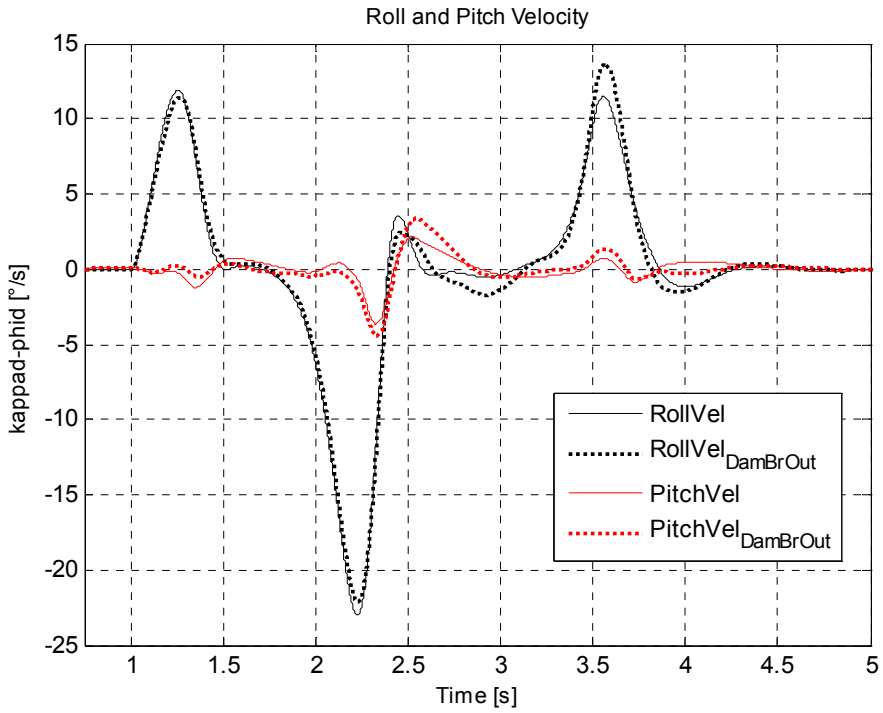

Figure 4.68 Roll and Pitch Velocities for Case 9- Damper 4 Failure

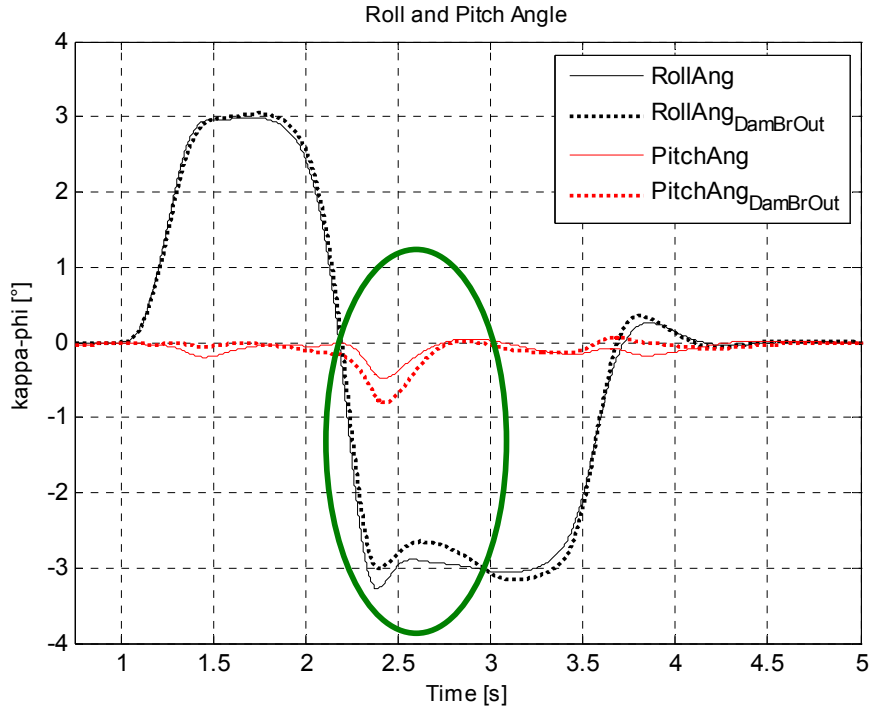

Figure 4.69 Roll and Pitch Angles for Case 9- Damper 4 Failure

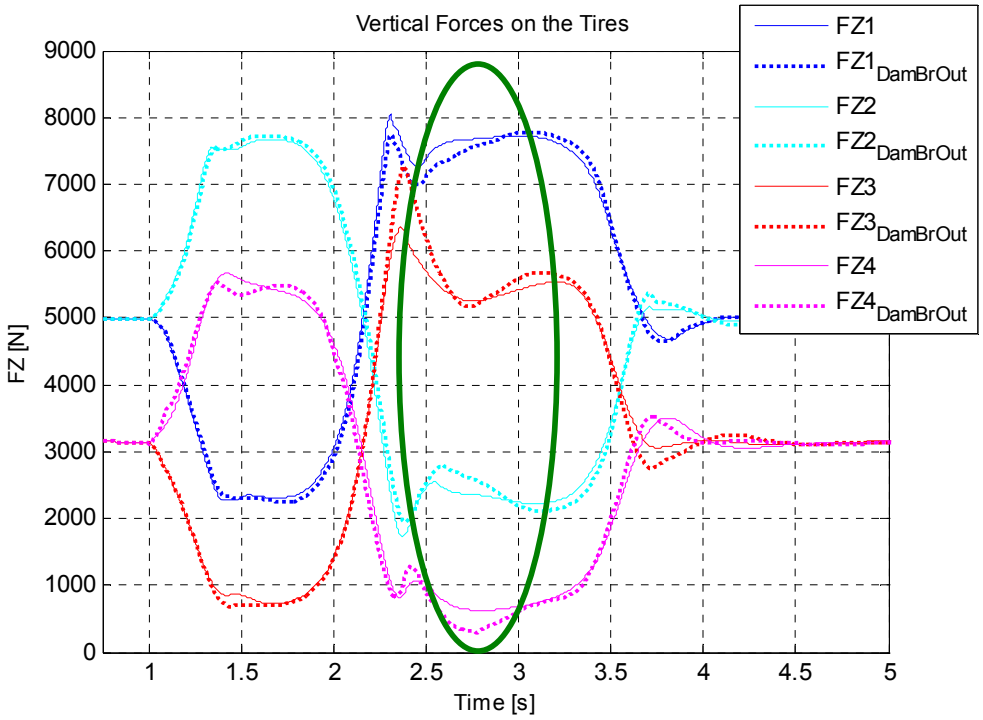

Figure 4.70 Vertical Tire Loads for Case 9- Damper 4 Failure

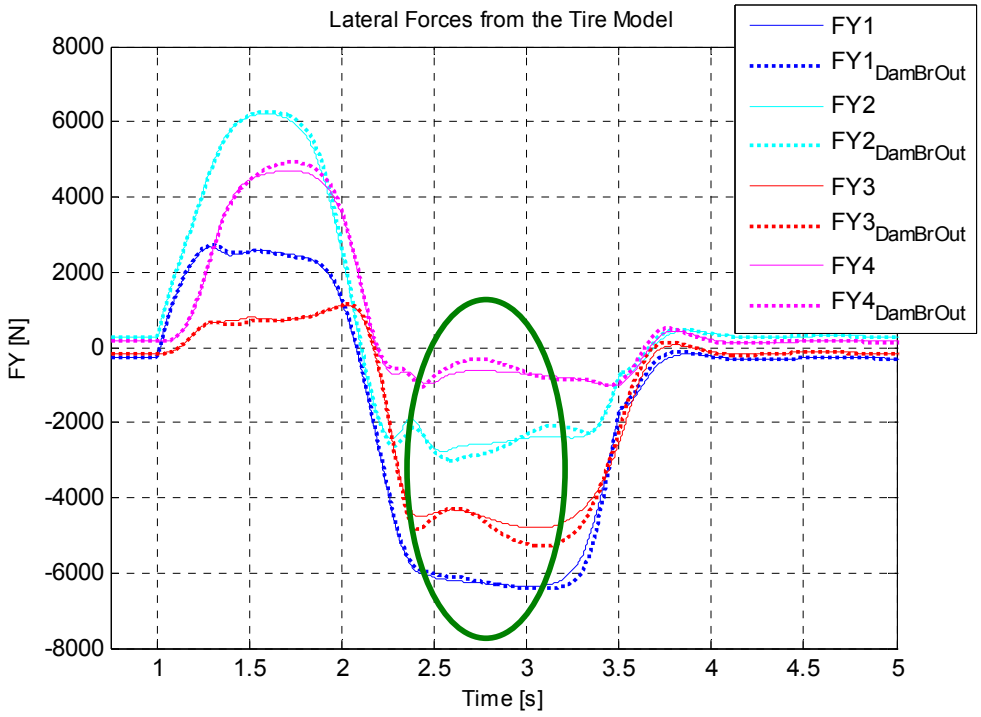

Figure 4.71 Lateral Tire Forces for Case 9- Damper 4 Failure

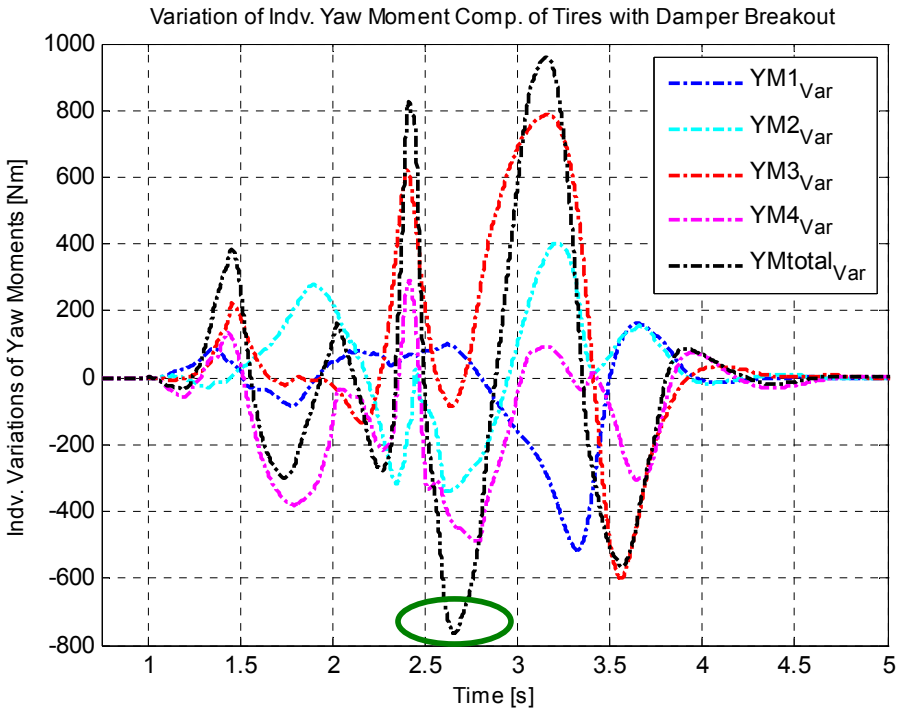

Figure 4.72 Variation of Yaw Moments for Case 9- Damper 4 Failure

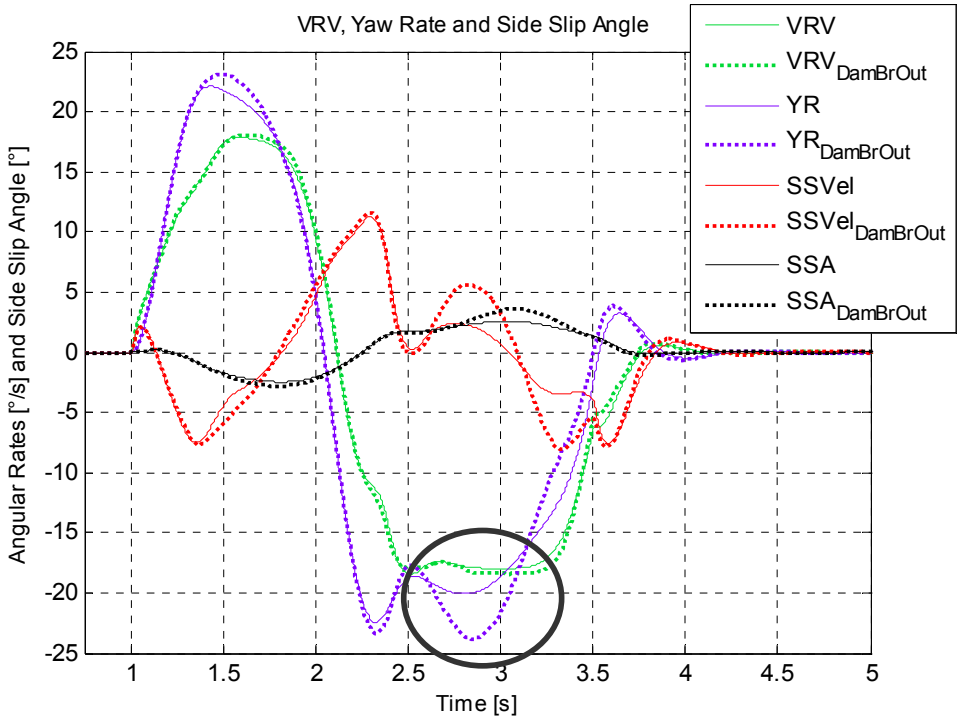

Figure 4.73 Calculation of Side Slip Angle for Case 9- Damper 4 Failure

4.2.2.4 CASE 10: STEP STEER RESPONSE WITH BRAKING

4.2.2.4.1 Failure of Damper 2 (worst case)

With a damper failure on tire 2 at the starting point of steering the responses become the most critical. A damper failure on tire 2 gives a harsher damping which means a greater damper force on the tire causing higher vertical loads throughout the entire maneuver. Since FX2 has attained a mechanical maximum, FY2 rises up consequently, which increases the total yaw moment and the side slip angle.

Due to the failure the body motions are also so effected that the body makes a lower roll and pitch and the other tire loads are also affected (i.e. FZ3 and FX3 are higher whereas FZ4 and FX4 are lower making a slight additional increase on yaw moment) which is an additional influence towards a more instable behaviour. Figures 4.74-4.80 demonstrate the influence of the failure explained above.

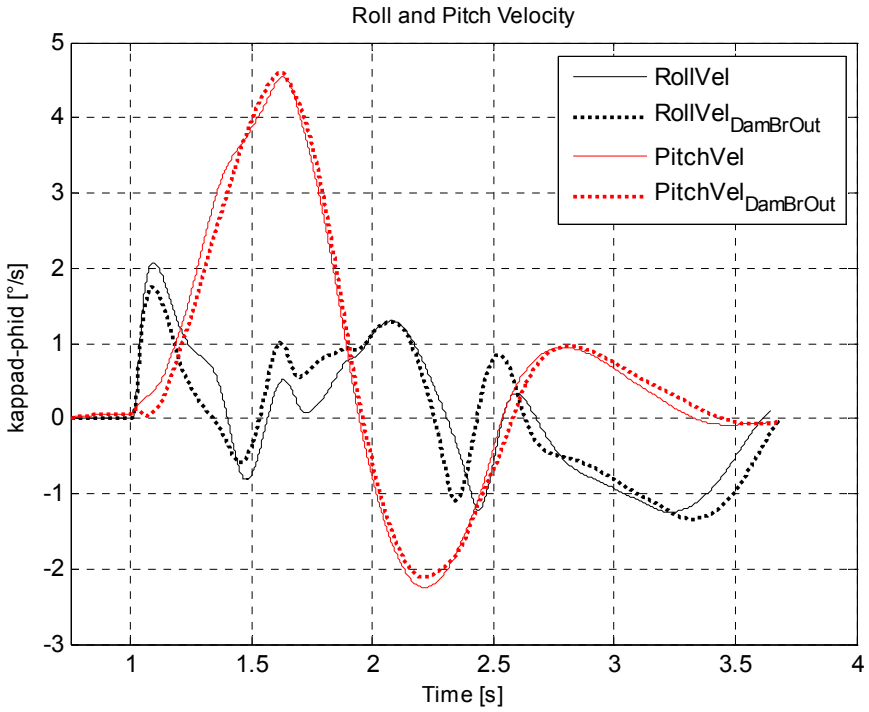

Figure 4.74 Roll and Pitch Velocities for Case 10-Damper 2 Failure

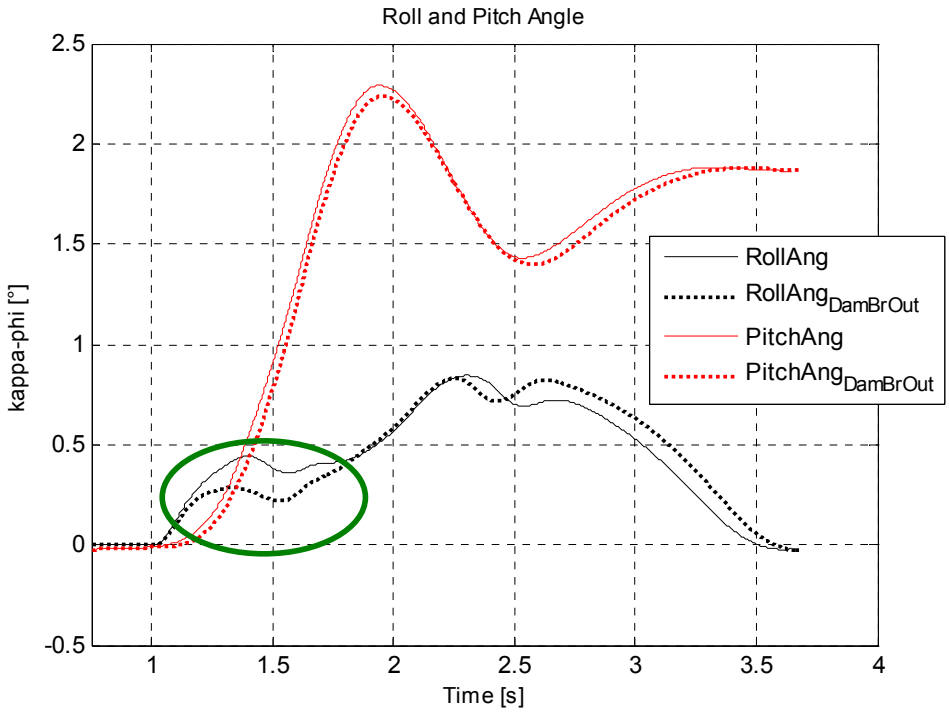

Figure 4.75 Roll and Pitch Angles for Case 10- Damper 2 Failure

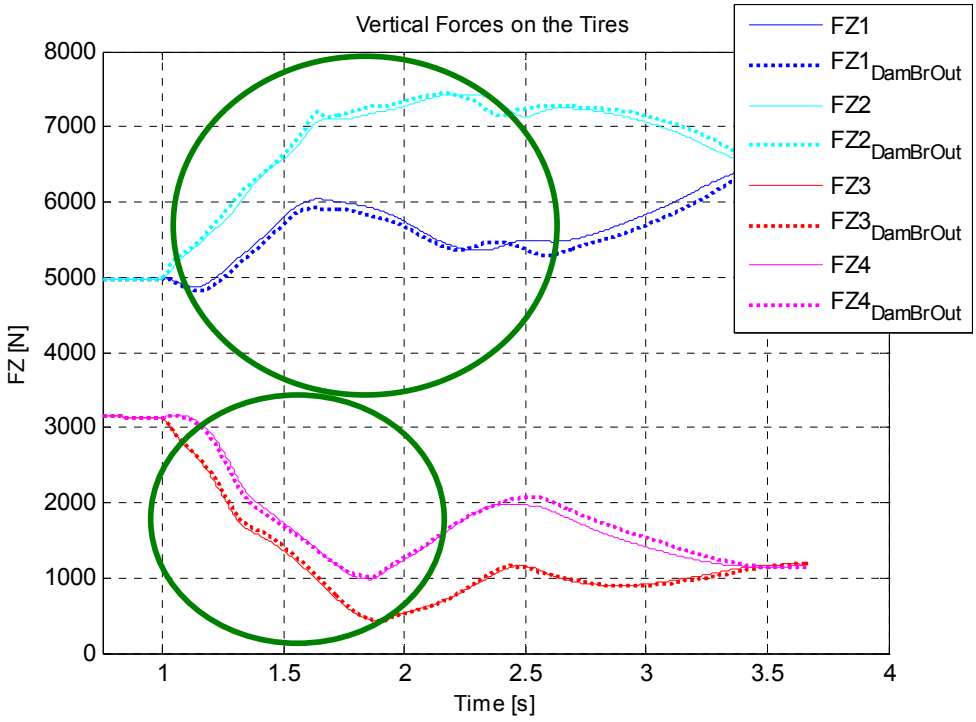

Figure 4.76 Vertical Tire Loads for Case 10- Damper 2 Failure

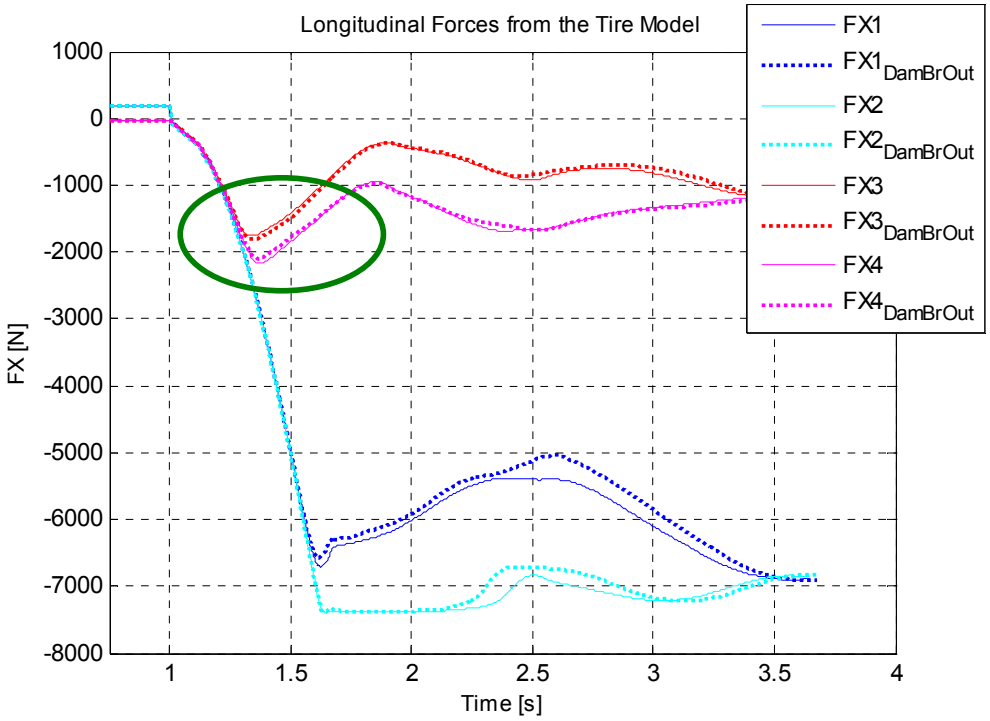

Figure 4.77 Longitudinal Tire Forces for Case 10- Damper 2 Failure

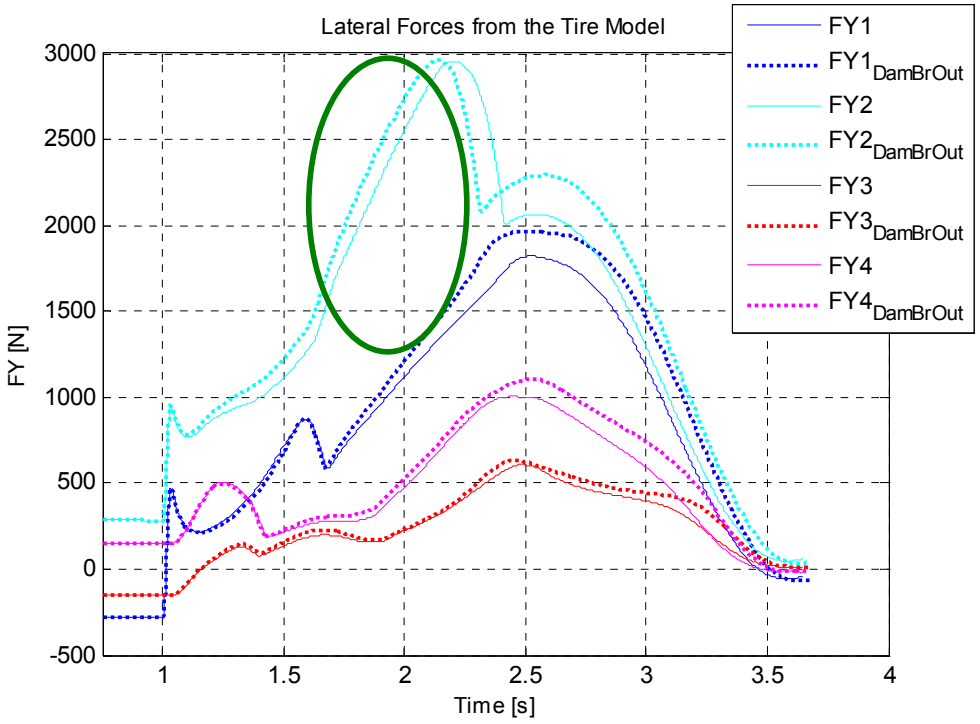

Figure 4.78 Lateral Tire Forces for Case 10- Damper 2 Failure

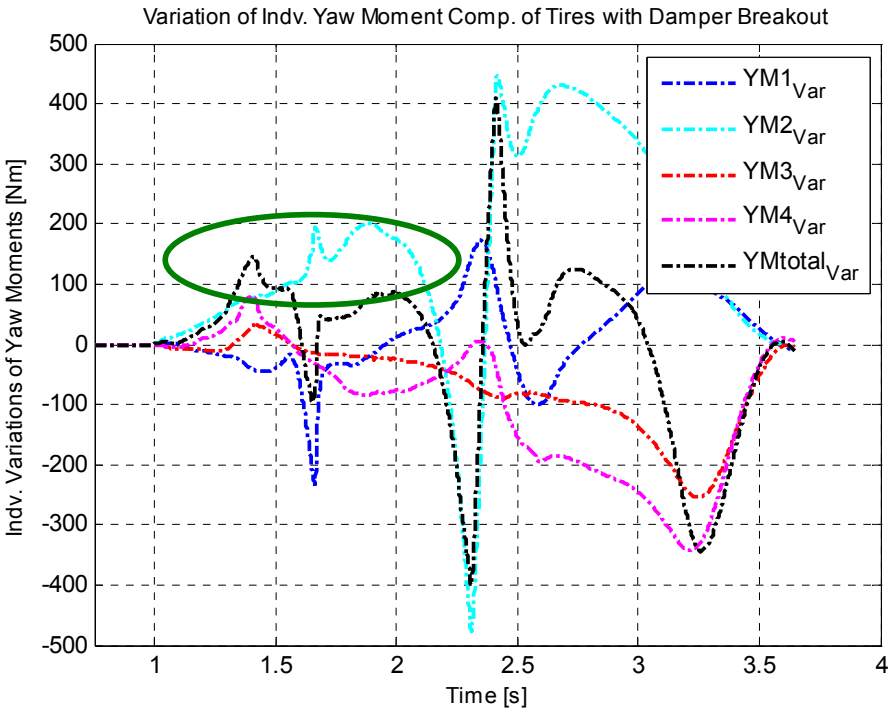

Figure 4.79 Variation of Yaw Moments for Case 10- Damper 2 Failure

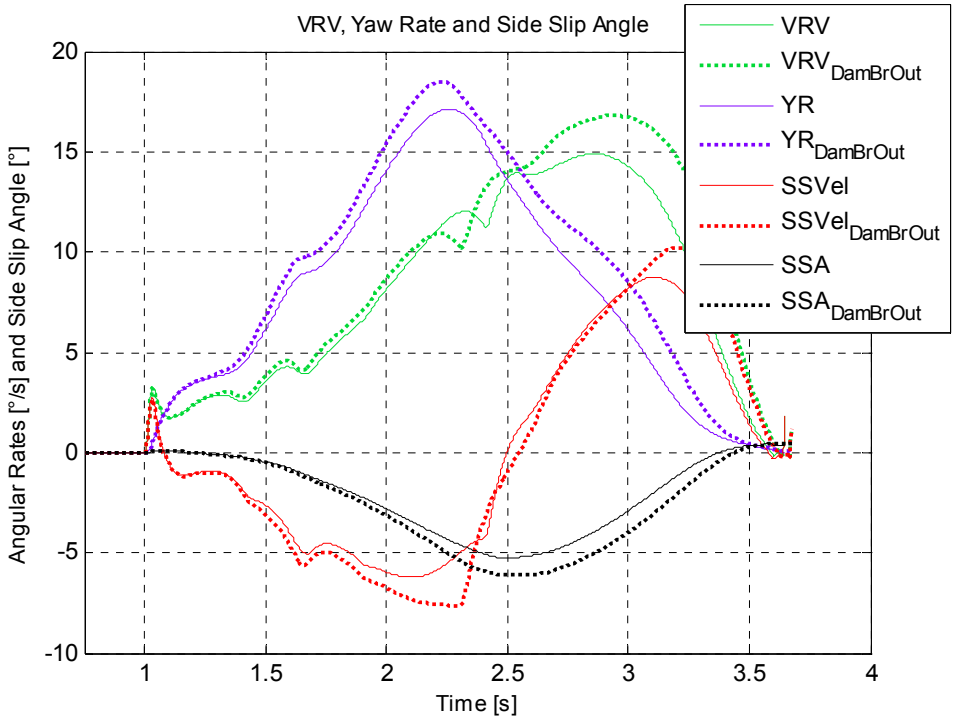

Figure 4.80 Calculation of Side Slip Angle for Case 10- Damper 2 Failure

4.2.2.5 CASE 11: CONTINUOUS SINE RESPONSE WITH BRAKING

4.2.2.5.1 Failure of Damper 3 (worst case)

In this case, the most critical point for damper 3 failure is the $\dot{\varphi}_{max}$ point since on that point the damper relative velocities (and consequently the damper forces) are the highest and also a damper failure on that point would decelerate the body motions to a maximum extent.

Due to the higher resisting force on tire 4, the tire is subjected to more extensional damping which makes the vertical load on tire 4 smaller, Figure 4.83. Because of that fact, the tire forces (longitudinal and lateral) on tire 4 are smaller. As a result a higher total yaw moment is obtained since load changes on tire 4 are decisive. Figures 4.81-4.87 demonstrate the influence of the failure explained above.

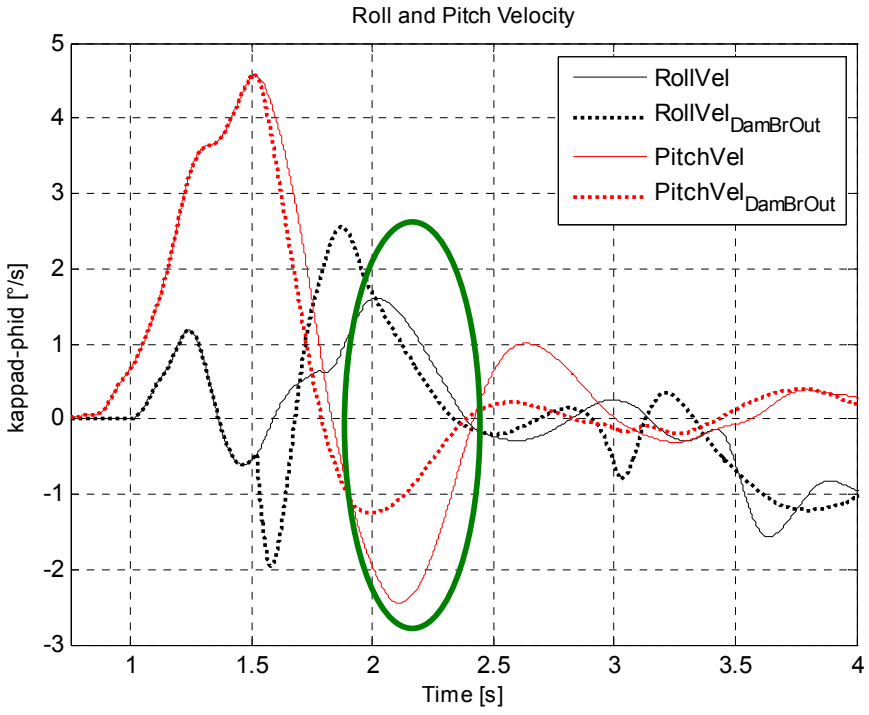

Figure 4.81 Roll and Pitch Velocities for Case 11-Damper 3 Failure

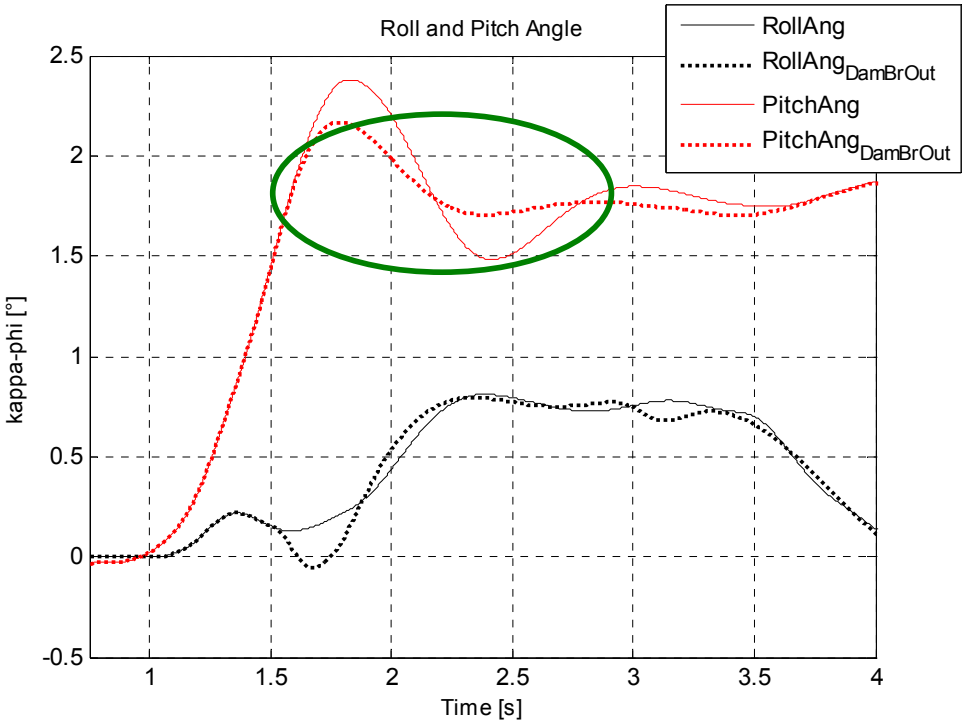

Figure 4.82 Roll and Pitch Angles for Case 11- Damper 3 Failure

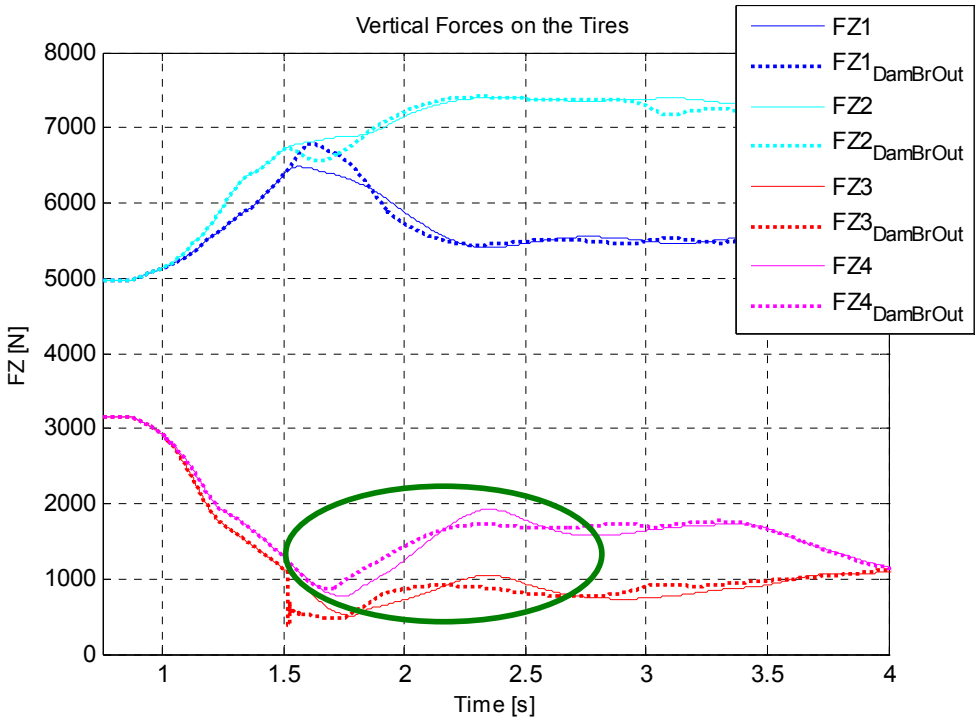

Figure 4.83 Vertical Tire Loads for Case 11- Damper 3 Failure

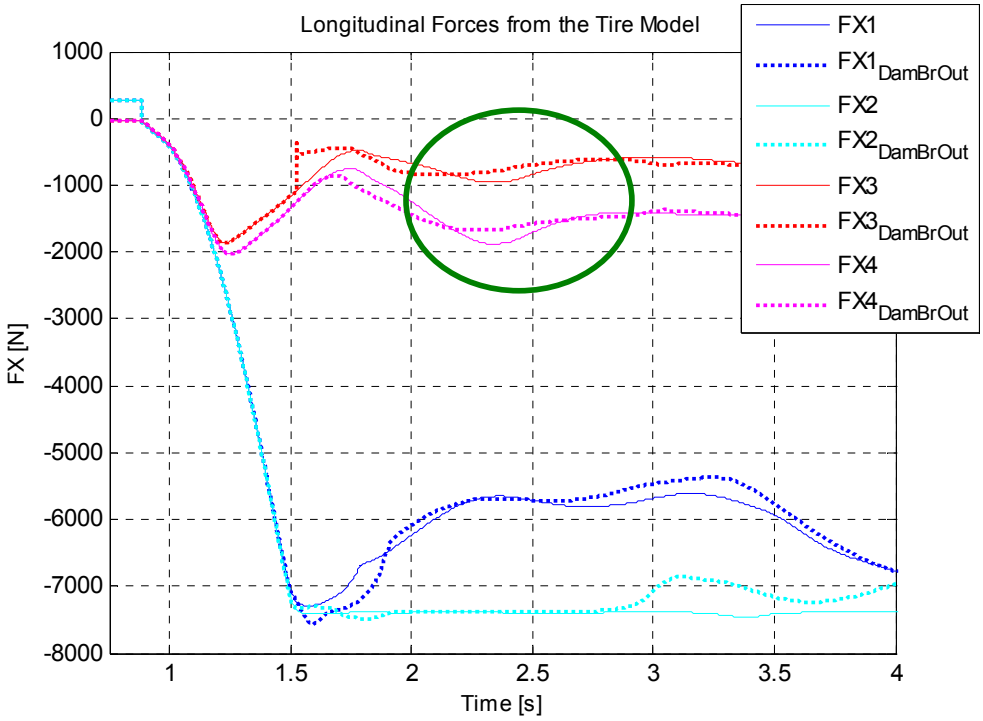

Figure 4.84 Longitudinal Tire Forces for Case 11- Damper 3 Failure

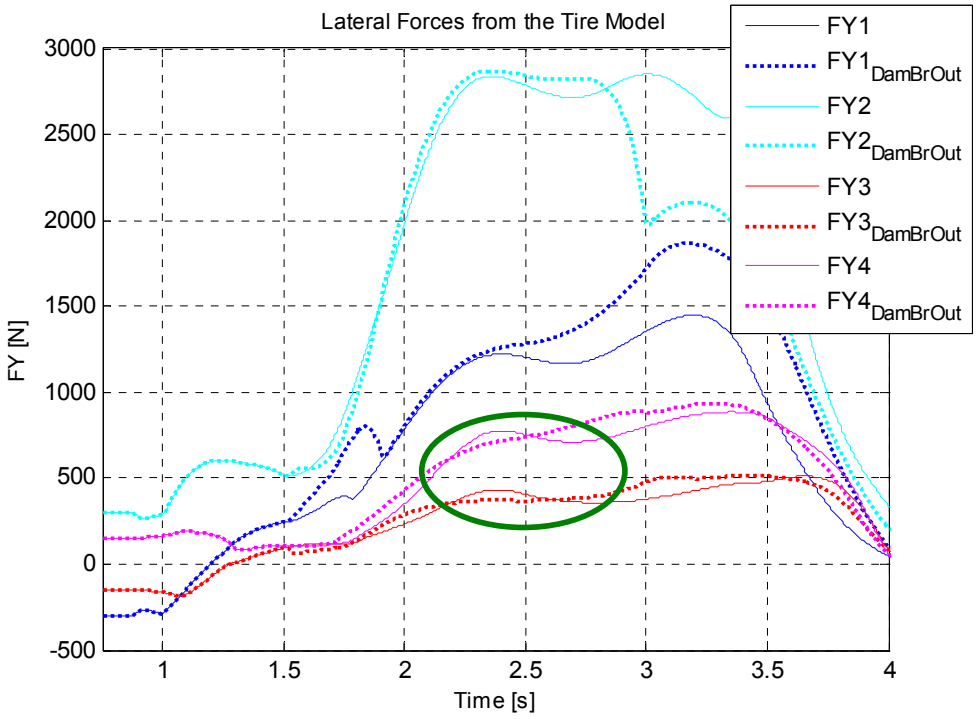

Figure 4.85 Lateral Tire Forces for Case 11- Damper 3 Failure

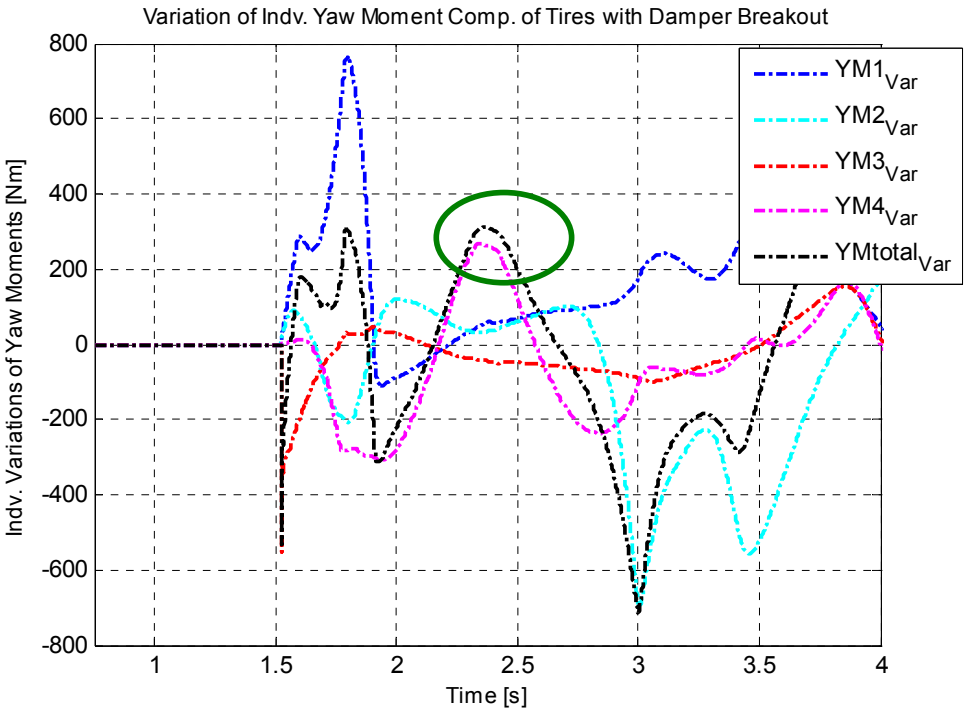

Figure 4.86 Variation of Yaw Moments for Case 11- Damper 3 Failure

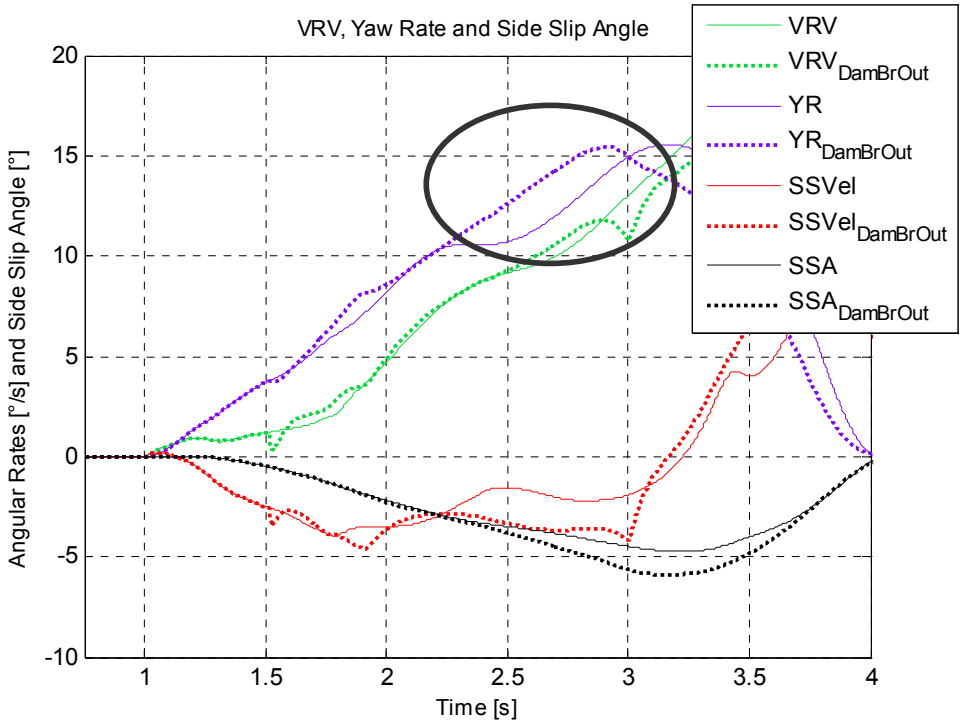

Figure 4.87 Calculation of Side Slip Angle for Case 11- Damper 3 Failure

4.2.2.6 CASE 12: SINE-DWELL RESPONSE WITH BRAKING

4.2.2.6.1 Failure of Damper 3 (worst case)

The most critical damper failure point for damper 3 is $\dot{\kappa}_{\min}$ point since a damper failure on this point decelerates the body motions to the maximum extent. This situation is similar to the damper failure scene of Case 10-Damper 3 Failure. But in this case the inner tire at the rear axle is 3 instead of 4 since the vehicle rotates in the other direction. With a damper failure on tire 3 at $\dot{\kappa}_{\min}$, due to a higher damping on tire 3, the pitching due to braking would be lower and the roll (towards left side on the right curve) would be smaller, Figure 4.89. Despite this fact, the tire load on tire 3 is lower since the damping resistance is higher and consequently the damper applies a more extensional damping force on the tire. With a lower vertical load also the tire forces are lower, which at the end results in an increased total yaw moment and side slip angle. Figures 4.88-4.94 demonstrate the influence of the failure explained above.

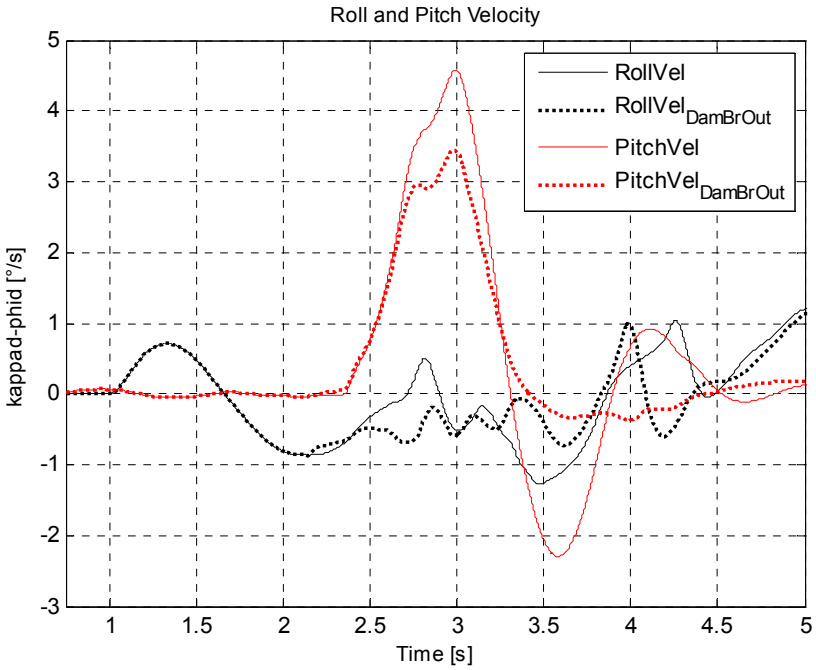

Figure 4.88 Roll and Pitch Velocities for Case 12- Damper 3 Failure

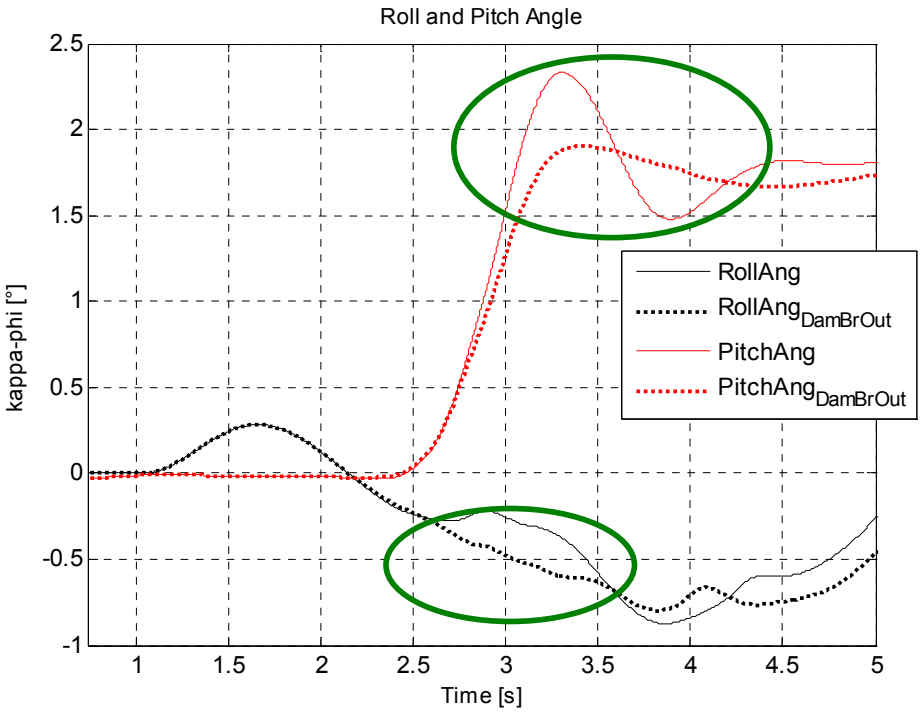

Figure 4.89 Roll and Pitch Angles for Case 12- Damper 3 Failure

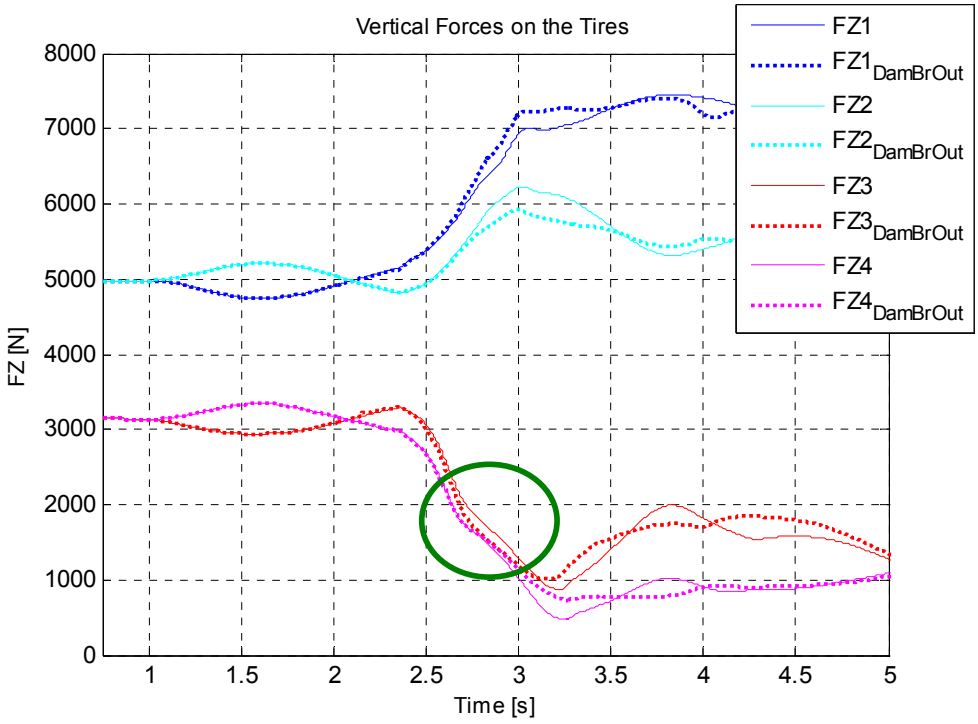

Figure 4.90 Vertical Tire Loads for Case 12- Damper 3 Failure

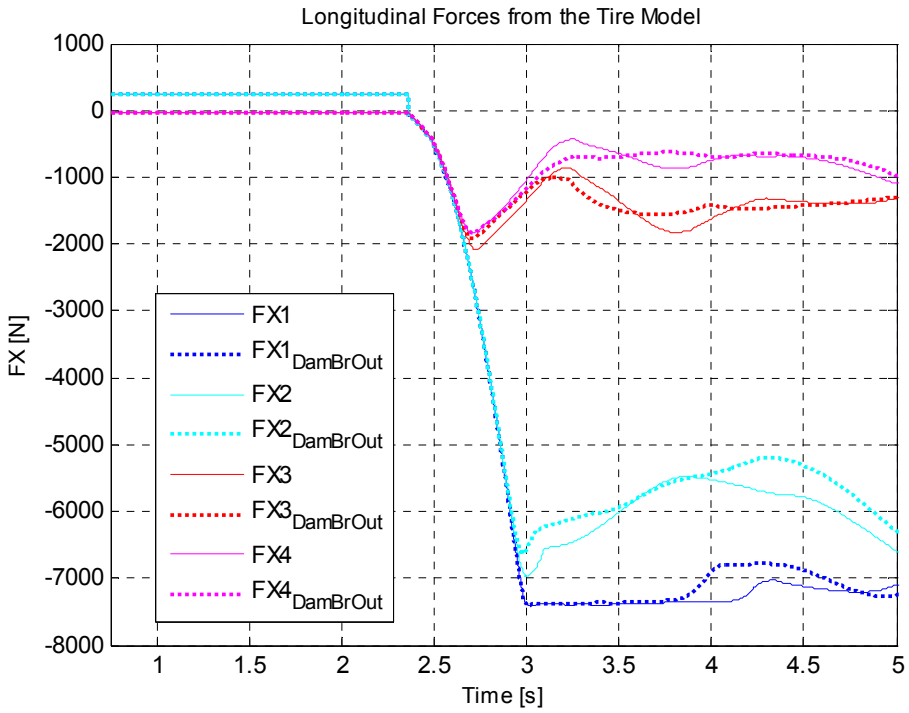

Figure 4.91 Longitudinal Tire Forces for Case 12- Damper 3 Failure

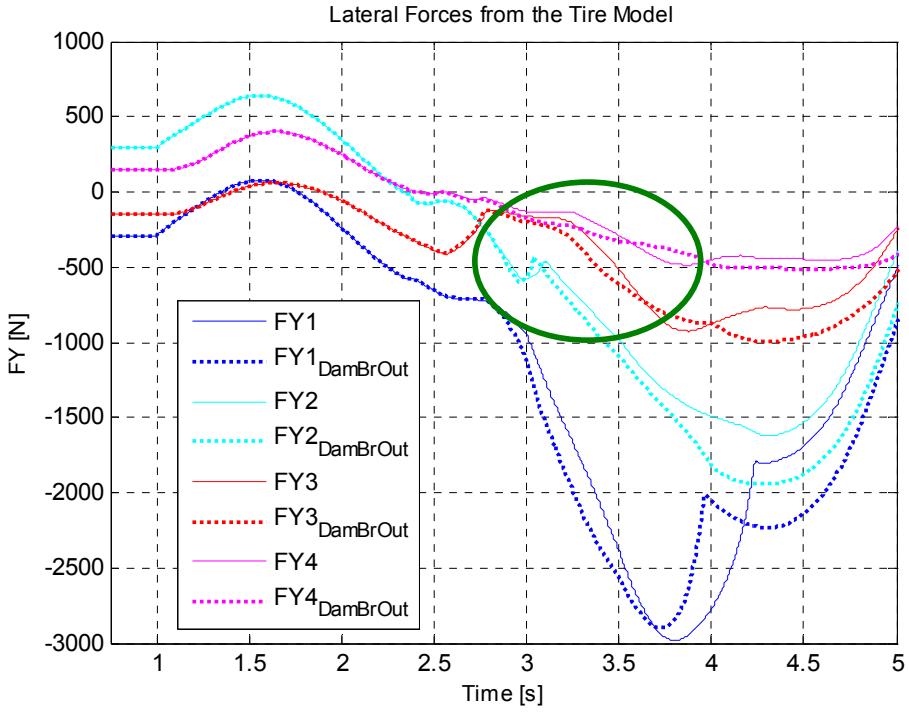

Figure 4.92 Lateral Tire Forces for Case 12- Damper 3 Failure

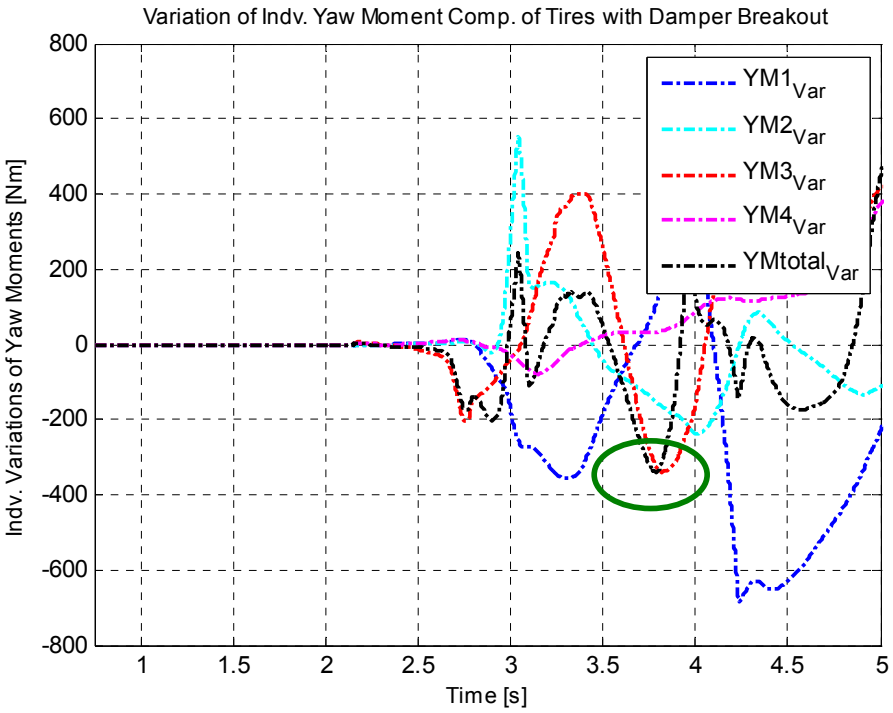

Figure 4.93 Variation of Yaw Moments for Case 12- Damper 3 Failure

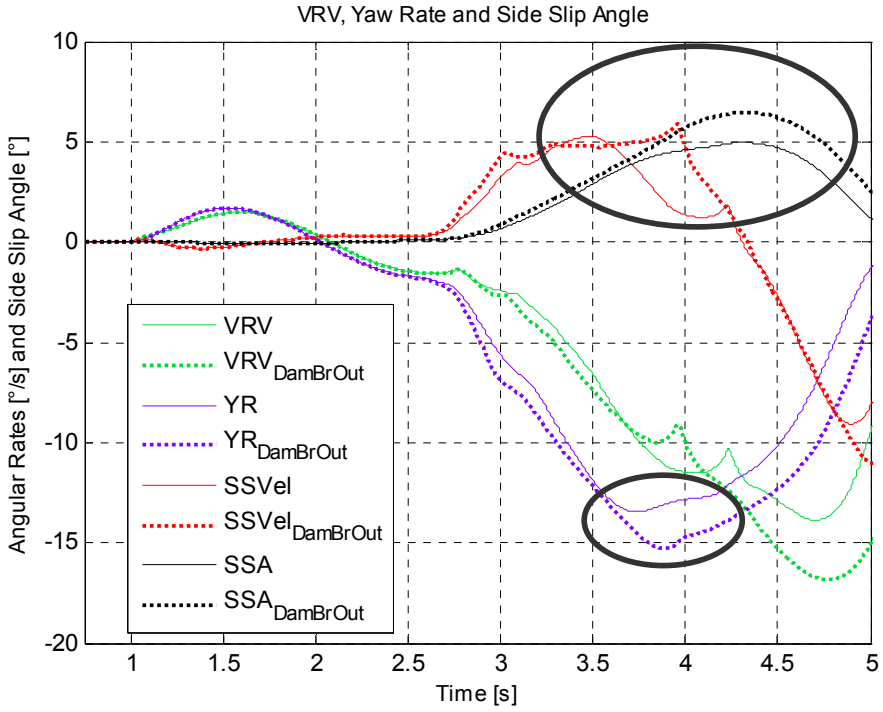

Figure 4.94 Calculation of Side Slip Angle for Case 12- Damper 3 Failure

4.3 EVALUATION OF THE RESULTS

In this section, a summary of the scenarios which are examined one by one in detail in the previous part is given. The results and outcomes obtained from the damper failure study are consequences of the case studies which are held through simulations of representative maneuvers and the two main types of damper failure. The results obtained in terms of the most critical cases concerning each case are given in the following table:

Table 4.3 The Summary of most critical Cases obtained from Damper Failure Study

	Mechanical or Software Failure		**Electrical Failure**	
Maneuver	**Without Braking**	**With Braking**	**Without Braking**	**With Braking**
Step Steer	D3 at Start	D1 and D3 at $\dot{\kappa}_{max}$	D4 at Start	D2 and D4 at Start
Continuous Sine	D3 at $\dot{\psi}_{max}$	D1 at Brake Start	D4 at Start	D3 at $\dot{\varphi}_{max}$
Sine-Dwell	D3 at $\dot{\psi}_{max}$	D4 at $\dot{\kappa}_{min}$	D4 at Start	D3 at $\dot{\kappa}_{min}$

The observations and the general summary of a damper failure simulation study with a realistic vehicle come out to be:

- Regardless of the maneuver being carried out, the most critical cases in an action without braking is obtained through the damper failure of tire 3 in the case of mechanical or software type of failures (in which the damper forces

attain a zero value with damper failure). This action is influenced by excessive additional fore motion especially if the driving condition involves a high level of lateral acceleration. With a fore motion the vertical loads and consequently the lateral loads on the front axle are greater in general, which is the main explanation towards more instable responses. In the modern applications, essential precautions are taken in order to avoid excessive pitching which would influence the vehicle stability.

- Similarly, concerning electrical failure phenomena, the most critical damper selection is damper 4 failure in driving situations usually without braking. This has the similar reason to the one with mechanical or software type of failures since greater damper forces on tire 4 influences greater fore motion. Here the difference can be explained with the concept of symmetricity i.e. the tires 3 and 4 are symmetrical to each other on the rear axle. Due to this symmetry it is obvious that damper softening failure on one side creates the similar effect in terms of vehicle handling with a damper hardening failure of influence on the other side. It means mechanical failure at one side has the similar influence on dynamics with an electrical damper failure on the other side. Therefore, if one damper is critical for one failure type for a certain maneuver, the symmetric one is the critical one for the other failure type in general. The characteristic point changes with the maneuver selection in mechanical and software type of failures whereas they do not in electrical failures. The reason behind that is the lateral tire force jump in tire 3 with failure, whereas tire 4 does not reveal such a jump. That is because on the spring-deflected side the vertical tire loads (tire force potential) are higher than the extended side. It means, since the vertical loads are higher, the tires on the spring-deflected side produces tire forces that are further from the friction circle boundary in comparison with the tires on the other side. Consequently it leads that the vertical tire jump due to failure at the spring deflected side would have a smaller effect on the lateral tire forces than the extended side. It should be noted from the explanations in the

previous part that in sine and sine-dwell maneuvers, a tire load jump has an effect towards stability on the point it takes place, however that effect is reversed when the vehicle turns in the other direction due to the second half cycle of the steering input.

- In case of maneuvers with braking, one side of the vehicle appears to be the critical side i.e. the dampers on that side are the critical ones for damper failure. Here, the mechanism is related to the influence of roll and pitch changes triggered by strong braking in case of failure and consequently the vertical load changes. For the step steer response maneuver, the critical damper selection is on the left side of the vehicle for mechanical or software type of failures, whereas for electrical failure it is on the right (spring-deflected) side. This difference can be explained with the type of failure, since disappearance of the damper forces (mechanical or software type failure) on one side leads to the same effects created as a result of damper stiffening on the other side. It can be claimed that it is roughly related to the direction of the shift in the body roll motion due to failure (leftwards or rightwards). Therefore in this case, softening on the left side gives the same effect with stiffening on the right (spring-deflected) side. The critical damper failure points (for the step steer responses) appear to be roll velocity maximums for mechanical or software type failures, whereas it is the steering start for electrical failure. This difference has a similar explanation with the *tire force jump effect* explained above. The side of the critical damper selection shifts for sine-dwell response with braking which can be explained with the altered turn direction of the vehicle.
- The similarity or correlation in terms of the critical damper and the critical damper failure time of the sine and sine-dwell responses attracts also attention which can be also related to the similarity in the maneuvers. Note that the first 2 cycles for sine and entire steering input for sine-dwell are analogous to each other except from the slight difference of *dwell time* included in sine-dwell maneuver. Additionally, the differences or the

correlations obtained between the 2 damper failure types for step steer responses also stand for the sine and sine-dwell maneuvers subjected to different damper failure means, the shift of the critical damper selection to the other side.

- The sine response maneuvers with braking are the exceptions which has slight or nearly no correlation to other maneuvers in terms of the damper criticality and critical damper failure point, which can be also related to the dynamics of the maneuver itself. In sine maneuvers a relative high frequency is given to the steering maneuver and with braking the maneuver seems to be increased in terms of its dynamicity. Nevertheless, there still seems to exist a correlation to results of other maneuvers in terms of similarity in the critical side (left or right selection, as explained above) which makes the results obtained from sine maneuvers reasonable.

CHAPTER 5

DISCUSSIONS AND CONCLUSIONS

The main goal of this study was to investigate the impact of damper failure phenomena on vehicle handling behaviour during critical driving conditions. To constitute a more in-depth and complete work, the phenomenon is examined under divided and expanded cases. The cases were to be examined in a detailed way and a general conclusion over the damper failure phenomena in terms of its criticality was to be obtained.

To justify the goal, a detailed literature survey work was carried out. It was realised that there exists a lack of studies which take concern to such a study in exact manner. The literature up to now has mainly focused on:

- the effects of some other chassis components; effects of their parameter selections on the vehicle stability,
- impact of worn dampers on roll and pitch velocities; but without further study,
- the control strategies used in active dampers, while switching the damper characteristics.

Therefore, the studies which have some connection to this study were taken into account and it was decided to contribute to those with a new point of view. Considering the work carried out and the outcomes arrived, it can be claimed that the goals have been achieved.

In order to represent the real-life on a software environment, it is required to prepare a detailed vehicle model and realistic maneuvers that a certain driver is able to perform. There is a requirement of a detailed modelling since the damper failure outcomes may be sensitive to a rough vehicle modelling or may lead to incorrect results with that type of a modelling. For that reason, the traditional vehicle

modelling principles with several number of engineering assumptions were abandoned and rather a certain level of assumptions (which are used to be made generally in vehicle modelling) are assured to ensure model accuracy. The tire model can be claimed to have sufficient detail, since it has been commonly used in vehicle dynamics modelling due to its high level of competence. However, there is still a certain trade-off point on which the model complexity is too high and consequently the maintenance of the model and the simulation speed would be inefficient. In the vehicle modelling this point has been attained.

In the analysis part the damper failure phenomenon has been divided to case studies to demonstrate the outcomes more systematically and to ensure an ease in the systematic to follow. The failure issue has been divided to 2 types in terms of its failure and the maneuvers have been examined under the two cases of *braking manuvers* and *maneuvers without braking*. Concerning the side slip angle maxima obtained through the damper failure applied at the *characteristic failure points* for each maneuver, the most critical damper selection and its failure point correspondence have been identified. After carrying out a detailed analysis for each case, a general conclusion over the impact of damper failure on the driving dynamics has been done.

Generally, it has been discovered that for mechanical or software type of failures, the inner tire at the rear axle is the most critical one for damper failure for maneuvers without braking depending upon the turning direction of the vehicle. Similarly for electrical failures and maneuvers without braking, the most critical tire came out to be the outer tire at the rear axle with characteristic points changed. For maneuvers with braking, generally the inner side has appeared to be the most critical for mechanical or software failure, whereas the outer side was critical for electrical failure experience. In general, relating to the results from the damper failure maneuvers, the most critical cases identified may be hazardous in terms of vehicle stability; that may lead to undesired consequences. It can thereby be suggested that the chassis assistance systems or driver warning systems may be integrated to notice a damper broken or interfere in case a damper failure occurs on a critical situation.

As a result it can be concluded that this study contributes to the literature, on researches and studies on vehicle handling and impacts of similar experiences on vehicle stability, since it evaluates the concrete consequences of damper failure phenomenon as to whether it can be dangerous or not.

Therefore, the study can be claimed to own a certain worth, in that it constitutes a proceeding to the studies focused on above and it is the single study which focuses on evaluating the concrete results of damper failure experience on driving behaviour.

It has been investigated throughout the study that, for driving conditions on dry asphalt surface, in some damper failure experiences for a number of test maneuver-damper selection-failure time combinations the resulting vehicle handling characteristics come out to be critical; i.e. resulting with up to **85 %** increase in the side slip angle maxima, Tables D.1-D.12. It appears to be a critical experience in that in such a case the desired and *expected* driving conditions are instantaneously and drastically changed. In case of such a damper failure, the driver may not be able to react so sudden and appropriate to compensate the failure effect. The solutions in application to damper failure experience seem to be the drive dynamics control algorithms like ESP, Active Yaw Control etc. However, some situations may exist in which these types of controllers may come out to be insufficient. The reason behind that assumption is that these algorithms run basing on a vehicle model, and the reliability of the algorithm depends on the accuracy and reliability of the model. Thus, the requirement of further studies or special safety measures concerning damper failure experience is related to the availability of an effective feedback of the failure information to those models included by such stability control algorithms.

5.1 FUTURE WORK

As mentioned, this study aimed to evaluate the impacts of damper failure process on vehicle handling. However, concerning the area of interest of the subject

and the tasks performed throughout the study, some future work would be valuable in terms of contributing the subject further:

- A variety in characteristics in vehicle parametrization may be developed to ensure more representative cases i.e. a completely oversteer or maybe a theoretically neutral steer vehicle may be simulated for damper failure and the shortcomings may be visualized,
- A research may be made leading towards the Driver Assistance Systems which may be worthwhile as precautions to avoid the consequences of damper failure,
- A test study furnishing the knowledge acquired throughout the thesis may be carried out. Therefore, a software algorithm is to be implemented to the switchable dampers which controls the characteristics in the desired manner, to apply the damper failure scenarios,
- More Driver Assistance Representations may be implemented on the vehicle model to visualise whether they have a positive impact on the consequences of damper failure,
- A Hardware-in-the-Loop (HIL) simulation can be carried out to obtain more accurate results at the end.

REFERENCES

[1] Brandon, P., Patel, A., Karwatzki, J., Ordys, A., "Adaptive Damper Modelling and Experimentation", Automotive Electronics, 2007 3rd Institution of Engineering and Technology Conference, June 2007

[2] Paz, O.D., "Design and Performance of Electric Shock Absorber", M.Sc. Thesis, Louisiana State University, December 2004,

[3] Mirzaei S., Saghaiannejad S.M., Tahani V., Moallem M., "Electromagnetic Shock Absorber", Electric Machines and Drives Conference, 2001

[4] Scienceline website, http://scienceline.org/ Last visited on 28.07.2009

[5] Wang, J., Dong, C., Shen, Y., Wei, J., "Robust modelling and control of vehicle active suspension with MR damper", Vehicle System Dynamics 2008, Vol.46, No.1, pp. 509-520

[6] Shen, Y., Golnaraghi, M.F., Heppler, G.R., "Load-leveling suspension system with a magnetorheological damper", Vehicle System Dynamics 2007, Vol. 45, No. 4, pp. 297–312

[7] Ko, Y., Heydinger, G. J., Guenther, D.A., "Evaluation of a Shock Model for Vehicle Simulation", SAE Paper 2007-01-0845

[8] Warner, B., Rakheja, S., "An Investigation of the Influence of High Performance Dampers on the Suspension Performance of a Quarter Vehicle", SAE Paper 962552, 1996.

[9] Soliman, A.M.A., Abd El-Tawwab, A.M., Crolla, D.A., "Adaptive Control Strategies for a Switchable Damper Suspension System", SAE Paper 960939, 1996.

[10] Abd El-Tawwab, A.M., Crolla, D.A., "An Experimental and Theoretical Study of a Switchable Damper", SAE Paper 960937, 1996.

[11] Hac, A., Bodie, M.O., "Improvements in vehicle handling through integrated control of chassis systems", International Journal of Vehicle Autonomous Systems (IJVAS) 2002, Vol. 1, No. 1, pp. 83-110

[12] Guba, S., Ko, Y., Rizzoni, G., Heydinger G.J., Guenther, D.A., "The Impact of Worn Shocks on Vehicle Handling and Stability", SAE Paper 2006-01-0563

[13] Gracia, A.G., Jimenez F., Páez J., Narváez A., "Theoretical and experimental analysis to determine the influence of the ageing process of the shock-absorber on safety", International Journal of Vehicle Design 2006, Vol. 40, Nos. 1/2/3, pp. 15-35

[14] Filiatrault, D.D., Cooper, P.J., "The Effect of Oversize Tires on Vehicle Dynamics and Crash Risk of Light-Duty Trucks", SAE Paper 2007-01-0847

[15] VCU Transportation Safety Training Center website, http://www.vcu.edu/cppweb/tstc/crashinvestigation/index.html Last visited on 21.10.2009

[16] Veloso, V., Magalhães, H.S., Bicalho, G.I., Palma, E.S., "Failure investigation and stress analysis of a longitudinal stringer of an automobile chassis", Engineering Failure Analysis 16 (2009) 1696–1702

[17] van Schoor, O., van Niekerk, J.L., Grobbelaar, B., "Mechanical failures as a contributing cause to motor vehicle accidents — South Africa", Accident Analysis and Prevention 33 (2001) 713–721

[18] Nishio, A., Tozu, K., Yamaguchi, H., Asano, K., Amano, Y., "Development of Vehicle Stability Control System Based on Vehicle Side Slip Angle Estimation", SAE Paper 2001-01-0137

[19] Pacejka, H.B., "Tyre and Vehicle Dynamics", Butterworth-Heinemann, Amsterdam 2006, Second Edition

[20] Pawellek, T., "Online-Applikation eines Fahrzustandsschätzers", Experimentelle Diplomarbeit, TU Braunschweig, September 2008

[21] Racer website, http://www.racer.nl/reference/pacejka_racer.htm/ Last visited on 12.08.2009

[22] Racer website, http://www.racer.nl/ Last visited on 12.08.2009

[23] Bridgestone website, http://www.bridgestone.eu/tyres/cars-suvs-and-4x4s/potenza-re040 Last visited on 21.10.2009

[24] Boßdorf-Zimmer, B., “Nichtlineare Fahrzustandsbeobachtung für die Echtzeitanwendung”, Schriftenreihe des Instituts für Fahrzeugtechnik TU Braunschweig, 2007

[25] Lecture Notes: Fahrzeugtechnik 3, Prof. Dr.-Ing. Ferit Küçükay, Institute für Fahrzeugtechnik, TU Braunschweig

[26] Lecture Notes: ME513 Vehicle Dynamics, Prof. Dr. Y. Samim Ünlüsoy, METU

APPENDIX A

VEHICLE DATA

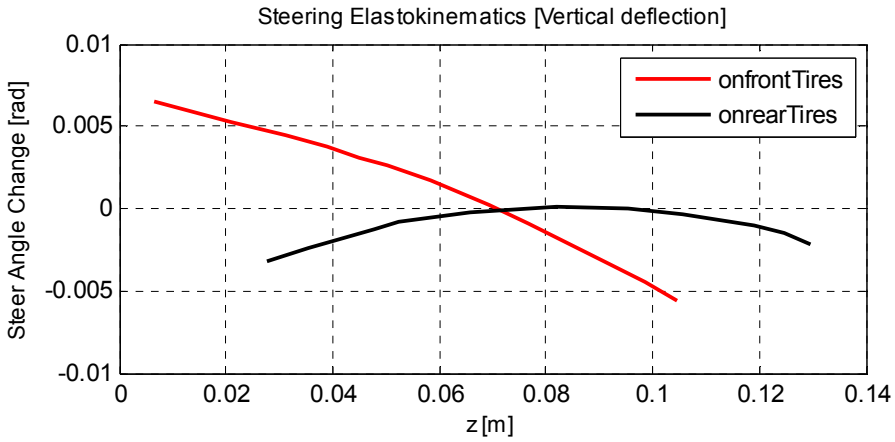

Figure A.1 Steering Elastokinematics dependent on vertical deflection

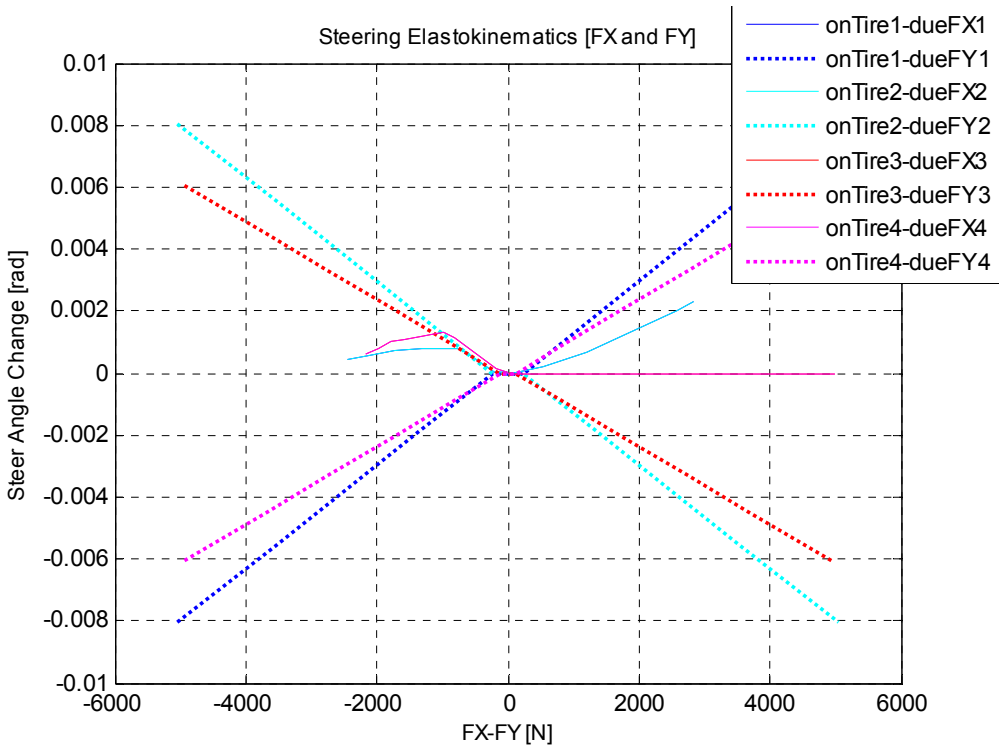

Figure A.2 Steering Elastokinematics dependent on FX and FY

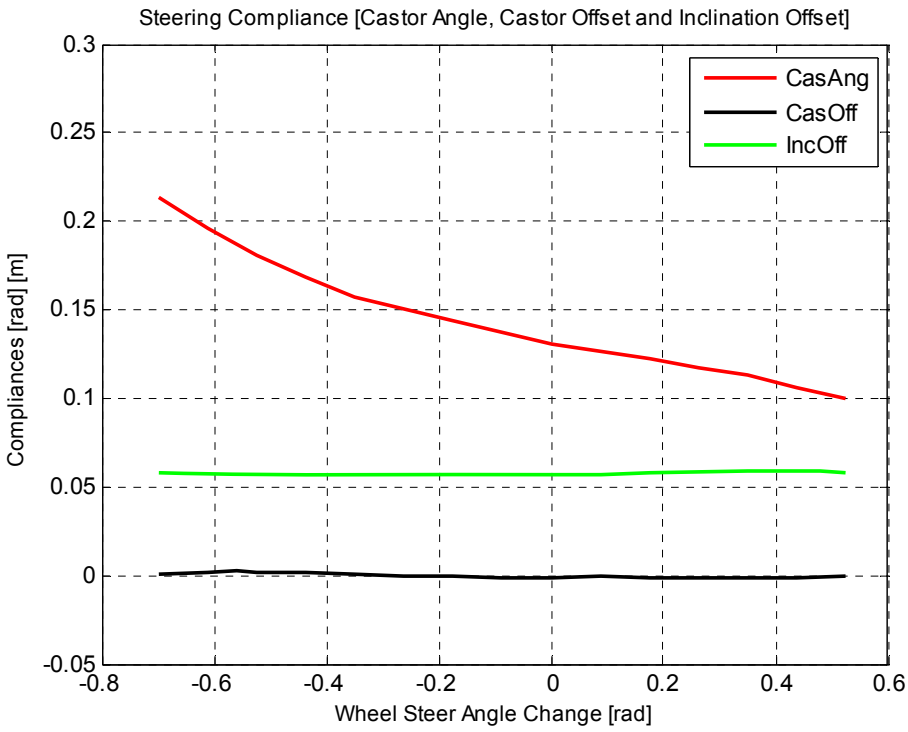

Figure A.3 Steering Compliance for Castor Angle, Castor Offset and Inclination Offset

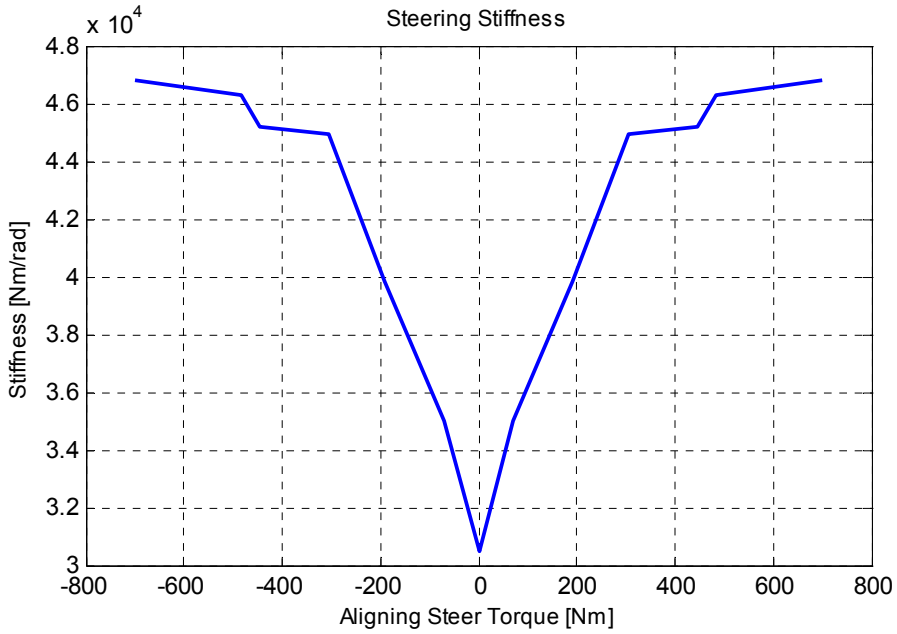

Figure A.4 Steering Stiffness dependent on Aligning Steer Torque

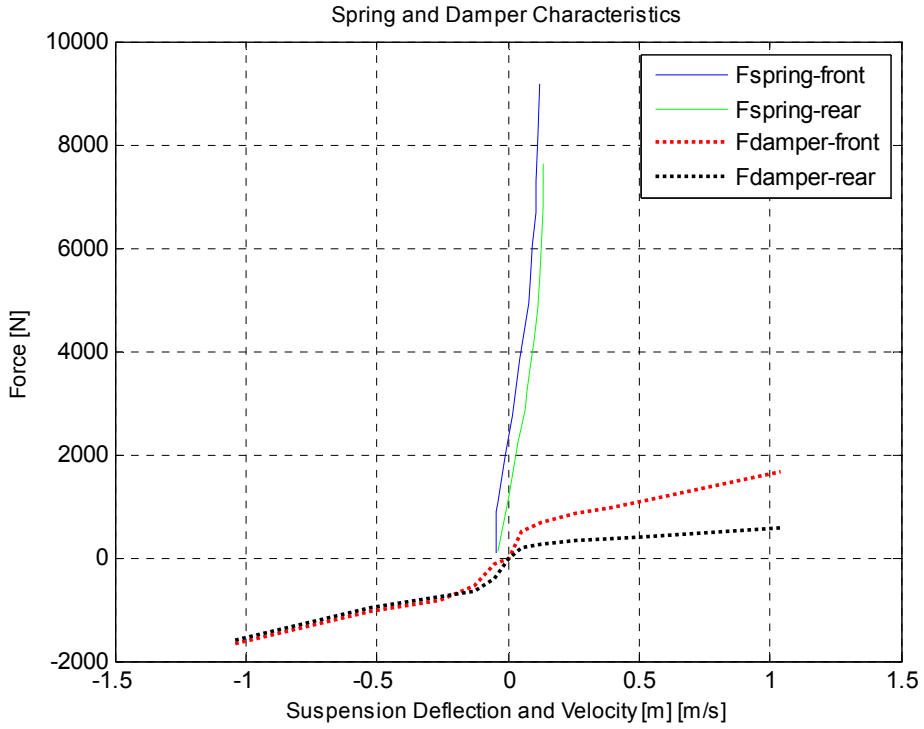

Figure A.5 Spring and Damper Characteristics

Table A.1 Vehicle Parameters

PARAMETERS	VALUE OR CALCULATED THROUGH
m	1656 kg
ma	m - mv - mh
mv	94 kg
mh	80 kg
mf	mv + mh
JX	560 kg/m2
JY	2200 kg/m2
JZ	2200 kg/m2
pv	-0.04419 m
ph	0.10576 m
ha	0.535 m
hv	0.296 m
hh	0.296 m

Table A.1 (continued)

lv	0.9959 m
lh	1- lv
l	2.577 m
lva	l - lha
lha	(lh*m - mv*l)/ ma
lvn	l
lhn	0
sv	1.530 m
sh	1.505 m
cstv	25364 Nm/rad
csth	16920 Nm/rad
cw1	5.662
cw2	0.3169
cw3	0.0023
h´	h* pv - (ph - pv)* lv/l
ε	0.0223 rad
rGA	0.022843 m
rst1	0.09 m
rst2	0.045 m
rh	0.045 m
rp	0.0275 m
rs	0.045 m
Jst	0.025 kg*m2
Jp	0.000151 kg*m2
JR	1.4 kg*m2
rdyn	0.3115 m
iL	15.911
Tl	0.02
iL	15.911
TIRE MODEL PARAMETERS	
Bx,Cx,Ex	16.8149, 1.6304, 1.2
b3,b4,b5	0.0011461, 29.5, 2.7433e-5
By,Cy,Ey	12.2128, 1.414, -0.99252
a3,a4,a5	120926.8451, 11843.7949, -0.2
Bz,Cz,Ez	9.8434, 2.4075, -1.7651
c3,c4,c5	-175.326, 86.5024, 0.031178
Byx,B2yx,Cyx	7.045, 6.3768, 1.0849
Bxy,B2xy,Cxy	24, 11.9084, 0.98877
E2x	-0.07375

APPENDIX B

MODEL AND MANEUVER SPECIFICATIONS

B.1 STEP STEER TIME DELAY

As explained in the maneuver definitions to ensure the real-life compatibility of a driver's reaction on the steering in the case of step steer input, a slight time delay is applied during the step. A realistic slope value **450°/s** for the linear function that is applied as a step function with delay in order to be realistic and to represent the sharp response of the driver.

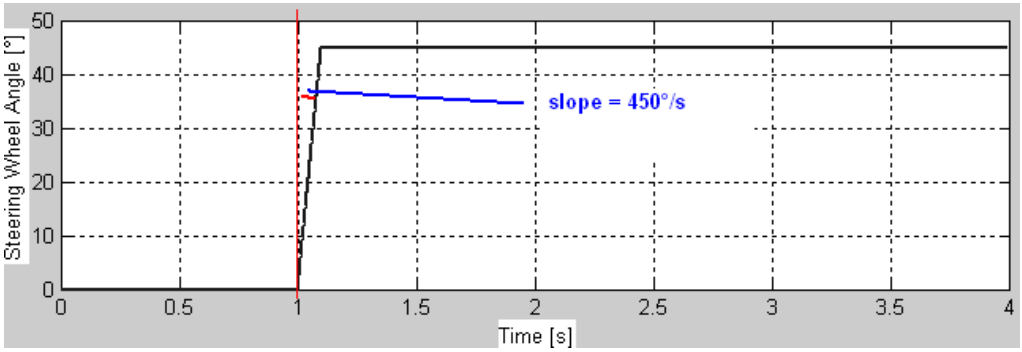

Figure B.1 Slope value used in the Step steer input

B.2 DAMPER FAILURE SWITCH

To interfere the suspension block (damper force generation) in accordance with the damper failure time and the force values to be generated as a result of failure some triggers are modelled which produce signals concerning the GUI parameters given by the user for damper failure. By this means the damper force signals are appropriately produced to the desired failure type, time and damper selection.

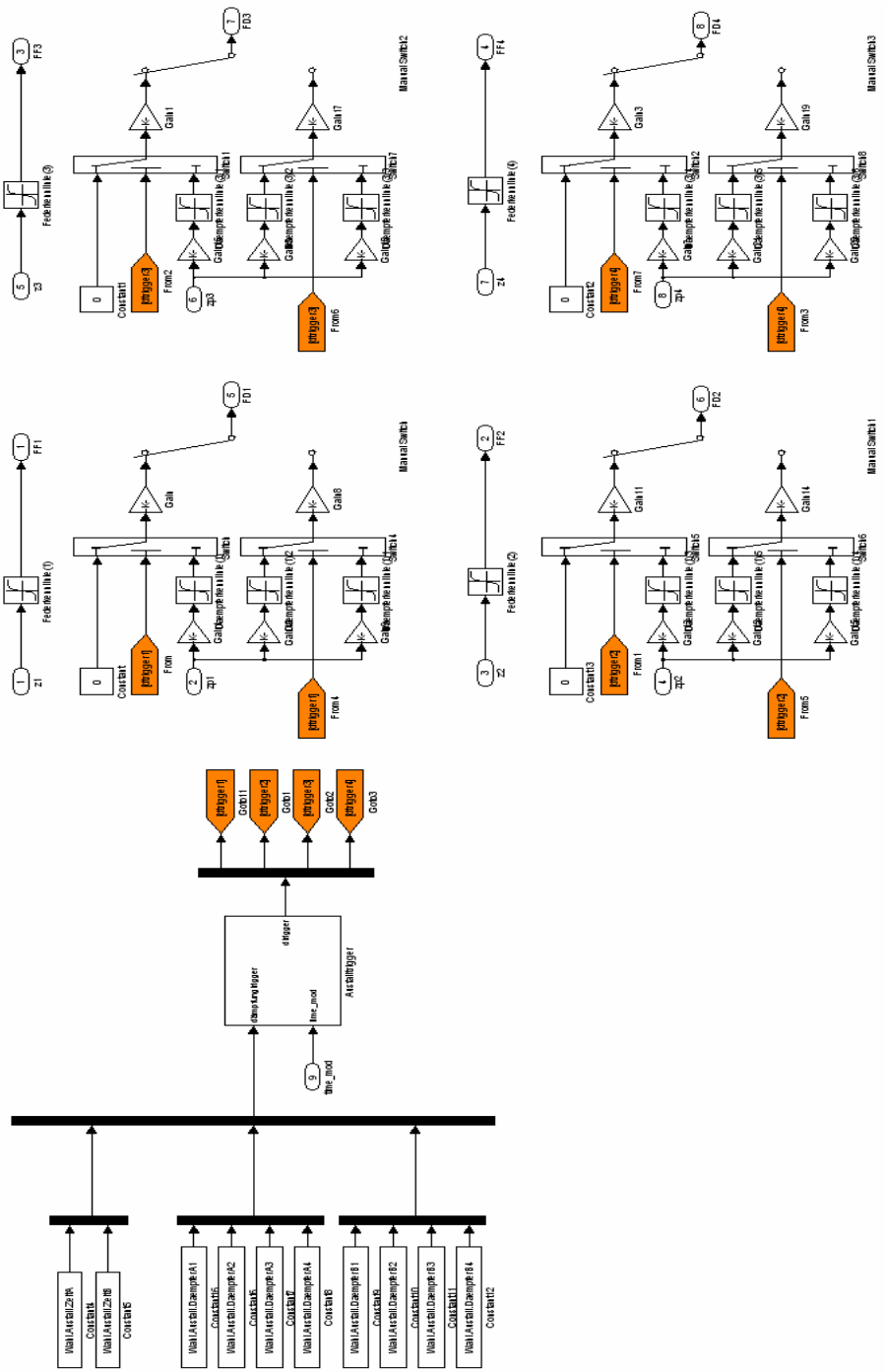

Figure B.2 Damper Force generation in connection with GUI Trigger signals

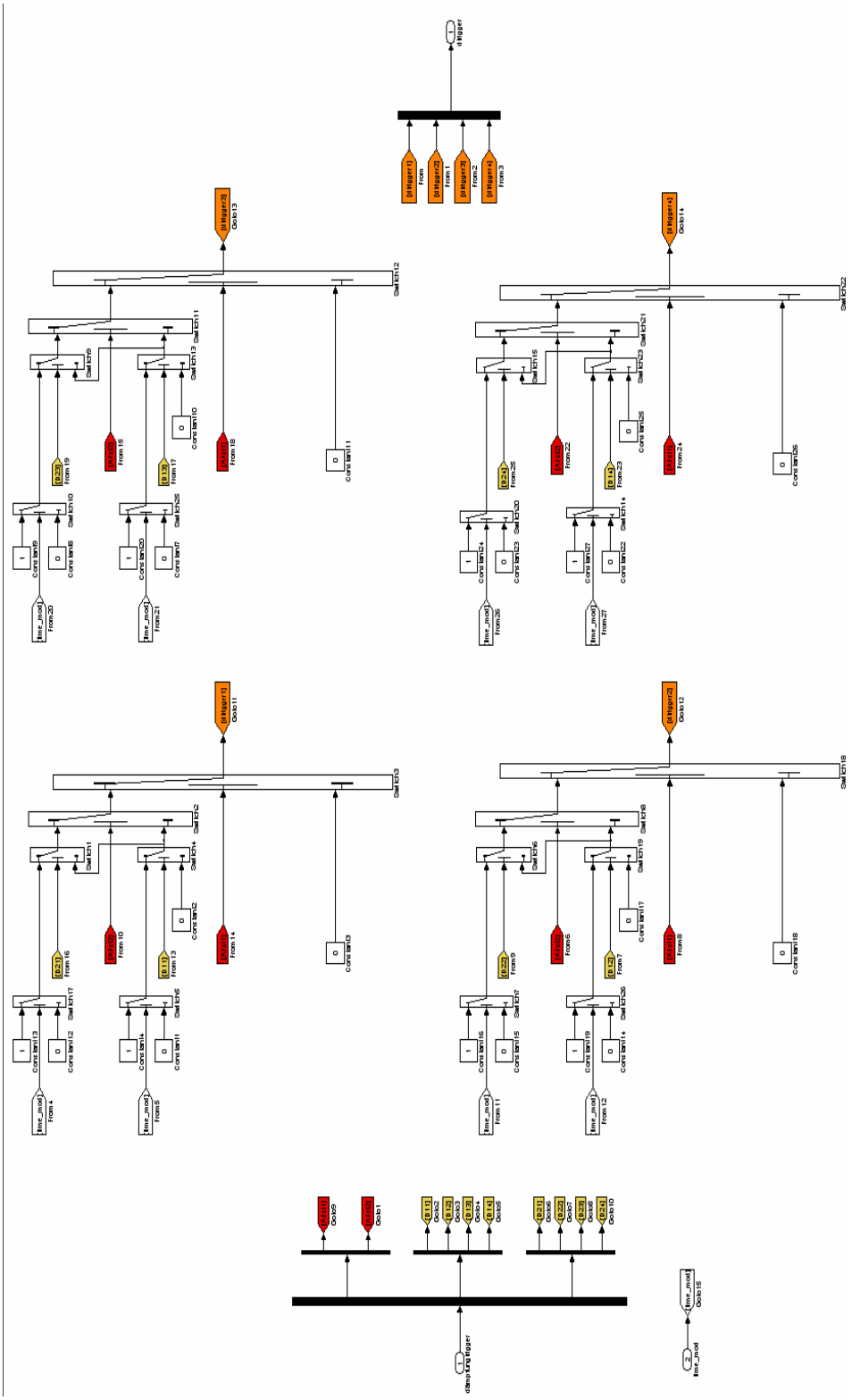

Figure B.3 Damper Trigger Signals Block

B.3 CRUISE CONTROL MODEL

The vehicle velocity should be kept constant for the maneuvers in the simulation work in order no to lose the lateral dynamics characteristics. For this purpose a cruise control block is implemented to the drive train block which produces the driving torque signal to the driven wheels as a function of vehicle desired longitudinal and actual speeds. The working principle of that model is closed loop feedback in terms of the vehicle velocity. The controller itself is designed applying an optimization study and finding out the usage of proportional gain only gives out the most appropriate outputs.

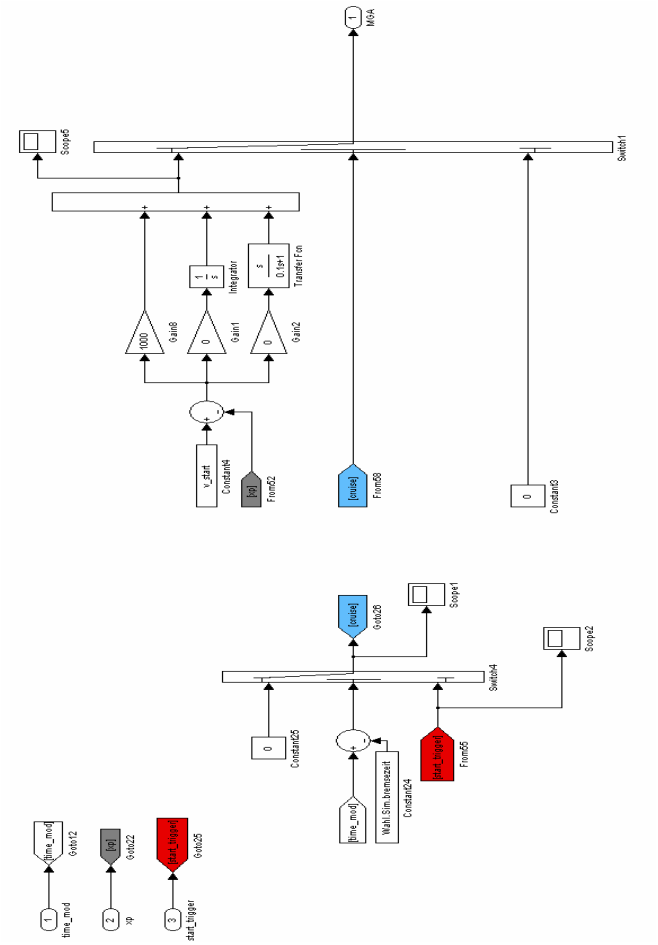

Figure B.4 Inside of the Cruise Control Model block

B.4 BRAKING STRATEGY

In estimation of braking times for the maneuver with braking, a certain strategy is used. This strategy is based on the selection of the most critical point which gives the most dynamic response in terms of vehicle lateral behaviour (yaw rate side slip angle, etc.) From the vehicle data, the braking time to attain maximum braking pressure (**100 bars**) is about **0.62 s**. Considering that information:

- The most critical point for braking for the step steer maneuver is the start point for steering (since by such means the transient dynamics of step region would be influenced on a maximum extent),
- The most critical point for sine and sine-dwell steer maneuvers is the point on which a braking ensures that the *roll angle or lateral acceleration peaks* are met with the point on which the maximum braking pressure is attained; the time point which is 0.62 seconds earlier than roll angle or lateral acceleration maxima. The points in italics are indications of the greatest lateral dynamics during the maneuver, i.e. coinciding the maxima of lateral and longitudinal behaviour ends up with the most dynamic vehicle lateral behaviour.

APPENDIX C

FRICTION CIRCLE CONCEPT

Throughout the damper failure analysis, the changes in the vertical loads caused by damper failure influence the tire loads. The relation between the vertical loads and the tire forces can be explained via the friction circle concept. It is already mentioned that the spring deflected side is less sensitive to tire load changes in terms of tire force alterations, since the resultant tire force in this side is further to the saturation point than the other side as the vertical loads are higher in this side due to spring deflection. This phenomenon can be explained via *friction circle*, which is a boundary for tire force resultant (vector sum of longitudinal and lateral forces). This boundary is defined (and a function of) the vertical tire load and the coefficient of adhesion between the road surface and the tire contact patch. The product of tire vertical load and coefficient of adhesion gives the maximum potential of tire force resultant on the tire, which is also called the *friction circle*. Due to that fact, the tire forces whose resultant is closer to that maximum (called also the saturation point) are more sensitive to tire load variations.

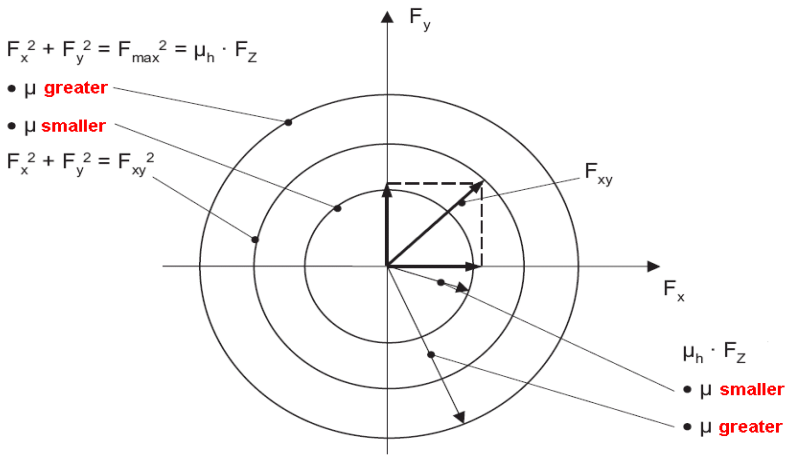

Figure C.1 Schematic explanation of the Friction Circle [23]

APPENDIX D

OTHER CASE STUDIES

D.1 CASE 1: MECHANICAL FAILURE FOR STEP STEER RESPONSE WTIHOUT BRAKING

D.1.1 Failure of Damper 1

In that dynamic maneuver, the most critical damper failure scene for damper 1 is obtained with a damper failure at $\dot{\psi}_{\max}$.

At that point with a damper failure the vertical tire load on tire1 increases instantaneously since the tensile damper force disappears with failure, Figure D.1. Since the tire forces on the left side of the vehicle are bounded by friction circle (the load is shifted to the right side due to roll motion), it consequently results in an increase in FY1 which increases the total yaw moment and consequently the side slip angle. It should be noted that, damper failure on tire1 in general does not lead to very instable responses in terms of lateral dynamics, but the damper failure at that characteristic point $\dot{\psi}_{\max}$ gives the most dynamic response among the other selections. The reason why it constitutes the most critical point is that the speeding up of the body roll motion due to failure (vanishing of the resisting damper force) does not decrease the vertical load on tire 1 very rapidly, since the motion itself is about to reach the steady state. On the contrary there exists a sufficient amount of damper relative velocity (i.e. damper force) to influence the dynamics. The point $\dot{\psi}_{\max}$ forms a good compromise in between. Figures D.1-D.4 demonstrate the influence of the failure explained above.

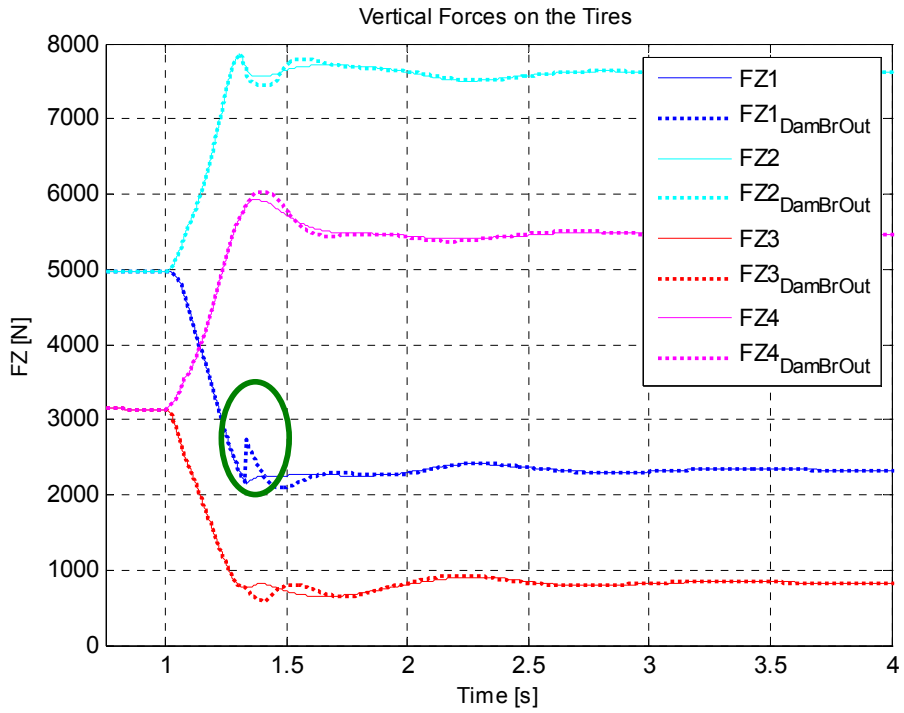

Figure D.1 Vertical Tire Loads for Case 1-Damper1 Failure

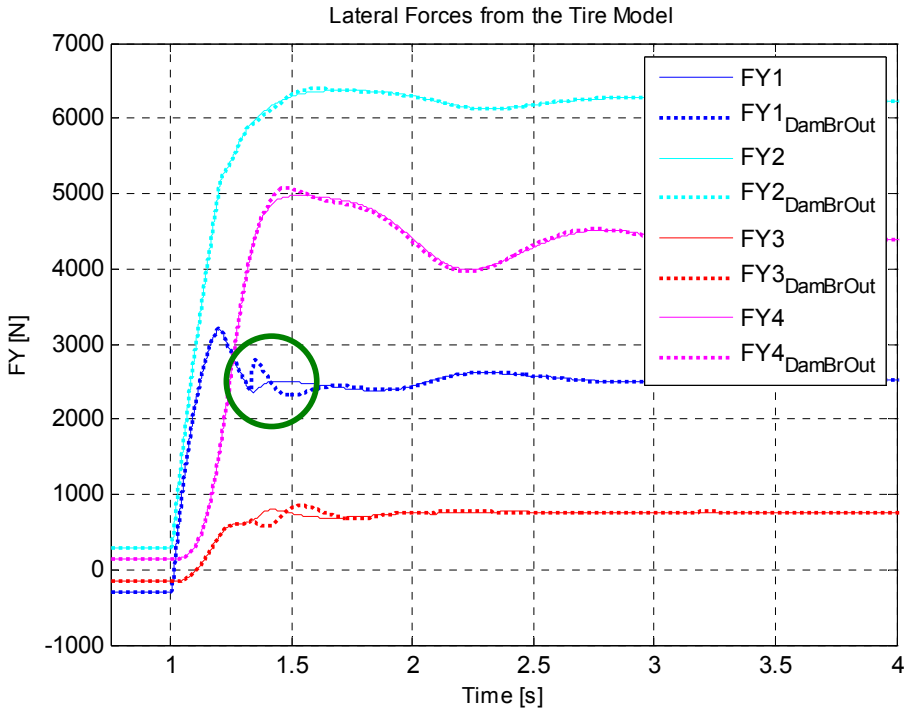

Figure D.2 Lateral Tire Forces for Case 1-Damper1 Failure

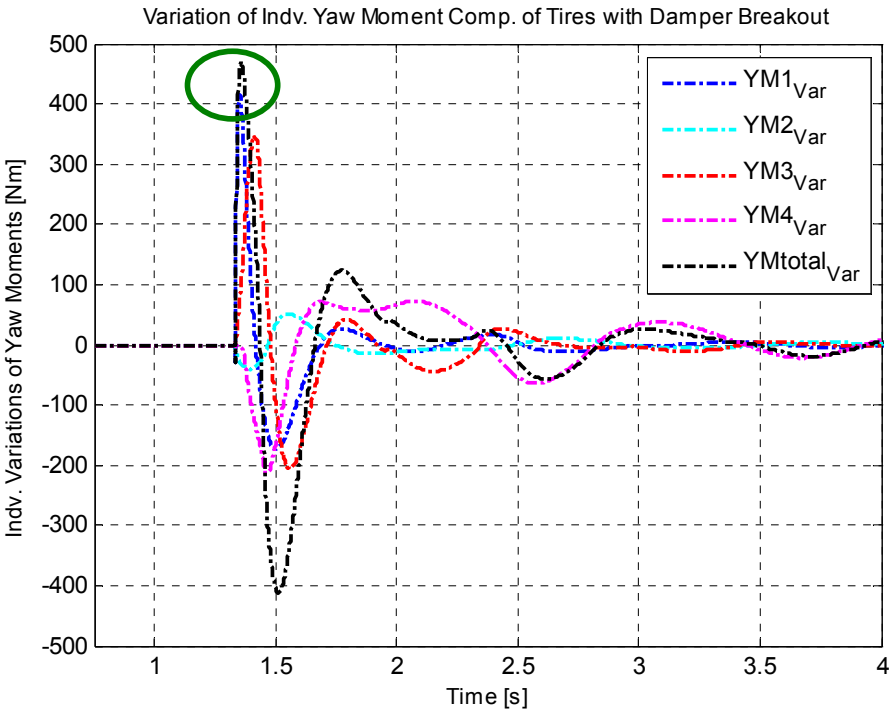

Figure D.3 Variation of Yaw Moments for Case 1-Damper1 Failure

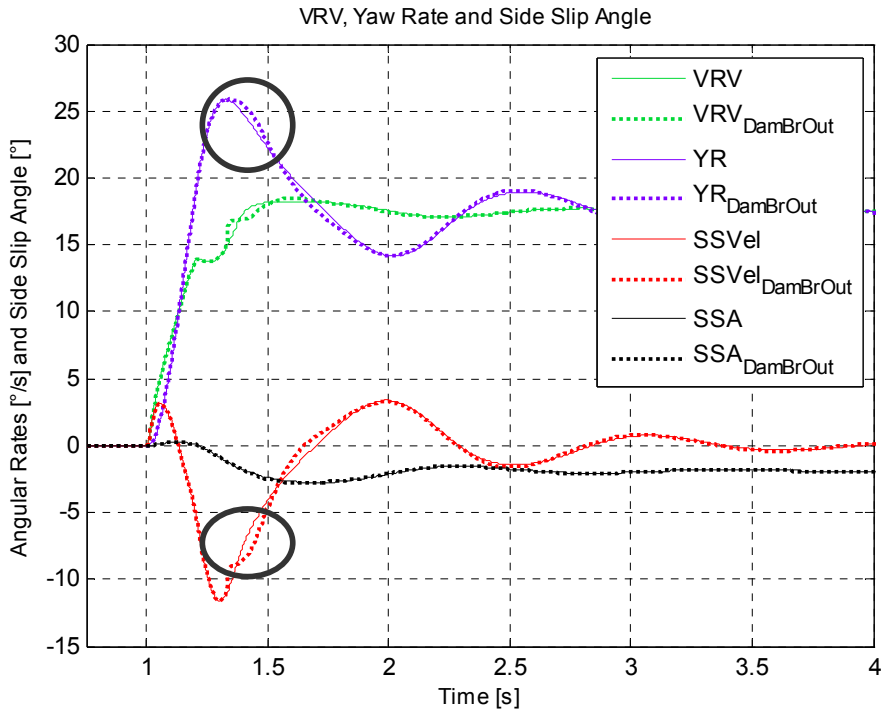

Figure D.4 Calculation of Side Slip Angle for Case 1-Damper1 Failure

D.1.2 Failure of Damper 2

In general the damper failure phenomenon is not critical for damper2 at all. However, the most dynamic case is obtained when the damper fails at the start of the steering maneuver. In that case, due to the decrease in body roll inertia force, the total lateral force is decreased at the point on which the steering step ends, Figure D.7. Due to some reaction to roll acceleration there is a turning point in vehicle lateral force and consequently the vehicle rotate velocity. Without damper force at tire 2 this reaction is sharper and at that point leads to a greater side slip angular peak velocity which is the only critical response in this case, Figure D.8. There is also a more oscillatory tendency in the body roll and pitch but these do not affect the overall yaw moment to a significant extent. Figures D.5-D.8 demonstrate the influence of the failure explained above.

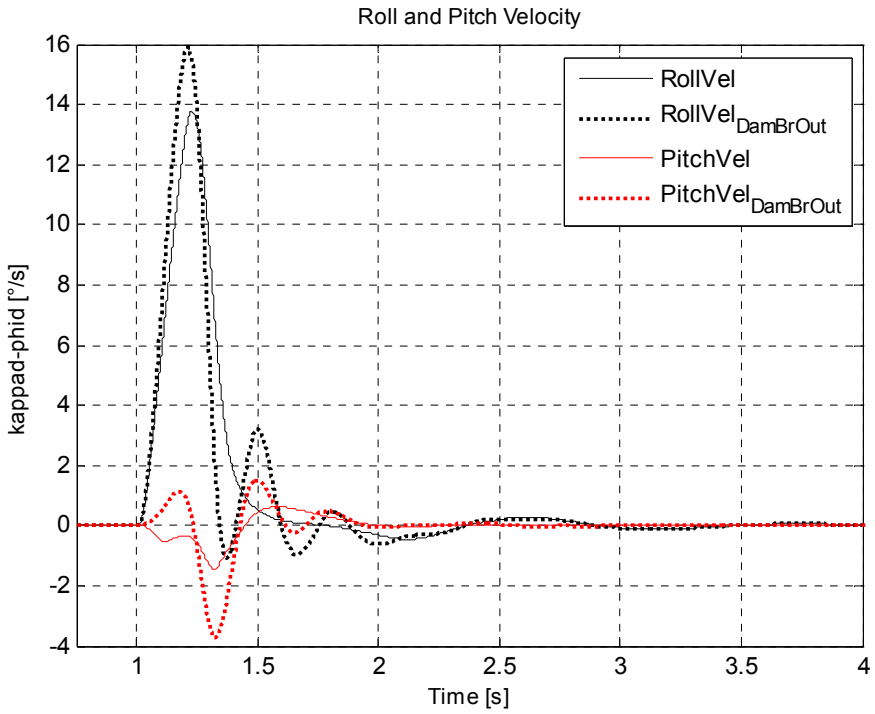

Figure D.5 Roll and Pitch Velocities for Case 1-Damper2 Failure

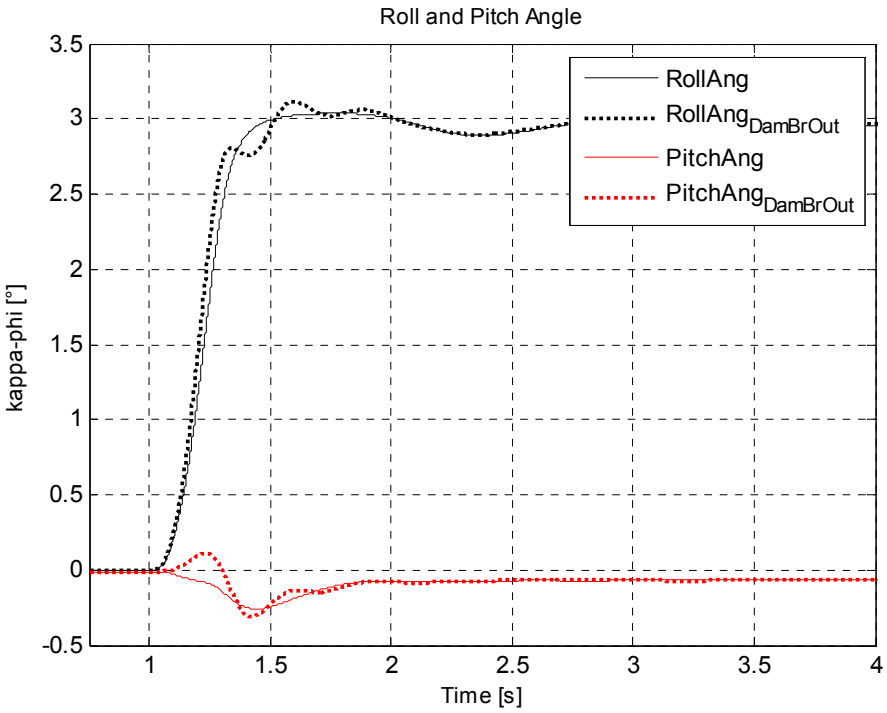

Figure D.6 Roll and Pitch Angles for Case 1-Damper2 Failure

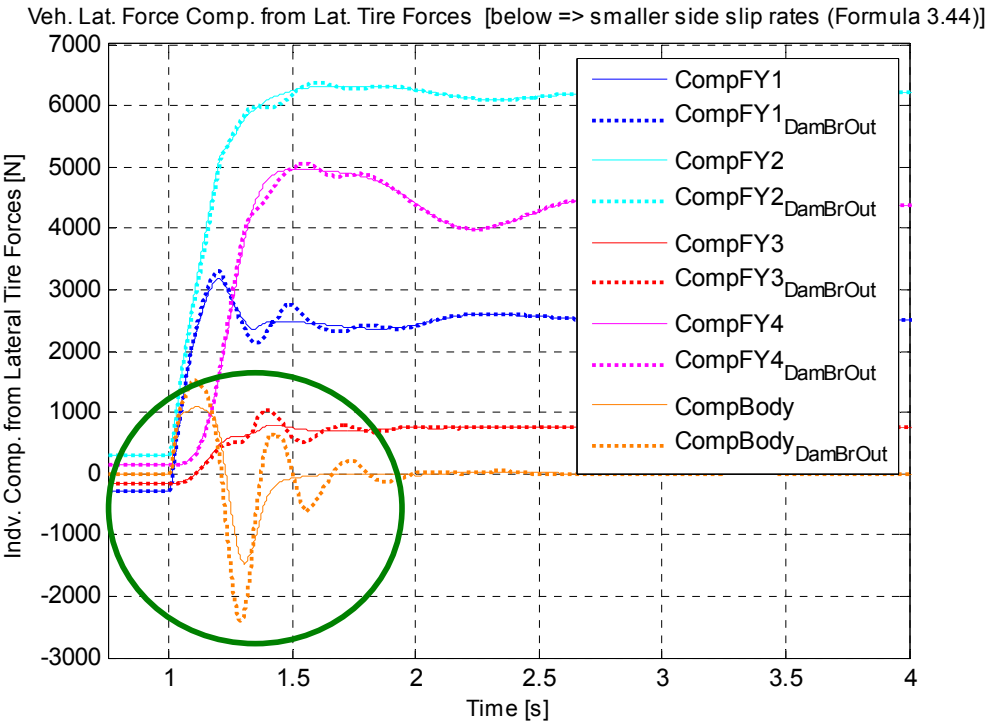

Figure D.7 Vehicle Lateral Force Components from FY for Case 1-Damper2 Failure

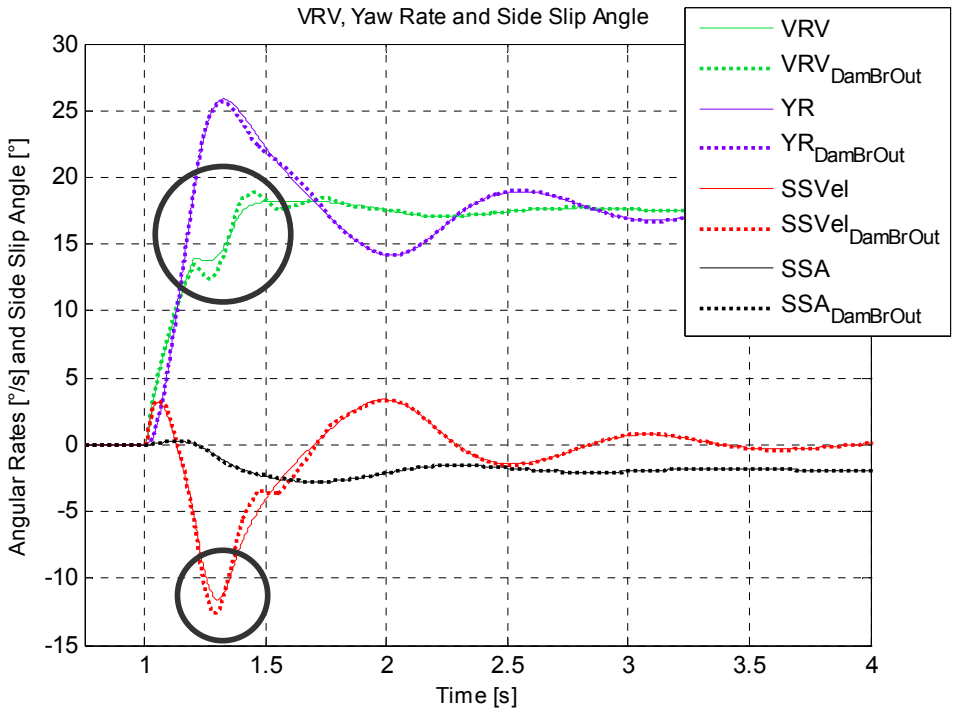

Figure D.8 Calculation of Side Slip Angle for Case 1-Damper2 Failure

D.1.3 Failure of Damper 4

With a damper 4 failure the overall behaviour is not much more critical again but slightly more dynamic. The most critical characteristic point for damper 4 failure is the maximum lateral acceleration $a_{y\max}$ on which the damper relative velocity of damper 4 is tensile and maximum. Due to settling pitch velocity, roll velocity is nearly zero at that point, Figure D.9. So through a damper failure at that point, the resisting force created by damper 4 in order to prevent the body to lean forwards and leftwards disappear. That changes the vertical loads and consequently the lateral forces of tires 1, 3, and 4 significantly (increase in 1 and decrease in 3 are decisive in that case) and the yaw moment is so effected that it rises together with slightly increasing side slip angle, Figure D.13 and D.14. Figures D.9-D.14 demonstrate the influence of the failure explained above.

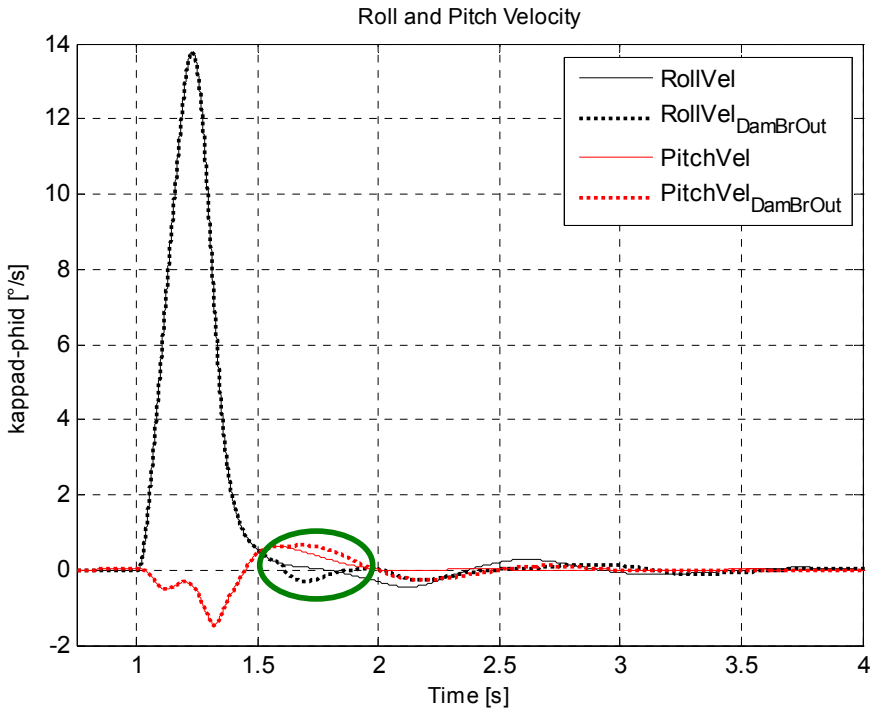

Figure D.9 Roll and Pitch Velocities for Case 1-Damper 4 Failure

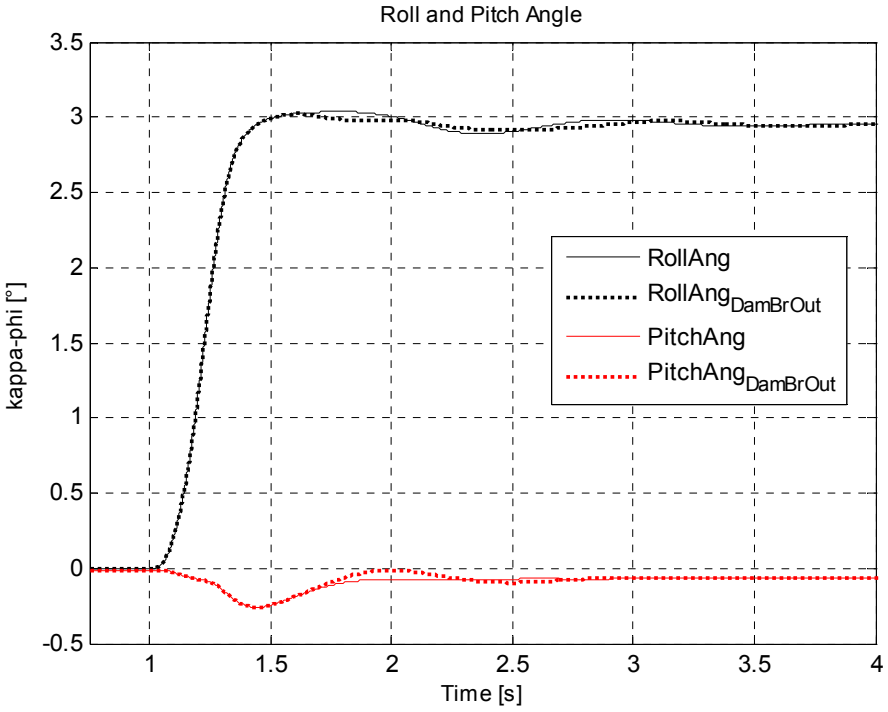

Figure D.10 Roll and Pitch Angles for Case 1- Damper 4 Failure

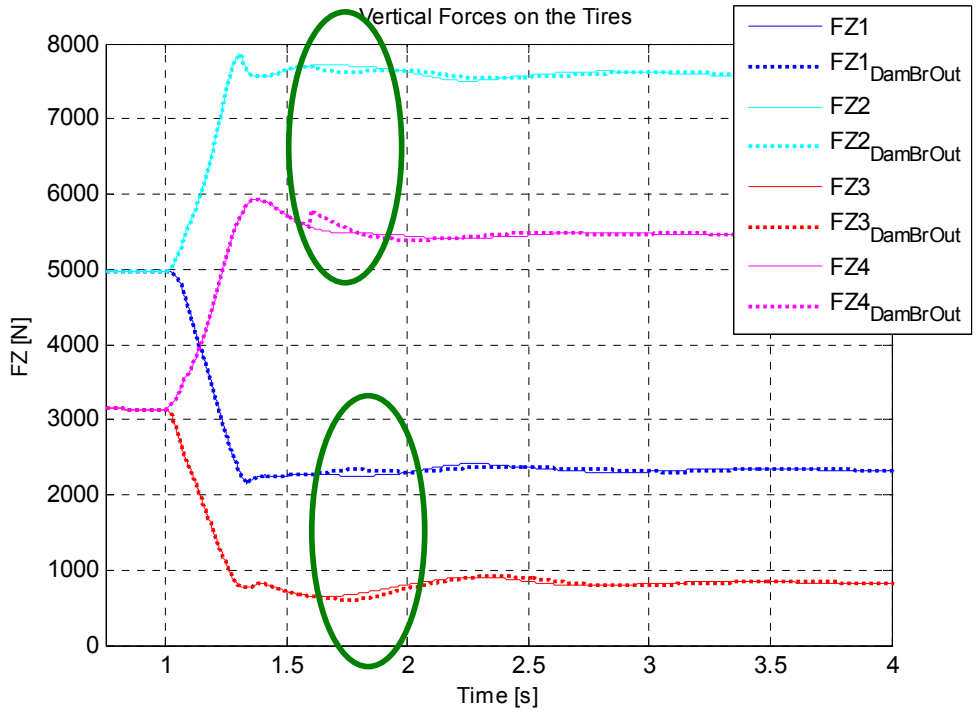

Figure D.11 Vehicle Tire Loads for Case 1- Damper 4 Failure

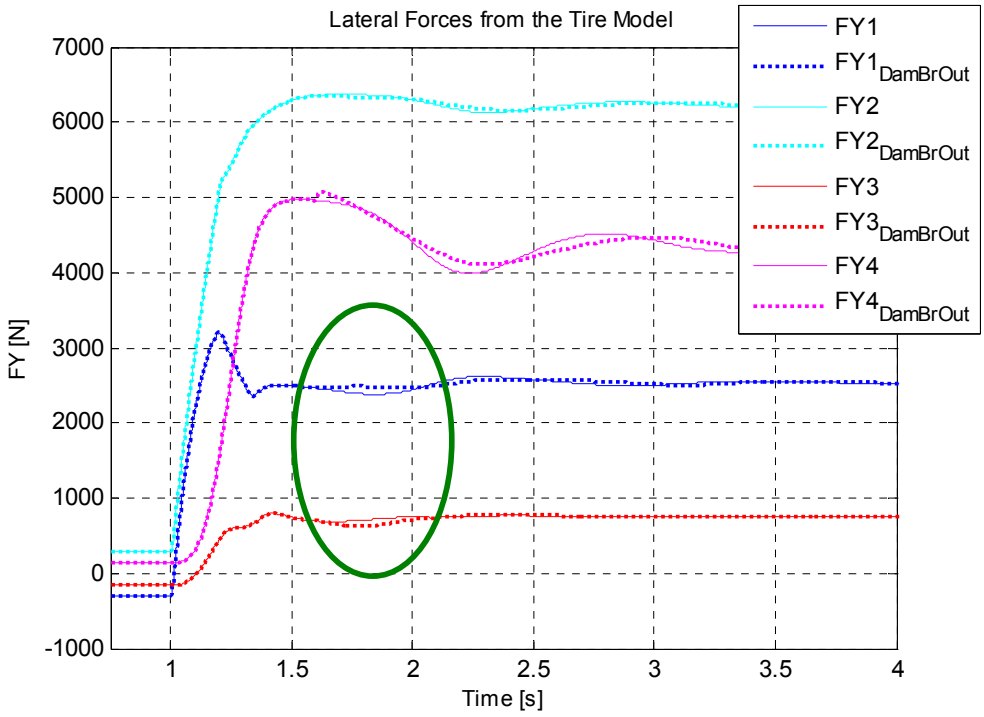

Figure D.12 Lateral Tire Forces for Case 1- Damper 4 Failure

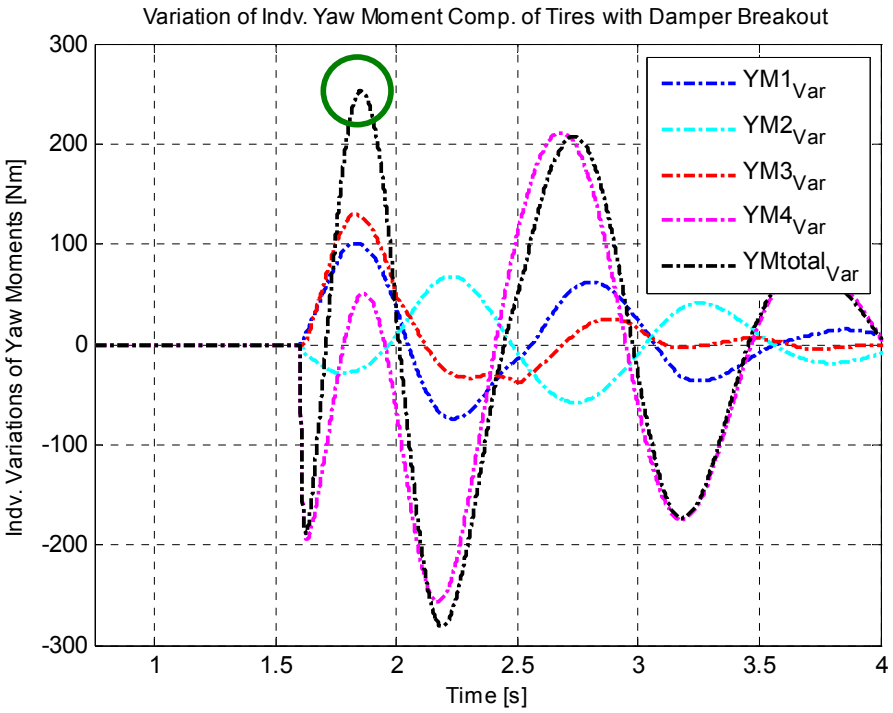

Figure D.13 Variation of Yaw Moments for Case 1- Damper 4 Failure

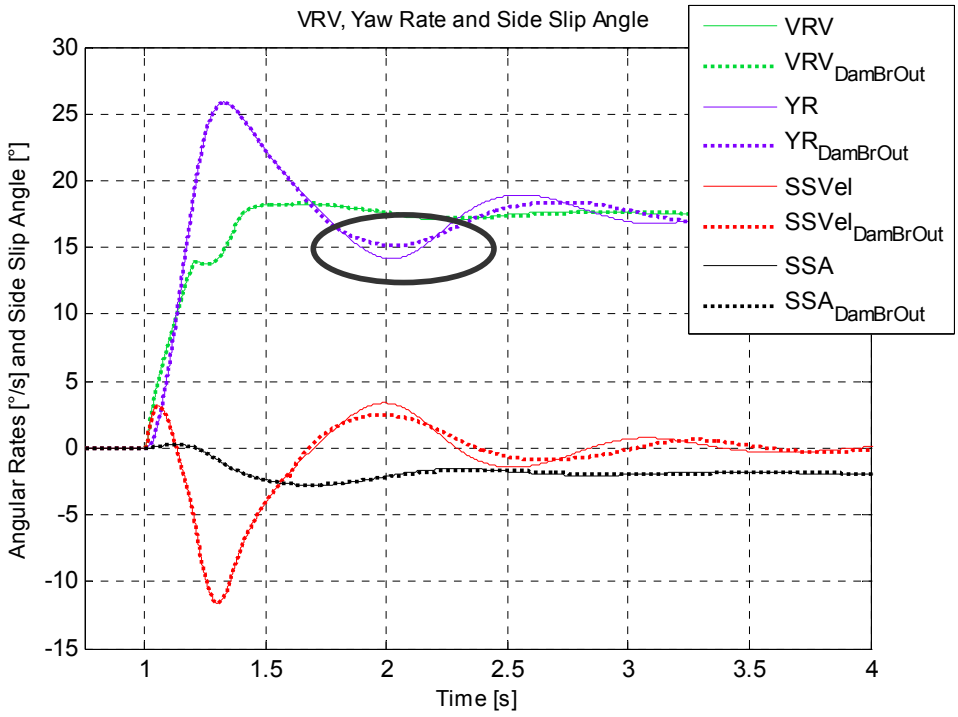

Figure D.14 Calculation of Side Slip Angle for Case 1- Damper 4 Failure

D.2 CASE 4: MECHANICAL FAILURE FOR STEP STEER RESPONSE WITH BRAKING

D.2.1 Failure of Damper 1

$\dot{\kappa}_{max}$ is the most critical point for damper 1 failure, since it accelerates the body pitch and roll motions to the greatest extent. It should be noted that $\dot{\kappa}_{max}$ point is the last dynamic point before the fore motion occurs due to braking. With a damper failure at this point, the pitching during the fore motion becomes greater and the roll motion is smaller, Figure D.15 and D.16. It can be also imagined that with the absence of damper force on tire1, as a result of harsh braking, the body leans on the tire 1 more.

Therefore, the vertical forces on tires 1, 2 and 4 change (i.e. FX3 smaller, FX4 greater and FY1 greater) so that the longitudinal and lateral tire forces at the end create a total yaw moment which rises up. Figures D.15-D.21 demonstrate the influence of the failure explained above.

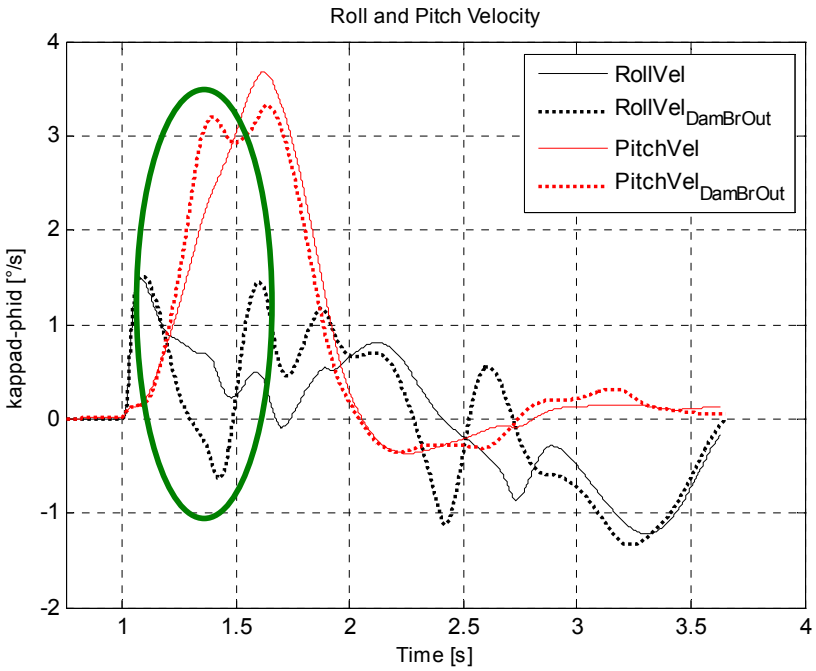

Figure D.15 Roll and Pitch Velocities for Case 4-Damper 1 Failure

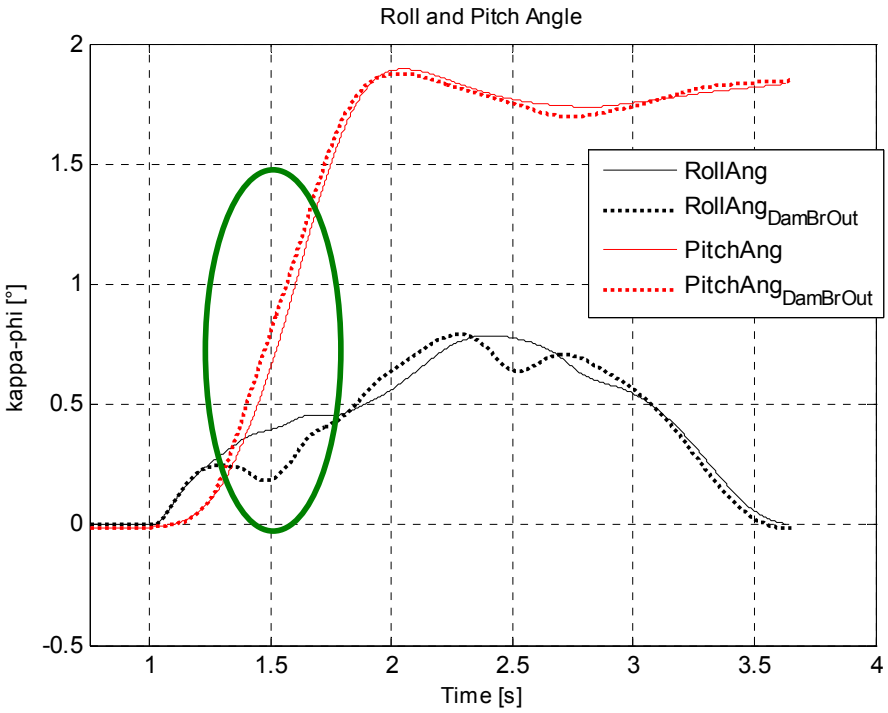

Figure D.16 Roll and Pitch Angles for Case 4-Damper 1 Failure

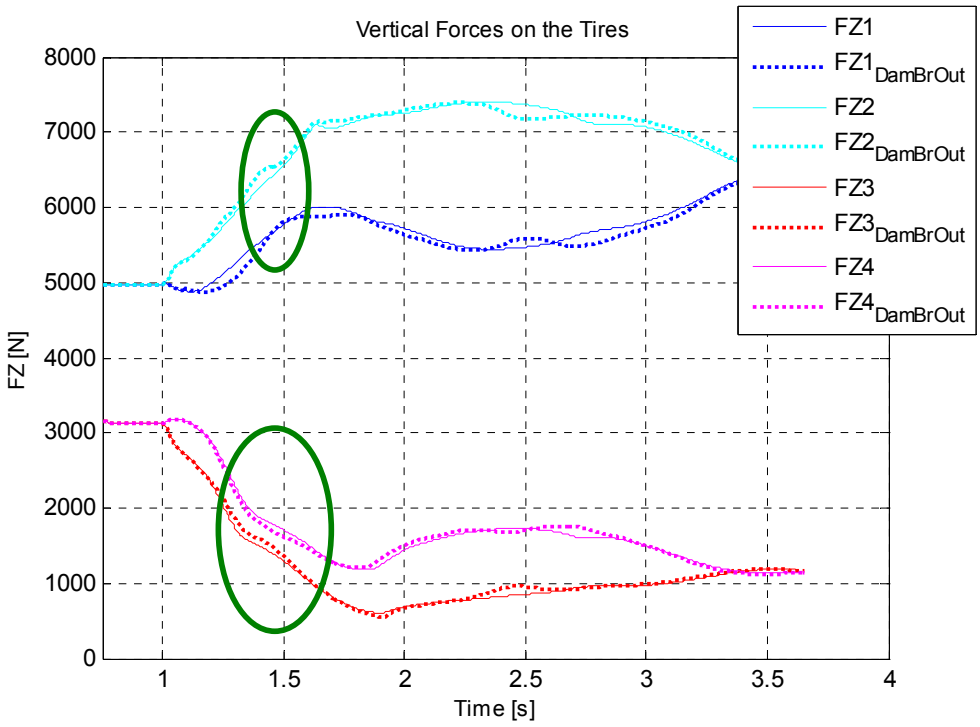

Figure D.17 Vertical Tire Loads for Case 4-Damper 1 Failure

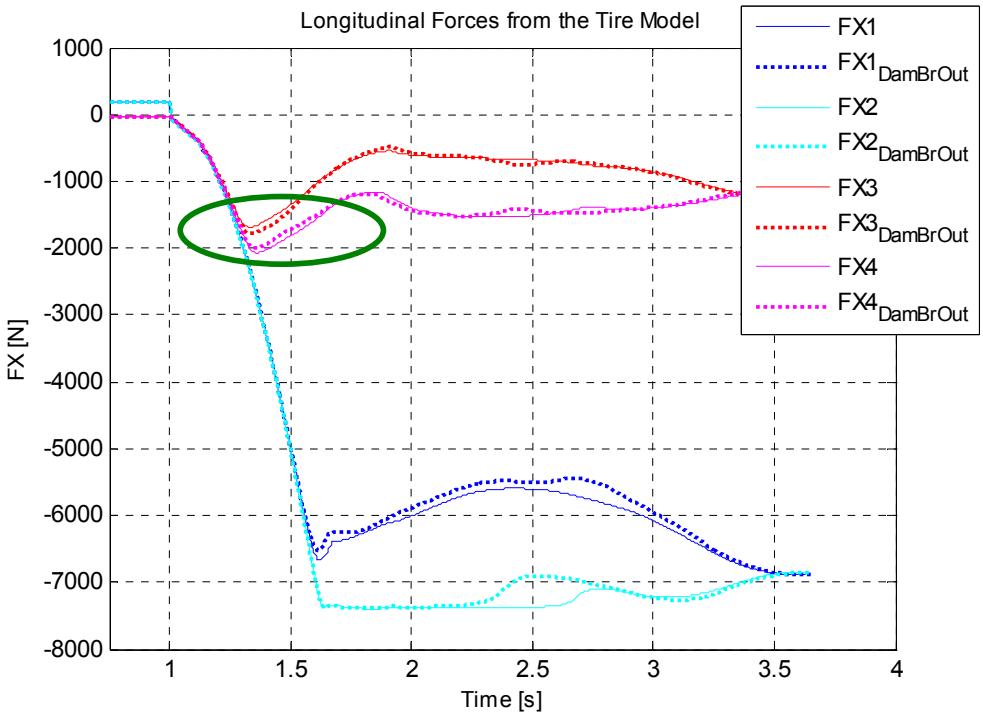

Figure D.18 Longitudinal Tire Forces for Case 4-Damper 1 Failure

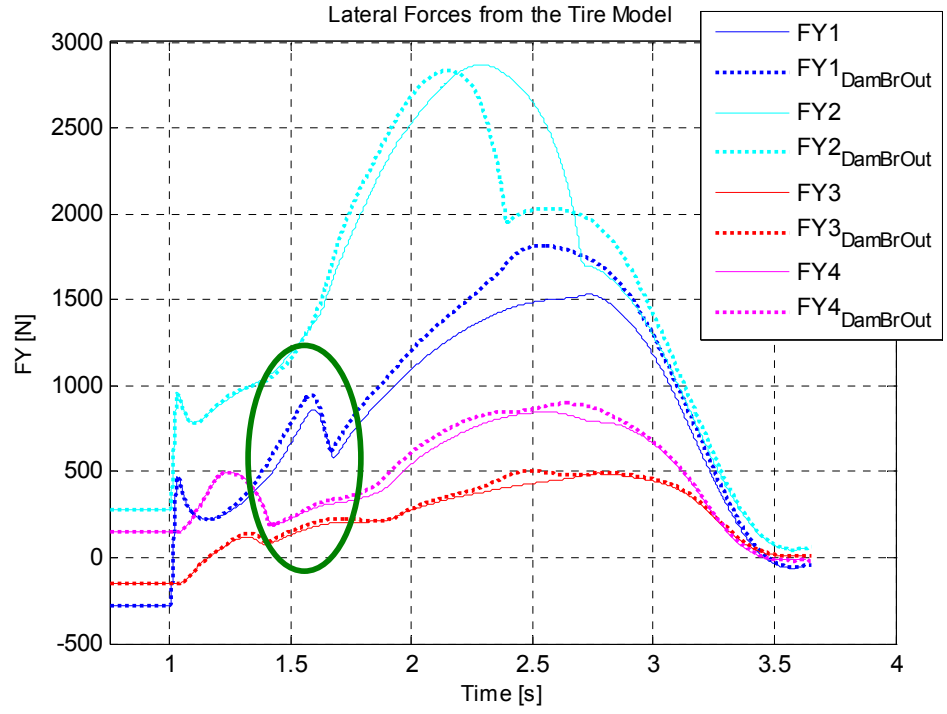

Figure D.19 Lateral Tire Forces for Case 4-Damper 1 Failure

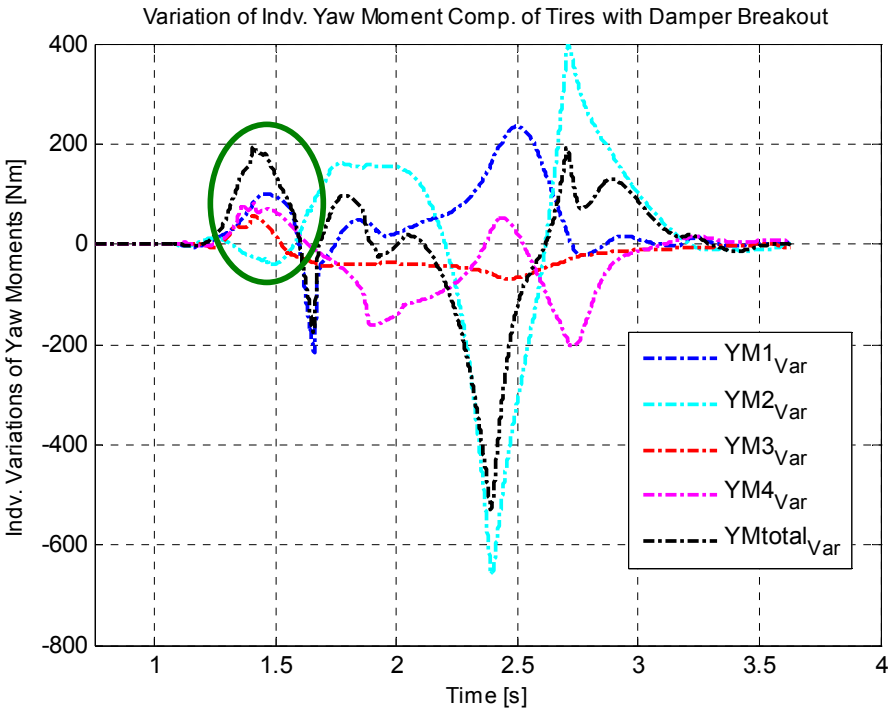

Figure D.20 Variation of yaw Moments for Case 4-Damper 1 Failure

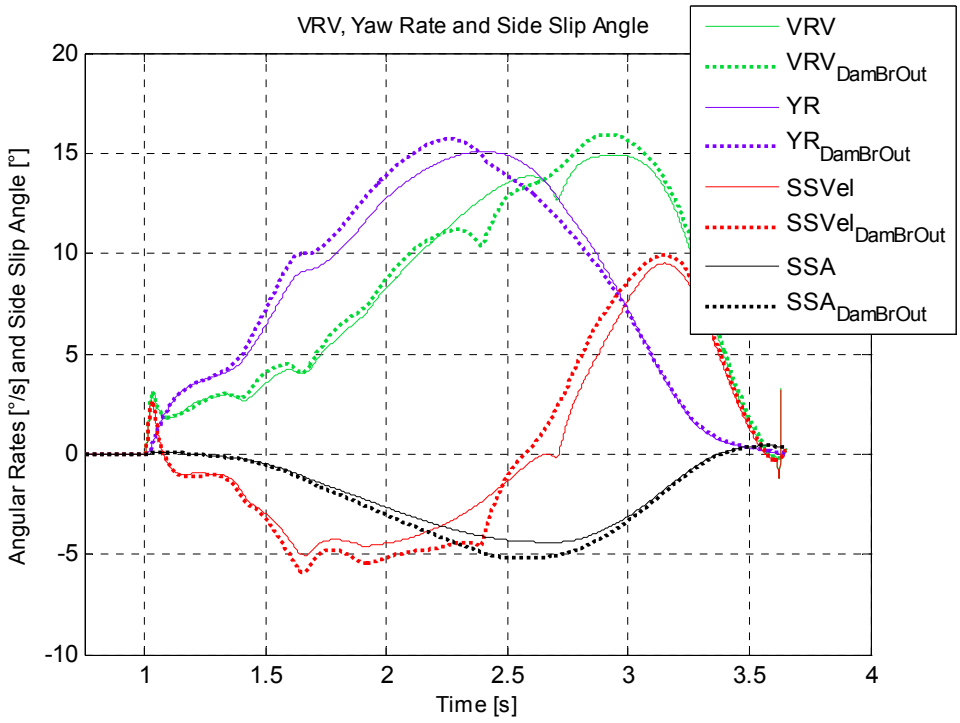

Figure D.21 Calculation of Side Slip Angle for Case 4-Damper 1 Failure

D.2.2 Failure of Damper 2

In general, damper failure on tire 2 does not result in a more dynamic tendency. However, φ_{max} is the most critical point on which the damper failure creates the most dynamic one when compared to the other points.

On that point, on tire 2 there exists a pure relative velocity (damper force) due to roll velocity, on φ_{max} the pitch velocity is 0, Figure D.22. Damper failure of tire 2 creates a comparatively large change in the lateral force (due to vertical force oscillation as a result of more oscillatory body motions), since longitudinal force FX2 is already at its maximum; mechanically limited since the achievable brake force in the brake drum is attained and the Friction Circle concept distributes all the tire force potential to FY2. That slight oscillation in FY2 is the only factor which influences the response in a more dynamic way. Figures D.22-D.27 demonstrate the influence of the failure explained above.

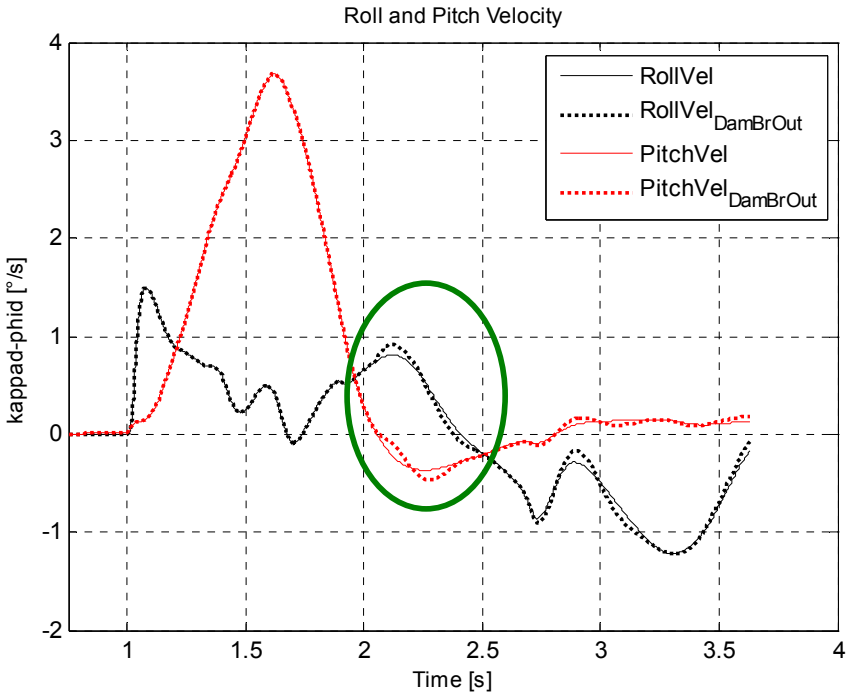

Figure D.22 Roll and Pitch Velocities for Case 4-Damper 2 Failure

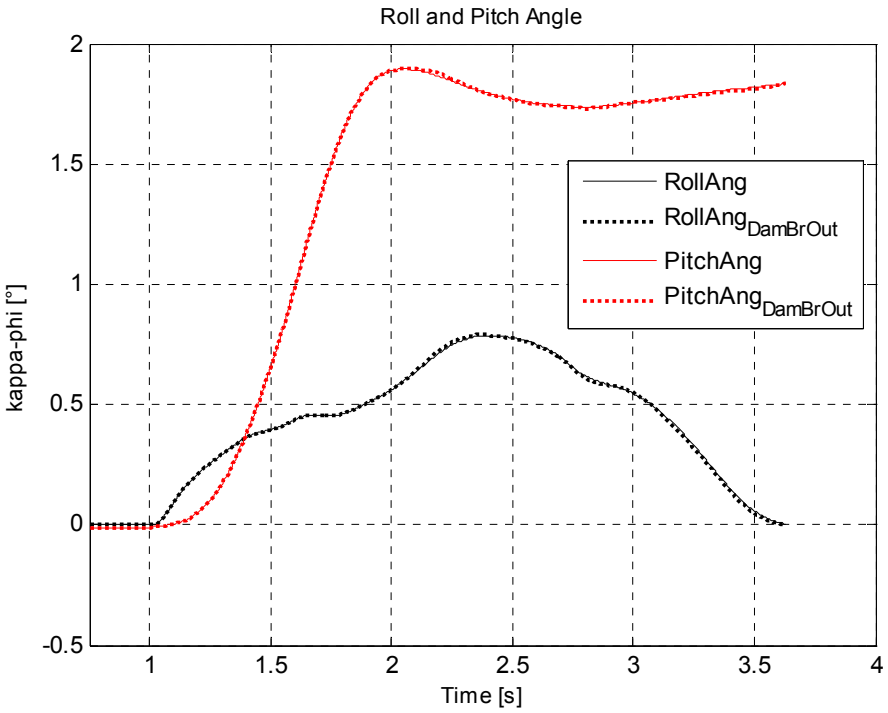

Figure D.23 Roll and Pitch Angles for Case 4-Damper 2 Failure

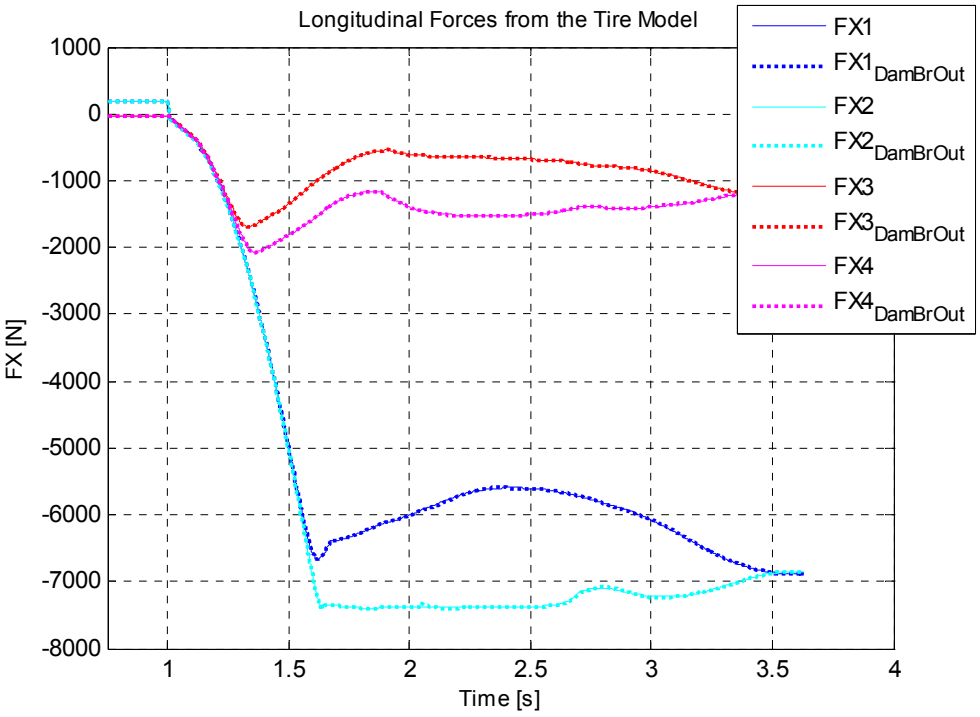

Figure D.24 Longitudinal Tire Forces for Case 4-Damper 2 Failure

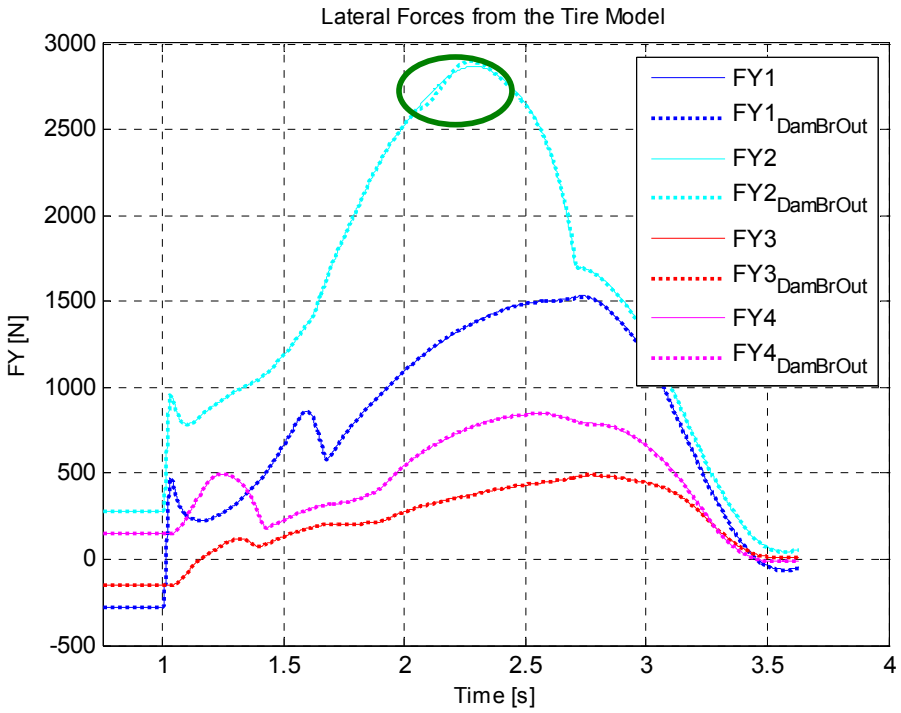

Figure D.25 Lateral Tire Forces for Case 4-Damper 2 Failure

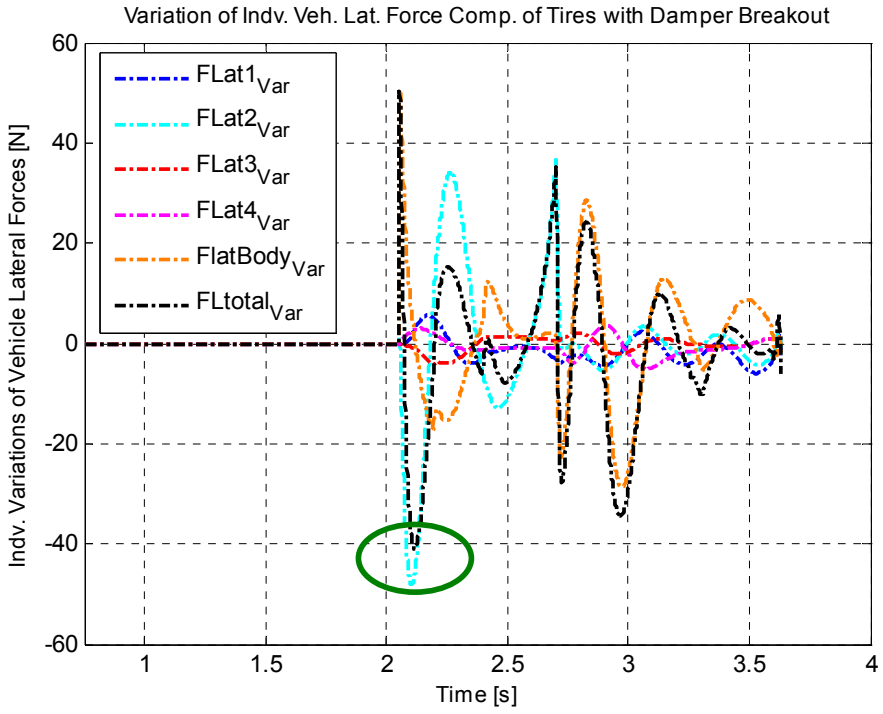

Figure D.26 Vehicle Lateral Force Components from FY for Case 4-Damper 2 Failure

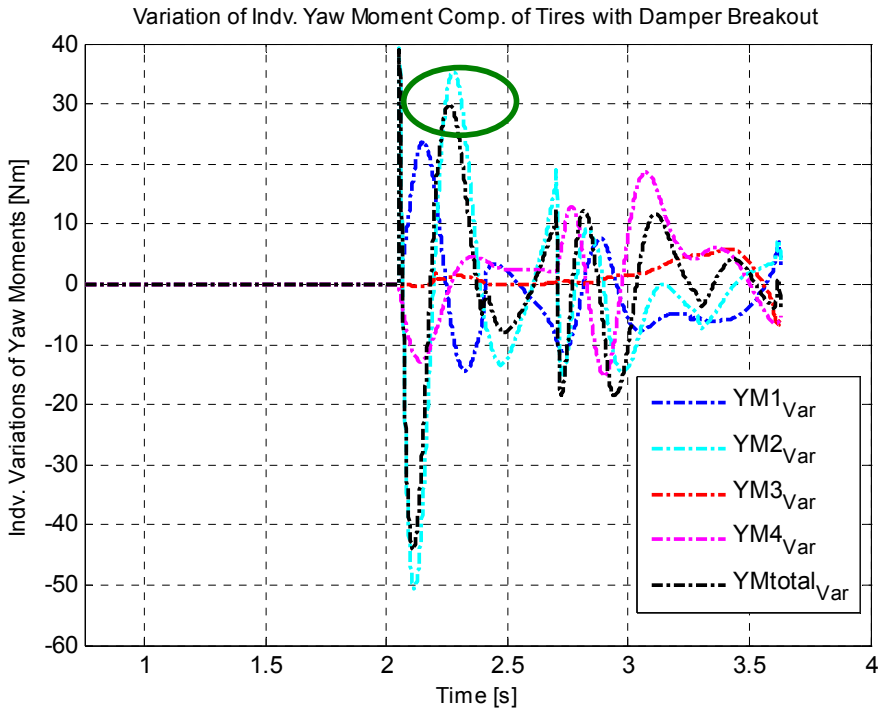

Figure D.27 Variation of Yaw Moments for Case 4-Damper 2 Failure

D.2.3 Failure of Damper 4

In general, damper failure on tire 4 gives out a slightly more dynamic response in side slip angle. φ_{max} is the most critical point since on that point the damper relative velocities are only due to roll (the pitch velocity is zero at that moment) and consequently a compressive one. Due to that fact a damper failure at that point results in the compressive damper force to disappear, the body will lean on tire 4, greater roll and smaller pitch, Figure D.29.

Due to greater roll the FY2 has a relative greater increase when compared to the variations on other tire forces (the increase in the vertical load on tire 2 is distributed only to FY2 since FX2 is at its mechanical limit) the vehicle has a slight tendency towards more dynamic response related to the increase in the total yaw moment. Figures D.28-D.34 demonstrate the influence of the failure explained above.

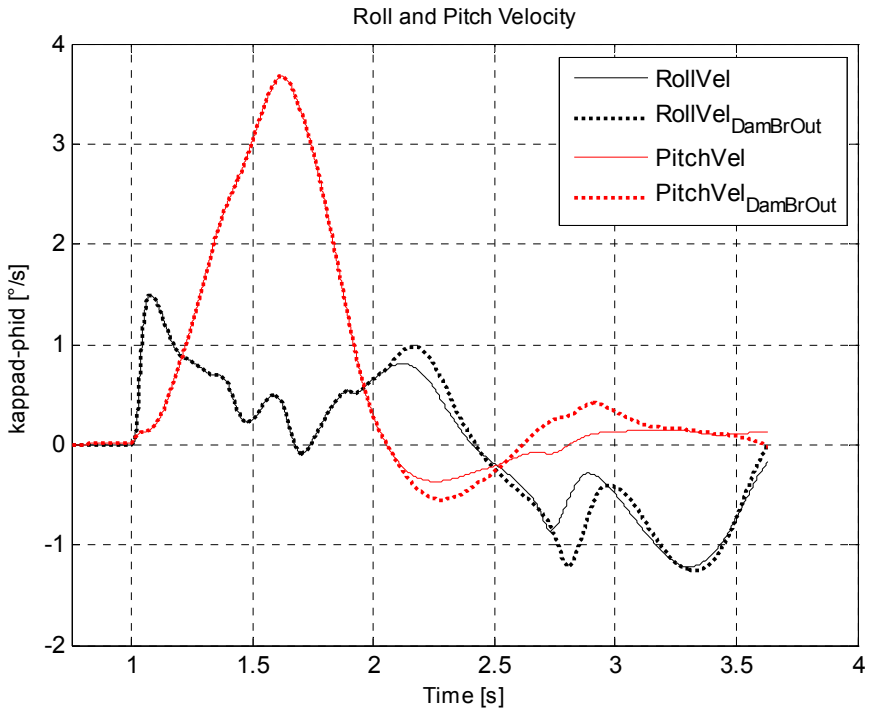

Figure D.28 Roll and Pitch Velocities for Case 4-Damper 4 Failure

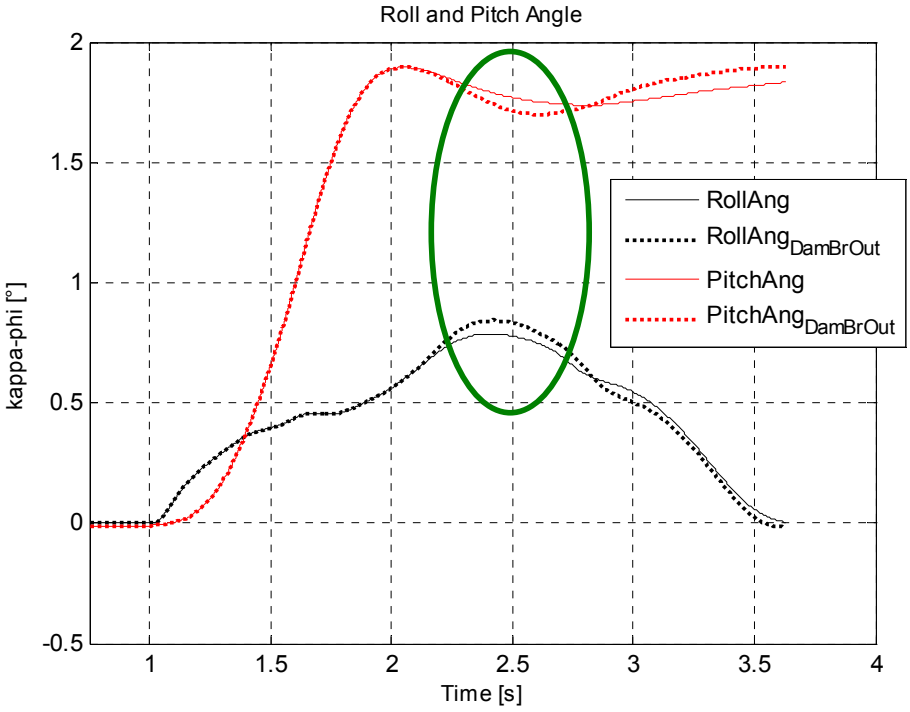

Figure D.29 Roll and Pitch Angles for Case 4-Damper 4 Failure

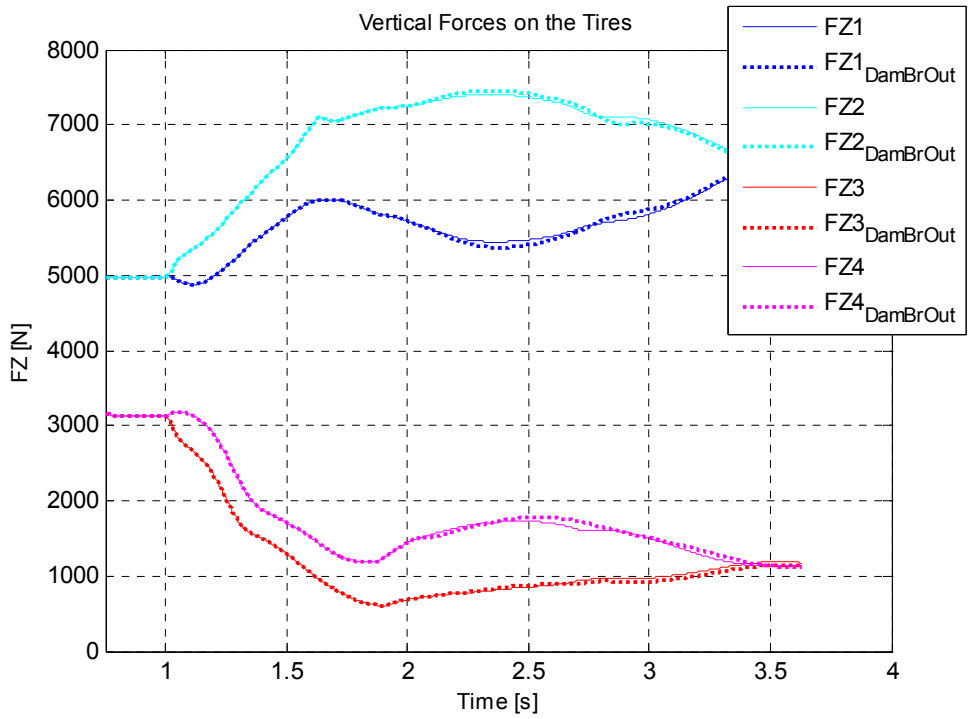

Figure D.30 Vertical Tire Loads for Case 4-Damper 4 Failure

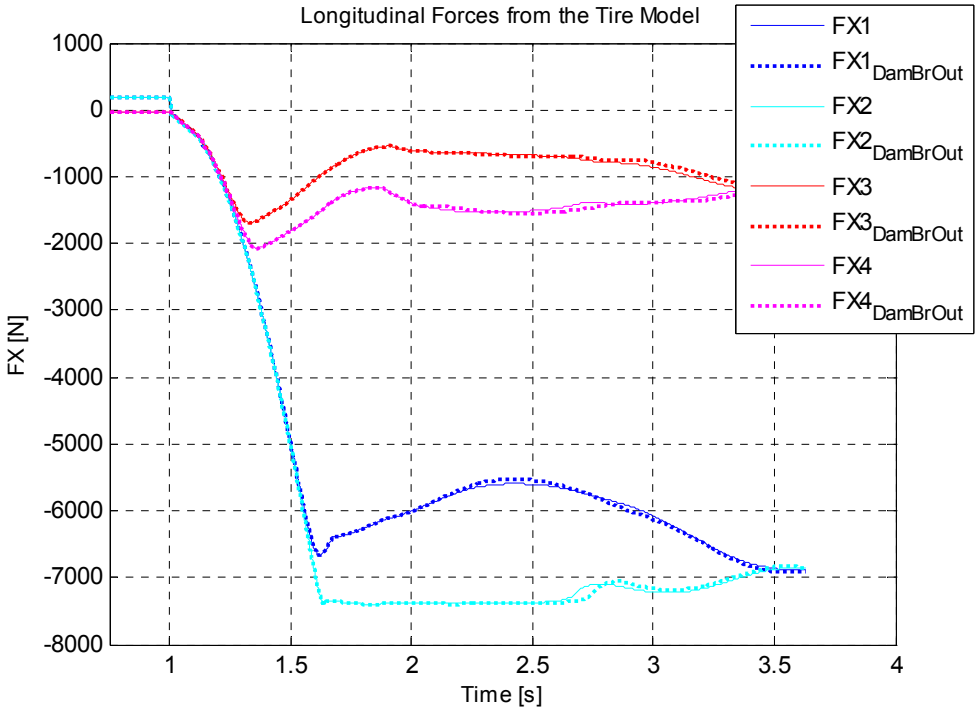

Figure D.31 Longitudinal Tire Forces for Case 4-Damper 4 Failure

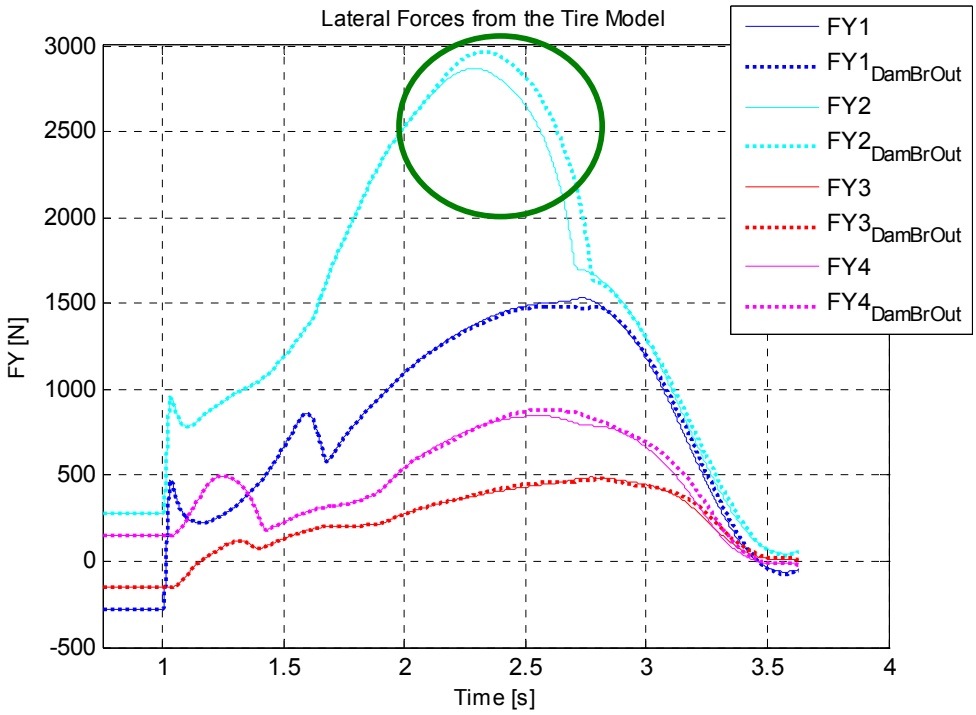

Figure D.32 Lateral Tire Forces for Case 4-Damper 4 Failure

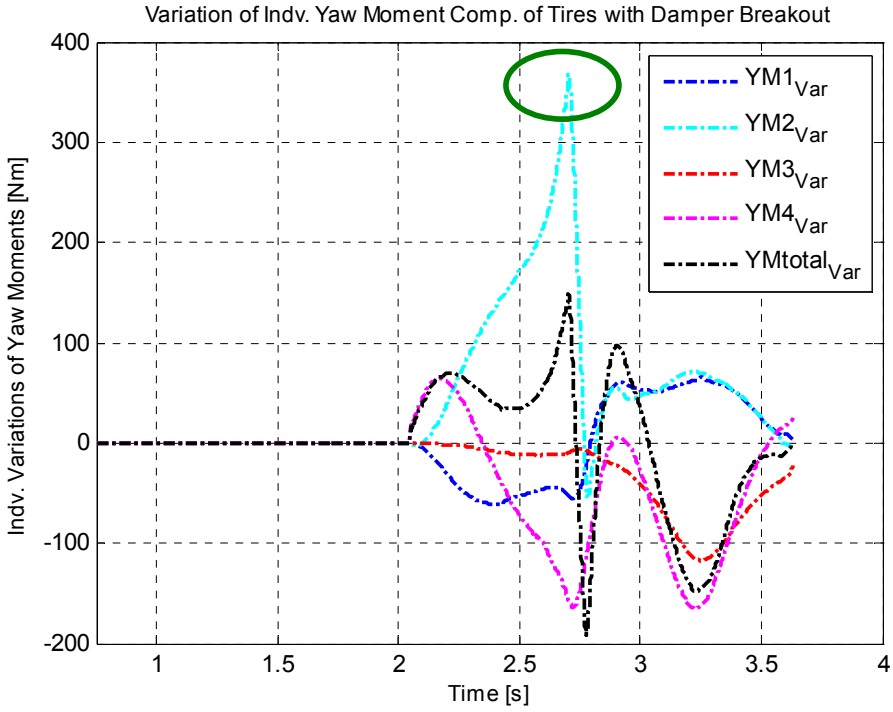

Figure D.33 Variation of Yaw Moments for Case 4-Damper 4 Failure

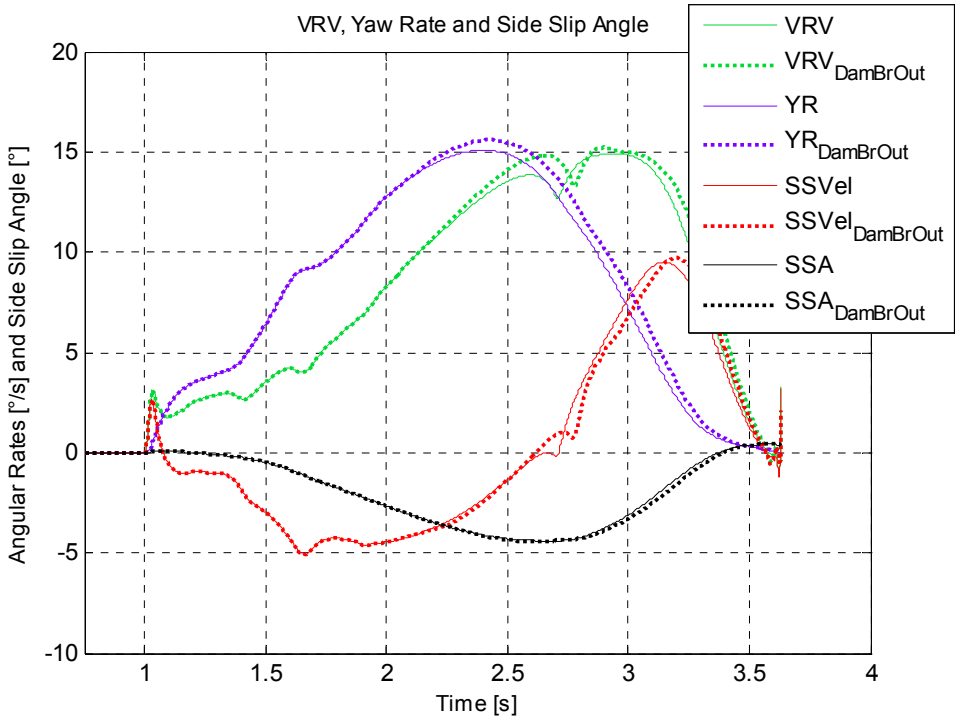

Figure D.34 Calculation of Side Slip Angle for Case 4-Damper 4 Failure

D.3 CASE 7: ELECTRICAL FAILURE FOR STEP STEER RESPONSE WITHOUT BRAKING

D.3.1 Failure of Damper 1

In general, the failure on tire 1 gives no significant critical responses. However, the damper failure at the characteristic point $a_{y\max}$ has the most dynamic influence on the responses. Firstly, with the damper failure the vertical load on tire 1 jumps up creating a greater lateral force on tire 1 (due to friction circle the FY1 is bounded with FZ1), Figure D.36. Secondly, due to greater damping force the body inertia forces due to roll acceleration is smaller which reduces the vehicle rotational velocity (VRV), Figure D.39. These two effects are the only dynamic influences to

the condition in this damper failure case. $a_{y\max}$ is the most critical point for damper 1 failure since at that point tire 1 has a compressive damper velocity (and damper force) and which is relatively high. Figures D.35-D.39 demonstrate the influence of the failure explained above.

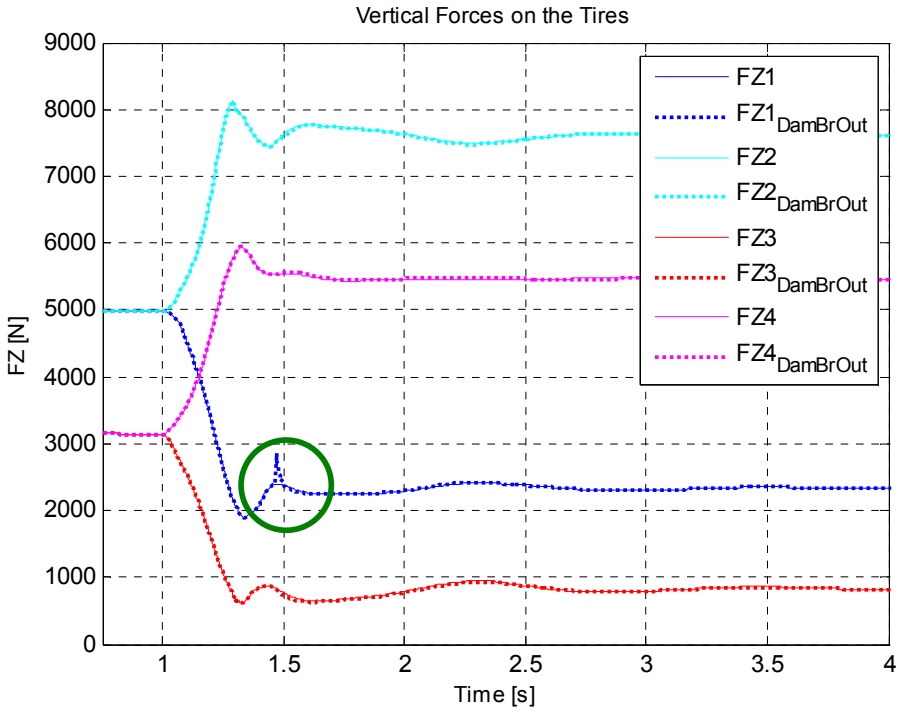

Figure D.35 Vertical Tire Loads for Case 7-Damper 1 Failure

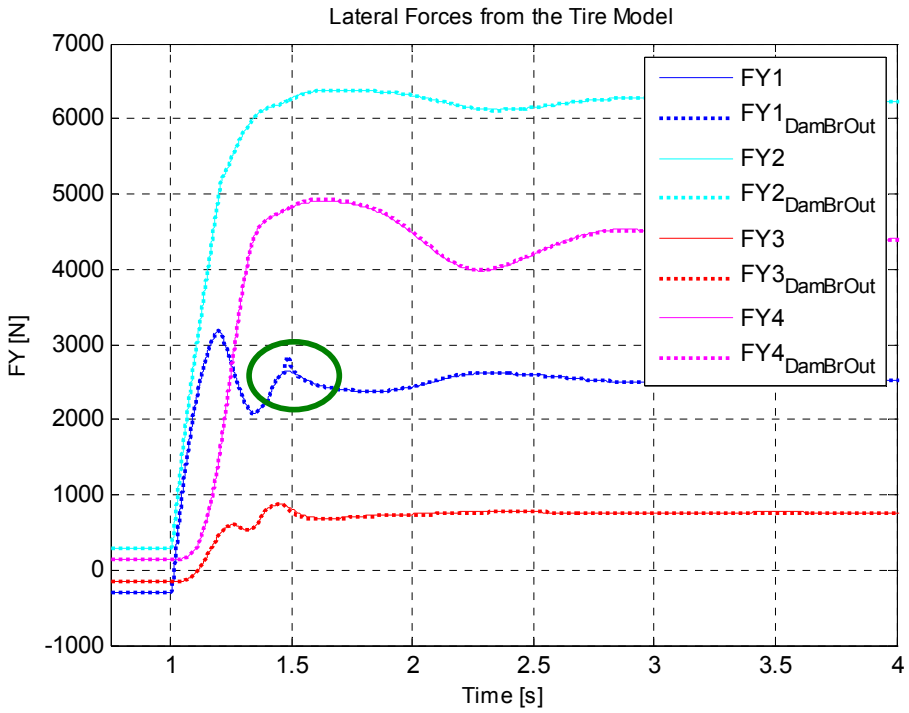

Figure D.36 Lateral Tire Forces for Case 7- Damper 1 Failure

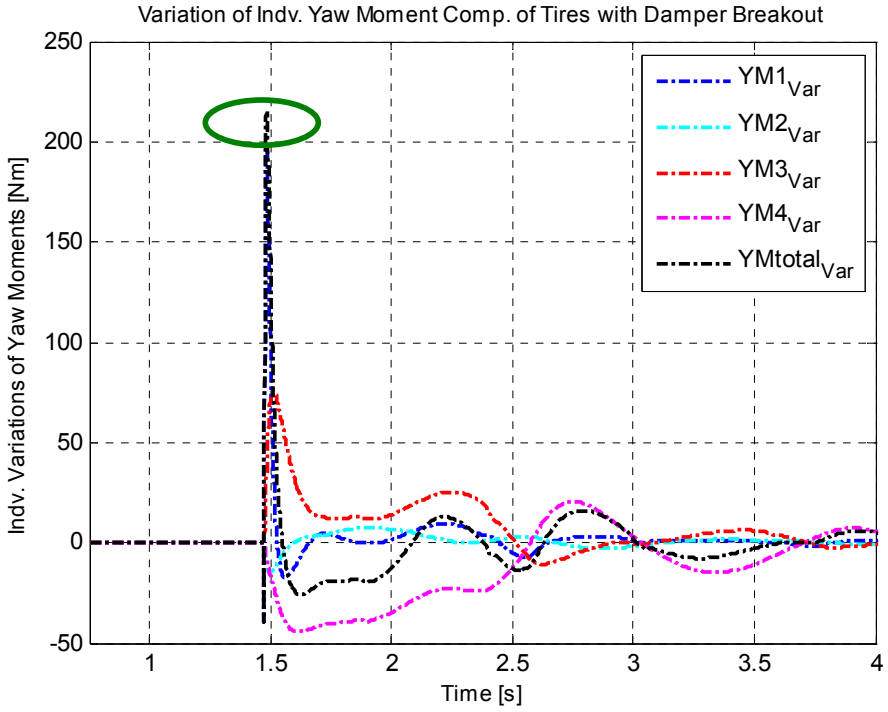

Figure D.37 Variation of Yaw Moments for Case 7- Damper 1 Failure

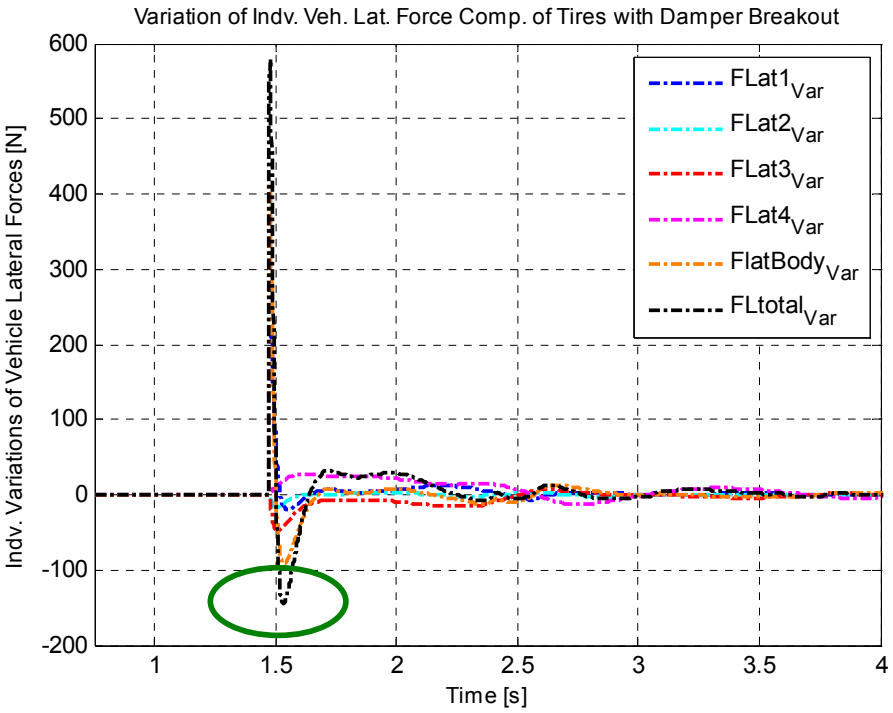

Figure D.38 Variation of Vehicle Lateral Force Components for Case 7- Damper 1 Failure

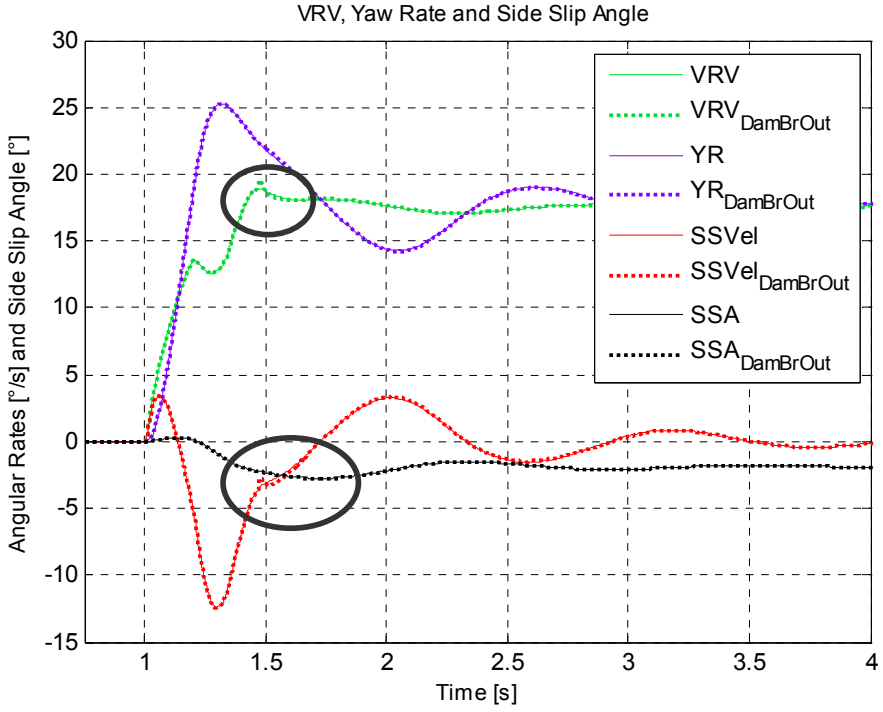

Figure D.39 Calculation of Side Slip Angle for Case 7- Damper 1 Failure

D.3.2 Failure of Damper 2

In general the damper failure on tire 2 is not critical, but the most dynamic influence is obtained with a damper break out at the characteristic failure point $\dot{\psi}_{\max}$ since that point is the last characteristic point before the overshoot of vehicle rotational velocity where the total lateral force starts to decrease. With a damper 2 failure on that characteristic point due to more resisting force the body roll inertia force comes out to be slightly smaller which as a result makes the VRV smaller in the region explained above, Figure D.42 and D.43. This is the only factor that has a dynamic influence on the overall response. Figures D.40-D.43 demonstrate the influence of the failure explained above.

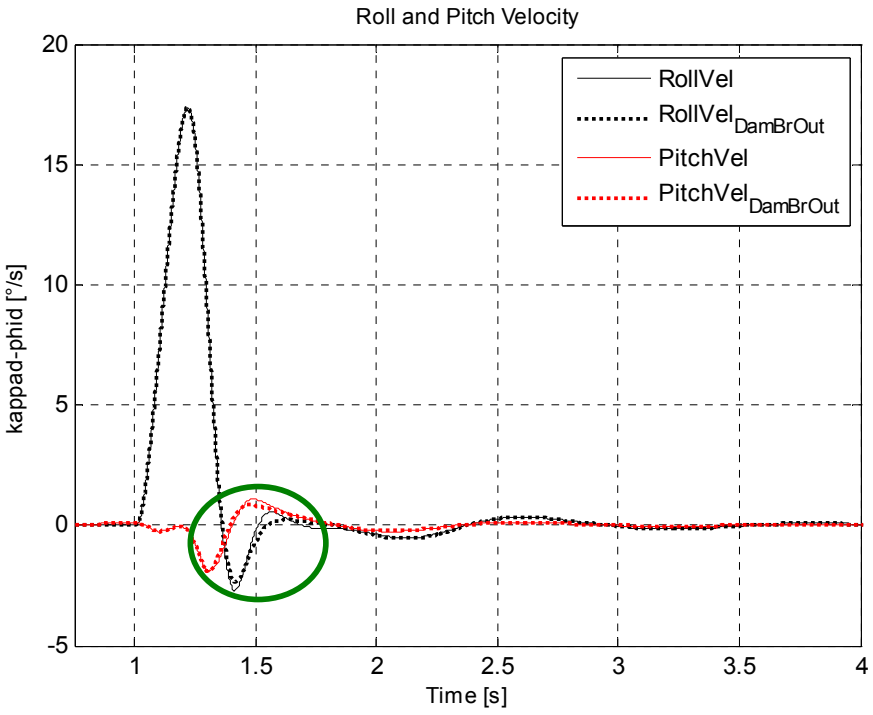

Figure D.40 Roll and Pitch Velocities for Case 7-Damper 2 Failure

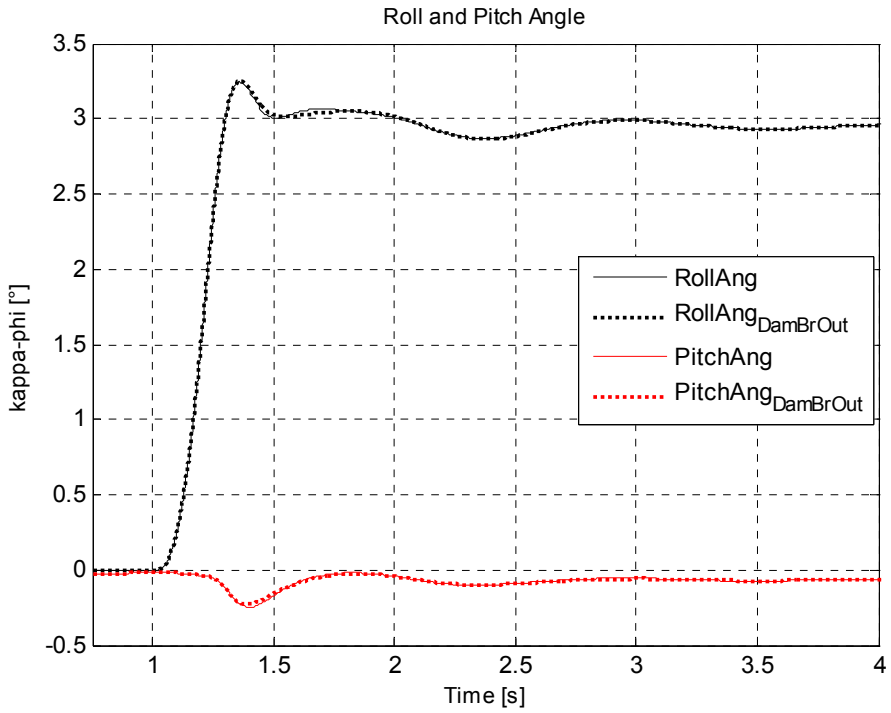

Figure D.41 Roll and Pitch Angles for Case 7- Damper 2 Failure

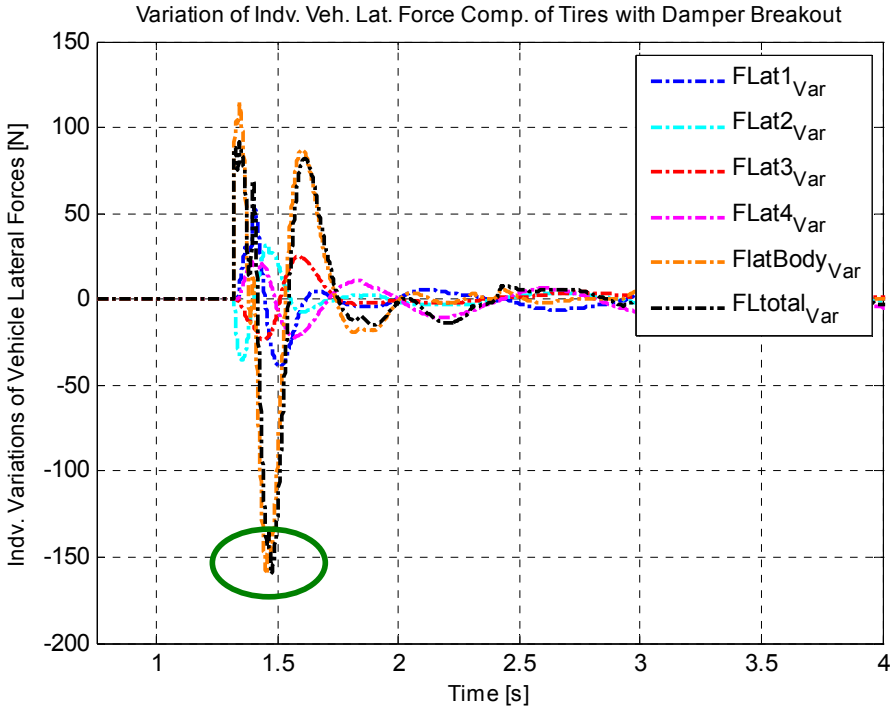

Figure D.42 Variation of Vehicle Lateral Force Components for Case 7- Damper 2 Failure

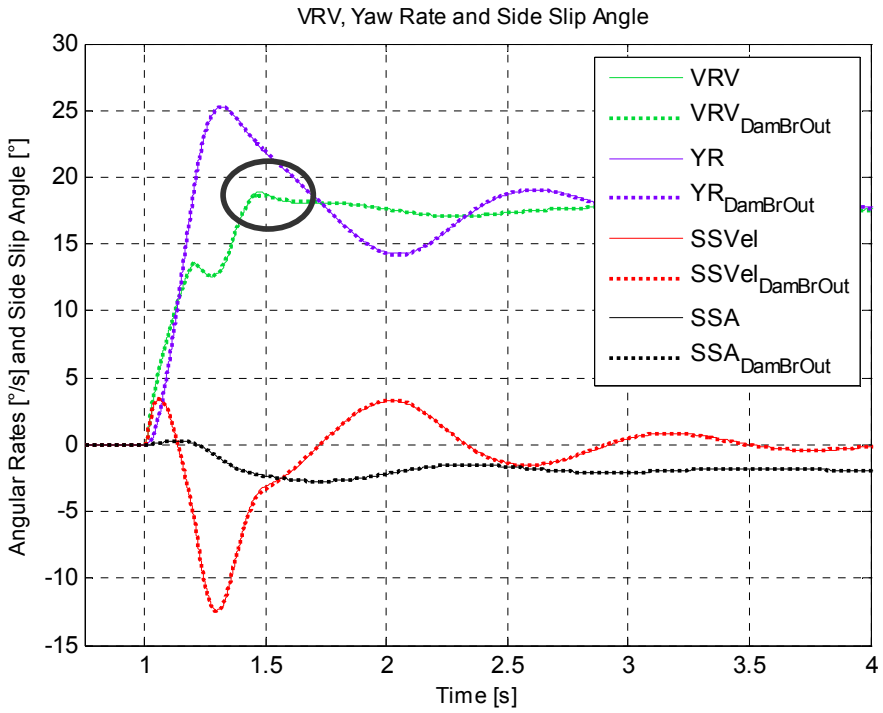

Figure D.43 Calculation of Side Slip Angle for Case 7- Damper 2 Failure

D.3.3 Failure of Damper 3

With a damper failure on tire 3 at the characteristic point $a_{y\max}$, a slightly more dynamic response is obtained which is the most critical response that is achievable. $a_{y\max}$ point is the most critical point for damper 3 failure, since at that point the tire 3 has a tensile and relative high damper relative velocity and thus damper force. So due to the damper failure tire 3 reveals a decrease in vertical load which results in a decrease in lateral force, too since lateral force on tire 3 is bounded by vertical load at that point. Since the damper forces after the failure are higher, the resistance to the motion of the body is more and the rise in the vertical load of tire 3 does not vanish so rapidly. Therefore, as a result, the total yaw moment is slightly higher and the tendency is slightly more dynamic. Figures D.44-D.47 demonstrate the influence of the failure explained above.

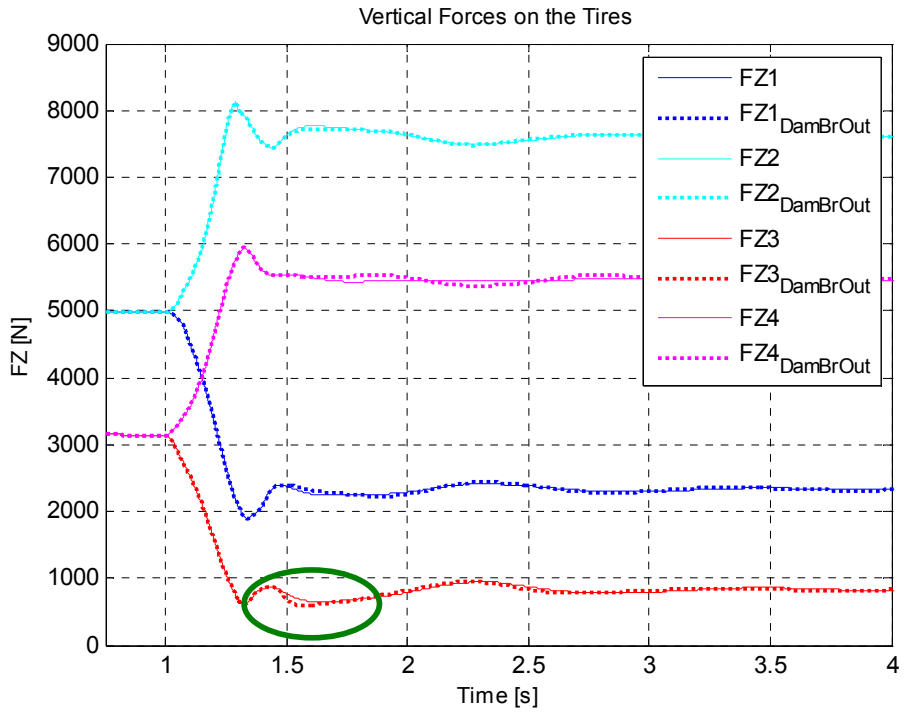

Figure D.44 Vertical Tire Loads for Case 7-Damper 3 Failure

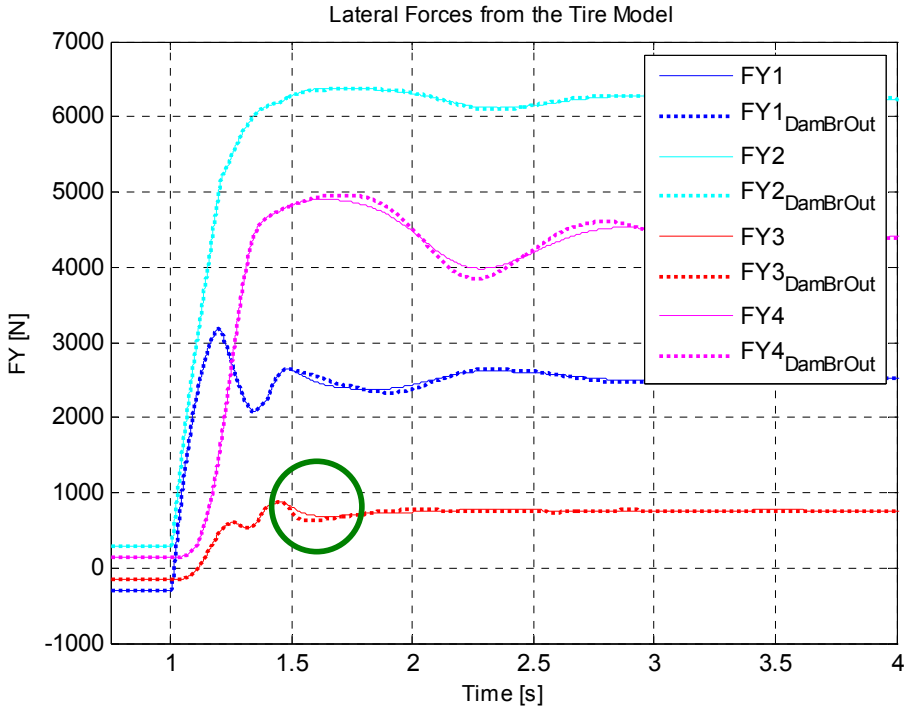

Figure D.45 Lateral Tire Forces for Case 7- Damper 3 Failure

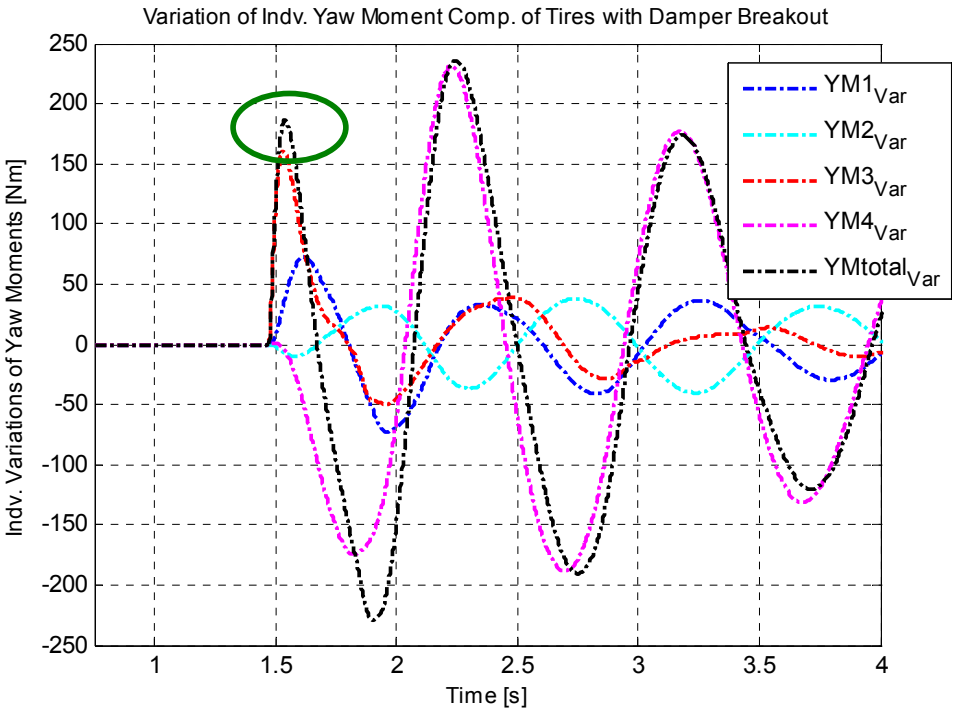

Figure D.46 Variation of Yaw Moments for Case 7- Damper 3 Failure

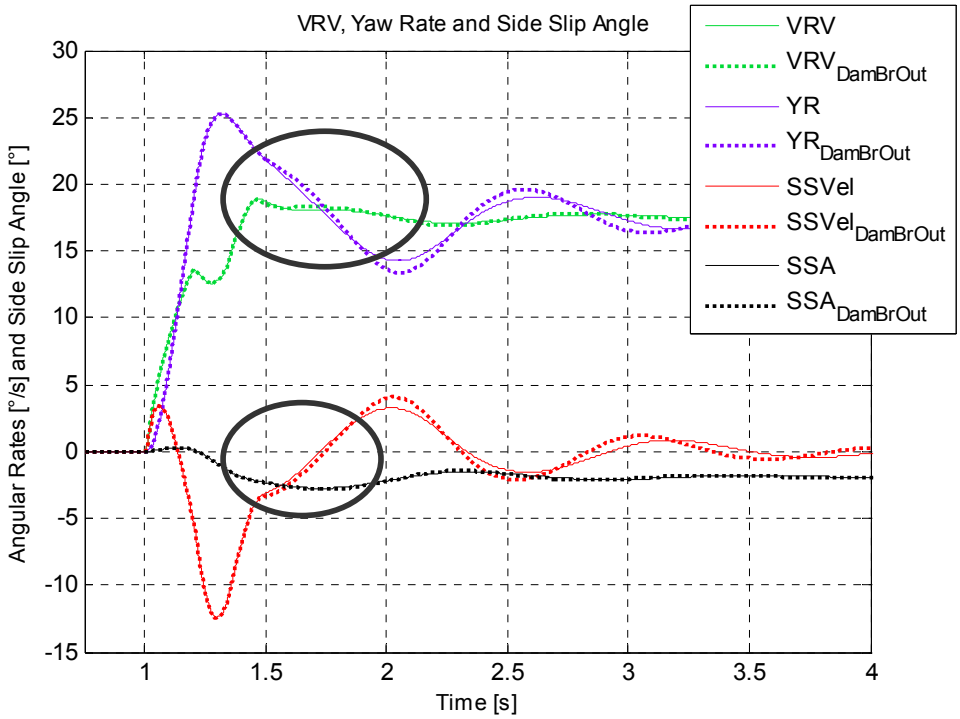

Figure D.47 Calculation of Side Slip Angle for Case 7- Damper 3 Failure

D.4 CASE 10: ELECTRICAL FAILURE FOR STEP STEER RESPONSE WITH BRAKING

D.4.1 Failure of Damper 1

In general a damper 1 failure in this case does not give more critical responses, but a failure at characteristic point $\dot{\varphi}_{max}$ creates the most dynamic case and slightly more critical response since at this point the damper velocities (damper forces) are the maximum.

With a damper failure on tire 1 at $\dot{\varphi}_{max}$ the body has a tendency to lean towards tire 2 more due to increased damper force on tire 1 which pulls the body away for greater roll angle, Figure D.49. Therefore, due to the increase in the tire load on tire 2 the FY2 also increases slightly (FY2 uses the entire potential of the increase in vertical load since FX1 has reached its maximum limit) which increases the total yaw moment and the dynamics of the vehicle slightly. Figures D.48-D.54 demonstrate the influence of the failure explained above.

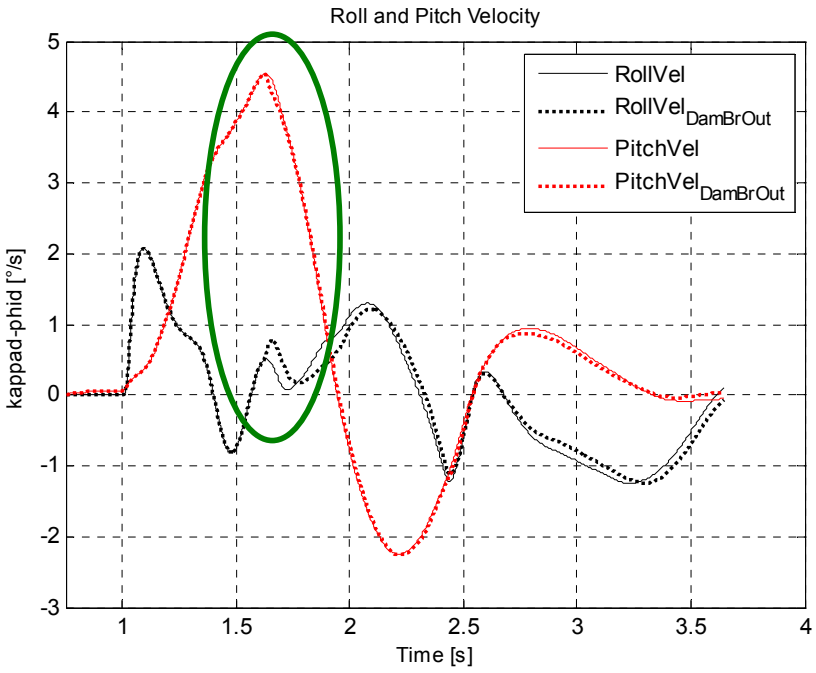

Figure D.48 Roll and Pitch Velocities for Case 10-Damper 1 Failure

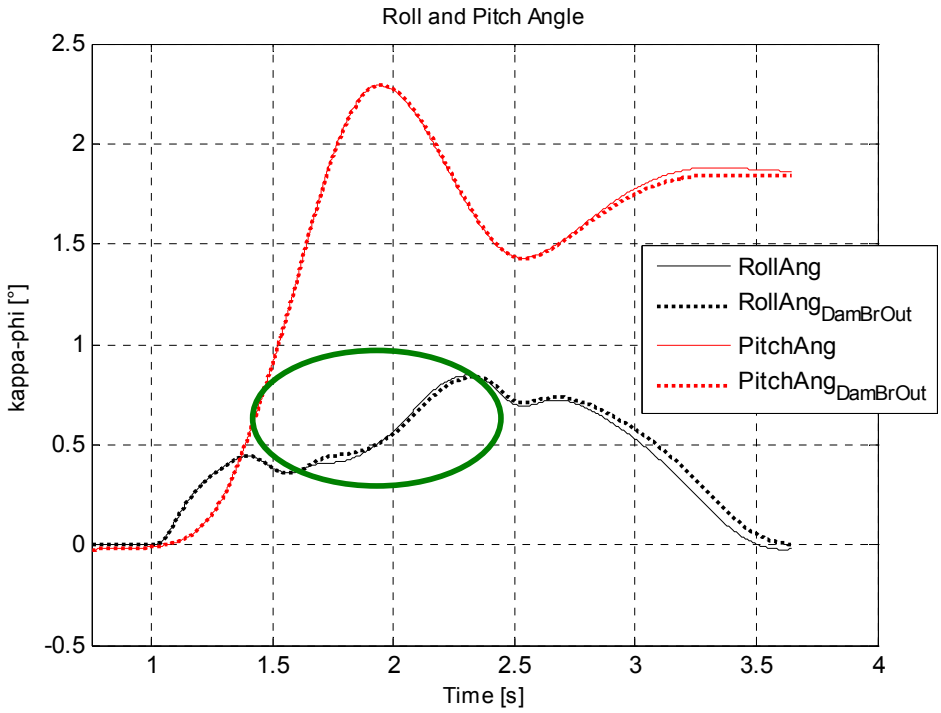

Figure D.49 Roll and Pitch Angles for Case 10- Damper 1 Failure

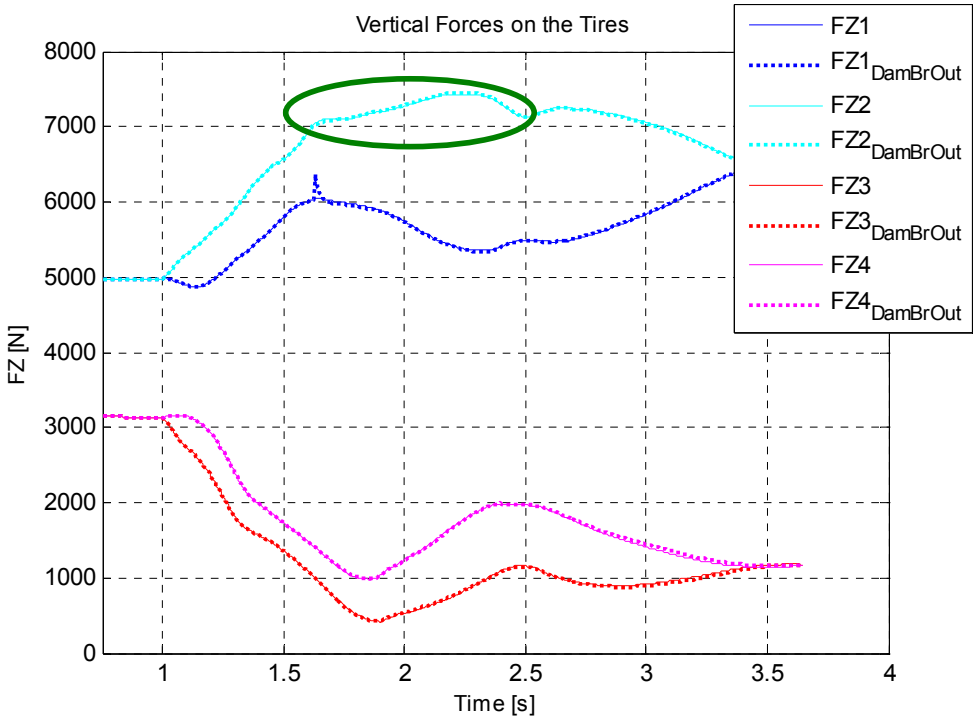

Figure D.50 Vertical Tire Loads for Case 10- Damper 1 Failure

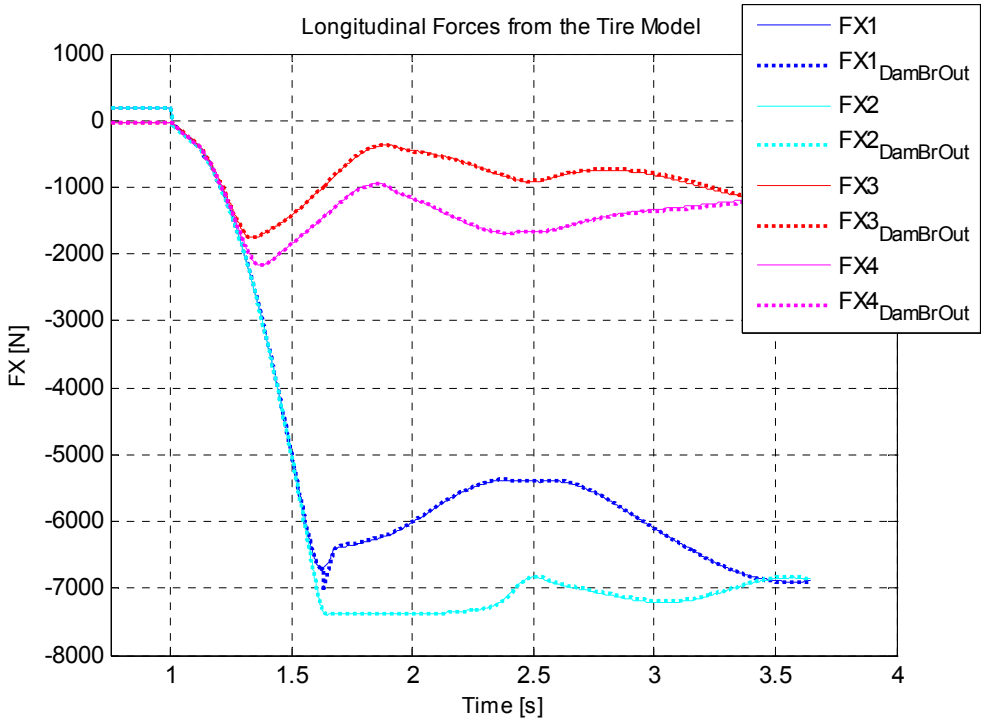

Figure D.51 Longitudinal Tire Forces for Case 10- Damper 1 Failure

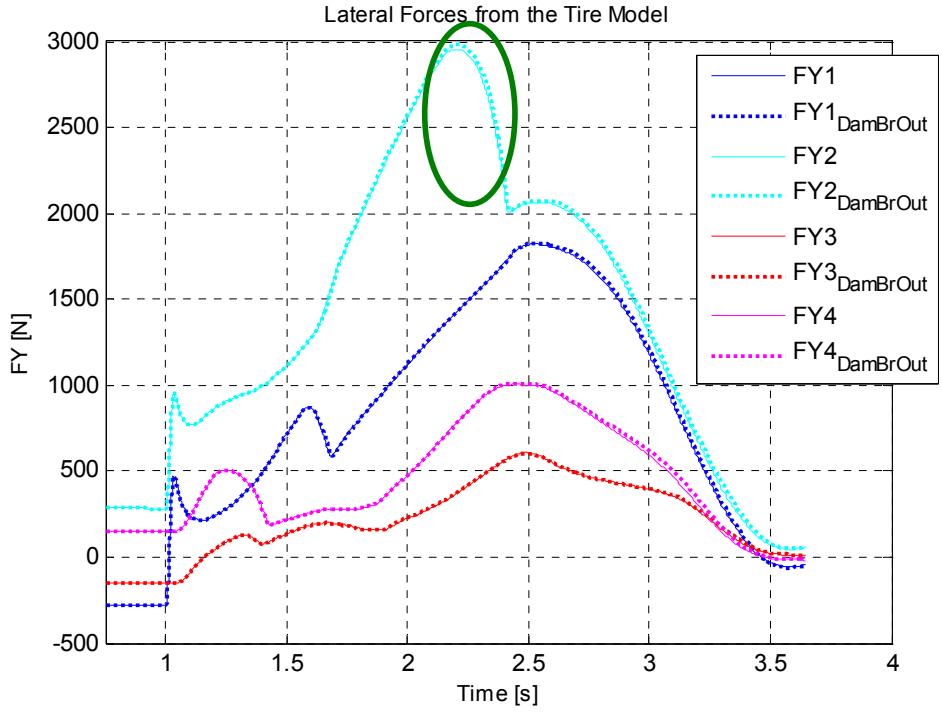

Figure D.52 Lateral Tire Forces for Case 10- Damper 1 Failure

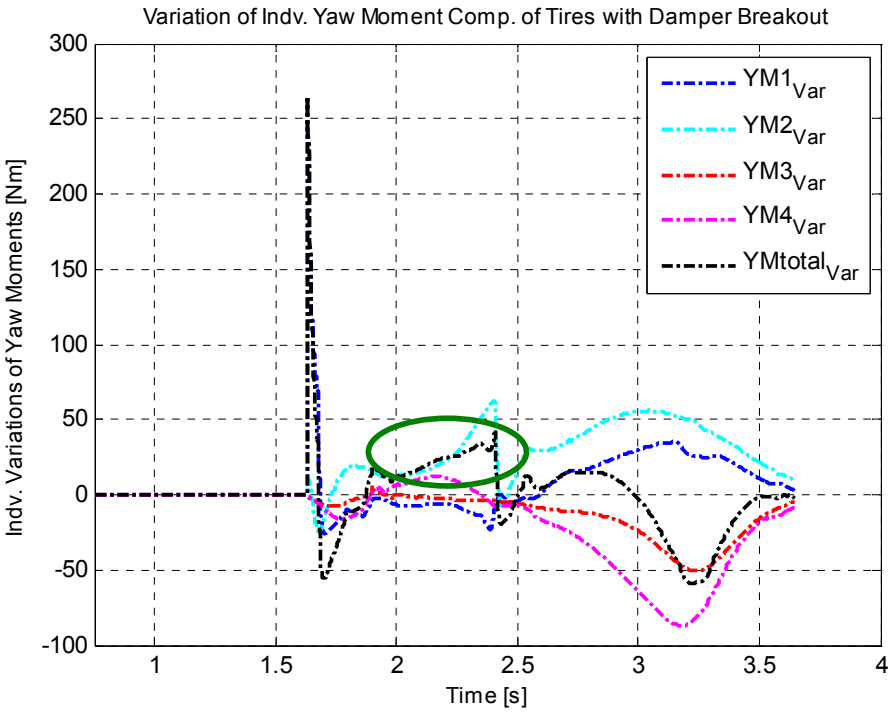

Figure D.53 Variation of Yaw Moments for Case 10- Damper 1 Failure

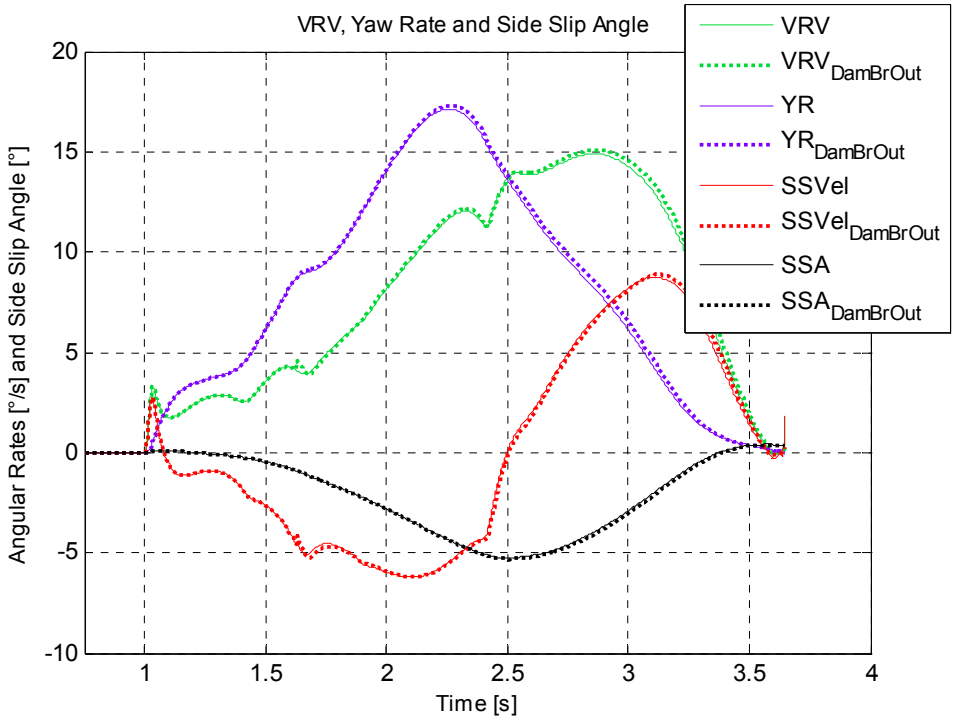

Figure D.54 Calculation of Side Slip Angle for Case 10- Damper 1 Failure

D.4.2 Failure of Damper 3

In general a damper failure of damper 3 does not create a more instable behaviour but rather a more stable behaviour through the entire characteristic points. Therefore, the most dynamic case is in fact the one without damper failure which keeps the original value of the side slip angle. A damper failure which would not influence the behaviour, i.e. at a point on which the responses reach the steady state and consequently there exists no damper relative velocity an damper force. So the only characteristic point matching with that explanation is the $\beta_{\max}$ point. Figure D.55 shows the resulting yaw rate and side slip angle.

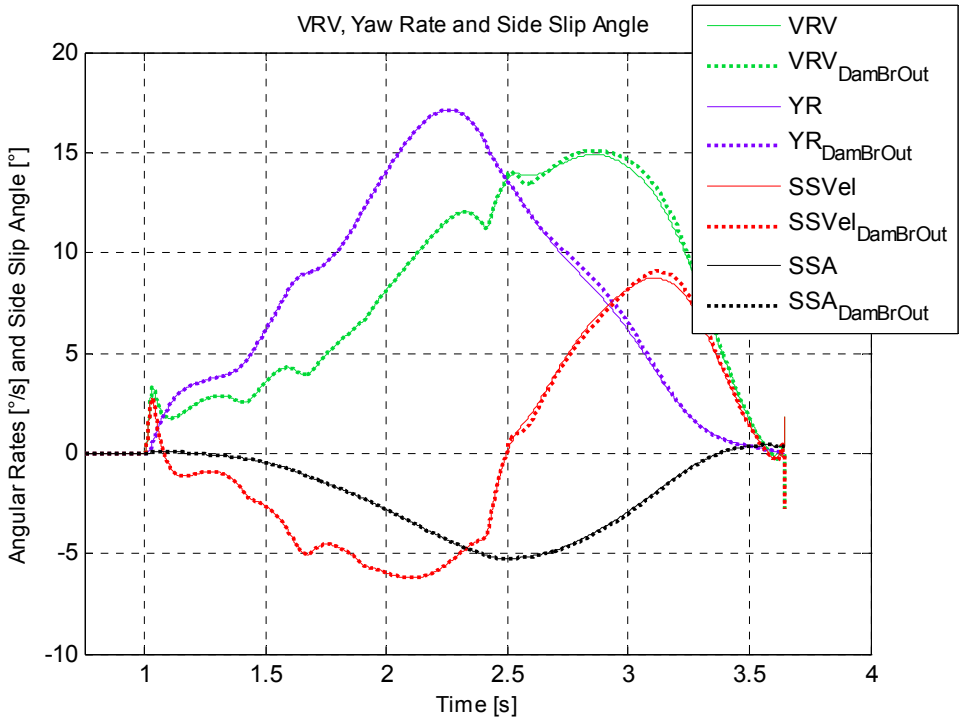

Figure D.55 Calculation of Side Slip Angle for Case 10-Damper 3 Failure

D.4.3 Failure of Damper 4

In this maneuver, the most critical point for damper 4 failure is the point for steering start since the entire maneuver would be influenced by the failed damper.

With a damper failure on tire 4 the damper force is higher and due to the higher resistance on tire 4 the body tends to lean onto tire 4 more which creates as a result a higher roll and lower pitch, Figure D.57. Consequently, due to greater tire load FZ2 the FY2 increases to a great extent (since FX2 is at its mechanical limit) and creates a higher total yaw moment. At the same time, due to a higher extensional force on tire 4 the vertical load on tire 4 is smaller which makes the FX4 also smaller. This also affects the total yaw moment in that it increases more. Figures D.56-D.62 demonstrate the influence of the failure explained above.

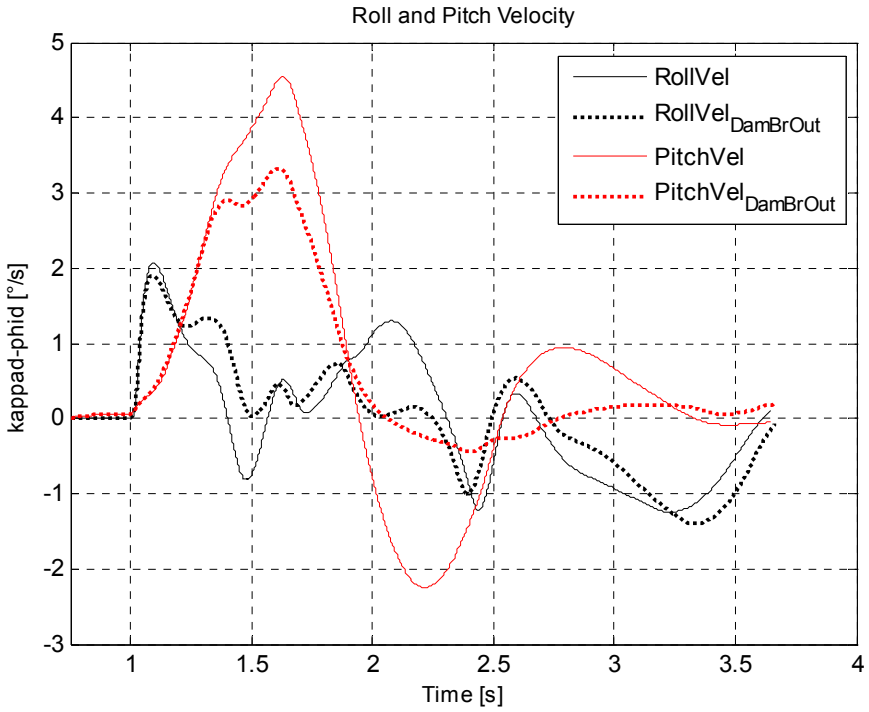

Figure D.56 Roll and Pitch Velocities for Case 10-Damper 4 Failure

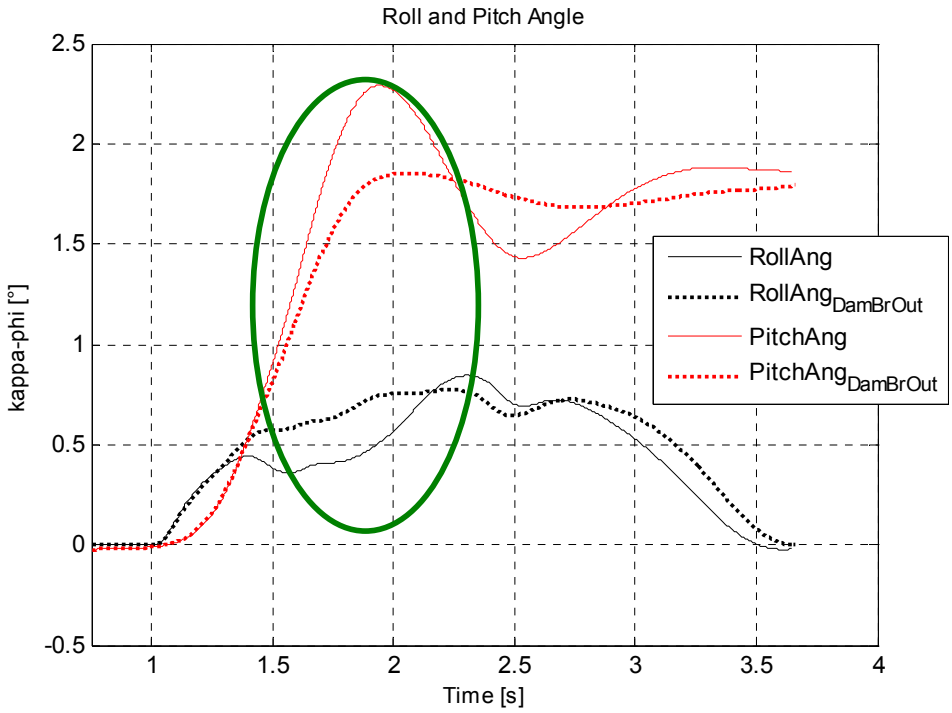

Figure D.57 Roll and Pitch Angles for Case 10- Damper 4 Failure

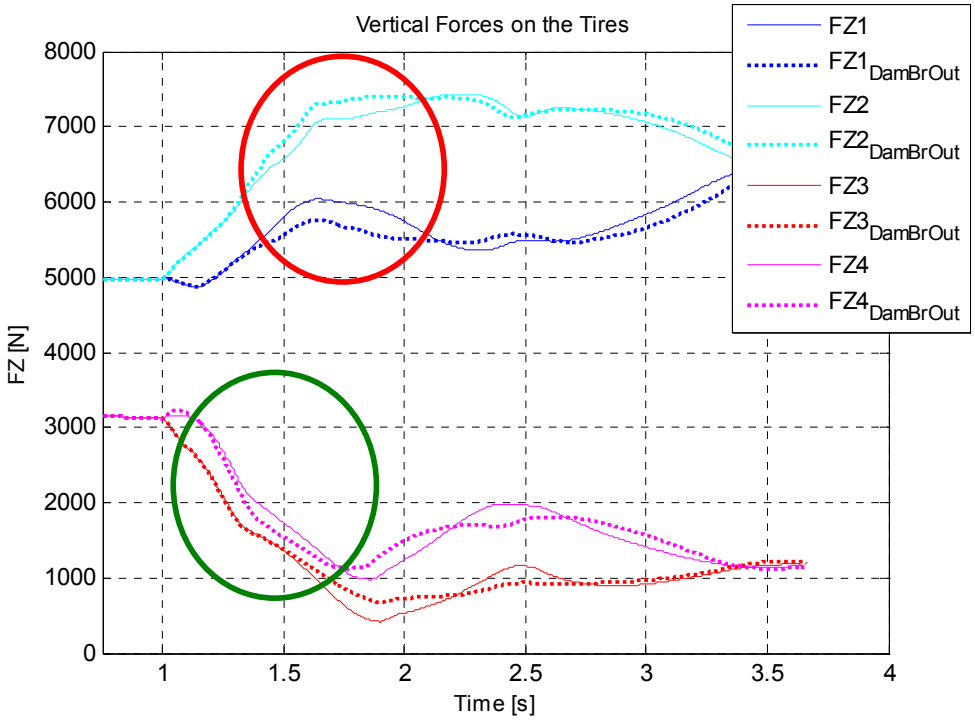

Figure D.58 Vertical Tire Loads for Case 10- Damper 4 Failure

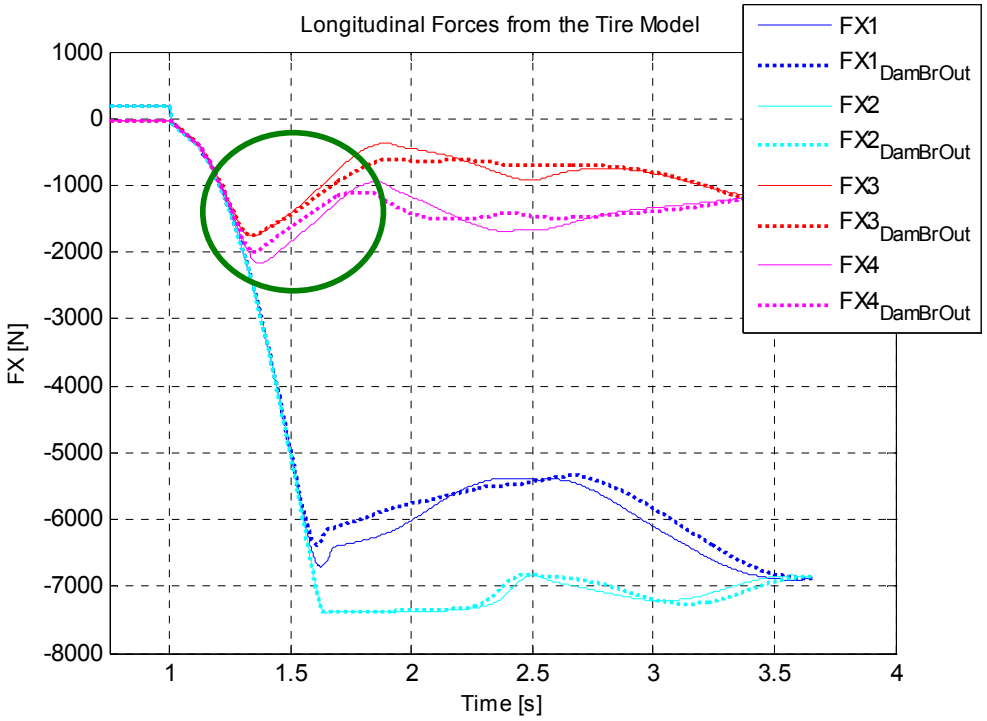

Figure D.59 Longitudinal Tire Forces for Case 10- Damper 4 Failure

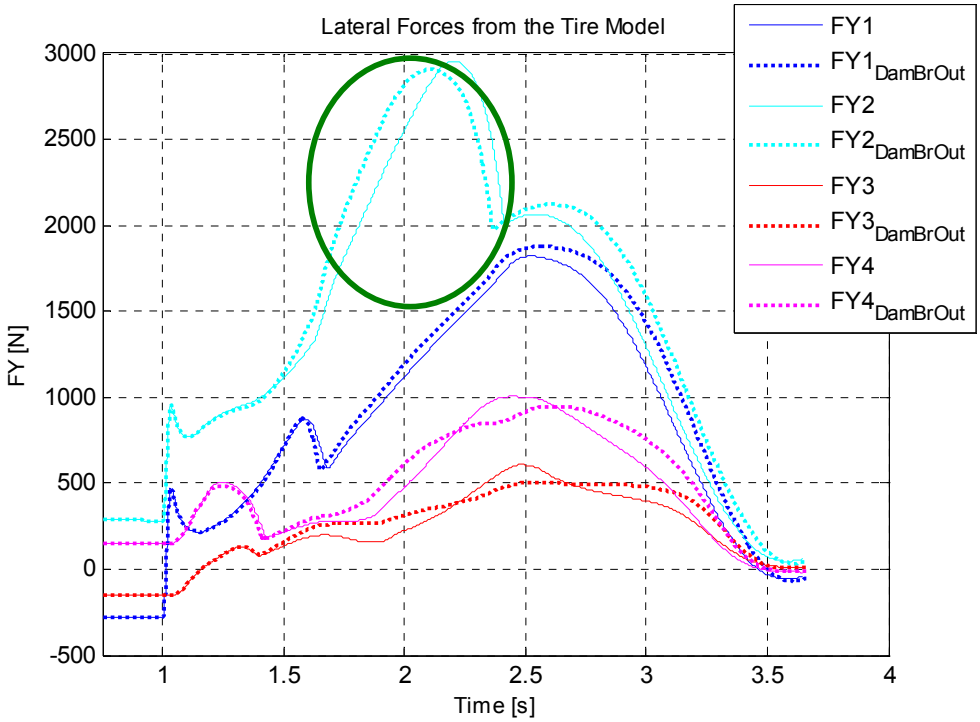

Figure D.60 Lateral Tire Forces for Case 10- Damper 4 Failure

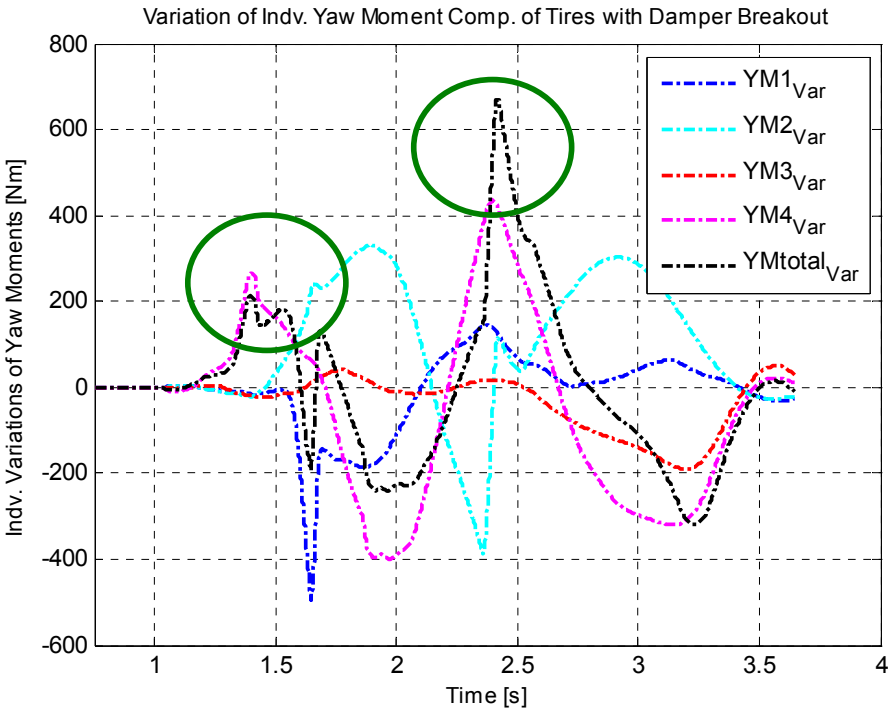

Figure D.61 Variation of yaw Moments for Case 10- Damper 4 Failure

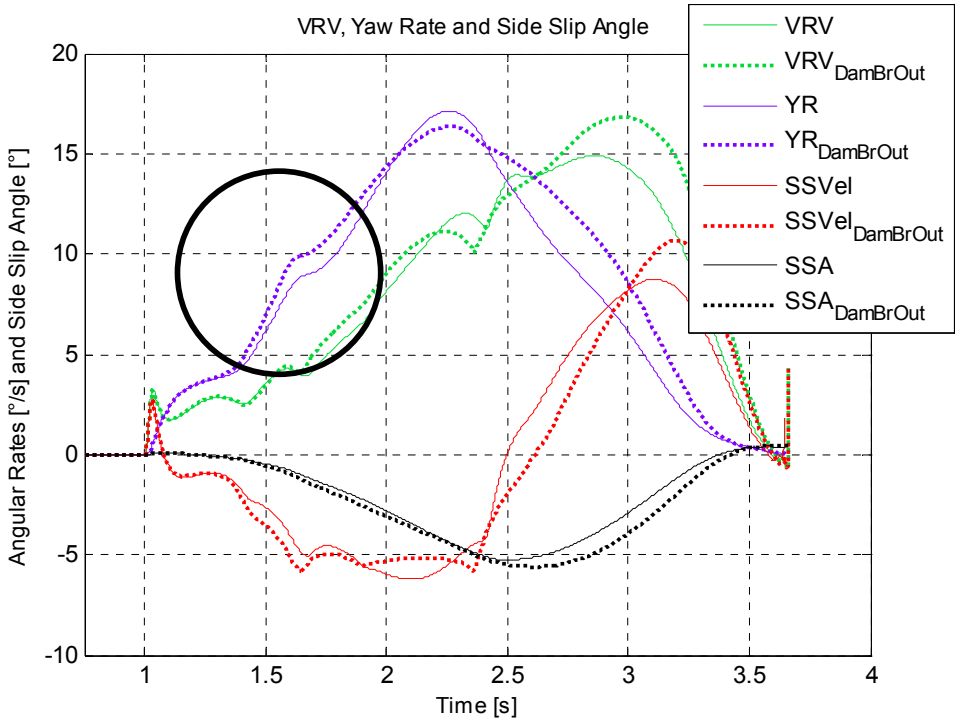

Figure D.62 Calculation of Side Slip Angle for Case 10- Damper 4 Failure

APPENDIX E

SIDE SLIP ANGLE VALUES OBTAINED FROM DAMPER FAILURE

Table D.1 Side Slip Angle peak values from Damper Failure Simulation for Case 1

Damper Failure		Side Slip Angle (β [°])			
At Point	At Time [s]	DA1	DA2	DA3	DA4
Without Failure	x	-2.77	-2.77	-2.77	-2.77
Start	1	-2.48	-2.78	-3.41	-2.53
$\dot{\kappa}_{max}$ = 13.79 °/s	1.23	-2.66	-2.71	-2.76	-2.53
$\dot{\psi}_{max}$ = 25.87 °/s	1.33	-2.79	same	-2.5	-2.67
$a_{y\,max}$ = 8.88 m/s2	1.6	same	same	-2.71	-2.75
β_{min} = -2.77°	1.7	same	same	same	same
κ_{max} = 3.04°	1.8	same	same	same	same

Table D.2 Side Slip Angle peak values from Damper Failure Simulation for Case 2

Damper Failure		Side Slip Angle (β [°])			
At Point	At Time [s]	DA1	DA2	DA3	DA4
Without Failure	x	2.22 (-2.48)	2.22 (-2.48)	2.22 (-2.48)	2.22 (-2.48)
Start	1	2.33	2.28 (-2.55)	2.88 (-3.0)	2.36 (-2.87)
$\dot{\kappa}_{max}$ = 9.78 °/s	1.28	2.36	2.28	2.88 (-2.59)	2.37 (-2.87)
$\dot{\psi}_{max}$ = 22.75 °/s	1.43	2.32 (-2.50)	2.27 (-2.50)	2.89	2.41 (-2.87)
$a_{y\,max}$ = 8.59 m/s2	1.64	2.32 (-2.49)	2.27 (-2.49)	2.87	2.44 (-2.87)

Table D.2 (continued)

κ_{max} = 2.97°	1.74	2.32 (-2.49)	2.27	2.87	2.49 (-2.87)
β_{min} = -2.48°	1.8	2.32	2.27	2.87	2.53 (-2.87)
$\dot{\kappa}_{min}$ = -21.75 °/s	2.24	2.29	2.27	2.85	2.36 (-2.89)
$\dot{\psi}_{min}$ = -23.1 °/s	2.33	2.30	2.27	2.85	2.33 (-2.90)
κ_{min} = -2.96°	2.44	2.30	2.27	2.86	2.32 (-2.91)
$a_{y\,min}$ = -8.65 m/s2	2.51	2.30	2.27	2.85	2.32 (-2.89)
β_{max} = 2.22°	2.84	2.30	2.27	2.84 (-2.55)	2.31 (-2.86)

Table D.3 Side Slip Angle peak values from Damper Failure Simulation for Case 3

Damper Failure		**Side Slip Angle (β [°])**			
At Point	At Time [s]	DA1	DA2	DA3	DA4
Without Failure	x	2.34 (-2.48)	2.34 (-2.48)	2.34 (-2.48)	2.34 (-2.48)
Start	1	2.46	2.62 (-2.55)	3.89 (-3.0)	2.36
$\dot{\kappa}_{max}$ = 9.78 °/s	1.28	2.49	2.62	4.11 (-2.59)	2.37
$\dot{\psi}_{max}$ = 22.75 °/s	1.43	2.46 (-2.50)	2.62 (-2.50)	4.17	2.41
$a_{y\,max}$ = 8.59 m/s2	1.64	2.45	2.62 (-2.49)	4.05	2.44
κ_{max} = 2.97°	1.74	2.45	2.62	3.89	2.49
β_{min} = -2.48°	1.8	2.45	2.62	3.82	2.53
$\dot{\kappa}_{min}$ = -21.75 °/s	2.24	2.38	2.43	3.05	2.46
$\dot{\psi}_{min}$ = -23.1 °/s	2.33	2.35	2.34	2.85	2.45
κ_{min} = -2.96°	2.44	2.36	2.33	2.81	2.42
$a_{y\,min}$ = -8.65 m/s2	2.51	2.36	2.33	2.73	2.36
β_{max} = -2.34°	2.96	2.34	2.34	2.34	2.34

Table D.4 Side Slip Angle peak values from Damper Failure Simulation for Case 4

Damper Failure		Side Slip Angle (β [°])			
At Point	At Time [s]	DA1	DA2	DA3	DA4
Without Failure	x	-4.39	-4.39	-4.39	-4.39
Start	1	-5.2	-3.56	-6.39	-3.98
$\dot{\kappa}_{max}$ = 1.5°/s	1.08	-5.2	-3.56	-6.43	-3.99
$\dot{\varphi}_{max}$ = 3.68°/s	1.62	-4.29	-4.24	-5.41	-3.64
φ_{max} = 1.89°	2.05	-4.35	-4.39	-4.63	-4.42
$a_{y\,max}$ = 2.63 m/s2	2.36	-4.38	-4.38	-4.5	-4.36
$\dot{\psi}_{max}$ = 15.09°/s	2.4	-4.38	-4.38	-4.52	-4.37
κ_{max} = 0.79°	2.41	-4.38	-4.38	-4.52	-4.37
β_{min} = -4.39°	2.71	-4.4	-4.24	-4.4	-4.4

Table D.5 Side Slip Angle peak values from Damper Failure Simulation for Case 5

Damper Failure		Side Slip Angle (β [°])			
At Point	At Time [s]	DA1	DA2	DA3	DA4
Without Failure	x	-3.32	-3.32	-3.32	-3.32
Start	0.88	-6.14	-1.90	-5.28	-1.54
$\dot{\kappa}_{max}$ = 0.78°/s	1.29	-5.62	-2.45	-5.13	-2.23
$\dot{\varphi}_{max}$ = 3.72°/s	1.52	-2.23	-3.66	-2.86	-5.72
φ_{max} = 1.99°	1.94	-3.30	-3.29	-3.31	-3.37
$\dot{\kappa}_{max}$ = 1.05°/s	2.03	-3.31	-3.30	-3.29	-3.35
$a_{y\,max}$ = 2.14 m/s2	2.49	same	same	-3.31	same
κ_{max} = 0.63°	2.5	same	same	-3.31	same
β_{min} = -3.32°	2.93	same	same	same	same
$\dot{\psi}_{max}$ = 10.85°/s	3.08	same	same	same	same

Table D.6 Side Slip Angle peak values from Damper Failure Simulation for Case 6

Damper Failure		Side Slip Angle (β [°])			
At Point	At Time [s]	DA1	DA2	DA3	DA4
Without Failure	x	4.59	4.59	4.59	4.59
Start	1	2.94	6.37	3.83	6.41
$\dot{\kappa}_{max}$ = 0.68 °/s	1.4	2.94	6.37	3.80	6.41
$\dot{\psi}_{max}$ = 1.72 °/s	1.53	2.94	6.37	3.79	6.41
$a_{y\,max}$ = 0.69 m/s2	1.59	2.94	6.37	3.78	6.41
$\dot{\kappa}_{min}$ = -0.96 °/s	2.2	2.93	6.36	3.76	6.44
$\dot{\varphi}_{max}$ = 3.78°/s	2.99	4.76	4.14	4.24	5.10
φ_{max} = 1.99°	3.42	4.56	4.55	4.71	4.57
$\dot{\kappa}_{min}$ = -0.87 °/s	3.57	4.57	4.57	4.69	4.54
$a_{y\,min}$ = -2.66 m/s2	4.1	4.58	4.58	4.59	4.58
κ_{min} = -0.79°	4.17	same	4.58	4.59	4.58
β_{max} = 4.59°	4.35	same	same	same	same
$\dot{\psi}_{min}$ = -14.8 °/s	4.42	same	same	same	same

Table D.7 Side Slip Angle peak values from Damper Failure Simulation for Case 7

Damper Failure		Side Slip Angle (β [°])			
At Point	At Time [s]	DA1	DA2	DA3	DA4
Without Failure	x	-2.74	-2.74	-2.74	-2.74
Start	1	-2.76	-2.62	-2.47	-3.15
$\dot{\kappa}_{max}$ = 17.37 °/s	1.22	-2.71	-2.73	-2.70	-2.88
$\dot{\psi}_{max}$ = 25.29 °/s	1.32	-2.75	-2.74	-2.82	-2.74
$a_{y\,max}$ = 9.11 m/s2	1.47	-2.77	-2.73	-2.83	-2.77
κ_{max} = 3.06°	1.7	same	same	-2.75	-2.74
β_{min} = -2.74°	1.73	same	same	-2.74	same

Table D.8 Side Slip Angle peak values from Damper Failure Simulation for Case 8

Damper Failure		Side Slip Angle (β [°])			
At Point	At Time [s]	DA1	DA2	DA3	DA4
Without Failure	x	2.29 (-2.47)	2.29 (-2.47)	2.29 (-2.47)	2.29 (-2.47)
Start	1	2.26 (-2.52)	2.23	2.50 (-2.84)	2.83 (-2.79)
$\dot{\kappa}_{max}$ = 11.91 °/s	1.26	2.26 (-2.50)	2.25	2.49 (-2.83)	2.83 (-2.65)
$\dot{\psi}_{max}$ = 22.12 °/s	1.44	2.27	2.25	2.49 (-2.83)	2.83 (-2.49)
$a_{y\,max}$ = 8.62 m/s2	1.58	2.27	2.25	2.49 (-2.83)	2.83 (-2.50)
κ_{max} = 2.99°	1.71	2.27	2.25	2.49 (-2.83)	2.83 (-2.49)
β_{min} = -2.47°	1.82	2.27	2.25	2.48 (-2.83)	2.82 (-2.49)
$\dot{\kappa}_{min}$ = -23.01 °/s	2.23	2.30	2.29	2.46 (-2.83)	2.83 (-2.49)
$\dot{\psi}_{min}$ = -22.44 °/s	2.33	2.31	2.33	2.45 (-2.83)	2.83 (-2.49)
κ_{min} = -3.28°	2.39	2.29	2.37	2.45 (-2.83)	2.82 (-2.49)
$a_{y\,min}$ = -8.9 m/s2	2.51	2.28	2.33	2.46 (-2.83)	2.82 (-2.49)
β_{max} = 2.29°	2.90	2.29	2.29	2.47 (-2.82)	2.80 (-2.48)

Table D.9 Side Slip Angle peak values from Damper Failure Simulation for Case 9

Damper Failure		Side Slip Angle (β [°])			
At Point	At Time [s]	DA1	DA2	DA3	DA4
Without Failure	x	2.58 (-2.47)	2.58 (-2.47)	2.58 (-2.47)	2.58 (-2.47)
Start	1	2.70 (-2.52)	2.43	2.37	3.59 (-2.79)
$\dot{\kappa}_{max}$ = 11.91 °/s	1.26	2.70 (-2.50)	2.44	2.35	3.57 (-2.65)
$\dot{\psi}_{max}$ = 22.12 °/s	1.44	2.72	2.45	2.33 (-2.56)	3.54 (-2.48)
$a_{y\,max}$ = 8.62 m/s2	1.58	2.72	2.45	2.32 (-2.53)	3.56 (-2.50)
κ_{max} = 2.99°	1.71	2.72	2.45	2.30 (-2.48)	3.59 (-2.48)
β_{min} = -2.47°	1.82	2.72	2.45	2.29	2.62
$\dot{\kappa}_{min}$ = -23.01 °/s	2.23	2.60	2.54	2.36	2.70
$\dot{\psi}_{min}$ = -22.44 °/s	2.33	2.59	2.58	2.27	2.64
κ_{min} = -3.28°	2.39	2.57	2.60	2.25	2.72
$a_{y\,min}$ = -8.90 m/s2	2.51	2.55	2.59	2.41	2.71
β_{max} = 2.58°	3.05	same	2.58	2.58	2.58

Table D.10 Side Slip Angle peak values from Damper Failure Simulation for Case 10

Damper Failure		Side Slip Angle (β [°])			
At Point	At Time [s]	DA1	DA2	DA3	DA4
Without Failure	x	-5.25	-5.25	-5.25	-5.25
Start	1	-4.37	-6.13	-3.24	-5.59
$\dot{\kappa}_{max}$ = 2.07°/s	1.1	-4.35	-6.09	-3.24	-5.59
$\dot{\varphi}_{max}$ = 4.55°/s	1.63	-5.31	-5.28	-4	-4.92
φ_{max} = 2.29°	1.95	-5.27	-5.26	-5.21	-4.99
$a_{y\,max}$ = 2.69 m/s2	2.27	-5.25	-5.26	-5.19	-5.17
$\dot{\psi}_{max}$ = 17.14°/s	2.26	-5.25	-5.26	-5.19	-5.17
κ_{max} = 0.84°	2.31	-5.25	-5.26	-5.21	-5.19
β_{min} = -5.25°	2.5	-5.25	-5.25	-5.25	-5.25

Table D.11 Side Slip Angle peak values from Damper Failure Simulation for Case 11

Damper Failure		Side Slip Angle (β [°])			
At Point	At Time [s]	DA1	DA2	DA3	DA4
Without Failure	x	-4.74	-4.74	-4.74	-4.74
Start	0.88	-2.77	-5.56	-1.65	-5.59
$\dot{\kappa}_{max}$ = 1.18°/s	1.24	-3.61	-5.67	-2.17	-5.17
$\dot{\varphi}_{max}$ = 4.57°/s	1.52	-4.46	-4.58	-5.83	-3.37
φ_{max} = 2.38°	1.83	-4.79	-4.81	-5.20	-4.33
$\dot{\kappa}_{max}$ = 1.61°/s	2.02	-4.77	-4.77	-5.11	-4.43
κ_{max} = 0.81°	2.39	-4.71	-4.74	-4.59	-4.91
$a_{y\,max}$ = 2.66 m/s2	2.43	-4.71	-4.74	-4.58	-4.91
β_{min} = -4.74°	3.23	-4.74	-4.74	-4.73	-4.74
$\dot{\psi}_{max}$ = 15.58°/s	3.17	-4.74	-4.74	-4.74	-4.74

Table D.12 Side Slip Angle peak values from Damper Failure Simulation for Case 12

Damper Failure		Side Slip Angle (β [°])			
At Point	At Time [s]	DA1	DA2	DA3	DA4
Without Failure	x	4.59	4.59	4.59	4.59
Start	1	6.40	3.37	6.43	3.54
$\dot{\kappa}_{max}$ = 0.71 °/s	1.34	6.40	3.37	6.43	3.54
$\dot{\psi}_{max}$ = 1.68 °/s	1.53	6.40	3.37	6.43	3.54
$a_{y\,max}$ = 0.68 m/s2	1.59	6.40	3.37	6.43	3.54
$\dot{\kappa}_{min}$ = -0.87 °/s	2.15	6.37	3.38	6.47	3.54
$\dot{\varphi}_{max}$ = 4.58°/s	3	4.96	5.12	5.15	4.88
φ_{max} = 2.33°	3.31	4.98	5.03	5.57	5.37
$\dot{\kappa}_{min}$ = -1.27 °/s	3.48	4.96	5.02	5.57	5.32
$\dot{\psi}_{min}$ = -13.45 °/s	3.74	4.96	4.99	4.77	5.09
κ_{min} = -0.79°	3.86	4.96	4.98	4.85	5.02
$a_{y\,min}$ = -2.82 m/s2	3.90	4.96	4.98	4.85	5.02
β_{max} = 4.59°	4.31	4.96	4.96	4.96	4.97